DISPERSION OF ATMOSPHERIC POLLUTANTS FROM POINT SOURCES IN A COASTAL ENVIRONMENT

by

Kenneth N. Rayner B.E.(Hons), M.Eng.Sc.

This Thesis is presented for

the Degree of Doctor of Philosophy of Murdoch University.

1987

:SSN 1030 0600
:SBN 0 7309 1607 3

ABSTRACT

This Thesis describes work undertaken by the author as part of a Government sponsored study of air pollution dispersion from industrial sources at Kwinana, Western Australia. The primary objective of the study was to develop predictive tools, in the form of computer models, which could be used in assessing air quality constraints on land use planning in the Kwinana area. A secondary objective was to develop models which could be adapted to apply to other areas of the State, both on the coast and inland.

The approach adopted to achieve these objectives was to identify those meteorological processes which significantly influence pollutant dispersion and to concentrate on developing conceptually simple, acceptably accurate model components which could be amalgamated into an efficient, flexible and robust dispersion model package. As far as possible, computation methods requiring only routinely available data were pursued, in view of the applications proposed for the model. The model components developed in the course of the study were:

(a) a model combining heat budget and bulk aerodynamic methods for computing surface turbulent fluxes, which requires routine single height meteorological data only and which accounts for the important stabilizing effect of surface evaporation;

(b) a model to describe the erosion of radiation inversions above a growing daytime well mixed layer, based on a parameterization of the turbulent kinetic energy budget of the layer;

(c) an efficient multi-source Gaussian plume dispersion model, incorporating simulation of the shoreline fumigation effect of elevated plumes entrained into a thermal internal boundary layer.

Each of these model components was successfully validated via comprehensive field experiments, which are described in the Thesis. The dispersion model displayed excellent accuracy in predicting daily or longer averages of sulphur dioxide measurements at a continuous monitoring station, but tended to under-predict high hourly averages.

The development and implementation of the above model components to simulate the various meteorological processes over a full twelve month period (with a ten minute timestep) for a very modest computing cost is considered to be a significant contribution to this field of study.

TABLE OF CONTENTS

LIST OF FIGURES

LIST OF TABLES

ACKNOWLEDGEMENTS

The bulk of work reported in this Thesis was completed as part of the Kwinana Air Modelling Study (KAMS). The author is indebted to his employer during this period, the Department of Conservation and Environment, for initiating the Study and providing the resources and facilities conducive to sound research. The Public Health Department similarly provided strong ongoing support. Special thanks go to Dr Bruce Hamilton for his foresight and guidance.

KAMS benefited from the contributions and specialist assistance of several organizations, including the Commonwealth Bureau of Meteorology, Western Australian Institute of Technology, Murdoch University, University of Western Australia and the State Energy Commission. Participation of these groups in intensive field experiments was of particular value. The contribution of continuous high grade emissions data by the various industries at Kwinana is also acknowledged.

The bulk of work in KAMS was completed by a small core group of full and part-time scientists, the activities of which were coordinated by the author. Work carried out by the author's colleagues which has been utilised in the preparation of this Thesis is acknowledged below.

Mr Vlado Raich successfully commissioned the electronic meteorological and data acquisition equipment and provided ongoing maintenance skills. Dr Don Martin played a major role in establishing the

monitoring programme and was also largely responsible for compiling the emissions data inventory. Mr John Rosher later assumed responsibility for both the monitoring programme and the data analysis and processing functions. John played a key role in the preparation for, and execution of, the major field experiments, and was primarily responsible for the development of an efficient multiple point source dispersion model, which was used by the author as the basis for development of a coastal dispersion model. John assisted with the computing tasks involved in testing and refining the coastal dispersion model, and subsequently carried out all of the dispersion simulations described in the KAMS Report (1982). Mr Vince Paparo assisted in several facets of the Study, (notably in the organization of tracer gas experiments) and undertook the major task of editing the final report. Dr Peter Rye was also closely involved in various facets of KAMS and was responsible for a separate stream of dispersion model development.

During 1982 and 1983, whilst employed by the State Energy Commission of W.A. (SECWA), the author coordinated two field experiments to study the growth of coastal internal boundary layers, as described in this Thesis. Mr Brian Bell of SECWA played a key role in preparation for, and execution of, these experiments, which included the use of a light aircraft to map the growth of the boundary layer. Brian also carried out the computer processing of data from these experiments using the models developed by the author in KAMS. Professor Des O'Connor of Murdoch University piloted the light aircraft and was strongly supportive of this work. As in KAMS, the Bureau of Meteorology

participated in the experiments, providing radiosonde data and expert advice. Mr Rosher and other staff from the Department of Conservation and Environment and Public Health also assisted in the experiments. The support of SECWA and notably Messrs Wulff and Colvin is gratefully acknowledged.

Dr Tom Lyons of Murdoch University was actively involved in KAMS and has been available at all times for scientific interaction. As the supervisor of this Thesis, Dr Lyons has provided valuable insights and constructive criticism.

Finally, thanks must go to Glenda for typing this Thesis, to Fred and Brian for proof-reading it, and to my wife, Robyn, and family for being extremely understanding and supportive whilst it was being completed outside normal work hours.

CHAPTER 1

INTRODUCTION

1.1 STUDY OBJECTIVES

Dispersion of atmospheric pollutants in coastal areas is a common concern of environmental and health agencies, since the population density of coastal areas is usually relatively high. The subject is also keenly studied by atmospheric scientists in view of the complexity of mesoscale wind patterns and mixing processes at coastal sites.

This Thesis describes theoretical and experimental work directed towards the development of computer models to describe the dispersion of pollutants from tall chimneys in a coastal environment. The bulk of this work was completed as part of the Kwinana Air Modelling Study (1978-82), of which the author was the Coordinator. Relevant theoretical and experimental work completed subsequent to that Study has also been included.

The Kwinana Air Modelling Study (KAMS) has been documented by the Department of Conservation and Environment (KAMS, 1982). An overview of the Study is provided in Chapter 2 of this Thesis. As the name implies, the aim of KAMS was to develop computer models of atmospheric pollutant dispersion in the Kwinana area, which is the State's major industrial area situated about 30 kms to the south of Perth. The main concentration of heavy industry at Kwinana is in a coastal strip

adjacent to Cockburn Sound which is a natural harbour protected by Garden Island. The prime objective behind the development of the computer models was to provide a predictive tool for use in assessing air quality constraints on land use planning (e.g. on future residential development adjacent to the industrial strip). A secondary general objective was to develop models which could be adapted to apply to other situations in the State, both on the coast and inland.

The stated objectives of KAMS had a major influence on the philosophy and direction of work. In order to meet the first objective, it was necessary for the models to be efficient (in terms of computer resources), flexible and robust (to provide results for widely varying conditions and scenarios without requiring significant modifications), whilst still describing the important meteorological phenomena with sufficient accuracy to make the results meaningful and reliable. Accordingly, models requiring numerical solutions to second or higher order primitive equations were deliberately avoided, with attention focussing instead on relatively simple conceptual models of meteorological phenomena which could be incorporated into algorithms within a computer model designed to run over extensive data sets (1-2 years) at minimal cost. The first objective also confined the region of interest to "local scale", i.e. the area surrounding industries within which significant concentrations of primary pollutants might occur (typically within 15 kms of the source). The second objective (applicability of the models at other locations) led to attention being focussed on models which could be run on routinely available data, as opposed to models requiring specialised and/or difficult-to-obtain data. This philosophy recognises that model

results are often required on a timescale far shorter than that required to collect a representative data set (1 to 2 years), and also that the logistics of collecting such data at remote sites may be prohibitive.

One of the main contributions of this Thesis will therefore be the description of a point source dispersion model optimised to meet the independent constraints of acceptable accuracy, efficiency, suitability for application to extensive data sets, flexibility, and dependence on routinely available data where practicable. Other contributions will be in the form of improvements or refinements to models of important meteorological processes and verification of these models via field experiments. These important meteorological processes will be identified in the next Section and a rationale given for the approach adopted to investigate them.

1.2 DISPERSION MODEL DEVELOPMENT METHODOLOGY

There are three fundamental steps in defining a methodology for dispersion model development:

(a) identify the important meteorological processes and characteristics of the pollutant sources which together will determine the ambient concentrations of pollutants in the area of interest;

(b) analyse each process or characteristic to determine how best to simulate it for the purposes of the model, and what information or data are required to do so;

(c) collate the findings and requirements from step (b) to determine

the optimum means of proceeding.

An overview of model development methodology employed in this Study, following these three steps, is given below. A series of figures is included to aid the discussion. Figure 1.1 is a schematic of the planetary boundary layer, included for the purposes of defining various meteorological parameters to be used in the discussion. Figures 1.2 to 1.6 are schematics of important meteorological processes which influence the dispersion of air pollutants in the Kwinana Area. In each figure, the meteorological parameters which together drive or influence the process are specified. Detailed theoretical descriptions of the meteorological processes, including the formal derivation of parameter relationships, will be given in the Chapters which follow.

1.2.1 IMPORTANT METEOROLOGICAL PROCESSES AND SOURCE CHARACTERISTICS

(i) Pollutant Source Location, Height and Strength

Location and height of chimneys in an industrial area are major determinants of the spatial distribution of pollutants. These parameters are easily specified within a computer model as three dimensional coordinates on a base map grid.

Pollutant concentrations are directly proportional to the rate of pollutant emission at the source. Data on pollutant emission rates for each source can be stored as a time sequence and accessed by a computer model.

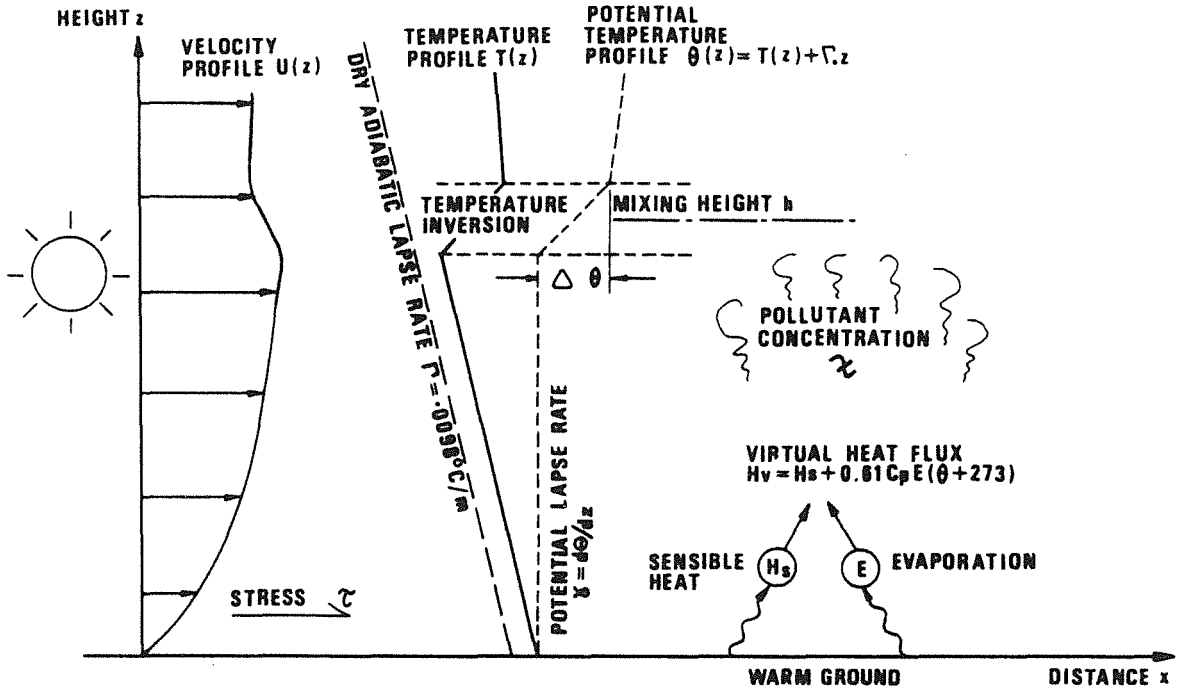

FIGURE 1.1 DEFINITION OF METEOROLOGICAL PARAMETERS IN THE PLANETARY BOUNDARY LAYER

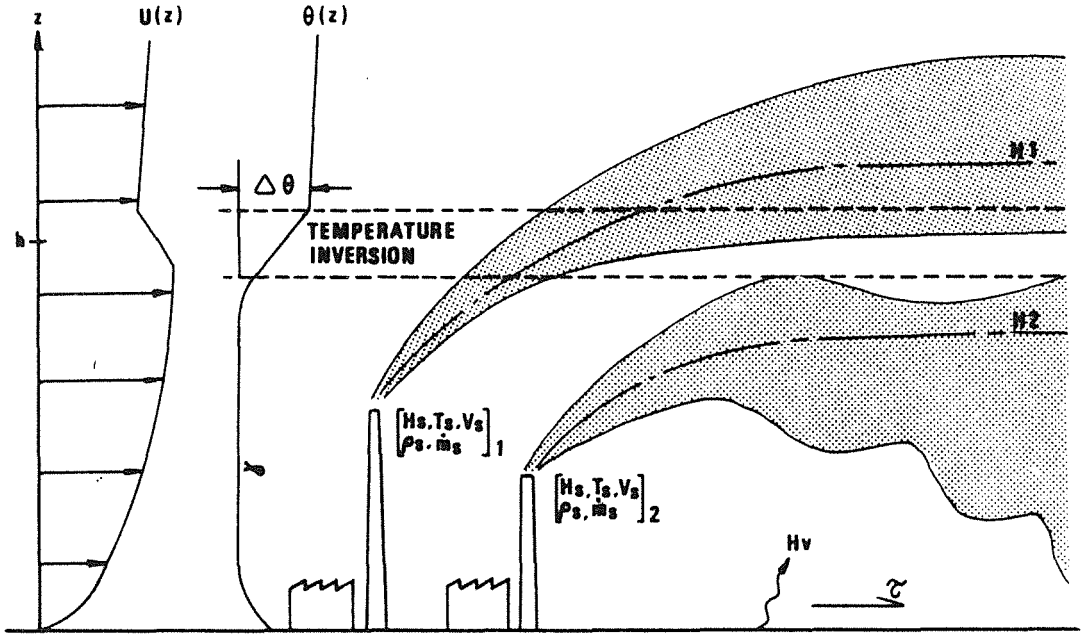

FIGURE 1.2 PLUME RISE AND EFFECT OF INVERSIONS

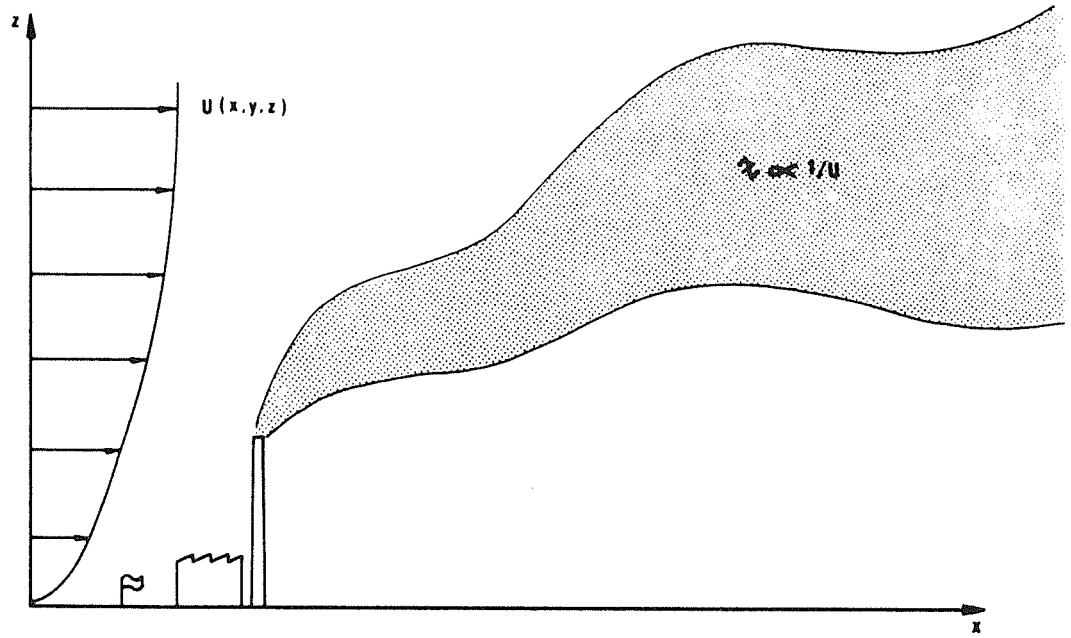

FIGURE 1.3 TRANSPORT OF POLLUTANTS

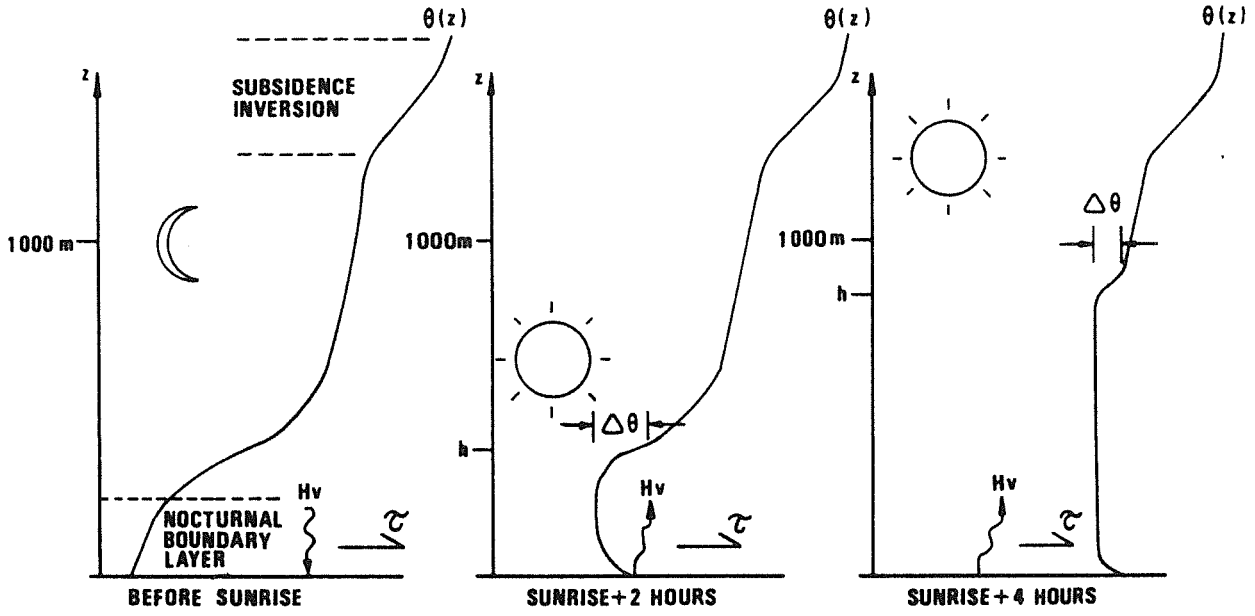

FIGURE 1.4 MIXING HEIGHT-WITHOUT COASTAL INFLUENCES

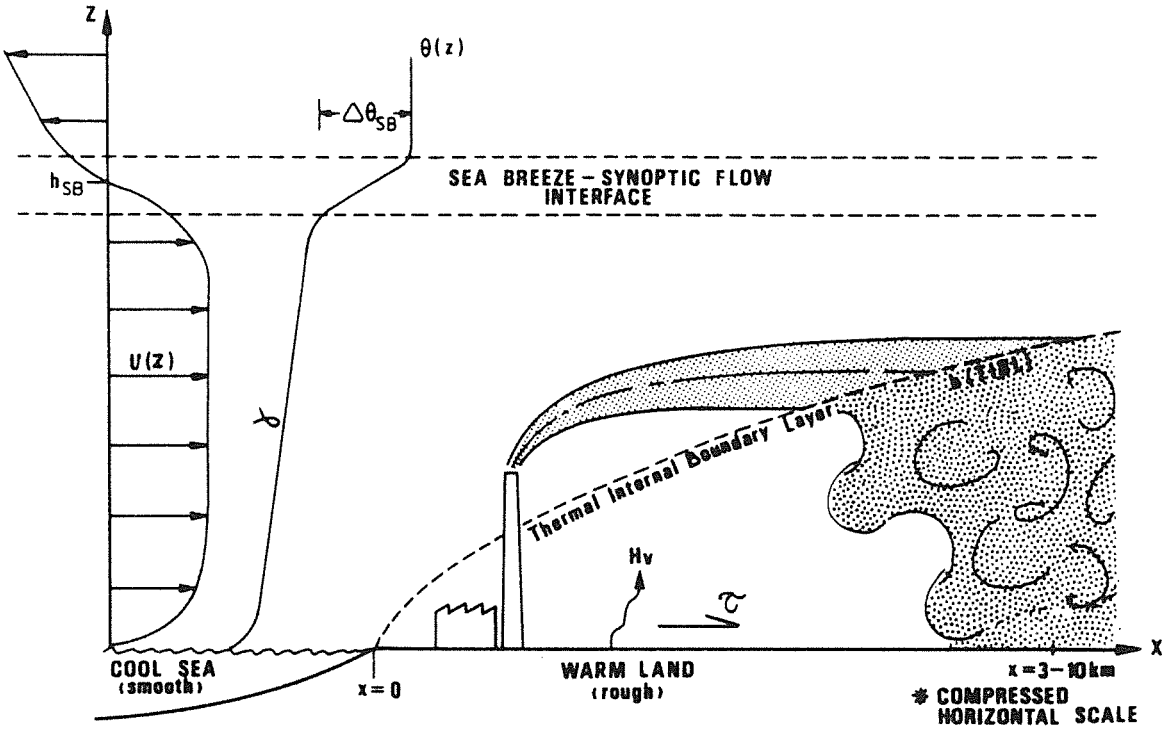

FIGURE 1.5 MIXING HEIGHT-SEA BREEZE WITH A TIBL

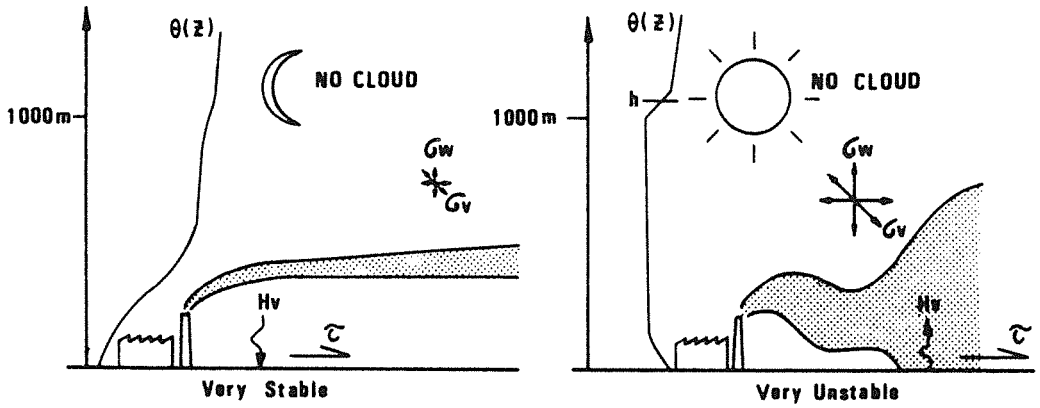

FIGURE 1.6 PLUME DISPERSION-INFLUENCE OF ATMOSPHERIC STABILITY

(ii) Plume Rise and Effect of Inversions

Buoyant chimney plumes rise and level within the planetary boundary layer as depicted in Figure 1.2. The height of rise H will depend on the initial plume characteristics (stack height Hs, temperature Ts, exit velocity Vs, density ρs, mass flow rates Ms) and on the meteorology, as described by Briggs (1975).

If the temperature lapse rate r is stable ($r > 0$), plumes will run out of buoyancy in the warmer air aloft and level out. In neutral or unstable conditions ($r \leq 0$), plumes will level out due to the mixing activity in the atmosphere, which will depend on surface turbulent fluxes of heat H_v and momentum τ, and the mixed layer depth h.

A plume may commence rising into a neutral or unstable layer and then intersect a very stable temperature inversion aloft, which acts like a "lid" with a strength $\Delta\theta$. If the plume temperature is still high enough it will penetrate the lid, as illustrated in Figure 1.2, but will not be able to disperse down through it again. If the plume is not warm enough, some or all of it will be trapped below the lid and the pollutants will be mixed back to ground in relatively high concentrations. $\Delta\theta$ is therefore an important parameter, as discussed by Manins (1979).

An increase in wind speed U will result in a decrease in plume height under all conditions.

(iii) Pollutant Transport

Pollutants at an elevated level in the planetary boundary layer are advected downwind at the speed of the wind at that height (see Figure 1.3). Concentration of pollutants is inversely proportional to this speed. The variation of wind speed U with height z becomes greater with increasing stability (Irwin, 1979b). These effects must be included in a model if surface wind data are to be used.

Surface wind speed U(x,y) and direction WD(x,y) may be significantly modified by topography or other changes in surface characteristics. For dispersion modelling over a large area, these changes may need to be measured or separately modelled.

(iv) Mixing Height - Without Coastal Influences

Figure 1.4 illustrates a sequence of events frequently observed in the planetary boundary layer adjacent to the earth's surface. At night-time, in the absence of extensive cloud cover, the ground cools by radiating heat upwards. The air next to the ground is also cooled by sensible heat transfer, leading to the gradual formation of a deep ground-based stable layer (called a radiation inversion). There is no "lid" as such, but plumes released within the layer will disperse slowly, dependent on the amount of turbulent mixing occurring, which in turn is determined by the surface cooling rate H_v and the stress τ (Mahrt, 1981). If clouds are present at night, their added radiation may be enough to prevent the stable layer forming (ie. by keeping H_v small).

Shortly after sunrise, there will be enough mixing energy available from surface heating and wind stirring (parameterized via H_v and τ) to commence eroding the stable temperature structure and forming a well mixed layer. The mixing and deepening of this layer will continue through the day, probably reaching 1-2 kms depth by mid-afternoon. During its growth, turbulent mixing at the top of the layer causes a relatively sharp temperature inversion $\Delta\theta$ to form, which acts as a "lid" to some plumes, as described in (ii) above. Hence it is important to describe the daytime evolution of mixed layer height h and inversion strength $\Delta\theta$ in the dispersion model. The key meteorological parameters are expected to be H_v , τ and $\theta(z)$ (Tennekes, 1973).

Subsidence inversions rarely form below 1,000 m in the South West of Western Australia and so are not a major consideration. If present, a subsidence inversion will slow the growth of the mixed layer when mixing reaches the inversion height.

(v) Mixing Height - Coastal Effects

Sea breezes along the W.A. coast typically take the form of a cool current of air, 300 to 500 m deep at the coast, with a strong inversion interface at its upper boundary. Pollutants released into the sea breeze will almost certainly be trapped therein. However, close to the coast, details of the sea breeze are not as important for dispersion modelling as those of the coastal internal boundary layer.

When onshore flows encounter the coastline, the sudden change in

surface roughness, heating and evaporation rates leads to the formation of an internal boundary layer over the land (see Figure 1.5). The situation of most interest in the current Study is the formation of a thermal internal boundary layer (TIBL) within cool onshore flow over warm land. In this situation the strength of turbulence (driven by convective heating) and hence also the dispersive capability of air within the TIBL is far greater than that of the marine air. Figure 1.5 shows a plume released in the stable flow of a sea breeze and dispersing only slowly until it intersects a growing TIBL, from where it is mixed rapidly to ground level, resulting in much higher short term concentrations than would otherwise occur at that distance from the source. This phenomenon is called "shoreline fumigation" (Lyons, 1975), and is a major consideration in dispersion modelling for coastal sites. To determine the location and strength of fumigation events it is necessary to predict the rate of growth of the TIBL, which is determined mainly by H_v, τ, layer mean velocity U and the temperature structure of the onshore flow, r(z) (Stunder and SethuRaman, 1985).

(vi) Pollutant Dispersion

After the initial rise stage, the pollutants in a plume are dispersed by the action of atmospheric turbulence. The level of turbulent mixing in the planetary boundary layer is commonly expressed as atmospheric stability, varying between the extremes shown in Figure 1.6. Turbulent velocity fluctuations σ_u, σ_v and σ_w (orthogonal components), which determine the rate of plume spread, may be related to various measures of atmospheric stability. The key parameters for determining stability

are H_v, τ and h (Hanna et al., 1977).

1.2.2 MODELLING METHODOLOGY

Given the above analysis of meteorological processes and the parameters on which these depend, an optimum approach to model development may be derived.

From inspection, the only key parameters which are provided directly by routine near surface measurements are the wind speed U(x,y) and direction WD(x,y). Horizontal variations of these parameters, although usually present and measurable, can most likely be classified as secondary effects for local scale studies over relatively featureless landscapes (such as at Kwinana). Mixing height may be directly measured by an acoustic sounder, but such measurement is far from routine.

The next class of parameters which may be identified are those which are directly calculable from surface meteorological data. Included in this group are:

(a) σ_v (from σ_θ and U, where σ_θ is the standard deviation of wind direction fluctuations);

(b) H_v and τ (from tower profile measurements or heat budget calculations).

The third identified group of parameters are those which depend on H_v and τ, plus other direct measurements. This group is comprised of various measures of the mixing height h, and inversion strength $\Delta\theta$, as

follows:

(c) Nocturnal boundary layer height h;

(d) Daytime mixed layer height h and lid strength $\Delta\theta$ (which depend also on a measured morning temperature profile $\theta(z)$);

(e) TIBL height h(x) (which depends also on measurements of the marine air temperature profile $\theta(z)$).

The fourth group of parameters are those which depend on H_v, τ and h. It may be noted at this stage that H_v, τ and h may be combined with mean air temperature (K) and other constants to describe the full range of atmospheric stabilities encountered in the planetary boundary layer. Any alternative scheme for describing atmospheric stability should be able to be related back to these parameters, unless it is deficient. This fourth group includes:

(f) "atmospheric stability";

(g) σ_u, σ_w (and σ_v as an alternative to measurement of σ_θ);

(h) U(z)/U(10) within the planetary boundary layer (without coastal effects);

(i) Plume levelling height H;

The final group of parameters must be treated as special cases:

(j) Potential temperature profile $\theta(z)$. For offshore flows, $\theta(z)$ is described with sufficient accuracy (for dispersion modelling purposes) by the simulation of h and $\Delta\theta$ (see (d) above). For the nocturnal case, $\theta(z)$ might be modelled if so desired, based on the cooling and mixing which occurs in the nocturnal boundary layer.

(k) Sea breeze parameters; h_{SB}, $\Delta\theta_{SB}$, $\theta(z)$, r(z), U(z). These

parameters might be obtained from sequential temperature and wind soundings (e.g. radiosondes tracked by double theodolite), but such measurements would obviously be confined to intensive field experiment periods. A numerical sea breeze model might also provide reasonable estimates, but the computing resources required to run such a model would similarly limit its application to short studies.

Experience at Kwinana (KAMS, 1982) and in other parts of the world (e.g. Portelli, 1982) indicates that, during sea breeze (or lake breeze) conditions, the maximum concentrations from tall stacks will generally be associated with fumigation in the TIBL, which occurs or at least commences prior to the distance at which TIBL growth is arrested by the top of the sea breeze. The sea breeze lid is therefore of secondary significance in terms of pollution impact, and an approximation of h_{sb} should be sufficient. Fortunately, the data gathered on sea breezes indicates that their characteristics are reasonably predictable, and that typical values of h_{sb}, $r(z)$, $\Delta\theta_{sb}$ and $U(z)$ may be assumed.

The above grouping of parameters has been on the basis of their dependence on other parameters, hence defining the order in which model computations should proceed. In practice, it is highly desirable to streamline models in order to reduce execution time, recognising that the final model run-time is likely to be very small compared to the computer time utilized in developing, debugging and testing the models. With this in mind, the model development undertaken in this

Study was completed in three separate sequential parts (i.e. three separate models), each providing a cumulative input data set to the next. The models and their respective output data were as follows:

(i) a combined heat budget - bulk aerodynamic model to provide H_v and τ (with other meteorological parameters carried through);

(ii) a mixing depth model to provide h and $\Delta\theta$ during day and night without coastal effects (with H_v, τ and other parameters carried through);

(iii) a multi-source Gaussian plume dispersion model incorporating calculation of TIBL height and shoreline fumigation, providing ground level concentration predictions (1 hour, 24 hour, monthly and annual averages) over a horizontal grid. Calculation of TIBL heights was logically included in the dispersion model, where downwind distance from the coast was readily calculated.

The model development methodology outlined above facilitated a clearly defined, objective study of the important meteorological processes by optimising the quality of input data at each step. Overall savings in computing costs were also significant. The methodology successfully implemented in this Study coincides very closely with the recommendations of a recent major workshop (Weil, 1985) sponsored by the American Meteorological Society and the U.S.E.P.A.

The structure of this Thesis follows the development of the models as outlined above. Following the outline of KAMS in Chapter 2, Chapter 3 describes various methods of computing H_v and τ and details the development and testing of a numerical model based on the surface heat budget. Chapter 4 provides a corresponding description of a mixing

depth model, which does not include coastal effects, and evaluates the model's performance against field observations. Chapter 5 deals with methods for calculating the growth of internal boundary layers, and presents the results of field studies which support the chosen formulae. Chapter 6 presents the theoretical basis of the KAMS multiple source Gaussian dispersion model, with particular emphasis on the theoretical description of the shoreline fumigation process. Experimental verification of the model is also presented. The application of the model to long term simulation of pollutant concentrations is described in Chapter 7. Chapter 8 provides a summary and conclusions.

The sequence of model development and of the chapters in this Thesis is depicted in Figure 1.7.

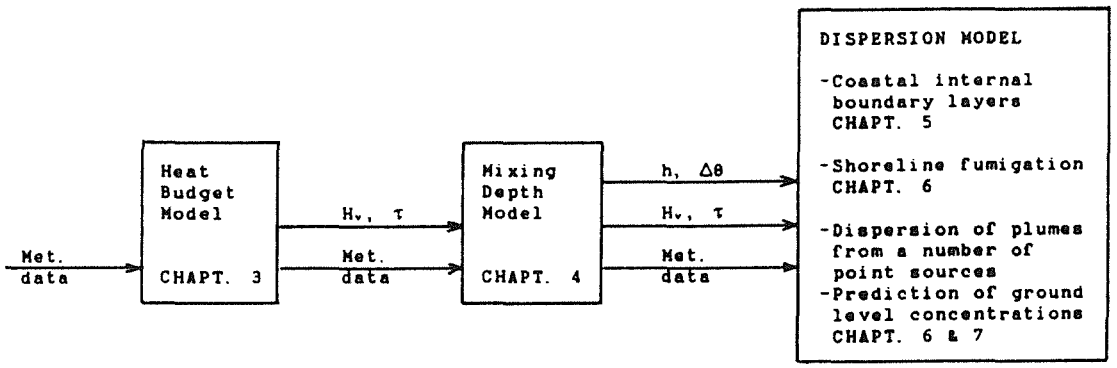

FIGURE 1.7 SEQUENCE OF MODEL DEVELOPMENT

CHAPTER 2

OUTLINE OF THE KWINANA AIR MODELLING STUDY

An outline description of the Kwinana Air Modelling Study is given here to establish the context within which most of the work described in this Thesis was carried out and, in particular, to describe the main sources of experimental data.

2.1 STUDY BACKGROUND

The Kwinana industrial area is depicted in Figure 2.1. Major industries identified on the map (mainly along the coast) include an alumina refinery (Alcoa), an 880 MW power station (SEC), a blast furnace and steel rolling mill (AIS), an oil refinery (BP), a fertilizer works (CSBP), a nickel refinery (WMC) and a cement works (CC). These and other smaller industries produce a variety of gaseous emissions. The emission of most significance from a health viewpoint, and the only one which was considered in KAMS, is sulphur dioxide (SO_2) produced primarily by the combustion of fossil fuels. As may be seen from Figure 2.1, there are sizable areas of urban development adjacent to the industrial strip. The small pockets of urban development at Wattleup and Hope Valley are poorly placed relative to the industrial area, being very close and downwind in sea breeze conditions. The first major investigation of air pollution in the Kwinana area was the Coogee Air Pollution Study, conducted in 1973-74. That Study was initiated to evaluate an urban development proposal for a tract of land immediately north of the industrial area. Whilst the

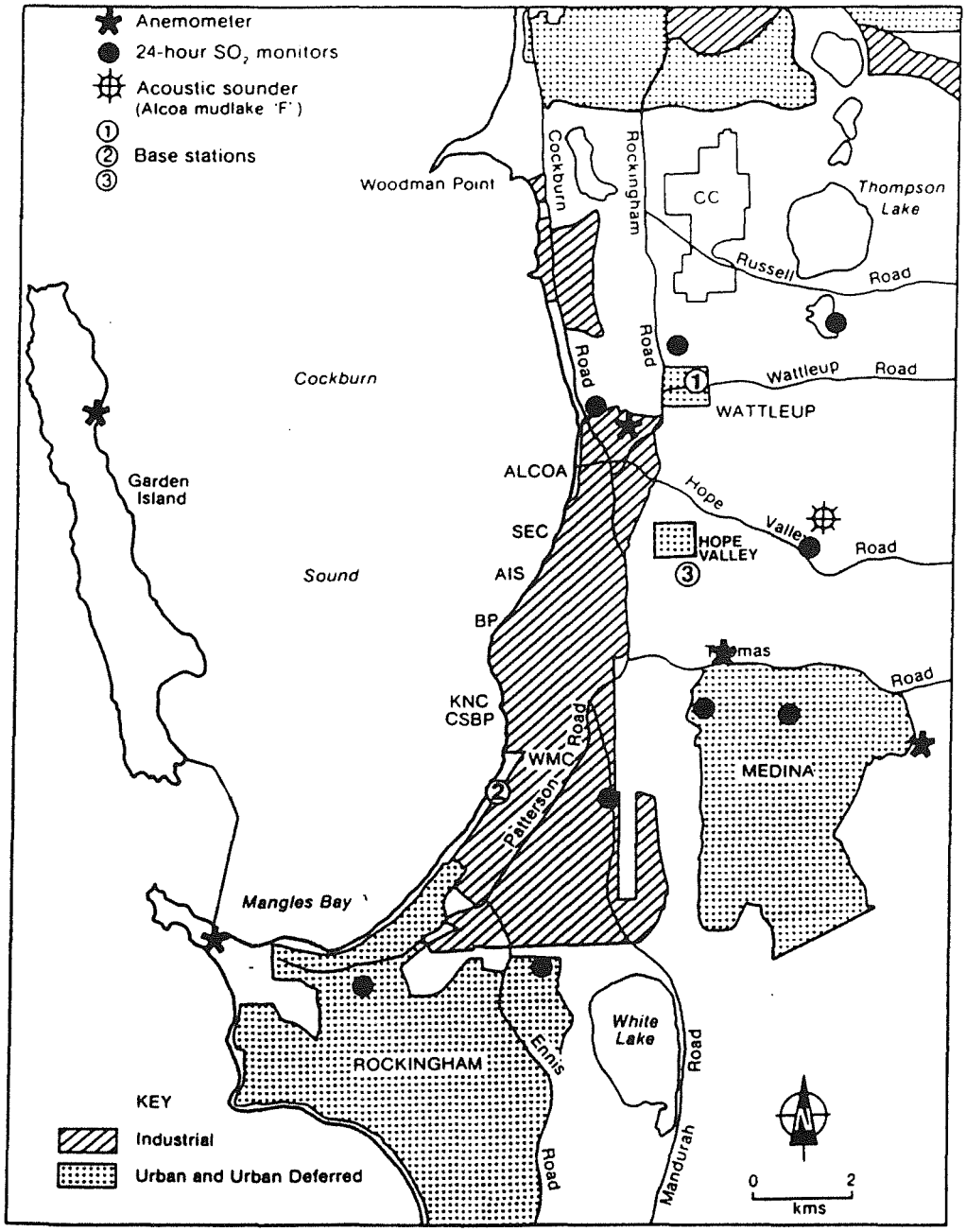

FIGURE 2.1 THE KWINANA AREA SHOWING THE LOCATION OF MONITORING INSTRUMENTS (KAMS, 1982)

Study was successful in opposing the development, primarily on the basis of SO_2 monitoring results, it also highlighted a lack of knowledge in the science of dispersion modelling applicable to coastal areas in the south-west of the State. The need for such a modelling capability was clearly recognised, in view of the potential for ill-informed land use planning decisions such as had led to the siting of the Wattleup township. The Kwinana Air Modelling Study was initiated as a direct result of this identified need.

KAMS was designed specifically as a study to develop modelling techniques which would be suited to a variety of applications, including land use planning, environmental impact assessment and pollution surveys. Accordingly, the monitoring of ambient SO_2 concentrations at a few locations was undertaken to provide data for comparison with model results, rather than to provide a representative picture of regional pollution levels. Continuous meteorological and emissions monitoring was undertaken to provide a data base for dispersion models, and three major field experiments were conducted to provide comprehensive data sets against which to test the various models. A summary of these components of KAMS is given below.

2.2 EMISSIONS INVENTORY

Each of the previously mentioned major industries cooperated by supplying a continuous record of SO_2 emission rates and other important emission parameters throughout the Study period.

The format and resolution of the data varied significantly for the

different industries, necessitating tailor-made procedures for digitising and processing the data in each case. Processed data from each industry was collated into a single file suitable for a multiple source dispersion model.

2.3 METEOROLOGICAL AND SULPHUR DIOXIDE MONITORING

Two base meteorological stations were operated throughout the study to provide a continuous record of important meteorological parameters. As shown on Figure 2.1, Base Station 1 was located in the Wattleup residential area and Base Station 2 further south at Kwinana. Following the acquisition of additional equipment in late 1979, Base Station 2 was relocated to a site at Hope Valley (Base Station 3). A photograph of Base Station 1 appears in Figure 2.2.

Base Stations 1 and 2 both consisted of an instrumented 10 m tower and an air-conditioned caravan housing electronic signal conditioning equipment, a continuous sulphur dioxide monitor and data logging equipment. The meteorological sensors used at these base stations, and the manufacturer's specifications for these sensors, were as follows:

- Wind Speed (10 metres): MRI model 1074 cup anemometer, consisting of a light bulb-photocell assembly, a light chopper disc and a tachometer to compute wind speed.

  Range 0 to 35 m/sec, Accuracy 0.1 m/sec.

- Wind Direction (10 metres): MRI model 1074, consisting of a ganged two-section potentiometer and a resistance-to-voltage conversion circuit.

  Range 0 to 540 degrees, Accuracy 3 degrees.

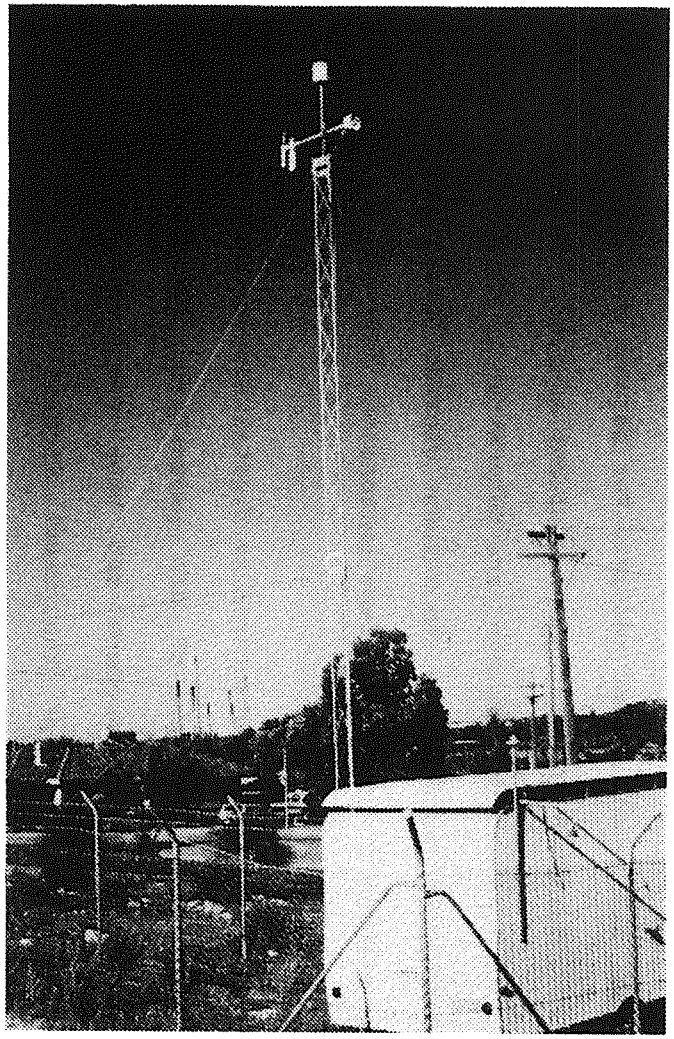

FIGURE 2.2 BASE METEOROLOGICAL STATION 1 AT WATTLEUP.

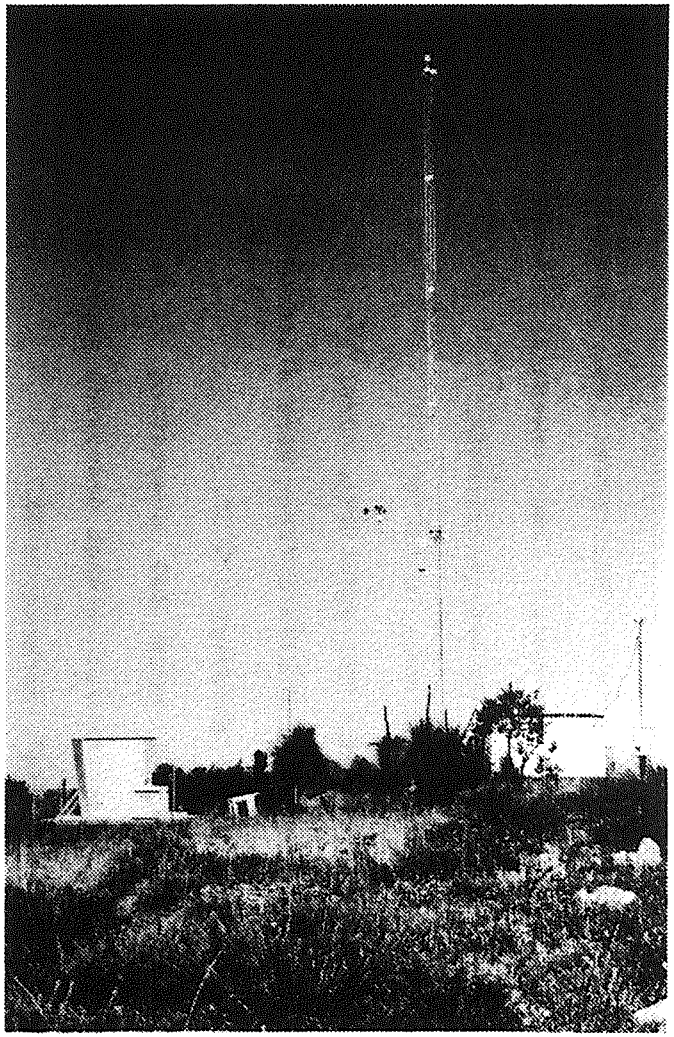

FIGURE 2.3 BASE METEOROLOGICAL STATION 3 AT HOPE VALLEY.

- Air temperature (10 metres): MRI model 842, consisting of an aspirated dual thermistor and resistor network with a resistance-to-voltage conversion circuit.
  Range -30 to 50 °C, Accuracy 0.15 °C.
- Dew Point (10 metres): MRI model 892, consisting of an aspirated lithium chloride sensor with bifilar wire electrodes.
  Range -50 to 50 °C, Accuracy 1.5 °C.
- Solar Radiation: MRI model 860, consisting of an Eppley Black and White Pyranometer with a high precision amplifier.
  Range 0 to 1400 W/m^2, Accuracy 2.5%.
- Sigma Theta (10 metres): MRI circuit 1431200 providing a continuous real-time standard deviation measurement of the wind direction from its mean over a 3-minute period.
  Range 0 to 45 degrees, Accuracy 2.5%.

Continuous air sampling and analysis for sulphur dioxide was carried out using a TRACOR 270HA atmospheric sulphur analyser. In the TRACOR, sulphur dioxide concentrations are determined by using an automatic gas chromatograph to separate the sulphur dioxide from other gases, and then passing it through a flame photometric detector.

EDAS 16 data loggers manufactured by Digital Electronics were used to record 10-minute averages of all parameters. The units utilize voltage-to-frequency converters and high speed counters to provide accurate scalar averages of the input signals, thus avoiding the aliasing errors inherent in many other logging systems.

Analysis of the meteorological data from the Kwinana Base Station (Base Station 2) showed that the site was less than ideal for the purposes of model development and validation. As mentioned above, a new site at Hope Valley was subsequently chosen as more representative of the whole of the study area. Base Station 3 was established at this new site in late 1979. The opportunity was also taken to significantly upgrade the Base Station. A 27 m tower was installed with wind and temperature being measured at two levels as seen in the photograph of the Station in Figure 2.3. Briefly, the additional sensors installed at Hope Valley were:

- Wind Speed, Wind direction, Air Temperature and Sigma Theta at 27 metres, all having the same specifications as their counterparts at 10 metres at Base Station 1.
- Net Radiation: Middleton Instruments net pyradiometer with precision amplifier.

  Range -700 to 800 W/m^2, Accuracy 3%.
- Relative Humidity at 10 metres: Vaisala humidity meter with precision amplifier.

  Range 0 to 100%, Accuracy 5%.
- Soil Temperature at 0.5 cm: Analog Devices, two terminal IC temperature transducer with associated circuitry for current to voltage conversion.

  Range 0 to 90 °C, Accuracy 0.5 °C.
- Soil Heat Flux at 1 cm: Middleton Instruments heat flux plate with precision amplifier.

  Range -150 to 200 W/m^2, Accuracy 5%.

Cassettes produced by the data loggers operating at the two Base Stations contained all the 10-minute average information from the meteorological and pollutant monitoring instruments. Additional information relating to instrument calibration, maintenance and general operation of the Base Station was recorded in log books.

The digital cassettes were read under program control to temporary magnetic cartridge storage on a mini-computer. This transfer allowed for the deletion or modification of records which were known to be of doubtful quality. The raw data were then plotted by the mini-computer to reveal any data errors or anomalies which had not been indicated in the log books, following which appropriate adjustments were made.

The corrected data were transferred to the central computer for final processing involving the application of predetermined calibration expressions to produce a time series of 10-minute average parameter values.

Data recovery rates from the meteorological base stations were generally very good, as illustrated in Table 2.1 which gives statistics for Base Station 1 over the full period of data collection. The period July 1979 to June 1980 was selected as the best period, and used in the final modelling exercises.

Table 2.1 Data recovery from Wattleup Base Station for the period 16 June 1978 to 2 February 1981.

INSTRUMENT	PERCENTAGE RECOVERY
Wind speed	86.2
Wind direction	96.2
Sigma Theta	96.2
Air temperature	97.3
Solar radiation	97.3
Dew point *	98.8
Sulphur dioxide	79.5
Data logger	97.3

* installed 25.4.79

A monostatic acoustic sounder was operated by Murdoch University at the site marked on Figure 2.1. This instrument did not provide a continuous record, and therefore the data were used for comparison with other estimates of mixing depth rather than direct input to the dispersion model. A second more powerful monostatic acoustic sounder was operated for short periods (notably during field experiments) at the Base Station 3 site.

Five continuously recording Lambrecht Woelfle anemometers were located in the study area to determine the wind field over the region. The instruments were mounted on wooden posts at a height of approximately 10 metres above the ground at sites shown in Figure 2.1.

In addition to continuous sulphur dioxide monitoring at the Base Station sites, air sampling for the determination of 24-hour average

sulphur dioxide concentrations at Kwinana was carried out using sequential samplers at nine sites (Figure 2.1). The analytical technique used in this work was a modified version of the pararosanaline method (West and Gaeke, 1956). Adjustments were made for the temperature-dependent decay rate of the absorbing complex for the computation of 24-hour average sulphur dioxide concentrations.

2.4 FIELD STUDIES

Three field studies were conducted during KAMS, as follows:

A. 2nd March 1978 - Study of Dispersion in the Sea Breeze

Inert tracer gas was released from a tall stack and sampled at 21 sites downwind of the stack, out to about 8 kms. Plume rise was estimated via photography of black smoke releases. Slow ascent radiosondes, tracked by double theodolites, gave vertical temperature and velocity profiles. Acoustic sounder data and Base Station data were also available.

B. 31st January 1980 - Study of Dispersion in the Sea Breeze

This experiment repeated the previous experiment with the addition of surface turbulent flux determination at Base Station 3.

C. 29th October 1980 - Study of Radiation Temperature Inversion Erosion

A record of the erosion of a ground based inversion was obtained from hourly radiosonde releases and an acoustic sounder record. Additional measurements at Base Station 3 allowed confident

determination of surface turbulent fluxes. The major industrial plumes were photographed at regular intervals to provide a visual record of plume behaviour as the inversion was eroded.

A detailed discussion of the experiments of 31st January 1980 and the 29th October 1980 will be given in the chapters which follow.

CHAPTER 3

ATMOSPHERIC SURFACE LAYER TURBULENT TRANSFERS

Turbulent transfers of heat, moisture and momentum in the atmospheric surface layer have been the subject of intense study over the past three decades. These fluxes must be included as boundary conditions in any modelling study of the lower atmosphere, and hence their accurate specification is of major importance.

As a result of this research, a variety of methods have been proposed for calculating the turbulent fluxes from measurement of mean flow parameters. The method adopted in the current Study, based on a heat budget in the atmospheric surface layer, is described in Section 3.3. The preceding Sections provide a discussion of theory which forms the basis of either the heat budget model, an alternative tower-profile method, or both. The tower-profile method was developed to provide a basis for model evaluation as described in Section 3.4.

3.1 SURFACE LAYER FLUXES AND PROFILES

3.1.1 SURFACE LAYER SIMILARITY THEORY

Monin and Obukhov (1954) proposed, on the basis of dimensional analysis, that any mean property of the turbulent flow may be described in terms of the dimensionless variable z/L, where z is the height above the ground and L, the Monin-Obukhov length, is defined as

$$L = - \frac{\rho C_p u_*^3 T}{kgH_*} \qquad (3.1)$$

Here, ρ is the air density, C_p is the specific heat capacity of air, u_* is the friction velocity, T is the mean absolute air temperature, k is the von Karman constant, g is gravitational acceleration and H_* is the sensible heat flux. L is a measure of the height of the sublayer within which thermally induced effects are not dominant. The buoyancy effect of water vapour may be incorporated via the virtual temperature $T_v = T(1 + 0.61q)$ to give

$$L = - \frac{\rho u_*^3 T_v}{kg(H_*/C_p + 0.61TE)} \qquad (3.2)$$

where q is the specific humidity and E is the mass flux of water vapour, (i.e. the evaporation rate).

Following Monin and Obukhov's hypothesis, the gradients of wind, potential temperature and specific humidity may be expressed as functions of the stability parameter z/L:

$$\frac{\partial U}{\partial z} = \frac{u_*}{kz} \Phi_M(z/L) \qquad (3.3)$$

$$\frac{\partial \theta}{\partial z} = \frac{\theta_*}{kz} \Phi_H(z/L) \qquad (3.4)$$

$$\frac{\partial q}{\partial z} = \frac{q_*}{kz} \Phi_W(z/L) \qquad (3.5)$$

where U is the wind velocity and θ is the potential temperature. The subscripts M, H and W refer to momentum, heat and water vapour respectively. The friction velocity and other terms with subscript "*" are defined in the definition of the various turbulent fluxes:

$$\frac{\tau}{\rho} = -\overline{u'w'} = u_* u_* \qquad (3.6)$$

$$\frac{H_s}{\rho C_p} = \overline{\theta' w'} = -u_* \theta_* \qquad (3.7)$$

$$\frac{E}{\rho} = \overline{q' w'} = -u_* q_* \qquad (3.8)$$

As is conventional, primes indicate the fluctuating component of a variable and the overbars denote a time average. τ is the stress, or negative momentum flux.

The development of instrumentation to directly measure turbulent fluxes of momentum, heat and moisture has permitted precise evaluation of the Φ functions. Dyer (1974) summarizes the various proposed forms and concludes that the following are most acceptable.

Unstable:

$$\Phi_M = [1 - \nu(z/L)]^{-1/4} \qquad (3.9)$$

$$\Phi_H = \Phi_W = [1 - \nu(z/L)]^{-1/2} \qquad (3.10)$$

where $\nu \approx 16$.

Stable:

$$\Phi_M = \Phi_H = \Phi_W = 1 + \alpha(z/L) \qquad (3.11)$$

where $\alpha \approx 5$.

Hicks (1976), in a re-analysis of the Hangara data (Clarke et al.,1971), found that (3.11) holds only for slightly stable conditions ($0 < z/L < 0.5$). For higher stabilities, he found that velocity profiles depart from the log-linear form of (3.11) toward a purely logarithmic form (Φ_M constant), but that this state is never reached. He further observed that in very stable conditions, the profile above a few metres becomes linear with height, indicating a decoupling of

this air from the surface, i.e.

$$dU/dz = cu_*/(kL) \qquad (3.12)$$

so $$\Phi_M = cz/L \qquad (3.13)$$

where c is a constant ($c \approx 0.8$)

Carsons and Richards (1978) lend their support to Hicks' (1976) findings and provide an empirical formula for the transition between (3.11) and (3.13):

$$\Phi_M = [8 - 4.25(z/L)^{-1} + (z/L)^{-2}], \quad (0.5 < z/L < 10) \qquad (3.14)$$

While it is well established that $\Phi_M = \Phi_H = \Phi_W$ for ($0< z/L <0.5$) there is currently no information on the relationship between the Φ functions at higher stabilities. It is assumed here that they are equal.

Following Paulson (1970) (3.3) to (3.5) may be integrated to the form:

$$U = \frac{u_*}{k}\left[\ln\left(\frac{z}{z_0}\right) - \psi_M\right] \qquad (3.15)$$

$$\theta - \theta_0 = \frac{\theta_*}{k}\left[\ln\left(\frac{z}{z_H}\right) - \psi_H\right] \qquad (3.16)$$

$$q - q_0 = \frac{q_*}{k}\left[\ln\left(\frac{z}{z_W}\right) - \psi_W\right] \qquad (3.17)$$

where z_0, z_H, z_W, are roughness lengths and subscript 0 indicates surface values. The ψ functions have the form

$$\psi = \int_{\zeta_0}^{\zeta} \frac{1 - \phi(\zeta)}{\zeta}\, d\zeta \qquad (3.18)$$

where $\zeta = z/L$ and $\zeta_0 = z_0/L$, z_H/L, or z_W/L as appropriate.

In neutral conditions ($\phi = 1$), $\psi = 0$ and (3.15) to (3.17) reduce to the familiar logarithmic profiles.

Paulson (1970) gives analytical solutions to (3.18). For the ϕ functions of (3.9) and (3.10) integration yields

$$\psi_M = 2\ln[(1 + x)/2] + \ln[(1 + x^2)/2] - 2\mathrm{Tan}^{-1}x + \pi/2 \qquad (3.19)$$

$$\psi_H = \psi_W = 2\ln[(1 + x^2)/2] \qquad (3.20)$$

where $x = [1 - \nu(z/L)]^{1/4}$. For ϕ given by (3.11)

$$\psi_M = \psi_H = \psi_W = -\alpha(z/L) \qquad (3.21)$$

Carson and Richards (1978) evaluate ψ numerically for the two regimes where $(z/L) > 0.5$, given by (3.13) and (3.14). Alternatively, to obtain an analytical solution, ψ may be evaluated separately for each regime.

For $(0.5 < \zeta \leq 10)$

$$\psi = \int_{\zeta_0}^{0.5} \frac{1 - \phi(\zeta)}{\zeta}\, d\zeta + \int_{0.5}^{\zeta} \frac{1 - \phi(\zeta)}{\zeta}\, d\zeta$$

$$= 0.5\zeta^{-2} - 4.25\zeta^{-1} - 7\ln(\zeta) - 0.852 \qquad (3.22)$$

For $\zeta > 10$

$$\psi = \int_{\zeta_0}^{0.5} \frac{1 - \phi(\zeta)}{\zeta}\, d\zeta + \int_{0.5}^{10} \frac{1 - \phi(\zeta)}{\zeta}\, d\zeta + \int_{10}^{\zeta} \frac{1 - \phi(\zeta)}{\zeta}\, d\zeta$$

$$= \ln\zeta - 0.76\zeta - 12.093 \qquad (3.23)$$

In obtaining the above results the lower limit of integration, ζ_0, has been taken as equal to zero. This approximation is obviously acceptable for smooth surfaces, where z_0, z_H and z_W are very small, but it would seem to be dubious for rough surfaces. However, Garratt

(1978a) has shown that the profile relations themselves only hold for heights $z > 100z_0$. Below this level the flow is modified by the wakes of individual roughness elements, producing a transition region where the diffusivity of momentum and heat is enhanced and, as a result, the gradients of windspeed and temperature (Φ_M and Φ_H) are smaller. Similar behaviour is envisaged for vapour flux. If measurement heights are kept above the transition layer then the approximation $\zeta_0 \approx 0$ will automatically be satisfied.

3.1.2 BULK AERODYNAMIC FORMULAE

It is feasible to determine turbulent fluxes from measurements of the vertical gradients of wind, temperature and humidity, using the theory presented thus far. Alternately, an integral approach may be used, where mean differences rather than gradients need to be measured. The bulk aerodynamic formulae, following this approach, may be written in the form

$$-\frac{\tau}{\rho} = \overline{u'w'} = -u_* u_* = -C_D U^2 \qquad (3.24)$$

$$\frac{H_s}{\rho C_p} = \overline{\theta' w'} = -u_* \theta_* = -C_H U(\theta - \theta_0) \qquad (3.25)$$

$$\frac{E}{\rho} = \overline{q' w'} = -u_* q_* = -C_W U(q - q_0) \qquad (3.26)$$

C_D, C_H and C_W are the respective bulk transfer coefficients. U, θ and q are measured at some reference height (usually 10 metres) and subscript 0 again refers to surface measurement. Given the widely reported result that $C_H \approx C_W$ (e.g. Hicks, 1975), implying that $z_H \approx z_W$, these will be treated together with a single subscript, HW.

Considering the theory discussed in preceding Sections, it is obvious that the bulk transfer coefficients will not be constants, but will be strongly dependent on stability. Several authors (Deardorff, 1968; Carson and Richards, 1978) have investigated this dependency. A similar analysis yields the following relations:

$$C_{HW} = k^2/[(\ln(z/z_0) - \psi_M)(\ln(z/z_{HW}) - \psi_{HW})] \quad (3.27)$$

$$C_D = k^2/(\ln(z/z_0) - \psi_M)^2 \quad (3.28)$$

For a given stability z/L, ψ_{HW} and ψ_M can be evaluated from (3.19) to (3.23). However, z/L is itself a function of the turbulent fluxes, so the fluxes cannot be explicitly calculated. Hicks (1975) suggests an iterative method of solution which works very well. The fluxes may be calculated from (3.24) to (3.26) using provisional estimates of the transfer coefficients C_D and C_{HW}. A provisional estimate of z/L may then be obtained from (3.2) and used to correct C_D and C_{HW} via (3.27) and (3.28). The process is repeated until z/L converges satisfactorily.

Neutral values of transfer coefficients may be calculated from (3.27) and (3.28) (with $\psi_M = \psi_{HW} = 0$) given values of z_0 and z_{HW}, which in turn must be determined experimentally. Determination of values appropriate for Kwinana is described in Section 3.3.4.

3.1.3 COMPUTING TURBULENT FLUXES FROM TWO-LEVEL TOWER MEASUREMENTS

Continuous measurement of wind speed, temperature and humidity at two levels on a tower gives the minimum data set which will allow computation of stress, heat and moisture fluxes without some knowledge

of the surface properties. The major disadvantage of this procedure is its sensitivity to measurement errors at either level, whether due to calibration error or long-term drift. Small absolute errors (e.g. ± 0.2°C), acceptable for mean measurements, may be unacceptably large when computing differences of the parameters between the two levels. For continuous monitoring purposes, the procedure demands precision instrumentation and frequent calibration checks. Furthermore, with only two levels, no redundant information is available to check the applicability of the flux-profile theory.

Measurement of humidity or a related parameter proved problematic in KAMS as it has for other research efforts (McKay, 1978). At no stage was continuous measurement of humidity at two levels contemplated. Measurement of wind speed and temperature at two levels was conducted at the Hope Valley Base Station on a research rather than routine basis. Whilst H_s and τ may be confidently estimated during fine weather, the effect of moisture flux on stability, described in (3.2), becomes important when the surface is moist following precipitation. The purpose in computing H_s and τ from two-level tower measurements in this project was to provide a check on the main method, to be described in Section 3.3.

Two methods of computing H_s and τ are described below; the first (A) using only tower data and the second (B) making use of a predetermined value of z_0.

Method A

Using two-level tower measurements, gradients of velocity and temperature may be calculated as indicated by Paulson (1970), e.g. for velocity:

$$\partial U/\partial z = (U_2 - U_1)/[(z_2 z_1)^{1/2} \ln(z_2/z_1)] \quad (3.29)$$

which holds at the geometric height

$$z = (z_2 z_1)^{1/2} \quad (3.30)$$

where $z_2 > z_1$. Alternatively, the gradients may be calculated from formulae given by Hicks (1976), (e.g. for velocity).

$$\partial U/\partial z = (U_2 - U_1)/(z_2 - z_1) \quad (3.31)$$

which holds at the height

$$z = (z_2 - z_1)/\ln(z_2/z_1) \quad (3.32)$$

This calculation is exact in neutral conditions and is accurate to ± 6% over the usually encountered stability range. Neglecting moisture effects, the Richardson number appropriate to height z may then be calculated:

$$Ri = \frac{g}{T} \frac{\partial\theta/\partial z}{(\partial U/\partial z)^2} \quad (3.33)$$

From this, and the general relationship $Ri = (z/L)(\Phi_H/\Phi_M^2)$, L may be computed:

$$L = z/Ri \ , \ (Ri < 0) \quad (3.34)$$

$$L = z(1 - \alpha Ri)/Ri, \ (0 \leq Ri \leq 0.143) \quad (3.35)$$

$$Ri = (z/L)/[8 - 4.25(z/L)^{-1} + (z/L)^{-2}], \ (0.143 < Ri < 1.318) \quad (3.36)$$

These relations are readily derived from (3.1), (3.33), (3.3), (3.4), (3.9) to (3.11) and (3.14). For stabilities higher than z/L = 10, Ri = 1.318 is constant. In other words, stabilities greater than z/L = 10 cannot be resolved by an analysis of the Gradient Richardson No.

Given z/L and the previously calculated gradients of velocity and temperature, u_* and θ_* are calculated from (3.3) and (3.4). H_s and τ then follow from (3.6) and (3.7).

Measurement inaccuracies for wind and temperature differences between the two levels are directly reflected in τ and H_s.

Method B

If z_0 has been determined with some confidence, it may be used in the determination of τ and H_s. As will be seen from the following, only one wind speed measurement level is required, with an associated potential saving in capital and operating costs.

Development of the "bulk" formulae used by this method is similar to that described in Section 3.1.2, but is set out in full for clarity.

A bulk equation for sensible heat is written as

$$H_s = - u_*\theta_* = \rho C_p C'_H U_2(\theta_2 - \theta_1) \qquad (3.37)$$

where C'_H is a modified transfer coefficient to be defined later.

Stress, as before, is given by

$$\tau = - \rho C_D U_2^2 \qquad (3.38)$$

Equation (3.3) is integrated between z_0 and z_2 (as in (3.15)) to give

$$U_2 = (u_*/k)[\ln(z_2/z_0) - \psi_H(\zeta_2, \zeta_0)] \qquad (3.39)$$

where $\psi_H(\zeta_2, \zeta_0) = \int_{\zeta_0}^{\zeta_2} \frac{1 - \phi_H(\zeta)}{\zeta} d\zeta$, $\zeta = z/L$ as before. (3.40)

Similarly, (3.4) may be integrated between z_1 and z_2 to give

$$(\theta_2 - \theta_1) = (\theta_* / k)[\ln(z_2/z_1) - \psi_H(\zeta_2, \zeta_1)] \quad (3.41)$$

where $\psi_H(\zeta_2, \zeta_1) = \int_{\zeta_1}^{\zeta_2} \frac{1 - \phi_H(\zeta)}{\zeta} d\zeta$ (3.42)

In neutral conditions, (3.37) to (3.42) yield

$$C_{DN} = k^2/[\ln(z_2/z_0)]^2 \quad (3.43)$$

$$C'_{HN} = k^2/[\ln(z_2/z_0)\ln(z_2/z_1)] \quad (3.44)$$

Under non-neutral conditions these same equations yield

$$C_D = k^2/[\ln(z_2/z_0) - \psi_H(\zeta_2, \zeta_0)]^2 \quad (3.45)$$

$$C'_H = k^2/\{[\ln(z_2/z_0) - \psi_H(\zeta_2, \zeta_0)][\ln(z_2/z_1) - \psi_H(\zeta_2, \zeta_1)]\} \quad (3.46)$$

If, as is common, a Bulk Richardson Number is defined as

$$Ri_B = g z_2(\theta_2 - \theta_1)/(T V_2^2) \quad (3.47)$$

it is readily shown that

$$Ri_B = (z_2/L)\, \beta(\zeta_2, \zeta_1, \zeta_0) \quad (3.48)$$

where $\beta(\zeta_2, \zeta_1, \zeta_0) = [\ln(z_2/z_1) - \psi_H(\zeta_2, \zeta_1)]/[\ln(z_2/z_0) - \psi_H(\zeta_2, \zeta_0)]^2$

Equation (3.48) may be plotted and so used to obtain either estimates of z/L from measured Ri_B, or an empirical expression for $z/L \sim f(Ri_B)$. Alternatively, H_*, τ and L may be determined by an iterative scheme similar to that described in Section 3.1.2.

Berkowicz and Prahm (1982b) describe a flux calculation procedure which is similar to the above, although they report problems in obtaining an iterative solution in stable conditions. Use of Hicks'

(1976) and Carson and Richards' (1978) recommended forms of the Φ functions (see (3.13) and (3.14)) avoids the iteration problem and gives a stable rapid solution for all values of z/L.

The apparent advantages of Method B over Method A are as follows. Given the presence of measurement inaccuracies in wind speed and temperature, Ri_B can be determined with much greater confidence than Ri which has the term $(U_2 - U_1)^2$ in its denominator. Whether Ri_B is used explicitly or implicitly (iterative scheme), the method is more stable, being sensitive to temperature difference inaccuracies alone. It does not suffer the error associated with calculating gradients in non-neutral conditions (albeit small) and, as stated above, requires only one wind measurement. The major disadvantage with Method B is in the uncertainty of the specification of z_0 (and hence C_D and C'_H). Roughness may possibly vary dynamically and may also vary with wind direction, an effect which could be accounted for if correctly determined. Berkowicz and Prahm (1982b) have assessed the potential errors associated with two-level wind speed measurement and roughness length determination and have argued that, provided $z_2 \gg z_0$, the latter error is likely to be much smaller.

Comparative testing of the two methods using data from two separate daily cycles gave closely corresponding results, as expected. Method B has been chosen as the standard method for comparison with alternative schemes, on the basis of the advantages described above.

3.2 HEAT BUDGET METHODS EMPLOYING SURFACE RESISTANCE CONCEPTS

The methods for turbulent flux calculation described thus far in this Chapter have relied on parameterization of the turbulent velocity, temperature and humidity fluctuations, and the associated turbulent fluxes, in terms of the mean components of each of these variables. Hence, for example, formulae for the heat flux $\overline{\theta' w'}$ have included mean velocities and temperatures. An evaluation of the heat budget in the surface layer of the atmosphere provides an additional item of information which may be utilized in determining the magnitude of turbulent heat fluxes. The heat budget may be expressed in the form:

$$G - R + H_s + H_L = 0 \qquad (3.49)$$

where G is the ground heat flux, R is net (short-wave plus long-wave) radiation and H_L is latent heat, given by

$$H_L = \lambda E \qquad (3.50)$$

The parameter λ is the latent heat of vaporization. In (3.49), H_s and H_L are positive upward, while R and G are positive downward.

The heat budget relation has been used in many different ways to develop computation schemes to suit various situations. For example, (3.49) may be re-expressed as

$$H_L = (R - G)/(1 + \beta) \qquad (3.51)$$

where β is the Bowen Ratio given by

$$\beta = H_s/H_L \qquad (3.52)$$

This ratio may be evaluated from the bulk aerodynamic formulae in (3.25) and (3.26) rewritten here for convenience:

$$H_s = \rho C_p C_H U(\theta_0 - \theta_z) \qquad (3.53)$$

$$H_L = \rho\lambda C_w U(q_0 - q_z) \qquad (3.54)$$

where subscripts 0 and z refer to the surface and a reference height respectively. Given the equality of C_H and C_W indicated in Section 3.1.2, the Bowen Ratio becomes

$$\beta = r(\theta_0 - \theta_z)/(q_0 - q_z) \qquad (3.55)$$

where $r = C_p/\lambda$. The temperature and humidity differences may in fact be taken between any two levels in the surface layer, given the similarity of the profiles of these two variables in the surface layer. It can be seen that the Bowen Ratio method provides a means of estimating latent (and hence also sensible) heat flux without the requirement for wind speed data.

An alternative well known method for calculating heat fluxes is that of Penman (1948). This method employs an alternative combination of the heat budget and bulk aerodynamic formulae set out above, and is clearly explained by Webb (1975). For a saturated surface, the Penman Equation takes the form:

$$H_L = \frac{s}{s+r}(R - G) + \frac{r}{s+r}\lambda E_a \qquad (3.56)$$

where $E_a = \rho C_W U(q_z^s - q_z)$.

The parameter s is the slope of the saturation curve $dq^s/d\theta$ at a temperature θ midway between θ_0 and θ_z, and superscript s refers to saturated conditions. Whereas the Bowen Ratio method avoids the need to measure wind speed, the Penman equation provides an estimate of latent heat (and hence also evaporation and sensible heat) from mean meteorological measurements at a single height. The Penman Equation still includes explicit dependence on the surface conditions via the transfer coefficient C_W, which is a function of surface roughness and atmospheric stability, as per (3.27).

If the surface is not saturated, then the Penman Equation becomes:

$$H_L = \frac{s}{s+r}(R - G) + \frac{r}{s+r}(\lambda E_a - \lambda E_{a0}) \qquad (3.57)$$

where $E_{a0} = \rho C_w U(q_0^* - q_0)$.

This formula is now explicitly dependent on specific humidity at two levels, one being the surface. Specific humidity at the surface is obviously not a routinely measured parameter, and so researchers have tended to search for alternative parameterizations of the term E_{a0}. The most widely accepted approach, also described by Webb (1975), is to define a surface resistance parameter, r_s, which is designed to provide a measure of the resistance to the transfer of vapour through the surface. The surface may be a combination of vegetation and bare earth. By definition,

$$E = \rho(q_0^* - q_0)/r_s \qquad (3.58)$$

For convenience, an atmospheric resistance parameter r_a is also defined by

$$E = \rho(q_0 - q_z)/r_a \qquad (3.59)$$

which, from (3.54), means that $r_a = 1/(C_w U)$. Penman's Equation may then be re-expressed as:

$$H_L = [s(R - G) + r\lambda E_a]/[s + r(1 + r_s/r_a)] \qquad (3.60)$$

The problem now reduces to one of evaluating r_s. Some of the necessary considerations and approaches followed in evaluating r_s are summarized below.

Most work which has employed the surface resistance formulation has been directed towards studying evapotranspiration from crops, forests or other types of vegetation (Monteith, 1973; Raupach and Thom, 1981).

Evapotranspiration predictions are required for a variety of reasons, including agricultural and forestry research, and as an input to mesoscale or global atmospheric models. The concept of surface resistance is meaningful when considering the transfer of water vapour through leaf stomata, which open and close to regulate the rate of vapour transpiration in response to various stresses on the vegetation. External stresses which are known to affect the transpiration rate are:

(i) degree of saturation of the soil in the root zone of the plant, which is in turn dependent on the history of rainfall, drainage and solar drying of the soil;

(ii) level of global radiation. Stomata are generally closed at night in the absence of sunlight;

(iii) ambient temperature;

(iv) presence of dew.

Many attempts to parameterize r_s in terms of these stresses are reported in the scientific literature, varying widely in their degree of empiricism . Smith and Blackall (1979) present a coarse categorization scheme for r_s (which varies over the enormous range of 0 - 4000) derived by matching Monteith's (1973) formula with independent estimates of heat fluxes. Berkowicz and Prahm (1982a) propose a simple empirical formulation for r_s which incorporates an intriguing mixture of diagnostic variables. At the other end of the scale, Deardorff (1978) presents an elaborate, complicated computation scheme for r_s and other terms in the heat and moisture budgets within a layer of vegetation. This scheme has subsequently been incorporated in a mesoscale numerical model described by McCumber (1980). In summary, it is apparent that the response of vegetation to the various

external stresses is very complex and will be the subject of much further study before any generalized, widely accepted parameterizations of r_s appear.

Despite the high degree of uncertainty about how to estimate r_s and the cumbersome nature of computation schemes, the surface resistance method still retains its attraction for many applications. For example, if mesoscale or regional predictions of turbulent surface fluxes are required, it is obvious that one or a few local measurements or predictions of these fluxes would not be representative, particularly if the density of vegetation cover varies across the region of interest. In this situation one would seek a spatial description of surface fluxes based on information about the spatial distribution of vegetation, water bodies, etc. The surface resistance method lends itself to this type of investigation. For example, the method is embodied in a study by Carlson et al. (1981) in which infrared satellite temperature measurements were used to determine the distribution of surface heat and moisture fluxes over urban and country areas.

The applicability of the surface resistance method to a local atmospheric dispersion study in a region of dense vegetation is less clear however. These types of studies generally employ a number of monitoring stations at representative locations, complete with data acquisition equipment. Therefore, the application of one of the measurement techniques (e.g. tower profiles, eddy correlation) may prove more viable, both in terms of ease of implementation and quality of results, than the application of a scheme for estimating r_s. The

requirement in air quality studies of short term accurate estimates of turbulent fluxes over dense vegetation is thought to be stretching the limits of the capability of the surface resistance method. And, if the heat budget concept is to be applied in this context, there is no current alternative to a complex paramaterization scheme for r_s.

At this juncture it is necessary to introduce a significant yet justifiable limitation to the scope of this aspect of the current Study, the need for which became apparent during the review of methods for estimating surface turbulent fluxes.

It was recognised that, although the heat budget method was not clearly viable for densely vegetated regions, it could be applied in a simplified form to sparsely vegetated areas. Along the south west coast of Western Australia, areas adjacent to the coast (such as Kwinana) are characterised by sandy soils and sparse scrubby vegetation which is shallow rooted. Consequently the transpiration rates are likely to be strongly correlated and in phase with soil surface moisture and so may be modelled as a simple amplification of soil evaporation. Based on this assumption, the need for complicated schemes for estimating r_s can be avoided, with attention being limited to describing evaporation from the soil.

Apart from the coastal plain in the south west, the bulk of the State could be described as sparsely vegetated relative to the forest areas of the south west. Much of this sparse vegetation regulates its transpiration rate so that it can survive the dry seasons. Therefore the above assumption is thought to hold as a good approximation for

the bulk of the State. This assumption would lose validity in areas with a significant density of large trees which tap into groundwater aquifers and do not regulate their stomatal resistance in dryer periods.

In view of the above, and in the light of the Study objectives spelled out in Chapter 1, development of methods for estimating turbulent fluxes from routinely available meteorological data was limited in application to areas of sparse vegetation. This limitation amounts to a recognition that the complications imposed by dense vegetation rule out a simple approach employing routine data. The limitation applies to surface flux determination only; it does not limit the applicability of the components of air dispersion modelling to be described in forthcoming Chapters.

Vapour loss from the soil is generally considered as a component of the total evaporation which is accounted for within the surface resistance method. In the limit of sparse or no vegetation this approach requires description of r_s related to the soil properties and behaviour only. At this point it should be recognised that, whereas surface resistance is a meaningful concept when considering the behaviour of leaf stomata, it does not have a corresponding tangible meaning when applied to soil. What is in fact meaningful is the recognition that the evaporation rate is directly dependent on the level of saturation of the soil surface, as reflected in the surface specific humidity q_0. Introducing r_s only serves to cloud the issue. This point is illustrated by the discussions of Webb (1984), Berkowicz and Prahm (1982a) and Smith and Blackall (1979) where the dependence

of r_s on the state of soil dryness is seemingly rediscovered from field data. DeHeer-Amissah et al. (1981) make the astounding observation that "there is also some indication that r_s decreases rapidly soon after rainfall".

Another aspect of the surface resistance method which gives cause for concern is the practice of closing the equation set by parameterizing the soil heat flux in terms of one of the other heat budget components. A common method, as used by DeHeer-Amissah et al. (1981), is to apply a relationship between soil heat flux G and net radiation R. Others, such as Berkowicz and Prahm (1982a) seek a relationship between G and sensible heat flux H_s. Van Ulden and Holtslag adopt a curious approach in which G is assumed to be proportional to $(\theta_0 - \theta_z)$ (i.e. proportional to H_s), which is in turn assumed to be proportional to R. (It may also be noted here that the use by these authors of an adjustable coefficient, α, to account for the effect of surface moisture on H_s is of little practical value since no generally applicable means of determining α is provided, nor is such likely to exist.) Deardorff's (1978) comment in regard to these types of methods is very relevant;

> "... since the negative soil heat flux equals the sum of all the atmospheric fluxes (as stated by the surface energy balance equation), any assumption that it is proportional to any particular component, or partial set of such components, seems dangerously nongeneral."

Even if such proportionality can be demonstrated to exist for the bulk of averaged data for a particular location, it will certainly not

exist for short term averages (e.g. 10 minutes - ¼ hour) during transition periods around sunrise and sunset. For example, there is a period of a few hours around sunset after a hot day when strong positive values of H_s will accompany negative values of G. The converse will be true after dawn following a cold cloudless night. These transition periods (particularly in the morning with a radiation inversion present) are very important in terms of pollution potential and so require accurate description. The transitional cooling of the ground close to the coast following the onset of a sea breeze is another case in point.

To summarise, the flux computation procedure ideally required for sparsely vegetated areas is one which employs a direct approach for calculating evaporation from the soil (i.e. avoids the surface resistance concept) and which employs a refined closure method for the equation set to enable the accurate calculation of fluxes necessary to compute atmospheric dispersion.

3.3 A HEAT BUDGET MODEL BASED ON SURFACE TEMPERATURE AND MOISTURE SIMULATION

The concept of a heat budget in the atmospheric surface layer can be ultilised along lines which differ from its conventional application to generate a model of surface turbulent fluxes which is more suited to the application of dispersion modelling. The important features of the model described in this Section are:

(i) surface temperature and humidity are directly computed, negating the need for a surface resistance parameter;

(ii) closure of the equation set is performed without the need for empirical relationships between terms in the heat budget equation;

(iii) the effects of atmospheric stability on turbulent fluxes is included;

(iv) short term (e.g. 10 minute) averages of fluxes and stability may be efficiently computed over extended periods (e.g. 1 year) providing output data ideally suited to the application of dispersion modelling.

The model is an adaption of that proposed by Deardorff (1978) which has been successfully applied in local scale planetary boundary layer models (Hoffert and Storch, 1979, Binkowski, 1983) and is also suitable for application in mesoscale numerical models. Apart from the relative simplicity of the model formulation (which conforms with theory presented thus far in this chapter) the main justification for adopting the model is its high level of skill in simulating experimental observations, as will be described in Section 3.4.

3.3.1 GROUND TEMPERATURE SIMULATION AND SENSIBLE HEAT TRANSFER

Deardorff (1978) compares several parameterizations of the soil surface temperature T_g against an accurate multi-layer soil model, and concludes that the method of Blackadar (1976) is superior. This method computes T_g via the equation

$$\partial T_g / \partial t = 2G/C_s - \Omega(T_g - T_d) \qquad (3.61)$$

where Ω is the earth's angular frequency ($7.27 \times 10^{-5} s^{-1}$) and T_d is a deep soil temperature (defined later). C_s is defined as

$$C_s = (2\rho_s c_s \lambda_s / \Omega)^{1/2} \qquad (3.62)$$

where ρ_s is soil density, c_s is soil specific heat and λ_s is soil heat conductivity. These parameters show strong dependence on soil moisture. Deardorff (1978), McCumber and Pielke (1981) and Binkowski (1983) present alternative empirical estimates of this dependence. The product $(\rho_s c_s \lambda_s / \Omega)^{1/2}$ is called the thermal inertia, and may be thought of as the resistance of a material to a change in temperature. Equation (3.61) is called a force-restore equation; the first term on the right hand side represents the forced heating or cooling, while the second term tends to restore the surface temperature to that of the soil at depth. Hoffert and Storch (1979) provide a derivation of this equation.

T_d, the deep or mean soil temperature may be estimated from an integral formulation based on the penetration depth of the annual thermal wave,

$$\partial T_d / \partial t = G/C_d \qquad (3.63)$$

where $C_d = (2\pi.365)^{1/2} C_s$

Given the above estimate of T_g, sensible heat is calculated via (3.25) where θ_0 is a combination of soil, grass and leaf temperatures, as assumed by Garratt (1978b). He utilized an expression of the form

$$(\theta_0 - \theta) = \beta_1(T_g - \theta) + \beta_2(T_{gr} - \theta) + \beta_3(T_l - \theta) \qquad (3.64)$$

where subscripts gr and l indicate grass and leaves. The coefficients β_1 to β_3 account for the relative surface area and external resistance to heat transfer of the three surface components. In the absence of radiometric measurements or representative β coefficients, it is necessary to assume that the effective surface temperature deviation is proportional to the ground surface temperature deviation, i.e.

$$(\theta_0 - \theta) = \beta'(T_g - \theta) \qquad (3.65)$$

The single coefficient β' accounts for patchy shading of the soil and for the limited heat transfer from vegetation. Equation (3.65) is consistent with (3.64) if the temperature deviation of each component is in proportion to the soil temperature deviation.

3.3.2 GROUND MOISTURE SIMULATION AND EVAPORATION

The moisture content of surface soil may vary between dry and saturated states and may change very quickly under the influence of evaporation or precipitation. Latent heat loss associated with evaporation may vary from an insignificant contribution to the heat budget (dry surface conditions) to being the dominant cooling mechanism (moist surface conditions). In view of the importance of surface moisture, Deardorff (1978) defines a moisture parameter, w, being the volume fraction of soil moisture (or depth of liquid/depth soil) and provides relations similar to those for surface temperature:

$$\partial w_g/\partial t = - C_1(E - P)/(\rho_w d_1) - (2\pi)^{-1} C_2 \Omega (w_g - w_d);\ 0 \leq w_g \leq w_{max} \quad (3.66)$$

$$\partial w_d/\partial t = - (E - P)/(\rho_w d_2) \quad (3.67)$$

where P is the precipitation rate and ρ_w is the density of water. The parameters d_1 and d_2 represent the depth to which the diurnal and annual moisture cycles respectively extend, with w_d being the average moisture content over the depth d_2. The coefficients C_1 and C_2, together with d_1 and d_2, need to be evaluated for a particular soil type. The parameter w_{max} is the maximum possible soil moisture content, above which run-off occurs.

In order to relate evaporation rate to soil surface moisture content, Deardorff postulates a modified bulk aerodynamic relationship

$$E = \rho C_H U \alpha [q_s(T_g) - q] \quad (3.68)$$

where $\alpha = \min(1,\ w_g/w_k)$

Here, w_k is that value, less than w_{max} at which the soil surface may be considered saturated (i.e. $q_0 = q^s(T_g)$, where superscript s indicates saturation). Comparing (3.68) and (3.26) it is apparent that

$$q_0 = \alpha q^s(T_g) + (1 - \alpha) q \quad (3.69)$$

3.3.3 RADIATIVE TRANSFERS

Varying levels of sophistication could be used in describing the components of radiation in the surface energy budget. The approach used here is tailored for the modelling philosophy described in Chapter 1, although some general principles are apparent.

From an inspection of (3.49) it may appear that a direct measure of

net radiation is the sole requirement. In practice however, there are significant problems with the use of measured net radiation:

(i) calculation rather than measurement of outgoing long-wave is preferable to provide feedback within the numerical computation of T_s;

(ii) it is difficult to find a location for a net radiometer over a surface area which may be classed as representative of the surroundings, particularly in the vicinity of an air quality monitoring station where the surface is usually highly disturbed;

(iii) birds (at least the Western Australian variety) delight in pecking holes in the polythene dome on the net radiometer. This proved to be a serious problem in KAMS.

Hence, although measurement of net radiation is strongly recommended, alternative methods for measuring or estimating the radiative components of the total balance are required.

Global radiation, being the sum of the direct and diffuse solar short-wave components, is a readily measured parameter and so its computation is not warranted, except perhaps to fill patches of missing data. Paltridge (1974), Davies et al. (1975) and Kahle (1977), for example, provide various methods for computing global radiation if required. Each method requires information on the scattering properties of the atmosphere and, importantly, the amount and type of cloud present. Lyons and Edwards (1981) have evaluated the method of Davies et al. (1975) and have found it to be capable of predicting daily global irradiation in Western Australia to within 15% of measurements.

A sizable proportion of the short-wave radiation is reflected from the surface. The surface short-wave reflectivity or albedo A is a function of surface type, surface moisture content, solar altitude and other factors, and also varies over different wave-lengths. Paltridge and Platt (1976) provide a simplified relation

$$A = A_1 + (1 - A_1) \exp[-\kappa(90° - a)] \qquad (3.70)$$

where $\kappa \approx 0.1$ and A_1 is the albedo for high solar elevations (i.e. near local noon). The solar altitude, a, is determined from

$$\sin a = \sin \Phi \sin \delta + \cos \Phi \cos \delta \cos h \qquad (3.71)$$

where Φ is the latitude, δ is the declination of the sun and h is the local hour angle of the sun. Further definition of terms is provided in Appendix A. Various values of A_1 for different surface types are provided by Paltridge and Platt.

Long-wave radiation is emitted by the ground surface and other objects in the range 6μ to 100μ for normal ambient temperatures. It may be calculated from the Stefan - Boltzmann Law

$$Q_{L\uparrow} = \varepsilon \sigma T_g^4 \qquad (3.72)$$

where ε is the surface emissivity and σ is the Stefan-Boltzmann constant ($\sigma = 2.0411 \times 10^{-7}$ kJ/m^2 hr K^4). Paltridge and Platt provide a table of ε for different surface types. If vegetation accounts for a significant fraction of the surface area then a surface area- weighted value of T^4 is required.

Long-wave radiation emitted by atmospheric water vapour and carbon dioxide is the last component of radiation to be considered. For the purposes of modelling it is most often calculated from a formula which

explicitly or implicitly includes the atmospheric water vapour content. The TVA (1972) evaluated alternative formulae and selected that of Swinbank (1963) for clear skies:

$$Q_{LI} = 5.31 \times 10^{-14} T^6 \ (mW\ cm^{-2}) \qquad (3.73)$$

where T is the absolute air temperature at normal measurement height. Paltridge (1970) provides estimates of the errors arising from the use of this formula; his graphs are reproduced below in Figure 3.1 and may be used to apply a correction to calculation if additional accuracy is required.

Equation (3.73) must be modified to include additional radiation from clouds, which reaches the surface through the atmospheric "window" between the wave-lengths of 8μ and 14μ. Since 70% of black body radiation at ambient temperatures lies outside this range, the contribution of clouds may be written as $(1 - 0.7)\varepsilon_c \sigma T_c^4 cc$, where subscript c refers to clouds and cc is the fraction of cloud cover over the total sky.

Paltridge (1970) found that for Aspendale the contribution for total cloud is approximately constant at 6 ± 0.5 $mW\ cm^{-2}$, so for partial cloud, $(1-0.7)\varepsilon_c \sigma T_c^4 cc \approx 6.0cc$. Alternately, the TVA (1972) accounts for the varying contribution of clouds dependent on their position in the sky (i.e. a lesser contribution for clouds near the horizon) by introducing the factor $(1 + 0.17\ cc^2)$ into (3.73), which is used here.

Whichever method is used to include cloud effects into (3.73), the problem remains to routinely estimate the cloud cover. It would be attractive in concept to estimate cloud cover from the measured

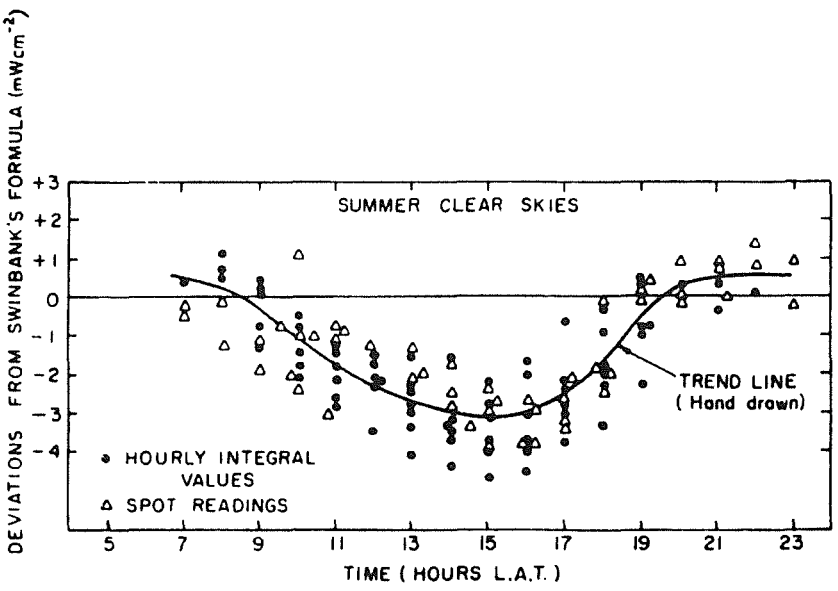

(a)

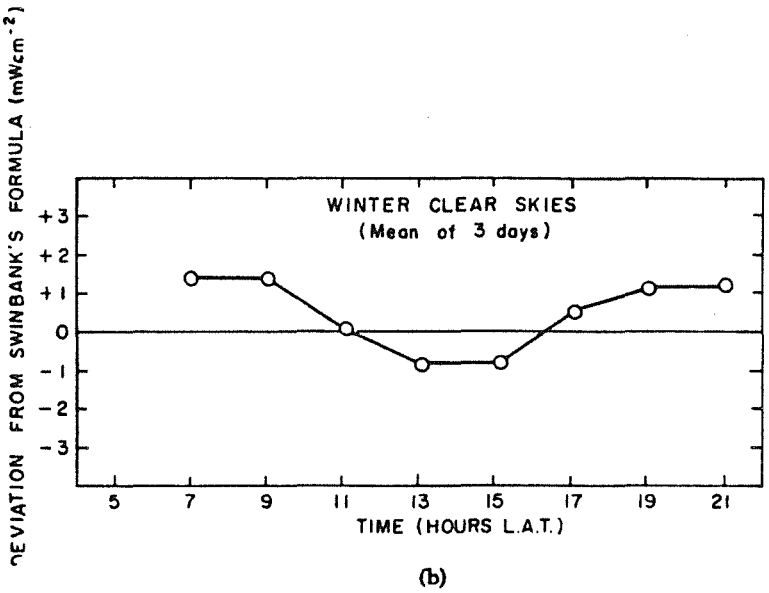

(b)

FIGURE 3.1 THE DEVIATION FROM SWINBANK'S FORMULA OF MEASURED CLEAR-SKY LONG-WAVE RADIATION AS A FUNCTION OF TIME OF DAY. (PALTRIDGE (1970))

fluctuation of global radiation. However, whilst direct solar radiation is simply related to cloud cover (i.e. direct radiation is obscured by cloud) diffuse shortwave radiation is related to cloud cover in a complicated way which is not well understood. It is notable that Paltridge and Proctor (1976) use calculations of direct and global radiation to infer diffuse radiation under cloudy skies. Hence, it seems impractical to extract cloud information from global radiation measurements alone. Figure 3.2 shows the complicated behaviour of measured global radiation under partially cloudy skies. Of particular interest are the peaks extending well above the superimposed clear-sky curve, indicating the enhancement of diffuse radiation by clouds.

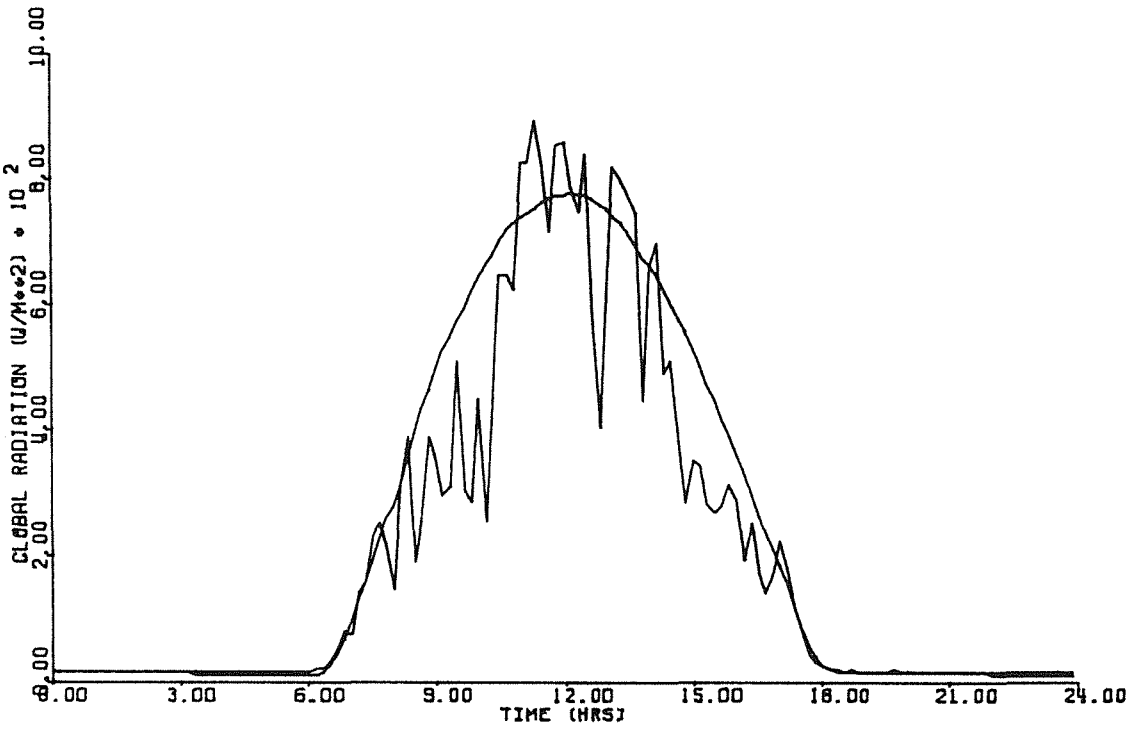

FIGURE 3.2 GLOBAL RADIATION UNDER PARTIALLY CLOUDY SKIES (KAMS DATA FOR DAY 1187)

Even if global radiation measurements could yield cloud information it would be of no use at night, which is the most important period for cloud effects. Although 6 mW cm^{-2} is small compared to the other long-wave contributions from (3.72) and (3.73), it is significant in the calculation of net long-wave radiation and may well prevent the formation of a night-time radiation inversion. The best means of estimating incoming long-wave radiation at all times appears to be direct measurement. This may be achieved by one of two methods:

(i) direct measurement by a pyrgeometer

(ii) fitting a black cavity shield to the lower face of a net radiometer and measuring the net radiometer output, cavity temperature and incoming short-wave radiation Q_{SI} with another radiometer. Q_{LI} then follows from

$$Q_{LI} = OUTPUT - Q_{SI} + \sigma T^4_{cavity} \qquad (3.74)$$

As an alternative to direct measurement of long-wave radiation, use can be made of cloud observations from meteorological offices or airports. In Australia, these take the form of three hourly observations of cloud height, type and fraction of sky covered.

3.3.4 MODEL INPUT DATA AND COEFFICIENTS

The meteorological Base Stations at Wattleup and Hope Valley provided the basic meteorological input data for the model in the form of accurate ten minute scalar averages. The relevant items of data for this model were wind speed, air temperature and dew point temperature measured at ten metres height, and global radiation.

Rainfall was not monitored at either meteorological Base Station during KAMS. Instead, pluviograph records for the entire period were obtained from Murdoch University and digitised to give a file of rainfall for each hour of the day (in tenths of a millimetre). Murdoch University is approximately 15 km NNE of Kwinana and 8 km inland from the coast (which runs approximately north/south). The model accessed the appropriate hourly values at the start of each timestep, and computed a precipitation rate.

Since no continuous measurements of incoming long-wave radiation were available, it was necessary to obtain cloud data for Perth Airport from the Commonwealth Bureau of Meteorology, in order to compute incoming long-wave radiation. Perth Airport is approximately 35 km NE of Kwinana and 20 km inland. The three hourly observations were taken to hold for the 90 minutes either side of the observation time. Atmospheric pressure data are similarly treated.

Table 3.1 lists the various coefficients and physical constants from the foregoing equations, together with chosen values and the sources of these values. Some of these chosen values are discussed below.

No attempt was made during the Study to analyse the soil from Kwinana to determine ρ_s, c_s and λ_s, so giving C_s for (3.61). Characterising soil types in this State is an important area of future work if this methodology is to be pursued. For the present Study, a representative value of C_s for the sand coastal plain was inferred from the data on various soil types given by Deardorff (1978). The value of C_d in (3.63) follows directly from this choice.

Param.	Value	Source
C_s	1.0×10^5 J m^{-2} K^{-1}	Deardorff(1978)
C_d	4.8×10^6 J m^{-2} K^{-1}	"
C_1	(see text)	"
C_2	0.9	"
d_1	0.1 m	"
d_2	0.5 m	"
w_k	0.3	"
w_{max}	0.4	"
A_1	0.2	Paltridge and Platt (1976)
ε	0.93	"
C_{DN}	8.0×10^{-3}	Kams fieldwork
C_{HN}	5.0×10^{-3}	and Garratt (1978b)
β'	0.7	"
Ω	7.27×10^{-5} s^{-1}	
ρ_w	1000. kg m^{-3}	
C_p	1010 J kg^{-1} K^{-1}	
L_e	2445 kJ kg^{-1}	
g	9.81 m s^{-2}	
k	0.41	

TABLE 3.1 Values of model coefficients and physical constants

Similarly, no information on local soil moisture characteristics was available or easily obtainable, so the scanty information provided by Deardorff (1978) was again utilized, giving the values of C_2, d_1, d_2, w_k and w_{max} in Table 3.1. The value of C_1 is obtained from the following expressions provided by Deardorff:

$$C_1 = 0.5, \quad w_g/w_{max} \geq 0.75$$

$$C_1 = 14 - 22.5[(w_g/w_{max}) - 0.15], \quad 0.15 < w_g/w_{max} < 0.75$$

$$C_1 = 14, \quad w_g/w_{max} \leq 0.15$$

The 27 metre tower at Hope Valley was equipped with three sensitive cup anemometers at logarithmic height intervals for the purpose of estimating displacement height D and roughness length z_0. Following Paulson's (1970) method, D was found to be zero, and the roughness length and the ten metre drag coefficient were determined to be 10 cm and 8.0×10^{-3} respectively. Using Garratt's (1978b) relationship of $z_0/z_H = 12$ gives $z_H = 0.008$, which in turn gives $C_{HN} = 5.0 \times 10^{-3}$.

It is necessary to quantify the coefficient ß' in (3.65) accounting for the area covered by vegetation which has different heat transfer characteristics. Site inspection, intuition and model testing has led to the plausible value ß' = 0.7. Further work involving radiometric temperature measurements of the various surfaces is required.

3.3.5 STRUCTURE OF THE COMPUTER MODEL

A flow diagram of the model is provided in Appendix B. A brief description of the main features follows.

The solution of the equations describing turbulent fluxes and the evolution of ground temperature and moisture is synchronised to the 10 minute meteorological data, producing output results at the end of each 10 minute period. The integration scheme employed is a fourth order Runge Kutta scheme which computes relative accuracy of integration via a fifth step and uses this test to govern its own timestep halving or doubling procedure.

Soil heat flux G and evaporation E are required to evaluate the differential equations. These may be determined:

(a) prior to the start of an integration step, using T_g and w_g from the previous timestep (as was done by Hoffert and Storch (1979));

(b) immediately prior to each Runge Kutta step, using the most recently integrated values of T_g and w_g;

Method (b) could be described as fully implicit except for the use of averaged meteorological data rather than instantaneous values. This method is recommended as T_g and w_g may vary markedly even over 10 minutes; hence method (a) would incur errors in flux computation. Additional computer run time for method (b) is minimal (~10% extra).

The iterative method of computing turbulent fluxes, outlined in Section 3.1.2, is ideally suited to continuous simulations like the present exercise. On the first calculation cycle, neutral transfer coefficients C_{DN} and C_{HWN} are read in and corrected for measurement height if necessary, then the stability dependent transfer coefficients are initialised to their neutral values. On subsequent calculation cycles, the fluxes are first calculated via (3.24), (3.25)

and (3.68) using the stability dependent transfer coefficients from the previous cycle. These fluxes are then used in (3.2) to evaluate z/L,(z = 10m) which is compared to the final z/L from the previous cycle to determine whether a "significant" (to be specified) change in stability has occurred. If so, the value of z/L is set to the current value, the transfer coefficients are corrected via (3.27) and (3.28), and the above process repeated iteratively until z/L converges satisfactorily. If z/L has not varied significantly (i.e. steady state conditions), control transfers immediately to final calculations of H_L, u_*, Q_{L0} and G. In this way, the lengthy calculations associated with (3.27) and (3.28) are avoided, resulting in rapid execution. Where iteration does occur, convergence usually occurs in one or two steps. This method is therefore preferred over that of Hoffert and Storch (1979) in which the complicated flux-profile relationships are solved at each timestep, and information from previous timesteps is neglected. In the current method, execution time can be reduced at the expense of precision by relaxing the convergence criterion for z/L.

Integration proceeds until the end of the 10 minute period is reached. The turbulent fluxes are evaluated one last time to utilize the final values of T_s, T_d, w_s and w_d. Results of the solution are then written to output files prior to the start of a new timestep. The main output file for use in dispersion models etc. has the form:

DATE DAY TIME H_v, u_*, 10/L, T_v, θ, U, direction, sigma

where H_v is the virtual heat flux defined as

$$H_v = H_s + 0.61C_p(\theta + 273)E \qquad (3.75)$$

Other output files may be optionally produced to show the balance of heat fluxes and the evolution of other parameters.

3.4 EVALUATION OF THE HEAT BUDGET MODEL

3.4.1 COMPARISON OF THE HEAT BUDGET AND PROFILE METHODS

Results of heat budget model have been compared against estimates of turbulent fluxes from the tower profile measurements and other monitoring results for three field experiment days during KAMS; 13/12/79, 31/1/80 and 29/10/80. The 13/12/79 experiment was an abortive tracer experiment which nevertheless provided valuable surface meteorological data.

For the purposes of the following discussion the heat budget and profile methods will be called SOIL and HVFLUX respectively, which were their assigned program names. HVFLUX is Method B described in Section 3.4.1.

Output from SOIL and HVFLUX is presented in plotted form in Figure 3.3(a) to (f). SOIL results appear as full lines throughout. For each experimental day there are four plots labelled (a) to (d) showing:

(a) modelled H_s from SOIL and H_s from the two - level tower measurements via HVFLUX (dashed line),

(b) modelled net radiation from SOIL and net radiation measured at the Hope Valley Base Station (dashed line),

(c) stability z/L at z = 10m, determined by SOIL and HVFLUX (dashed line),

(d) modelled surface ground temperature T_g from SOIL, with actual measured values plotted as crosses.

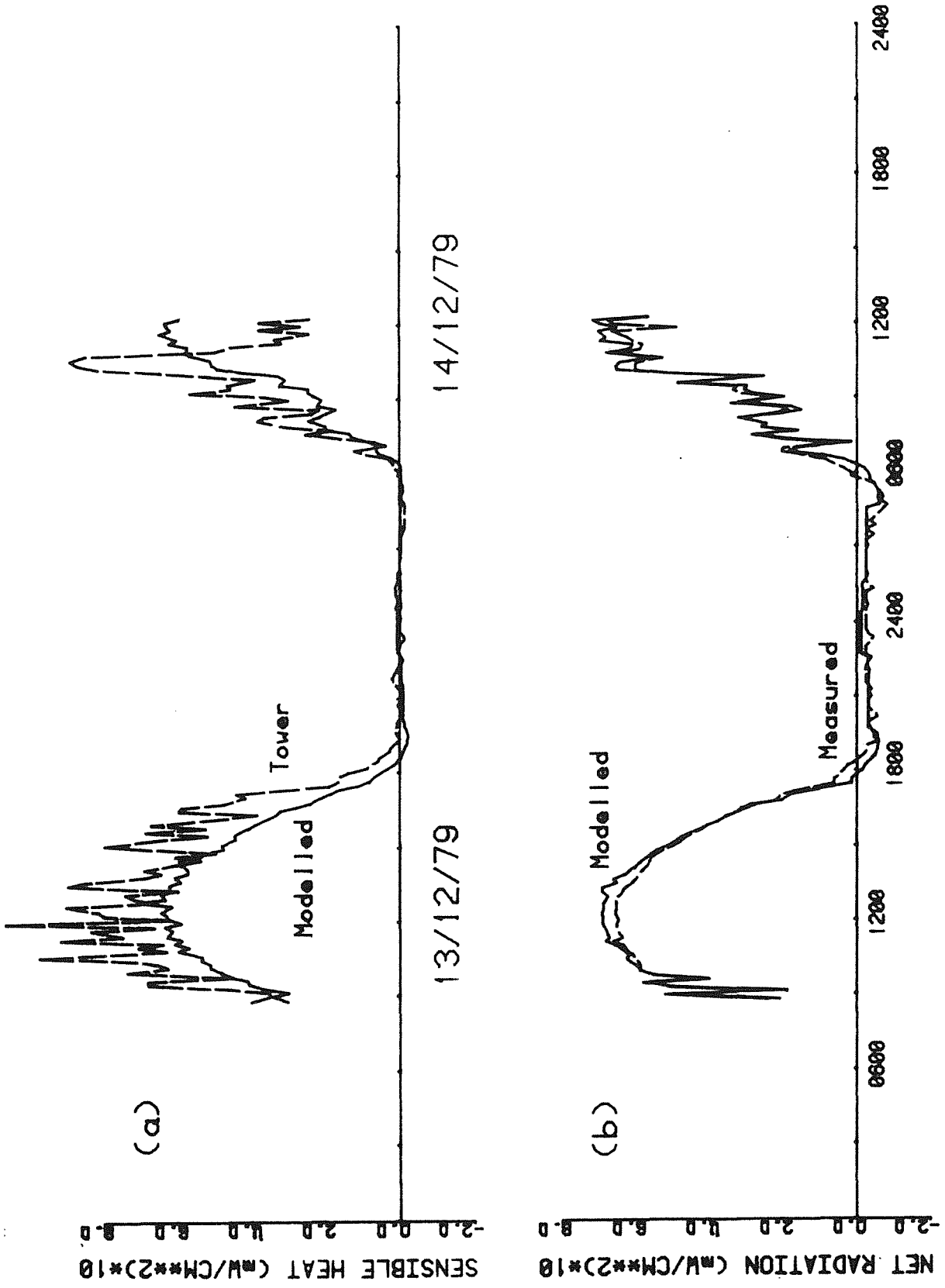

Figure 3.3(a) Results of Model SOIL, Profile method HVFLUX and measurements for 13/12/79.

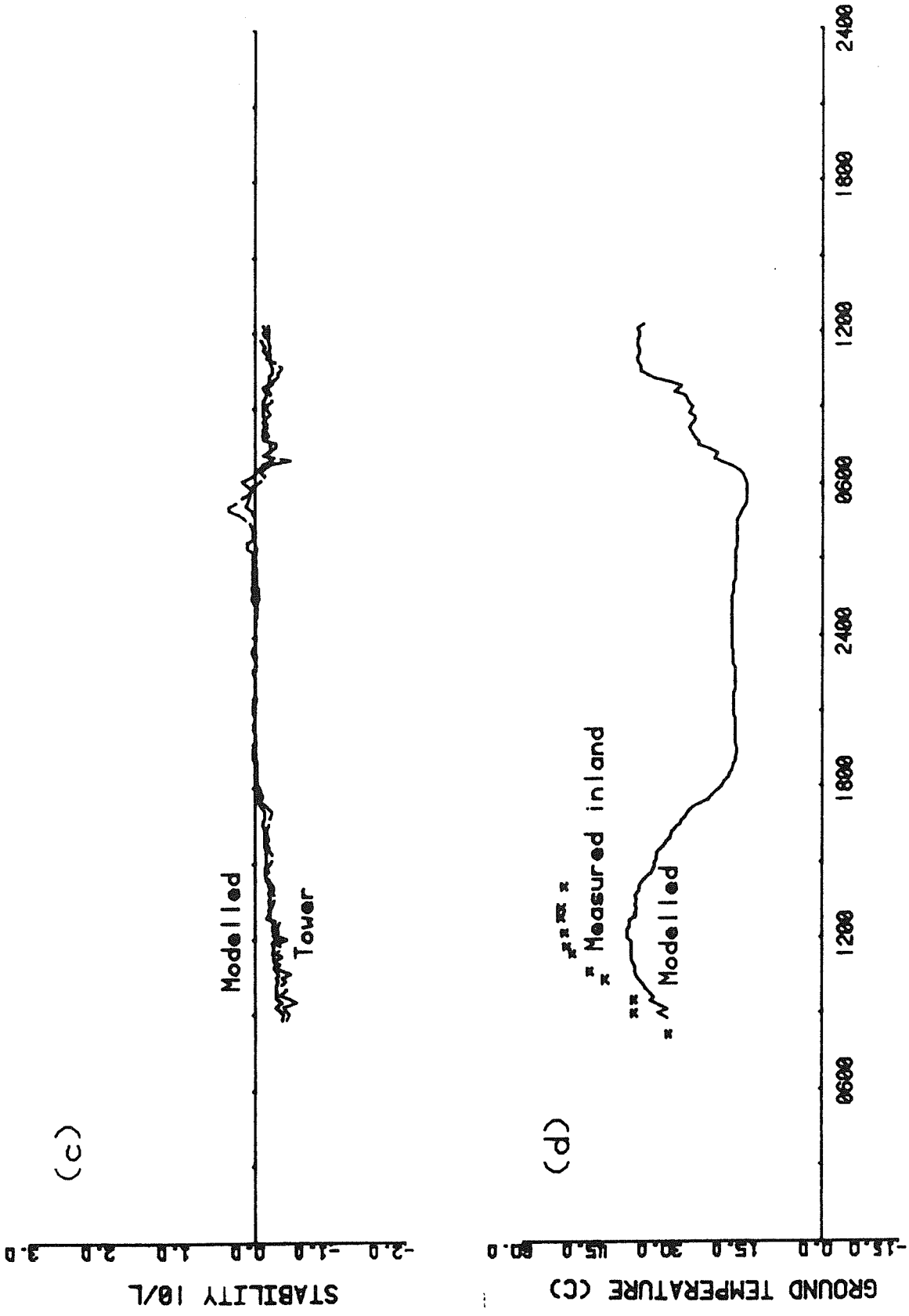

Figure 3.3(b) Results of Model SOIL, Profile method HVFLUX and measurements for 13/12/79.

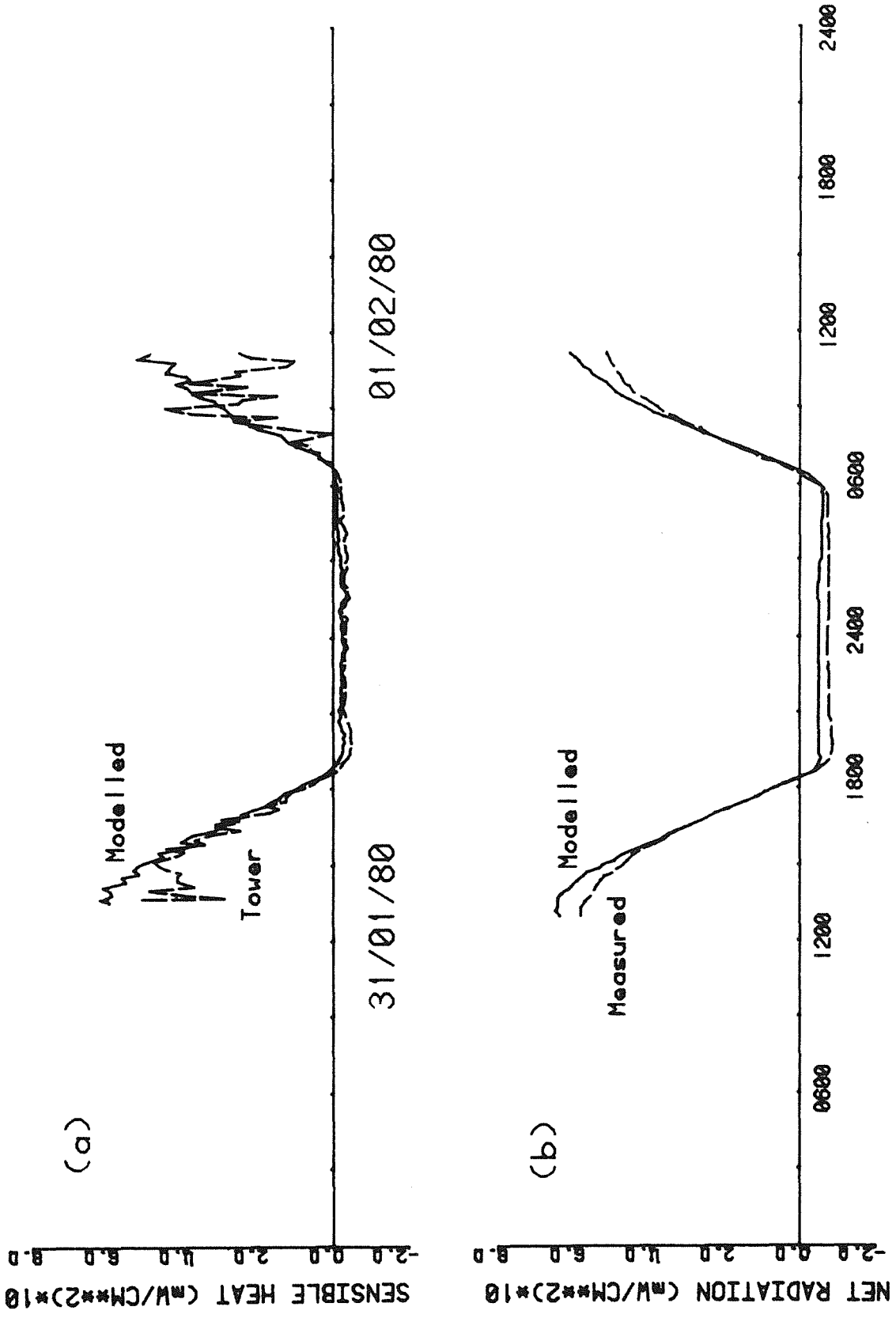

Figure 3.3(c) Results of Model SOIL, Profile method HVFLUX and measurements for 31/01/80.

Figure 3.3(d) Results of Model SOIL, Profile method HVFLUX and measurements for 31/01/80.

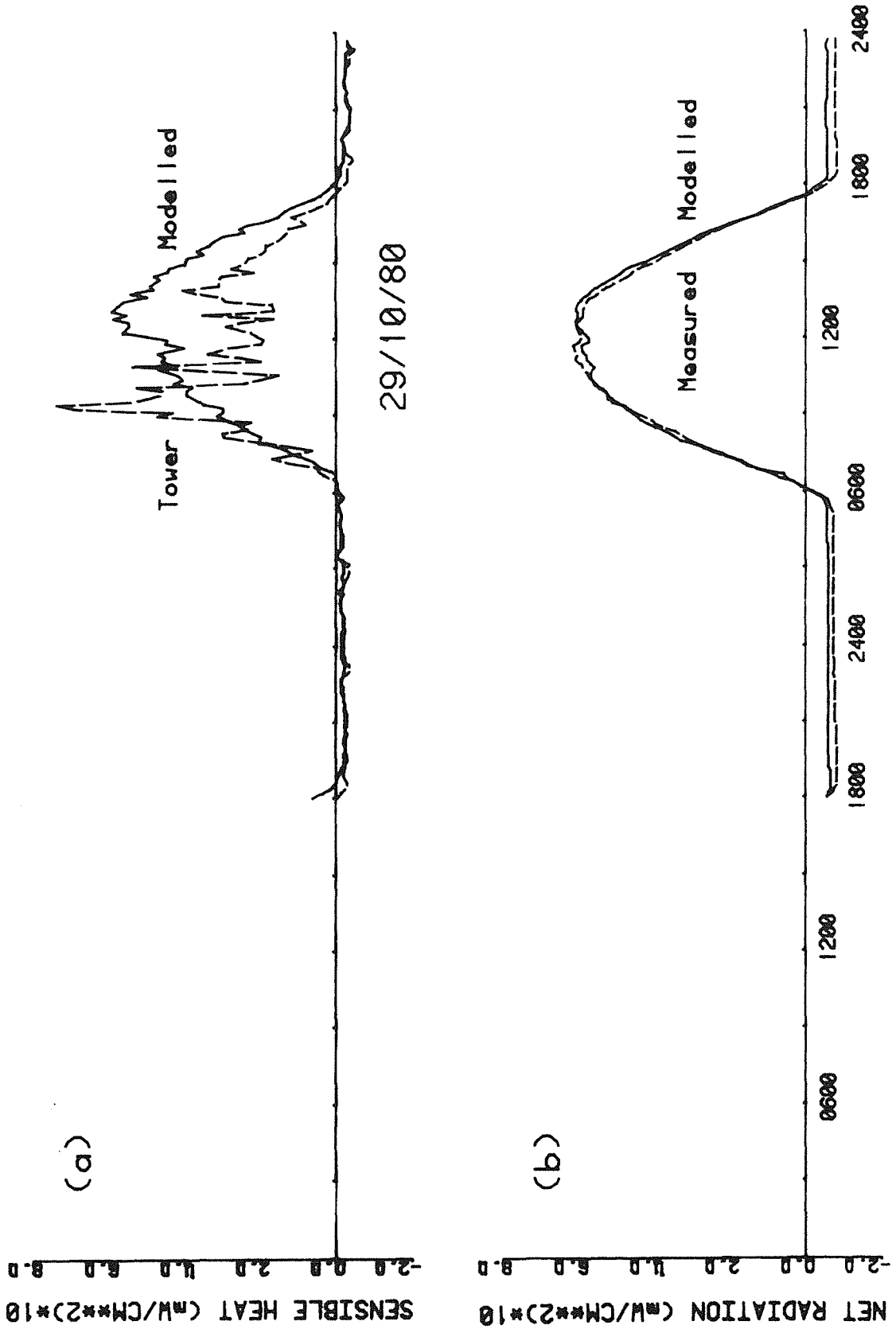

Figure 3.3(e) Results of Model SOIL, Profile method HVFLUX and measurements for 29/10/80.

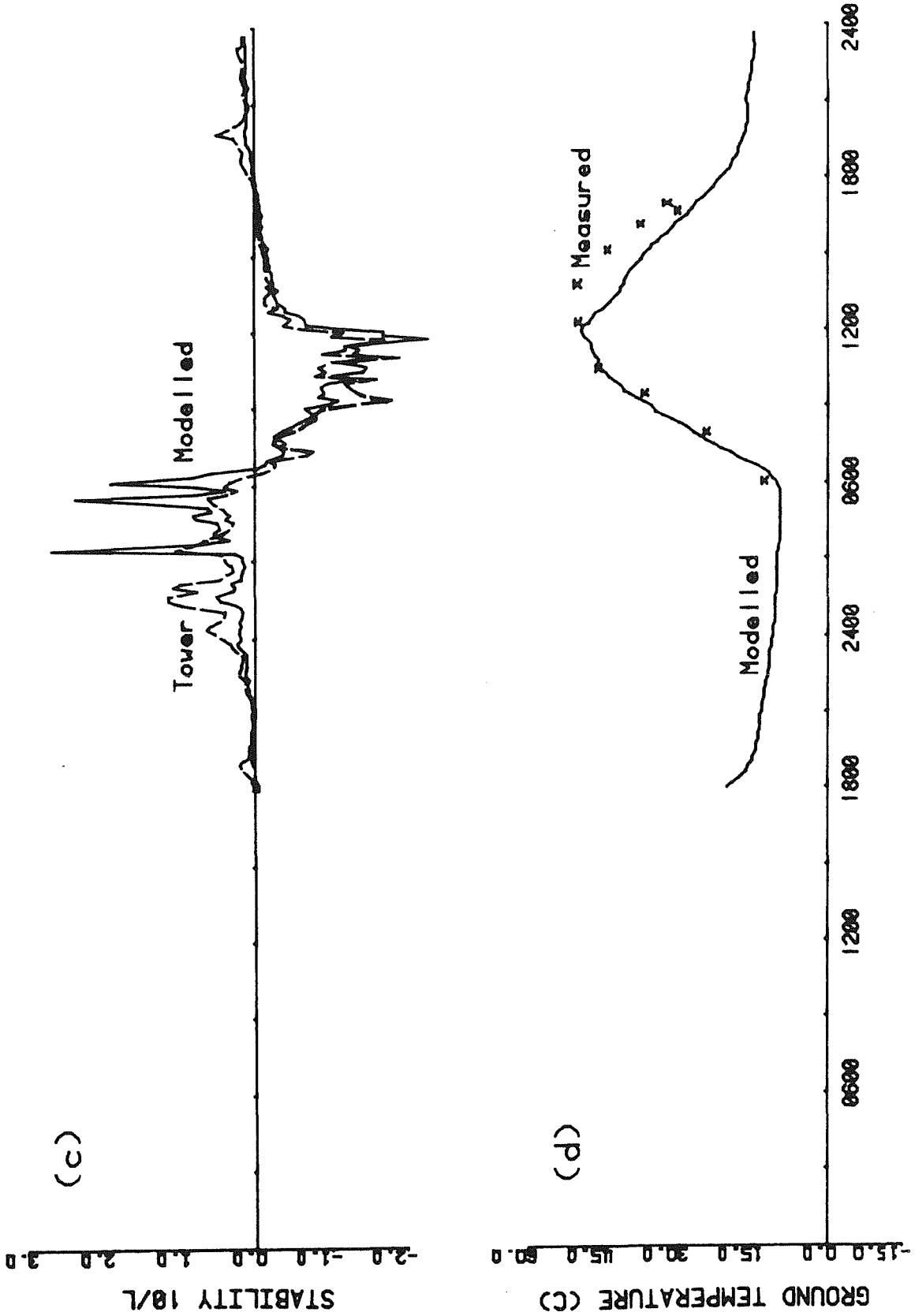

Figure 3.3(f) Results of Model SOIL, Profile method HVFLUX and measurements for 29/10/80.

The most important output parameter is H_s (or H_v in wet conditions) as this largely determines the state of turbulence in the planetary boundary layer within which industrial plumes disperse. The heat budget computation in the model ensures that the prediction of $H_s + H_L$ is very stable, e.g. it varies little with even large changes in the model coefficients. Other model outputs like T_s, u_* and hence also L are not similarly constrained and therefore show greater sensitivity to variations in model coefficients.

The apparent variability of H_s during daytime for all periods is consistent with the expected spatial variability of convective turbulence, but is over-enhanced by the method of computation in HVFLUX. In HVFLUX, a new independent estimate of Ri (and hence z/L) is computed for each 10 minute period giving a new C_H value. Hence the effect of short term peaks in $(\theta_2 - \theta_1)$ are magnified in H_s. Spatial or temporal averaging of Ri would provide a much smoother result. Viewed overall, however the comparison between the SOIL and HVFLUX values of H_s is fairly good. The shapes of the diurnal curves compare well on the 13/12/79, when fresh synoptic south-westerlies blew all day. The uncertainty in H_s from the HVFLUX profile method is at least as large as the apparent difference in results on that day. Results from the 29/10/80 show a clear drop in the HVFLUX value of H_s following the onset of a sea breeze just prior to noon. The ground temperature measurements also indicate that the rate of heat removal from the ground is not as high as indicated by SOIL, even though strong cooling would be expected under the cool sea breeze. It appears that heat transfer in sea breeze flows is less than that indicated by the ground/air temperature difference, presumably because the surface

layer profiles of mean temperature and wind have not reached equilibrium over the Hope Valley Base Station. If this is so, it would follow that the HVFLUX estimates of H_s (determined from measurements above 10 m) would be under-predicted, compared with the SOIL results being over-predicted. This problem was not anticipated given that the minimum fetch/height ratio (at the top of the tower) is approximately 100 in westerly winds, and is generally much larger. Peterson (1969) indicates that fetch/height ratios of 100 or more should ensure equilibrium conditions. The problem warrants a detailed micrometeorological investigation which is beyond the scope of this Study.

Net radiation figures are strongly dominated by the solar components during the day, but comparison of measured and modelled values provides, at all times, a check on the model's ground temperature simulation. The best results obtained are for the morning of 29/10/80 during which time surface (top millimetre or so) ground temperature was accurately measured. Winds were from the north east up to 1000 m height and hence the turbulence in the growing mixed layer was well developed, with no major upwind horizontal inhomogenieties. The results indicate that the model is clearly capable of simulating the ground temperature under these conditions. Analysis of the observed inversion erosion described in Chapter 4 supports the estimates of H_s from the model, which in turn agrees roughly with the tower estimates.

The measured soil temperature values on 13/12/79 and 31/1/80 have been included not for direct comparison but rather to illustrate a point. These values were measured at a radiosonde release point 3 km inland

from the Hope Valley Base Station and with a greater downwind fetch in the sea breeze of at least 6 km. Observations on 31/1/80 indicated that:

(i) the sea breeze reached Hope Valley approximately 30 minutes before the radiosonde site;

(ii) ambient air temperatures were 3° to 4°C higher at the radiosonde site between 1200 and 1500;

(iii) wind speeds were up to 30 per cent lower at the radiosonde site for the same period.

Although the south-westerly winds were well established on 13/12/79, similar air temperature and wind speed differences were present between the two sites. The large difference between modelled and measured (radiosonde site) ground temperatures is therefore to be expected and it is clearly not correct to assume horizontal uniformity of T_g, as does Venkatram (1977) for computing the growth of thermal internal boundary layers. Nevertheless, the net radiation plots indicate that the modelled ground temperature at Hope Valley is somewhat low, consistent with the foregoing conclusion that SOIL over-estimates H_s in sea breezes and other onshore flows.

Daytime computations of stability (10/L) compare favourably with those from the tower, indicating that momentum flux ρu_*^2 is also modelled successfully.

The usefulness of the Perth Airport cloud observations for computing incoming longwave is seen on the evening of 13/12/79. The heat fluxes computed and calculated for this evening are very small; a feature of cloudy nights.

On both the evening of the 31/1/80 and the morning of the 29/10/80 prior to sunrise, the computed negative net radiation is slightly too small. Whilst a number of factors may influence the computed net radiation, the only two significant potential causes for the observed under-prediction are:

(i) C_s too low,

(ii) Q_{LI} too large.

A low value of C_s would result in a low predicted T_s with an associated reduction in outgoing long-wave radiation leading to the observed under-prediction. A large value of calculated Q_{LI} would directly cause the observed under-prediction. However, whilst both potential causes would affect net radiation in the same sense, they would affect predicted atmospheric stability in contrasting senses;

(i) would lead to over-prediction of z/L

(ii) would lead to under-prediction of z/L

Although the night-time estimates of 10/L for both experimental periods show some variations between SOIL and HVFLUX predictions, there is no consistent bias which would support either (i) or (ii). Overall, the prediction of all parameters (including net radiation) over the night periods are considered satisfactory.

It is interesting to discover that, for given values of ε, C_s and cloud amount, night-time H_s is quite stable and insensitive to the value of C_{HN} This comes about because, in stable conditions, C_H is reduced markedly by very small changes in $(\theta - \theta_0)$ and so varies over a large range. Two differing values for C_{HN} may reduce to the same C_H in stable conditions for virtually the same value of $(\theta - \theta_0)$ (i.e.

the same Tg). Both ($\theta - \theta_0$) and H_s will therefore be determined almost solely by the balance of terms in the heat budget.

Field measurements need to be conducted in order to determine all of the model coefficients in Table 3.1 prior to the model being used in regulatory applications . No assessment of the accuracy of the model's soil moisture simulation has been possible, as no data are available for comparison. The simulation described in the next Section gives reason for some confidence however.

3.4.2 A SAMPLE MODEL SIMULATION INCLUDING RAINFALL

A sample run of three days in August 1980, including twelve hours of rain, is presented in plotted form in Figure 3.4(a) and (b), and it serves to illustrate the importance of accounting for soil moisture. The first day, 8/8/80, is reasonably sunny for a winter's day (see the net radiation curve); hence the ground temperature rises appreciably and the upward sensible heat H_s dominates over the latent heat H_L. Murdoch University records indicated that twenty five millimetres of rain fell in the eleven hours commencing at 0100 on the 9/8/80 with the heaviest falls following the passage of a cold front at 0300 (see the air temperature trace) . The model response is very credible. The soil moisture content w_s rises rapidly above the saturation level following the onset of heavy rain. Evaporation is inhibited by high humidity and so H_L remains small. The sudden drop in air temperature results in a short period of unstable conditions (positive H_s) during which time the ground cools rapidly. Net radiation shows the presence of total cloud cover prior to sunrise and the stability during this

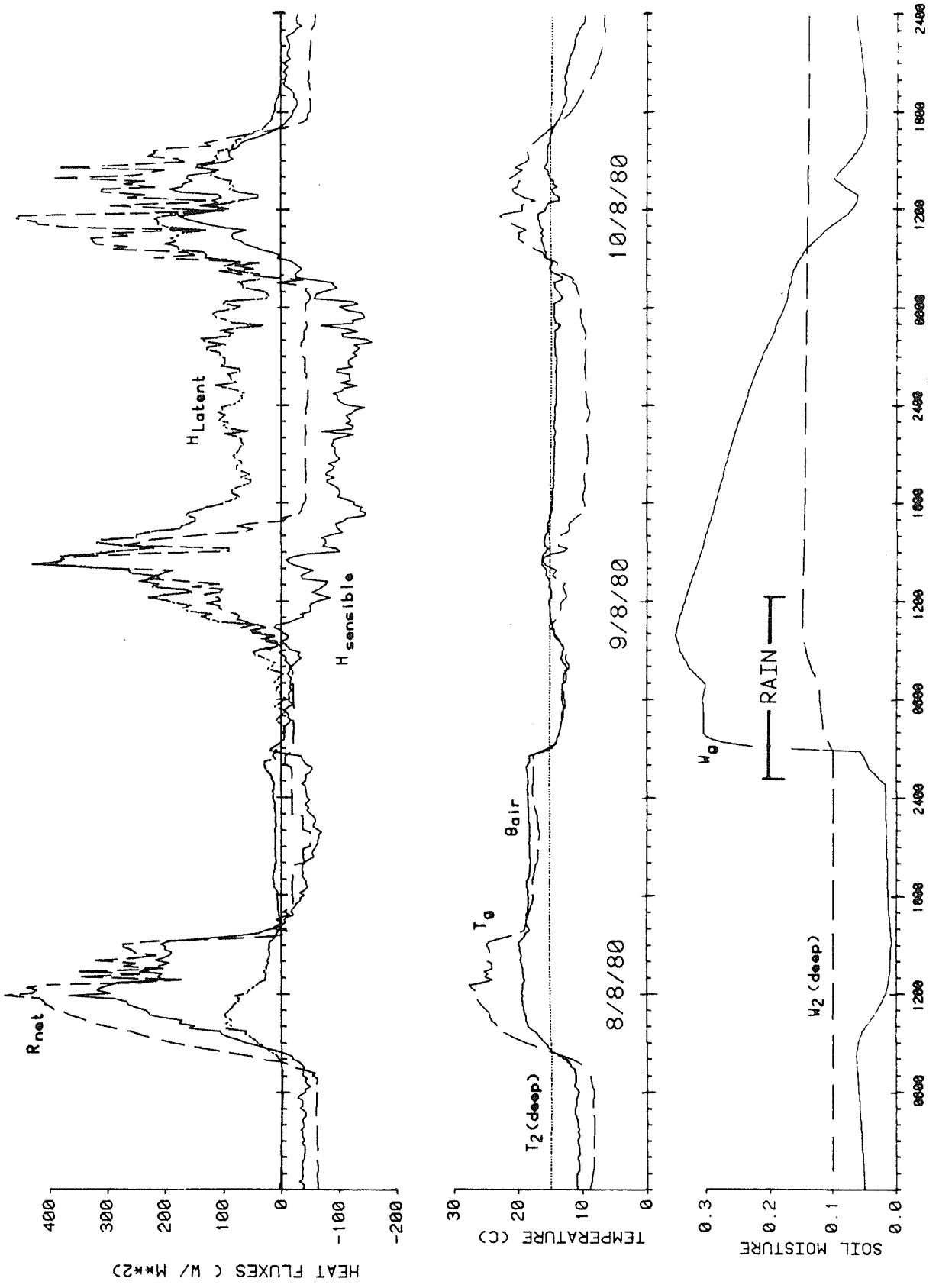

FIGURE 3.4(a) THREE-DAY SOIL SIMULATION WITH RAINFALL

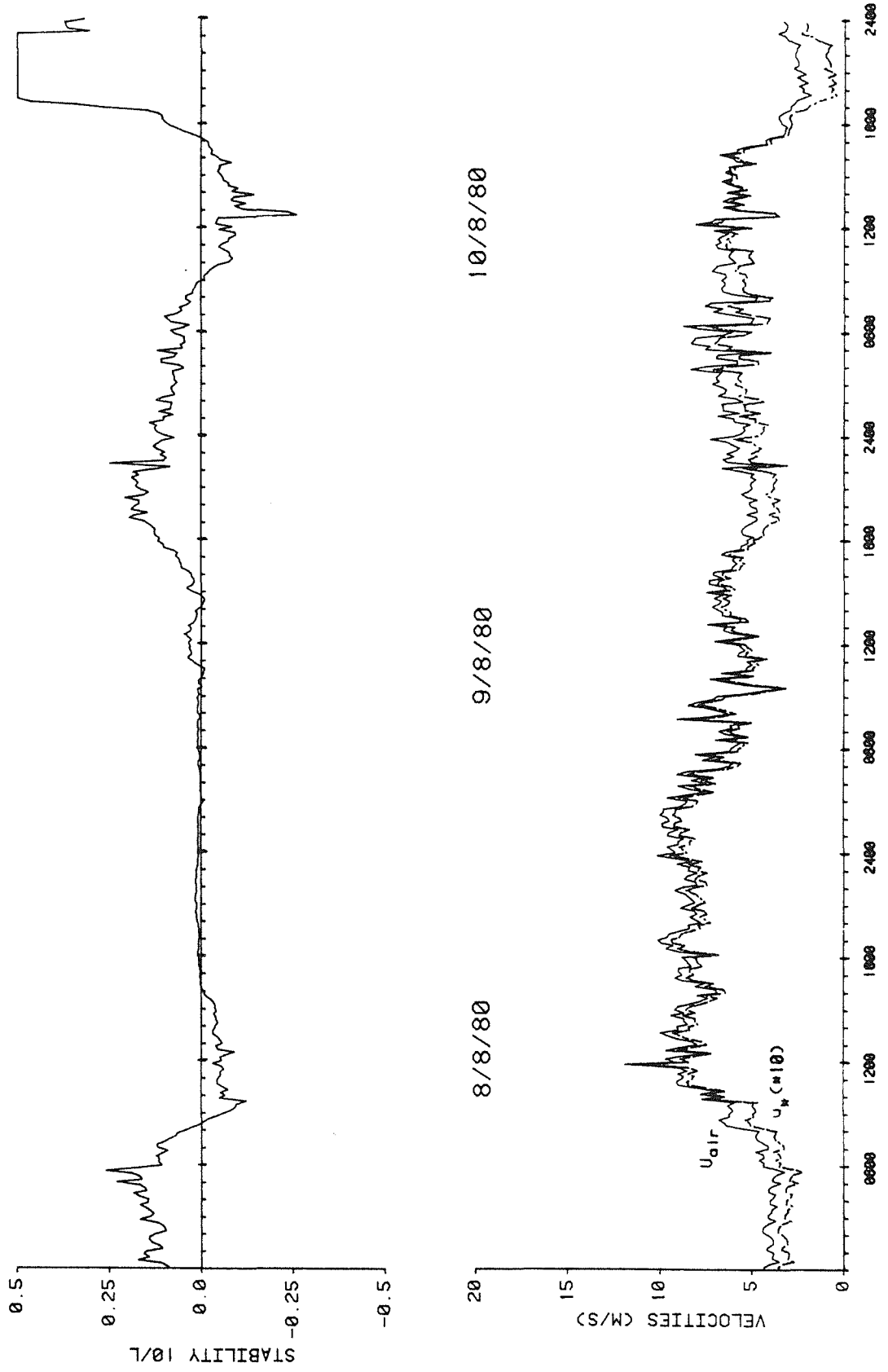

FIGURE 3.4(b) THREE DAY SOIL SIMULATION WITH RAINFALL

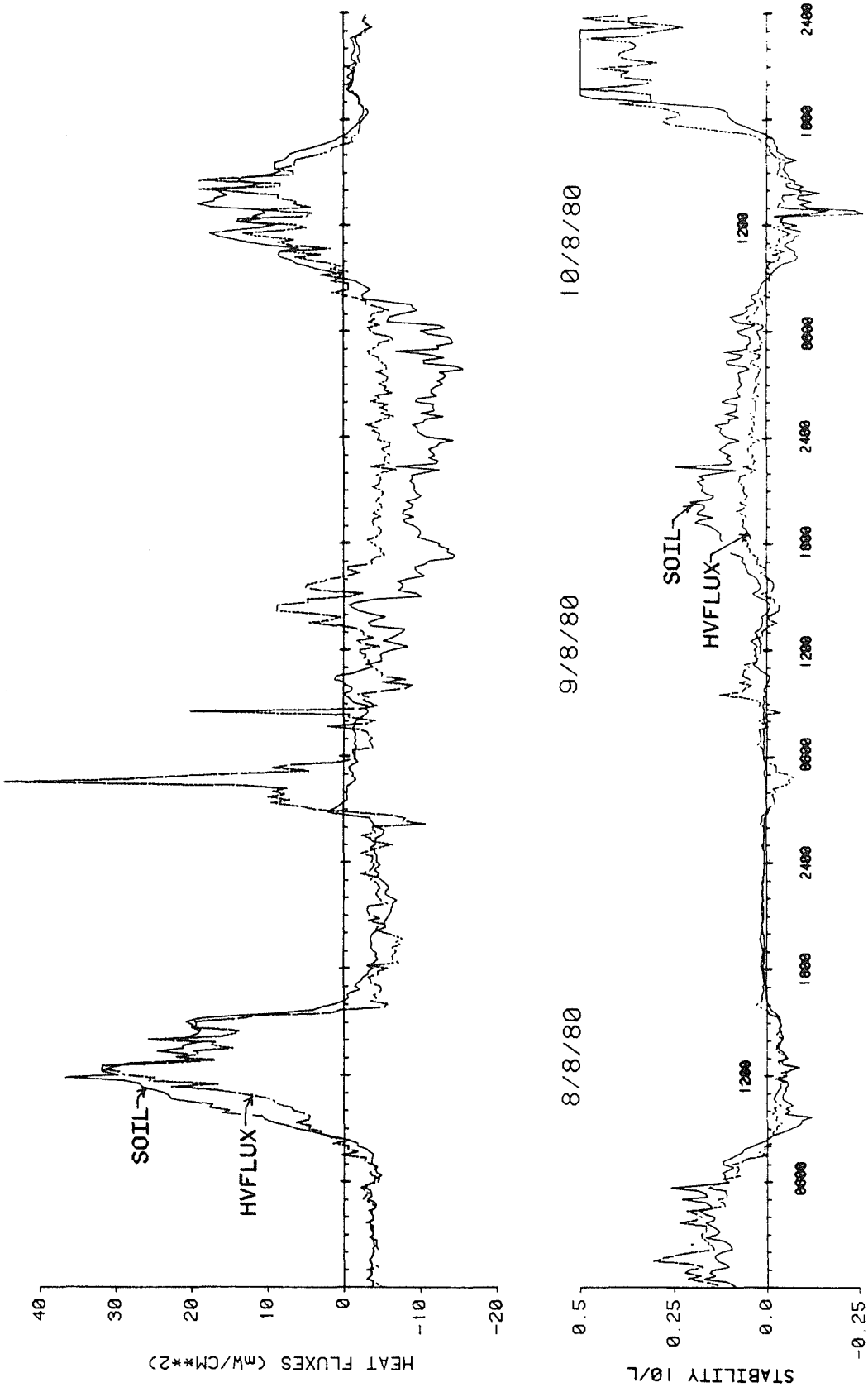

FIGURE 3.4(c) THREE DAY SOIL SIMULATION WITH RAINFALL

period is very close to neutral. During the daylight hours of 9/8/80, the loss of latent heat exceeds the incoming net radiation resulting in negative H_s and a T_s estimate which stays low all day. After the rain ceases, the soil starts to dry out in a reasonable fashion, with only a slight increase in soil moisture associated with 0.4 mm of rain on the 10/8/80. The surface drying rate has not been verified for Kwinana soil types. During the daylight hours of the 10/8/80, latent heat loss is less than the previous day (due to lower surface moisture) so that H_s becomes positive after 0900.

The two plots in Figure 3.4(b) show wind speed and friction velocity u_* (amplified ten times), both of which are moderately high over the three days, and also the stability 10/L over the three days. The absolute values of 10/L are generally low, due to seasonal effects and to the moderately high values of u_*. However the diurnal patterns of stability are representative and important. On the 8/8/80 there is a normal cycle of night-time stable and daytime unstable conditions typical of dry sunny days. On the 9/8/80 however, 10/L stays slightly positive virtually all day due to the downward sensible heat flux H_s. Significantly different dispersion characteristics would be expected on this day compared to the previous day. A morning radiation inversion would not form due to the almost neutral nocturnal conditions, and daytime dispersion of pollutants would be inhibited even in the sunny periods following the rain, as there would be no thermal convection in the planetary boundary layer. The effect of the rain period is felt through to mid-morning on the 10/8/80, at which time mildly unstable conditions are re-established.

Figure 3.4(c) presents a comparison (as far as is possible) between the results from SOIL and the tower profile method HVFLUX over the same period. (Moisture buoyancy effects are not included in HVFLUX so stability is slightly over-estimated in these calculations.) The increase in stability associated with rainfall is seen in the HVFLUX estimates of 10/L and its effect is seen in the estimates of H_s. The main differences between the SOIL and HVFLUX estimates, and likely explanations for these, are as follows:

(i) HVFLUX calculates lower values of negative H_s and 10/L during the day of 9/8/80 (including a short period of slightly unstable conditions in the afternoon). Although there are several factors which may have contributed to the difference in estimates, the most significant likely explanation is that the simulated soil surface moisture content was too high during this period, leading to over-estimation of H_L. This in turn is well explained by the fact that the soil at Kwinana is primarily deep, well drained sand, implying a large value of C_2 in (3.66). The need to determine soil characteristics for use in the model has already been mentioned. It may be noted however that the two estimates of 10/L still generally fall into a single Pasquill-Gifford stability category (Golder, 1972).

(ii) HVFLUX output shows an unstable period following the passage of the cold front, with very large associated values of H_s for the next three hours. The response of SOIL during this period has already been described. A simple assessment of the heat budget shows that the large H_s values are unrealistic. It is apparent that, during this period of fairly strong winds, the 27 m measurement level was not within the equilibrium boundary layer

and so the calculations are unreliable.

Both of the above problems relate to inadequate data and do not reflect significantly on the credibility of the model. Even with the apparent errors the results compare favourably with the tower estimates and certainly capture the essential features of the stabilizing effect of rainfall. The comparison of estimates for the 10/8/80 is good and demonstrates the stability of the model. Clearly, the model provides a viable means of estimating surface layer fluxes and stability, from single level measurements, which is far superior to the "rule of thumb" procedures usually employed in dispersion modelling. The method of Pasquill and Gifford (see Turner, 1970), reproduced in Table 3.2, is implicitly an energy budget approach to determine a stability scale which is related in some fashion to L. The

Surface Wind Speed (at 10 m), m sec^{-1}	Day			Night	
	Incoming Solar Radiation			Thinly Overcast or ≥4/8 Low Cloud	≤3/8 Cloud
	Strong	Moderate	Slight		
< 2	A	A-B	B		
2-3	A-B	B	C	E	F
3-5	B	B-C	C	D	E
5-6	C	C-D	D	D	D
> 6	C	D	D	D	D

The neutral class, D, should be assumed for overcast conditions during day or night.

TABLE 3.2 Key to stability categories (Turner (1970))

method completely neglects the partitioning of sensible and latent heat however, and does not account for site to site variations in any of the parameters of Table 3.1. Other researchers (e.g. Hanna et al.,

1977; Kristensen, 1982; van Ulden and Holtslag, 1985) similarly point to the limitations of the method. McCumber and Pielke (1981) and Ookouchi et al. (1984) report that soil moisture is a key factor in describing the turbulence and growth of the planetary boundary layer. Variation of soil moisture within normal ranges has a far greater effect than changes in albedo, surface roughness or soil conductivity. It follows directly that soil moisture is a key factor in evaluating dispersion of chimney plumes. It is not the intention here to criticise methods such as the one described above, which have been developed to facilitate simple engineering calculations. However, given reasonable estimates of soil heat and moisture retention characteristics, the present model is also capable of routine, efficient application whenever standard meteorological data are available, and the achievable enhanced accuracy is strong justification for its use.

Extensive testing of the model has proven it to be very stable and efficient, executing in a fraction of a second per day of simulation on modern mainframe computers. The model is well suited to simulation over extended periods (one or more years).

3.5 SUMMARY OF FINDINGS

The aim of this Chapter has been to develop a model to routinely estimate turbulent transfers in the atmospheric surface layers. These in turn may be used to estimate the level of turbulent energy in the planetary boundary layer which determines its dispersive capability.

Tower profile estimates of turbulent fluxes have proven valuable in this project for validating the heat budget model. The quality of results depends heavily on the quality of equipment and associated calibration procedures however, due to the method's sensitivity to small errors in mean measurements. Equipment and manpower costs, plus the logistics of equipment installation and operation, render the method unsuitable for many situations, particularly where dispersion estimates are required fairly promptly.

The present Study is limited in application to sparsely vegetated areas, which is a reasonable description of the plain immediately adjacent to the coast near Perth and is a good description of vast areas of Western Australia.

The principal advantage of the heat budget method employed by the Model SOIL is that it utilizes routinely available single height observations, with only standard accuracy requirements. It is related to the conventional means of stability estimation (Pasquill - Gifford classification) and is therefore conceptually easy to understand. Unlike the tower profile method however, it is dependent on a variety of surface characteristics which must be defined for each site. Further work is required to characterise soil types at Kwinana and elsewhere in the State.

Results from the model have been shown to compare favourably with tower profile calculations. Hence the model may be used with some confidence to process the KAMS Base Station data for the full Study period.

CHAPTER 4

MIXING IN THE ATMOSPHERIC BOUNDARY LAYER

Dispersion of pollutants in the atmospheric boundary layer is strongly influenced by two meteorological parameters, namely the stability or mixing capability of the air and the height to which mixing occurs, or the mixing depth. As will be seen later, these two parameters are inter-dependent although they are frequently considered to be independent by dispersion modellers. By way of definition, the mixing depth is that depth or height of the atmospheric boundary layer within which turbulent motions are able to disperse airborne contaminants (Pasquill, 1974). Above this level, the air is gravitationally stable with relatively little or no turbulent activity and may act as a "lid" to the vertical transport of pollutants. It is important to determine the strength of the lid in order to decide whether hot buoyant chimney plumes can penetrate it and so exit the turbulent boundary layer. The purpose of this Chapter is to develop a model of mixing depth which will provide estimates for subsequent use in dispersion modelling.

In dispersion calculations, mixing depths are of most importance when they are shallow (e.g. a few hundred metres). Large mixing depths need not be specified with great accuracy as they have little effect on the rise and dispersion of plumes. The present study is therefore focussed on an examination of the meteorological phenomena which produce limited mixing and therefore potentially higher pollutant concentrations near the ground. The following phenomena were

identified as being of possible concern:

(i) daytime well mixed layers beneath radiation inversions;

(ii) nocturnal boundary layers;

(iii) shallow sea breezes;

(iv) internal boundary layers at the coast during onshore winds.

Daytime mixed layers and nocturnal boundary layers will be addressed in this Chapter. Mixing depths associated with coastal effects (i.e. sea breezes and internal boundary layers) will be treated in Chapters 5 and 6.

4.1 REVIEW OF METHODS FOR ESTIMATING DAYTIME MIXED LAYER DEPTH

Mixing depth is most commonly determined or inferred from measurements in the planetary boundary layer, either by regular radiosonde releases or by acoustic sounding. Measuring temperature profiles with radiosondes is a labour-intensive task usually confined to short-term field experiments. Mixing depths are commonly inferred from a single morning radiosonde record and the evolving daytime surface temperature. As will be discussed in Section 4.7, however, this method is subject to significant errors.

Acoustic sounders potentially provide the best option for obtaining routine continuous measurements of mixing depth. However, there are several drawbacks associated with acoustic sounding. The sounder record reveals levels in the atmosphere at which there are significant turbulent density fluctuations. Interpretation of the record to infer mixing depth is frequently very subjective (Russell and Uthe, 1978;

Clark et al. 1977) and should be attempted by experienced meteorologists only. In many cases, the record is unclear or non-existent, leading to considerable uncertainty. A combination of unclear records and instrument malfunction may result in data recovery which is poor relative to other meteorological sensors, which in turn limits the direct usefulness of the data for dispersion modelling. Such was the experience in KAMS, although other users (e.g. Russell and Uthe, 1978) report high reliability. One must therefore attempt to model the evolution of mixing depth, either as a means of filling data gaps or as an alternative to the use of acoustic sounder data. There are clear advantages in having a "stand-alone" mixing depth model; acoustic sounders can then be used for verification purposes, but would not be mandatory for a dispersion study. This approach is followed in the current Study, consistent with the Study objectives.

As with other models developed here, the fundamental objective is to produce reasonably reliable results over long periods using routinely available data and minimal computing resources. Consequently, the model development described herein represents the simplest practicable approach to obtain reliable estimates of mixing depth h and inversion strength $\Delta\theta$.

The growth of well mixed layers has been the subject of intense theoretical study for a number of years, by meteorologists in relation to the atmospheric boundary layer, and by oceanographers and engineers in relation to the surface layer of the ocean or of lakes. The approach which is of most interest here (relative to the stated aims above) is the development of "slab" models in which the vertical

distributions of temperature, velocity and other constituents are specified (either explicitly or implicitly). As Niiler and Kraus (1977) point out, the simplicity and physical insight afforded by this approach is adequate justification for pursuing it. Tennekes and Driedonks (1981) state that this approach provides adequate accuracy for operational purposes with relatively little effort. Accordingly, the slab model approach will be considered exclusively.

Whilst atmospheric and marine well mixed layers are governed by the same set of physical relationships, the study of the subject in the two disciplines has tended to be divergent. This has occurred partly because the differing importance of individual mixing mechanisms in the two fluids has required differing emphases, and partly because of poor communication and cross-fertilization of ideas. Tennekes and Driedonks (1981) discuss these differing approaches, including the convention amongst oceanographers to deal with integral formulations of the energy budget in the well mixed layer whilst meteorologists prefer to examine the local energy balance at the top of the well mixed layer. There is really no substantial reason for the different approaches, as demonstrated below.

There is widespread agreement on the basic physical relationships which together describe the formation and growth of well mixed layers in the atmosphere or water bodies. These will be described in Section 4.2. On the other hand, there is no clear consensus on the form of parameterization schemes which must be employed to allow the various components of the turbulent energy budget to be estimated. These

schemes will be discussed in Section 4.3 in the context of a review of relevant literature, both historic and recent. The preferred parameterization scheme, developed by Rayner (1980) for a water reservoir and adapted during KAMS for the atmospheric boundary layer will also be described in Section 4.3.

4.2 DAYTIME WELL MIXED LAYER INTEGRAL RELATIONS

Following the method of Rayner (1980) for a water reservoir, the integral relations for a well mixed atmospheric layer are derived as follows.

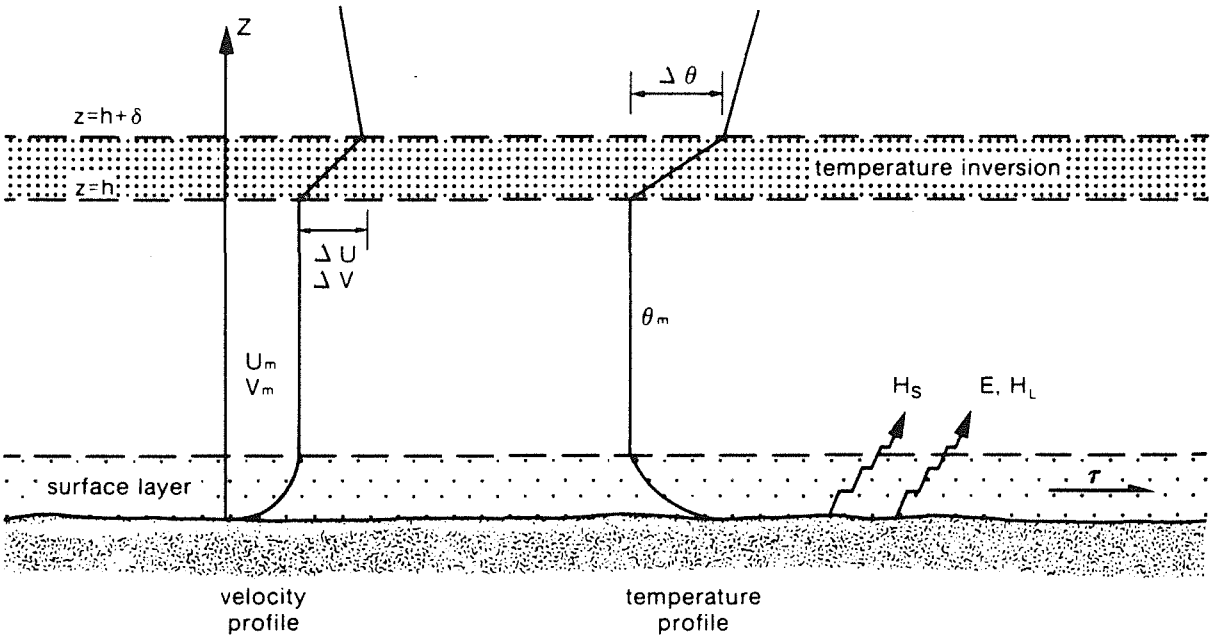

FIGURE 4.1 WELL MIXED LAYER PARAMETERS (KAMS, 1982)

Figure 4.1 shows schematically a well mixed layer above the earth's surface, bounded by an elevated temperature inversion. Wind speed and

virtual potential temperature are assumed to be uniform below the inversion, except for the shallow surface layer where the familiar logarithmic profiles are found. The parameters not employed previously (in Chapter 3) are:

U_m, V_m mixed layer velocity components

θ_m mixed layer virtual potential temperature

ΔU, ΔV inversion velocity jump components

$\Delta\theta$ inversion virtual potential temperature jump

z height variable

h height of inversion base

δ inversion thickness

Hereafter, the name well mixed layer will be abbreviated to WML, and the word temperature will mean virtual potential temperature.

Assumptions implicit in the formulation of WML models are:

(1) The WML is uniformly mixed with constituent profiles as shown in Figure 4.1, and moves as a slab.

(2) Horizontal advection of temperature or velocity variations may be ignored; hence the model is one-dimensional.

It is not strictly necessary to specify uniform profiles of temperature and velocity in order to use the integral approach described below. Instead, it is necessary that, at every level within the WML, the appropriate temperature and velocity scales are the layer averages of each variable, so that the integral method will correctly describe the various physical mechanisms involved in WML formation.

To obtain a solution giving the WML temperature, velocity and depth over time, the one-dimensional equations for heat, momentum and turbulent kinetic energy must be solved throughout the layer. With the assumed structure of Figure 4.1, it is possible to integrate these equations over the full depth ($0 \leq z \leq h+\delta$) and so include the integrated influence of all the relevant terms.

4.2.1 CONSERVATION OF HEAT

The one-dimensional equation of virtual heat (hereafter called heat), neglecting radiative transfers, may be written as

$$\partial\theta/\partial t = - \partial\overline{\theta' w'}/\partial z \qquad (4.1)$$

Manins (1982) points out that horizontal advection of heat may be important, however lack of horizontal temperature gradient data usually precludes the inclusion of these effects. Driedonks (1982) determined that horizontal advection was not important in his data set. He also determined that humidity variations may be important which supports the use of virtual temperature and virtual heat.

Integration of (4.1) across the WML and the inversion, assuming δ is very small (to be discussed later) and neglecting turbulent fluxes above $z = h + \delta$, gives

$$h d\theta_m/dt = \Delta\theta dh/dt + H_v/(\rho C_p) \qquad (4.2)$$

The right hand first term comes directly from the application of Leibnitz's Rule, recognising that the integration limit $z = h + \delta$ varies with time. Failure to apply this Rule has led some researchers into error and unnecessary complications, as will be seen later.

4.2.2 CONSERVATION OF MOMENTUM

The equation for horizontal momentum may be split into x and y components, with mean velocities U and V respectively:

$$\partial U/\partial t = fV - fV_g - \rho^{-1}\partial\tau_x/\partial z \qquad (4.3)$$

$$\partial V/\partial t = -fU + fU_g - \rho^{-1}\partial\tau_y/\partial z \qquad (4.4)$$

where U_g and V_g are the components of the geostrophic wind, and f is the Coriolis parameter. Above the inversion where the stress is negligible, (4.3) and (4.4) describe the inertial oscillation of the air mass, as discussed by Manins (1982). Below the inversion these equations may be integrated over the WML depth to give:

$$h\frac{\partial U_m}{\partial t} = fV_m h - f\int_0^h V_g\,dz + \Delta U\frac{dh}{dt} - \frac{\tau_x}{\rho} \qquad (4.5)$$

$$h\frac{\partial V_m}{\partial t} = -fU_m h + f\int_0^h U_g\,dz + \Delta V\frac{dh}{dt} - \frac{\tau_y}{\rho} \qquad (4.6)$$

To evaluate the integrals in (4.5) and (4.6), one must specify $U_g(z,t)$ and $V_g(z,t)$ which in turn requires knowledge of the synoptic scale horizontal temperature gradients as functions of z and t.

4.2.3 CONSERVATION OF TURBULENT KINETIC ENERGY

Following Denman (1973), the equation for turbulent kinetic energy (hereafter TKE) may be written as:

$$\underset{(1)}{\frac{1}{2}\frac{\partial E}{\partial t}} = \underset{(2)}{-\overline{u'w'}\frac{\partial U}{\partial z}} \underset{(3)}{-\frac{\partial}{\partial z}\left[\overline{w'\left(\frac{p'}{\rho}+\frac{E}{2}\right)}\right]} \underset{(4)}{-\frac{g}{\rho}\overline{\rho'w'}} \underset{(5)}{-\varepsilon} \qquad (4.7)$$

The various numbered terms are defined below.

(1) time rate of change of turbulent kinetic energy, E, in the WML, where $E = \overline{(u'^2 + v'^2 + w'^2)}$

(2) production of TKE due to the working of the Reynolds stress ($\overline{u'w'}$) on the mean shear,

(3) divergence of the vertical flux of TKE induced by pressure (p') and velocity fluctuations at the upper and lower boundaries,

(4) TKE expended in working against buoyancy forces ($g\overline{\rho'w'}/\rho = -g\overline{\theta'w'}/T_v$), recalling that θ is virtual potential temperature,

(5) rate of destruction of TKE by viscous dissipation.

Unlike temperature and velocity, it is not reasonable to consider TKE as being well mixed throughout the layer (see Willis and Deardorff, 1974). For the purpose of this analysis, a vertically averaged level of TKE may be defined:

$$E_m = \frac{1}{h}\int_0^h E\, dz \qquad (4.8)$$

Similarly, a vertical averaged WML dissipation rate is:

$$\varepsilon_m = \frac{1}{h}\int_0^h \varepsilon\, dz \qquad (4.9)$$

Integration of (4.7) across the WML and the inversion yields:

$$\frac{1}{2}h\frac{dE_m}{dt} = -\frac{E_m}{2}\frac{dh}{dt} - \int_0^{h+\delta} \overline{\underline{u}'w'}\frac{\partial \underline{U}}{\partial z}dz - \left[\overline{w'\left(\frac{p'}{\rho} + \frac{E}{2}\right)}\right]_{z=0}$$

$$+ \frac{gh}{2T_v}\left[\frac{H_v}{\rho C_p} - \Delta\theta\frac{dh}{dt}\right] - \varepsilon_m h \qquad (4.10)$$

where turbulent fluxes and energy loss via internal waves above the inversion have been neglected.

4.3 PARAMETERIZING THE DAYTIME TURBULENT ENERGY BUDGET

The integrated turbulent kinetic energy equation (4.10) is clearly not in a form suitable to yield information on MML growth. The various source and sink terms must first be parameterized in terms of measurable mean flow quantities. As previously mentioned there has been a considerable volume of work published over the past two decades describing alternative parameterization schemes for application to the atmospheric and marine well mixed layers. The generalised parameterization scheme proposed by Rayner (1980) for a water reservoir (which is summarized by Spigel, Imberger and Rayner, 1986) has been adapted to describe the growth of atmospheric well mixed layers.

4.3.1 MECHANICAL MIXING AT THE SURFACE

Near the surface, there is a contribution to TKE from shear production and pressure fluctuations in the boundary layer. Kraus and Turner (1967), and Niiler and Kraus (1977) describe these contributions as the working of the wind, given by the stress times a wind velocity scale. This may be expressed in the form:

$$-\int_0^h \overline{\underline{u}'w'}\frac{\partial \underline{U}}{\partial z}dz - \left[\overline{w'\left(\frac{p'}{\rho}+\frac{E}{2}\right)}\right]_{z=0} = \frac{C_N{}^3}{2}u_*{}^3 \qquad (4.11)$$

where u_* is the friction velocity and C_N is a constant (to be specified) which relates to production of TKE but does not attempt to account for dissipation, which is handled separately.

4.3.2 SHEAR INDUCED MIXING AT THE INVERSION

TKE is also produced by shear across the inversion. Employing integration by parts, it is simply shown that:

$$-\int_{h}^{h+\delta} \overline{\underline{u}'w'} \frac{d\underline{U}}{dz} dz = \frac{1}{2}\left[\Delta U^2 + \Delta V^2\right]\frac{dh}{dt} \qquad (4.12)$$

This result indicates that the kinetic energy lost due to entrainment of quiescent fluid becomes available to work locally to further deepen the layer. Pollard, Rhines and Thompson (1973) and Manins (1982) considered this term to represent the dominant mixing mechanism. By equating this source term with the buoyancy sink term in (4.10), these authors derive a Froude No. criterion,

$$Fr = gh\Delta\theta/[T_v(\Delta U^2 + \Delta V^2)] = 1 \qquad (4.13)$$

In other words, growth of the MML occurs whenever $Fr \to 1$. Although shear production may be a dominant mechanism in the ocean MML, it has been found to be generally a secondary mechanism in the atmosphere and so the Froude No. criterion is not generally applicable. This issue will be addressed further in Section 4.3.8.

4.3.3 BUOYANCY INDUCED MIXING

The term $ghH_v/(2\rho C_p T_v)$ is, by definition, $\frac{1}{2}w_*^3$ where w_* is the buoyancy velocity scale first introduced by Deardorff (1970). A useful feature of the integral approach in Section 4.2 is that terms like w_* are formally derived rather than having to be introduced via an external scaling argument, as done by Zeman and Tennekes (1977).

4.3.4 COMBINED SURFACE ENERGY SOURCES

It is convenient to combine the surface mechanical and buoyancy source terms of Sections 4.3.1 and 4.3.3 into a single parameter:

$$\tfrac{1}{2}q_*^3 = \tfrac{1}{2}(w_*^3 + C_w^3 u_*^3) \qquad (4.14)$$

Again, this combination occurs as a matter of course in following the integral approach. By way of contrast the derivation of a combined surface source term for the local energy balance approach is confused. Driedonks (1982) and Tennekes and Driedonks (1981) both speak of a "useful interpolation formula" but are unable to agree as to whether the square or cube of the source terms should be added. The form of (4.14) (adding the cube of w_* and u_*) is clearly correct; it correctly accounts for the case of weak mixing when surface cooling is occurring but $C_w^3 u_*^3 > -w_*^3$.

4.3.5 DISSIPATION

There are differing views in the marine and atmospheric literature on the most appropriate means of parameterizing dissipation of TKE. Niiler and Kraus (1977) favour the reduction of each individual source term by an efficiency factor. Mahrt and Lenschow (1976), Zeman and Tennekes (1977) and others favour a combined parameterization of the form:

$$\varepsilon_m h = \tfrac{1}{2} C_\varepsilon E_m^{3/2} \qquad (4.15)$$

The laboratory experiments of Willis and Deardorff (1974) support this form for surface sources of TKE, and hence it is adopted here. However, as pointed out by Rayner (1980) and Driedonks (1982), it is likely that a large fraction of the TKE generated by shear at the

inversion is dissipated locally without being fed into the MML. In other words, shear generated TKE is expended locally in smearing the interface (i.e. increasing the local potential energy) and by dissipation. Therefore, it seems appropriate to parameterize the local dissipation due to shear at the inversion by a separate efficiency factor C_s, yielding the modified shear production term

$\frac{1}{2} C_s(\Delta U^2 + \Delta V^2)dh/dt$.

Zeman and Tennekes (1977) include a separate dissipation term for the thin inversion region where h is not the appropriate length scale. The appropriate form of this term is not clear, and its inclusion has been found to give no significant improvement (Driedonks, 1982) so it will not be included in the present Study.

4.3.6 CLOSURE ASSUMPTION

The vertical integral models of Miller and Kraus (1977) neglected terms in (4.10) involving the TKE level E_m in order to close the equation set. However, the formulation of Tennekes (1973) suggests a closure scheme whereby E_m may be explicitly retained. He argues that the TKE flux convergence beneath the inversion must scale as σ_w^3/h, where σ_w^2 is the vertical component of TKE and σ_w is taken as a vertical velocity scale. This flux in turn provides the energy for local sinks at the inversion. Tennekes (1973) identified only one sink (apart from dissipation), being the energy required to entrain fluid into the MML, as represented by the term $\frac{1}{2} gh\Delta\theta(dh/dt)/T_v$ in (4.10). Zeman and Tennekes (1977) subsequently introduced a second sink term to account for the energy required to "spin up" the entrained

quiescent fluid, as represented by the term $-\frac{1}{2} E_s(dh/dt)$ in (4.10). The detailed derivation of this term described by these authors corresponds to the simple application of Leibnitz's Rule in the integral method.

Tennekes and Driedonks (1981) state that most authors agree on the use of a flux convergence hypothesis along the above lines if a local energy budget is employed. In fact, this perceived difference between the local and integral approaches has no substance, since a corresponding hypothesis may be employed in the integral method.

Considering the integrated energy balance of (4.10) Rayner (1980) hypothesised a similar energy transfer mechanism to provide closure. This is stated here in two parts:

i) The flux of TKE directly below the inversion may be modelled by $-\frac{1}{2} C_F E_s^{3/2}$ where $E_s \propto \sigma_w^2$,

ii) This flux, together with any local TKE production, supplies all energy sinks at the inversion.

From inspection of (4.10) the following expression satisfies (i) and (ii) above:

$$-\frac{C_F}{2} E_s^{3/2} = \frac{C_S}{2}\left[\Delta U^2 + \Delta V^2\right]\frac{dh}{dt} - \frac{gh\Delta\theta}{2T_v}\frac{dh}{dt} - \frac{E_s}{2}\frac{dh}{dt} \qquad (4.16)$$

Equation (2.10) may now be rewritten as two equations with the foregoing parameterizations introduced:

$$dE_s/dt = [q_s^3 - (C_F + C_\varepsilon)E_s^{3/2}]/h \qquad (4.17)$$

$$dh/dt = C_F E_s^{3/2}/[E_s + gh\Delta\theta/T_v - C_S(\Delta U^2 + \Delta V^2)] \qquad (4.18)$$

Given values for the various coefficients and the necessary meteorological data, equations (4.17), (4.18), (4.2), (4.5) and (4.6) may be solved to evaluate E_m, h, θ_m, U_m and V_m.

4.3.7 EVALUATION OF COEFFICIENTS

Information from field and laboratory experiments may be employed to evaluate the coefficients C_F, C_E, C_N and C_S. The following items of information allow this evaluation with a degree of redundancy for checking purposes.

(a) Willis and Deardorff (1974):

$E_m/2 = K_{em} w_*^2$, $K_{em} \approx 0.4$

for steady-state, free convection conditions. Steady-state, in the present context, means constant surface inputs (i.e. q_*^3 constant).

(b) Willis and Deardorff (1974), Kaimal et al. (1976), Mahrt and Lenschow (1976):

$\varepsilon_m = K_\varepsilon w_*^3$, $K_\varepsilon \approx 0.4 \rightarrow 0.5$

for steady-state, free convection conditions.

(c) Willis and Deardorff (1974), Stull (1976):

$\overline{\theta' w'}(h)/\overline{\theta' w'}(0) = K_a$, $K_a \approx 0.1 \rightarrow 0.3$

for steady-state, free convection entrainment of a strong density jump.

(d) Deardorff (1974):

$dh/dt = K_w w_*$, $K_w \approx 0.2$

for steady-state growth of a convective layer into a neutral environment.

(e) Wu (1973), Kato and Phillips (1969):

$$dh/dt = K_p u_*^3 T_v/(gh\Delta\theta), \quad K_p \approx 0.234 \text{ (Wu)}$$

$$\approx 2.5 \text{ (Phillips)}$$

for steady-state growth of a layer with a strong density jump. In Wu's experiment, turbulence was generated by wind shear in a wind/wave tank, with negligible internal shear. The Kato and Phillips experiments were conducted in an annular tank with surface shear. Internal shear generation of TKE was important in this case.

(f) Tennekes and Lumley (1972):

$$dh/dt = K_u u_*, \quad K_u \approx 0.3$$

for growth of a layer into a neutral environment with turbulence generated by surface wind shear.

Rayner (1980) derived the following relationships between the model coefficients and those represented in the experimental information:

$$C_F = K_a(2K_{em})^{-3/2} \tag{4.19}$$

$$C_E = (1 - K_a)(2K_{em})^{-3/2} \tag{4.20}$$

with the redundant information

$$K_u = C_F(C_F + C_E)^{-1/3} \tag{4.21}$$

Also,

$$C_N^3 = K_p/K_a \tag{4.22}$$

with the redundant information

$$K_u = C_F C_N(C_F + C_E)^{-1/3} \tag{4.23}$$

or

$$C_N = K_u(C_F + C_E)^{1/3}/C_F \tag{4.24}$$

with the redundant information

$$K_p = K_a C_N^3 \qquad (4.25)$$

A comprehensive analysis of the various combinations of these coefficients was carried out, bearing in mind the experimental uncertainty of values stated in (a) to (f) above. A self-consistent set, chosen as a result of this analysis, is as follows:

$K_{es} = 0.4$, $K_e = 0.41$, $K_a = 0.18$

$C_F = 0.25$, $C_E = 1.15$, $K_u = 0.22$

Equations (4.22) and (4.23) give (for $K_p = 0.234$)

$C_N = 1.09$ $K_u = 0.25$

Equations (4.24) and (4.25) give (for $K_u = 0.3$)

$C_N = 1.33$ $K_p = 0.42$

These values of K_{es}, K_e, K_a and K_u are within 10% of their expected values, as detailed in (a) to (f) above, giving confidence to the method of determination. K_u calculated from (4.23) is somewhat lower than the expected value. Alternatively, the calculated value of K_p from (4.25) is somewhat larger than Wu's estimate from (e). The latter is accepted as correct on the basis that in Wu's experiment, the wind/wave interaction would not have been fully developed in his small (2.3 m long) tank. The chosen value is much smaller than that for the Kato and Phillips experiment, as would be expected if internal shear was dominant in their case.

It should be noted at this point that the acceptance of a K_p value of 0.42 differs significantly from the value of 5 derived by Kantha et al. (1977) and utilized by Driedonks (1982) in order to simulate his field data. Further discussion on this important issue will be deferred until Section 4.6 where it can be viewed in the light of KAMS

field data.

The only coefficient as yet undetermined is C_s. Experimental evidence from which to determine C_s is sparse. Sherman, Imberger and Corcos (1978) summarise the available information, concluding that $C_s = 0.3$ is the best available estimate. From this and other papers it appears that C_s may fall between 0.2 and 0.5.

4.3.8 COMPARISON WITH OTHER MODELS

The model described in the foregoing Section is the only one known to the author which explicitly retains the TKE variable E_m in the solution. Imberger (1985) evaluated this model's performance in simulating a diurnal cycle of heating and mixing within Kellington Reservoir for which a comprehensive, high quality set of data was available. The model showed a high level of skill in simulating the temperature structure throughout the day, supporting the results of Rayner (1980). Imberger examined the relative importance of various terms in the model equations and demonstrated that the energy storage term, hdE_m/dt, plays a significant role in regulating the mixing in the diurnal mixed layer when surface meteorological forces are variable. Since the surface forcing term q_*^3 is proportional to the cube of the wind velocity, it is important to ensure that short term (e.g. 10 minute) wind speed maxima are not averaged out in the input data. By directly computing the energy storage via (4.17), and utilizing this value to compute the the "spin up" term in the denominator of (4.18), fluctuating meteorological data may be accepted without impacting on the numerical stability of the model.

The importance of the time derivative of E_a in a model of the atmospheric MML is somewhat less than in a model of diurnal cycles in a water body. Apart from the transient periods around sunrise and sunset, there is a close balance in the atmosphere between sources and sinks of energy, with the sources being dominated by convective mixing, which is itself governed by the surface heat budget and therefore not subject to large rapid fluctuations. A good approximation to the MML behaviour can therefore be obtained from a simplified model which neglects the temporal TKE term, in which case (4.17) and (4.18) reduce to a single equation:

$$dh/dt = C_K q_*^3/[C_T q_*^2 + gh\Delta\theta/T_v - C_S(\Delta U^2 + \Delta V^2)] \qquad (4.26)$$

where $C_T = (C_F + C_E)^{-2/3}$

$C_K = C_F/(C_F + C_E)$

An entrainment relation in the form of (4.26) was first proposed by Sherman, Imberger and Corcos (1978) for oceans or lakes, although some aspects of their derivation differ from the above. It is also essentially the same as that proposed by Driedonks (1982) for the atmosphere, if the inversion-base dissipation term used by that author is neglected.

Given the values of C_F and C_E derived in the previous Section, the coefficients in (4.26) have the values $C_K(=K_a) = 0.18$ and $C_T = 0.8$. The value of $C_K \approx 0.2$ has wide acceptance. The value of C_T derived by Driedonks (1982) is unfortunately affected by his acceptance of the Kantha et al. (1977) result, as previously mentioned, and so cannot be meaningfully compared to the above figure. However, the definition of

C_T and the method of evaluation are identical. Driedonks (1982) finds the "spin up" term $C_T q_*^2 dh/dt$ to be of little importance in modelling his field data. Nevertheless, there are clearly occasions on which the term would be significant and so it should be retained.

Noting the foregoing favourable comparison with other water and air studies, it is appropriate to restate that the generalised model given by (4.17) and (4.18), and the simplified version given by (4.26), have been developed using a combination of accepted principles from both oceanographic and atmospheric research, demonstrating that the conventional methods in these two fields of research can be reconciled into a generalised approach.

Driedonks (1982) and Driedonks and Tennekes (1984) discuss problems experienced in solving their version of (4.26) due to the behaviour of the shear term growing and forcing the denominator to turn negative, thus giving nonsensical results. It is evident that the numerical solution employed by these authors is not suited to the task. A stable scheme, employing a dynamic timestep adjustment process, will correctly model the rapid deepening rates which accompany shear growth and will ensure that the denominator stays positive. If the scheme in use is not capable of solving (4.26) directly, an explicit form of (4.26) may be used, as follows:

$$dh/dt = [C_K q_*^3 + C_S(\Delta U^2 + \Delta V^2)R]/[C_T q_*^2 + gh\Delta\theta/T_v] \qquad (4.27)$$

where R is an entrainment rate determined from the preceding timestep.

Having identified the numerical problem, Driedonks and Tennekes assume tentatively that inversion shear effects can be incorporated into

other shear effects associated with surface friction. Whilst this assumption may not lead to significant errors when modelling atmospheric MMLs it is clearly inappropriate for water bodies, where the timescale for changes in mean MML momentum (and hence also ΔU and ΔV) is far greater than the timescale for changes in wind-induced stress.

Meteorologists are in disagreement over the relative importance of the inversion shear mechanism: Manins (1982) considers it to be the major mechanism, while Mahrt and Lenschow (1976) and Deardorff (1979) consider it to be almost always insignificant in the atmosphere (but not the ocean). Driedonks (1982) obtained good agreement between field results and model results with the shear contribution neglected.

There have been two recent developments relating to the shear production mechanism. Firstly, Deardorff (1983) has developed an elaborate scheme in which the thermocline or inversion thickness δ is assumed to represent the integral length scale at the interface. He parameterizes δ/h in terms of three separate Richardson Numbers based on surface stress, convection and internal shear respectively. Secondly, Spigel et al. (1986) have extended the integral approach to include a thick interface, in order to more accurately model MML deepening when internal shear is a dominant mechanism. The resultant equations are far more cumbersome than those presented above. Both of these developments may be applied to the atmospheric MML, but they are primarily aimed at marine or reservoir MMLs where internal shear is known to be important. Driedonks and Tennekes (1984) choose not to pursue Deardorff's (1983) method on the basis that it is unlikely to

lead to significantly better predic ions in atmospheric problems.

Inclusion of the inversion shear terms in (4.2.6) necessitates the solution of the momentum equations within and above the MML, which in turn requires knowledge of the synoptic horizontal temperature gradients (see the discussion in Section 4.2.2). Such data are not readily available on a routine basis and hence there appears to be no way of confidently computing the inversion shear contribution for most applications.

Investigation of the importance of inversion shear contribution in the present Study was limited to a single field experiment, which will be discussed in Section 4.6. On the basis of the negative finding from that investigation, and the points discussed above, the shear term has been neglected in the mixing depth model.

4.4 NOCTURNAL BOUNDARY LAYERS

The nocturnal boundary layer (NBL) is that layer adjacent to the earth's surface within which turbulence generated by shear stress persists against the damping forces of the stable vertical temperature gradients, which are established by radiative cooling of the surface. The turbulent kinetic energy level, indicated by the magnitude of σ_w, has its maximum at the surface and decreases to zero at the top of the NBL.

Weil (1985) provides a very useful overview of the state of knowledge relating to diffusion in the nocturnal boundary layer, including a

brief review of methods for predicting the NBL height. His stated primary reason for determining the NBL height within a dispersion analysis is to determine whether buoyant emissions from elevated sources lodge above the NBL or within it. Plumes which level out above the top of the NBL are expected to have no ground level impact on the surrounding region (i.e. they will not mix to ground level). The NBL height is also employed in a parameterization of σ_w, which Weil suggests may be used to calculate vertical dispersion.

Having introduced the NBL at the start of this Chapter as an example of limited mixing which may potentially be of concern (i.e. by causing elevated ground level concentrations), it will now be argued that the height of the NBL is not a parameter of interest in the current Study. This in turn will justify the avoidance of what is a major research topic in itself. In this regard Mahrt (1981) points out that the stable planetary boundary layer height is one of the most difficult characteristics of the stable boundary layer to determine from observations and that such a determination should be avoided where possible.

As will be described in greater detail in Chapter 6, it is standard practice to include "reflection terms" within a Gaussian plume model which simulate the "lid" effect at the top of the daytime MML and the continued mixing throughout the MML of pollutants which may have reached the height of the lid at some distance downwind. If NBLs were to be considered within a model, it would not be valid to treat them in the same way as daytime well mixed layers because:

(a) they are not well mixed,

(b) they have no capping "lid".

In other words, there is no analagous mechanism of "reflection" at the top of the NBL. Any pollutants which reach the upper limit of a NBL will be trapped rather than reflected, since the turbulent energy level and associated mixing rate at this height are very small (Caughey et al., 1979).

Accordingly, it is thought that the only valid direct use of the NBL height in a conventional Gaussian plume model is in determining whether a plume has risen above the NBL and therefore may be considered to have zero impact on the surrounding area.

As stated in Chapter 1, the current Study objectives limit the region of interest to within about 15 km of the source, within which distance the most significant primary pollution impacts will be experienced. Over this relatively short distance, the impact of plumes from elevated sources in stable conditions is very small (in most cases negligible), whether or not the plumes escape above the NBL. Consequently there is little justification in the current Study for including a simulation of NBL heights.

On a more general basis, it may be argued that the phenomenon of plumes escaping NBLs should be neglected in air pollution prediction models as a conservative measure, at least until such time as the confidence in accurately predicting NBL heights reaches a reasonable level. The penalty associated with neglecting NBL heights is minor; relatively low levels will be predicted at large distances from the

source. Short term (e.g. one hour average) levels predicted in this way are likely to be small compared to the levels which may actually occur during morning fumigation events, that is, when a plume originally trapped above the NBL is engulfed by a growing daytime mixed layer. Modelling of fumigation is of far greater importance than modelling the trapping or otherwise of elevated plumes in stable conditions, but it will not be addressed in this Study, again because of the limited scale of interest.

The intentions stated above are simply achieved in a conventional Gaussian plume model by setting the "mixing height" equal to a very large number in stable conditions, so that the "reflection" calculations are not invoked. An estimate of the NBL height is required each morning shortly after sunrise however, to provide an initial value for the well mixed layer height simulation. As Tennekes (1973) points out, the precise value chosen initially tends not to be particularly important because the well mixed layer height simulation rapidly loses its dependence on the initial value. Accordingly, the simple NBL height formula proposed by Venkatram (1980a) was adopted:

$$h = 2.4 \times 10^{3}\ u_{*}^{3/2} \qquad (4.28)$$

This formula showed considerable skill in describing the data analysed by Venkatram, and is attractive in that it is well behaved around the evening and morning transition periods, even though it does not directly apply to these periods. To take account of the slow response of the NBL to changing winds, u_{*} may be averaged over the hour (or thereabouts) preceding the morning prediction.

4.5 A MODEL OF ATMOSPHERIC MIXING DEPTH

The computer model described in this Section was developed to predict the mixing depth associated with radiation inversions, based on the theory presented in Sections 4.2 and 4.3. In this model, subsidence inversions modify the growth of the mixed layer via their presence in the initial model temperature profile taken from an airport radiosonde record. However, subsidence is not dynamically modelled.

A flow diagram of the model is provided in Appendix C. The computer model employs a number of innovative features necessary to implement the theoretical results. These are described below, together with an overview of the model structure.

4.5.1 MODEL INPUT DATA

The main input data file is the output file of the model SOIL described in Chapter 3. The contents of this file are:
DATE DAY TIME H_v, u_*, 10/L, T_v, θ, U, direction, sigma.
Here, θ is the potential air temperature measured at 10 m height, and T_v is the corresponding absolute virtual temperature. Wind direction and sigma (direction variation) are carried passively through the model so as to be included in the output file for subsequent use in a dispersion model.

4.5.2 NIGHT TO DAY TRANSITION

At the start of each modelled day, as signified by a change of day

number in the input data, the times of sunrise and sunset (in minutes) are computed. A summary is given in Appendix A of the solar radiation theory involved in this computation.

A continuous check is maintained to see if the model time has advanced to that of sunrise. Following sunrise, the model initiates a check to determine if there is sufficient production of turbulent kinetic energy at the surface to increase the mixing height above the calculated NBL height; i.e. q_*^3 from (4.14) is positive. Typically, this may occur half an hour after sunrise, by which time the solar heating is significant. From this time until sunset or later, the mixing depth will be determined from a solution of (4.26) and (4.2).

4.5.3 DETERMINING THE INVERSION TEMPERATURE JUMP

Equations (4.26) and (4.2) both contain the term $\Delta\theta$, being the jump in temperature across the inversion. This may be expressed as

$$\Delta\theta = \theta_m - \theta_i \qquad (4.29)$$

where θ_i is the temperature immediately above the inversion (see Figure 4.2). With θ_m coming from the solution of (4.2), it remains to specify or compute θ_i throughout the day.

The only viable option in this Study was to utilise the morning (0700 WST) radiosonde data from Perth Airport, which were processed to produce virtual potential temperature profiles up to 5000 m. (WST denotes local (Western) standard time.) It is assumed that the temperature structure above the modelled mixed layer remains unchanged

from that of the morning sonde profile: hence the dynamics of subsidence, horizontal temperature gradient advection and radiation divergence are neglected. The neglect of the first two of these influences is supported by the findings of Driedonks (1982) and radiation divergence is likely to be a detectable influence at night-time only. For the purposes of dispersion modelling, these assumptions are expected to be quite satisfactory, since early morning limited mixing depths will be calculated with maximum confidence, and accuracy will be less important later in the day when mixing depths are large. Values of θ_i throughout the day are extracted from the profile for the current mixing height, as will be described in the next Section.

4.5.4 DAYTIME INITIALIZATION

The following procedures are invoked by the model at the time q_* first goes positive after sunrise.

(a) Loading a Morning Temperature Profile (SUBROUTINE LOAD)

The processed sonde profile for the morning is read in with the following format:

DATE DAY TIME NN BST (HEIGHT - TEMPERATURE PAIRS)

where NN is the number of pairs and BST is the 10 m level temperature from the Wattleup Base Meteorological Station at the sonde release time . (This temperature value is inserted into the sonde data when the data are being processed.)

The program which processes the radiosonde data ensures that there are no time gaps in the processed file by inserting records, if necessary, with zero levels (i.e. NN = 0) Other anomalies can also cause profile deletion, giving NN = 0. If such a record is encountered, the model sets the ground level temperature $\theta(1)$ equal to BST. It then synthesises a profile using the default lapse rates which are read in at the commencement of a model run. This default information specifies a standard shape of temperature profile for each month, determined from prior extensive visual inspection of sonde data.

The radiosonde data may produce profiles up to only a limited height, probably reflecting instrument failure. These profiles are extended to 5000 m by appending profile levels which follow the standard shape for that month.

These correction procedures, whilst scarcely ideal, are necessary to improve continuity of the model. Fortunately, they are required infrequently..

(b) Correcting the Time Difference

It is most unlikely that the model time at which q_* goes positive will be exactly the sonde release time (usually 0700). If the model time indicates commencement of mixing prior to 0700 (e.g. during summer) the sonde profile is likely to show a modified structure near the ground from which it is difficult to infer the

"unmixed" profile shape. Alternatively, mixing may commence after 0700 (e.g. in winter), in which case the sonde profile should be quite representative of the initial "unmixed" profile. The profile correction procedure adopted is as follows: the lowest (ground level) profile temperature is corrected for the change in temperature between sonde release time and model time by subtracting the corresponding change at the Wattleup meteorological station - hence the requirement of BST in the sonde data. If significant mixing has modified the sonde profiles, the second and higher levels may also warrant correction, but this is not practicable.

(c) Specifying the WML Temperature

The final step in the process of specifying the vertical temperature profile for a day is to determine an appropriate initial value for the WML temperature θ_w. The initial value for the WML depth (or inversion height) h is taken as the calculated value of the NBL height. Determination of θ_w depends on the position of the inversion relative to the sonde levels, which may fall into one of two categories:

(i) $z(1) < h < z(2)$

In this case, the inversion is below the first elevated level z(2). $\theta(1)$ is constrained to be less than $\theta(2)$ (i.e. a stable density structure). Figure 4.2 illustrates the following points. The best available estimate for θ_w is $\theta(1)$, as this value will

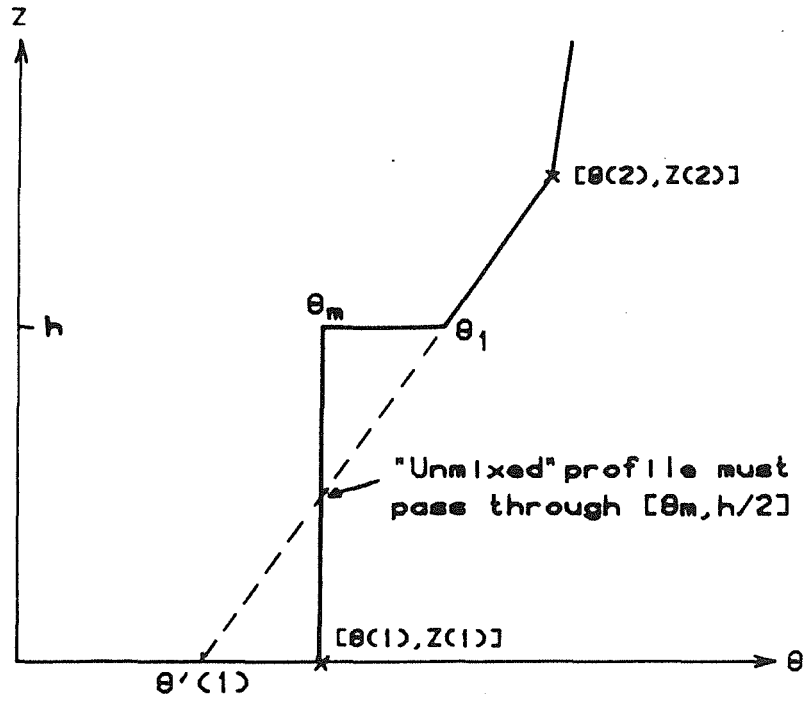

FIGURE 4.2 INVERSION IN LOWEST SONDE PROFILE LAYER

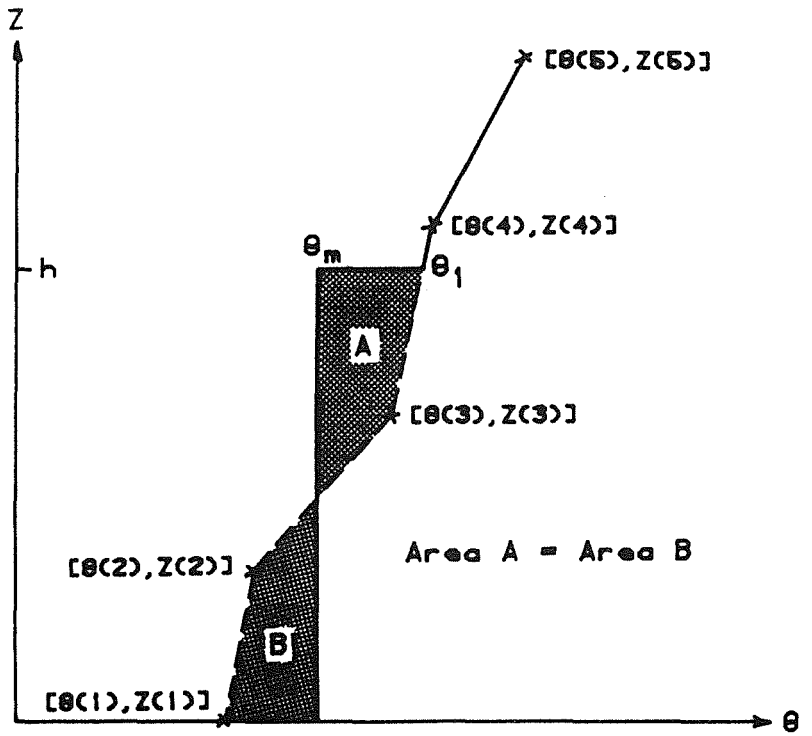

FIGURE 4.3 INVERSION IN AN ELEVATED SONDE PROFILE LAYER

reflect the existing mixing at the time. (Recall that q_* goes positive only when there is enough energy input to fully mix the NBL and deepen it further, so mixing within the NBL will be at least partially established at this time.) It is also necessary to know the slope of the temperature profile above h in order to determine θ_1 by linear interpolation as the simulation proceeds. For this purpose, having set θ_m, $\theta(1)$ is modified to an 'unmixed' value shown as $\theta'(1)$ such that the heat content of the layer is conserved. It is easily shown that

$$\theta'(1) = \theta(1) - \frac{h}{2}\left[\frac{\theta(2) - \theta(1)}{z(2) - z(1)}\right] \qquad (4.30)$$

θ_1 is subsequently determined from

$$\theta_1 = \theta'(1) + [h - z(1)]\left[\frac{\theta(2) - \theta'(1)}{z(2) - z(1)}\right] \qquad (4.31)$$

(ii) $h > z(2)$

If the initial MML height places the inversion in an elevated layer of the sonde profile, the only consistent approach is to apply conservation of heat and so determine θ_m. This procedure is shown schematically in Figure 4.3, where the shaded areas are equally distributed about the MML profile. As before, the profile is constrained to be stable, i.e. $\theta_m < \theta_1$. The value of θ_1 (and hence $\Delta\theta$) in the layer z(J) to z(J+1) are subsequently determined from

$$\theta_1 = \theta(J) + [h - z(J)]\left[\frac{\theta(J+1) - \theta(J)}{z(J+1) - z(J)}\right] \qquad (4.32)$$

4.5.5 DAYTIME INVERSION EROSION

Integration of the layer deepening and heat equations (4.26) and (4.2), to give the evolution of h and θ_* throughout daylight hours, is performed by a fourth order Runge Kutta scheme as described in Section 3.3.5. At each Runge Kutta step, q_*^3 and $\Delta\theta$ are evaluated and used to compute the derivatives. The integration time-step is matched to the 10 minute meteorological flux data although the integration scheme does invoke time-step halving if necessary to maintain numerical stability.

4.5.6 WELL MIXED LAYER STAGNATION AND TRANSITION TO THE NOCTURNAL SITUATION

The computation of q_* described in Section 4.5.2 continues throughout the day. If q_* goes negative, a check is made to see if the model time has passed the time of sunset. It is possible that q_* may go negative during the day due to a change in meteorological conditions (especially solar insolation or rainfall). In this event, the WML is assumed to be stagnant (h does not change) and (4.2) is solved alone to describe the change of θ_*. If however the model has advanced past sunset, it sets h to a large recognisable number (usually 999 m) for the rest of the nocturnal period. The NBL height from (4.28) is in fact calculated throughout the night so that the averaged values are available at the time of sunrise.

4.5.7 MODEL OUTPUT DATA

Data records in the output file have the following format:

DATE DAY TIME h, H_v, u_*, 10/L, T_v, θ, U, Direction, Sigma, θ_s, $\Delta\theta$

Nocturnal records omit the last two variable, θ_s and $\Delta\theta$, and are easily identified by this omission plus the large constant value of h.

4.6 SIMULATION OF AN OBSERVED RADIATION INVERSION EROSION

In order to test the model described in Section 4.5, a field study of radiation inversion erosion was conducted on the 29th October 1980. In brief, the key elements of the field study were:

(i) hourly slow-ascent radiosonde releases with dual theodolite tracking to provide estimates of the time evolution of temperature and velocity profiles,

(ii) operation of a monostatic acoustic sounder,

(iii) routine measurements at the Hope Valley Base Station, augmented by measurements of net radiation, ground heat flux and ground temperature, giving a comprehensive set of data from which turbulent fluxes could be calculated.

Calculation of turbulent fluxes via the heat budget model (SOIL) and the tower profile method (HVFLUX) for this field study has been described in Section 3.4. The results of calculations have been replotted in Figures 4.4 and 4.5 in a slightly different form (notably the inclusion of mean wind speed and friction velocity). The calculation results will not be rediscussed except to note that during

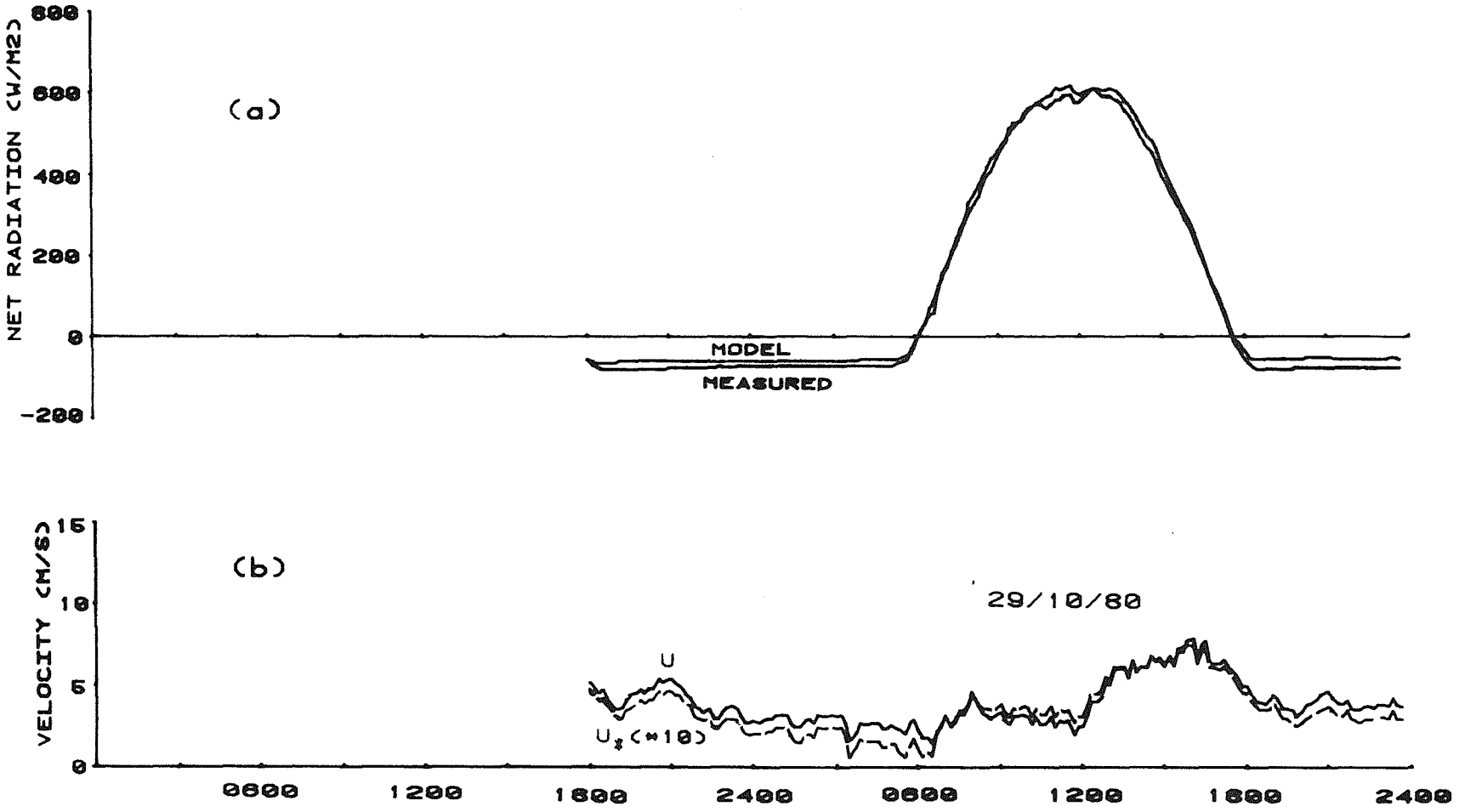

FIG 4.4 RESULTS OF MODEL SOIL

(a) Modelled and measured net radiation
(b) Wind speed(measured) and frict.velocity(modelled)

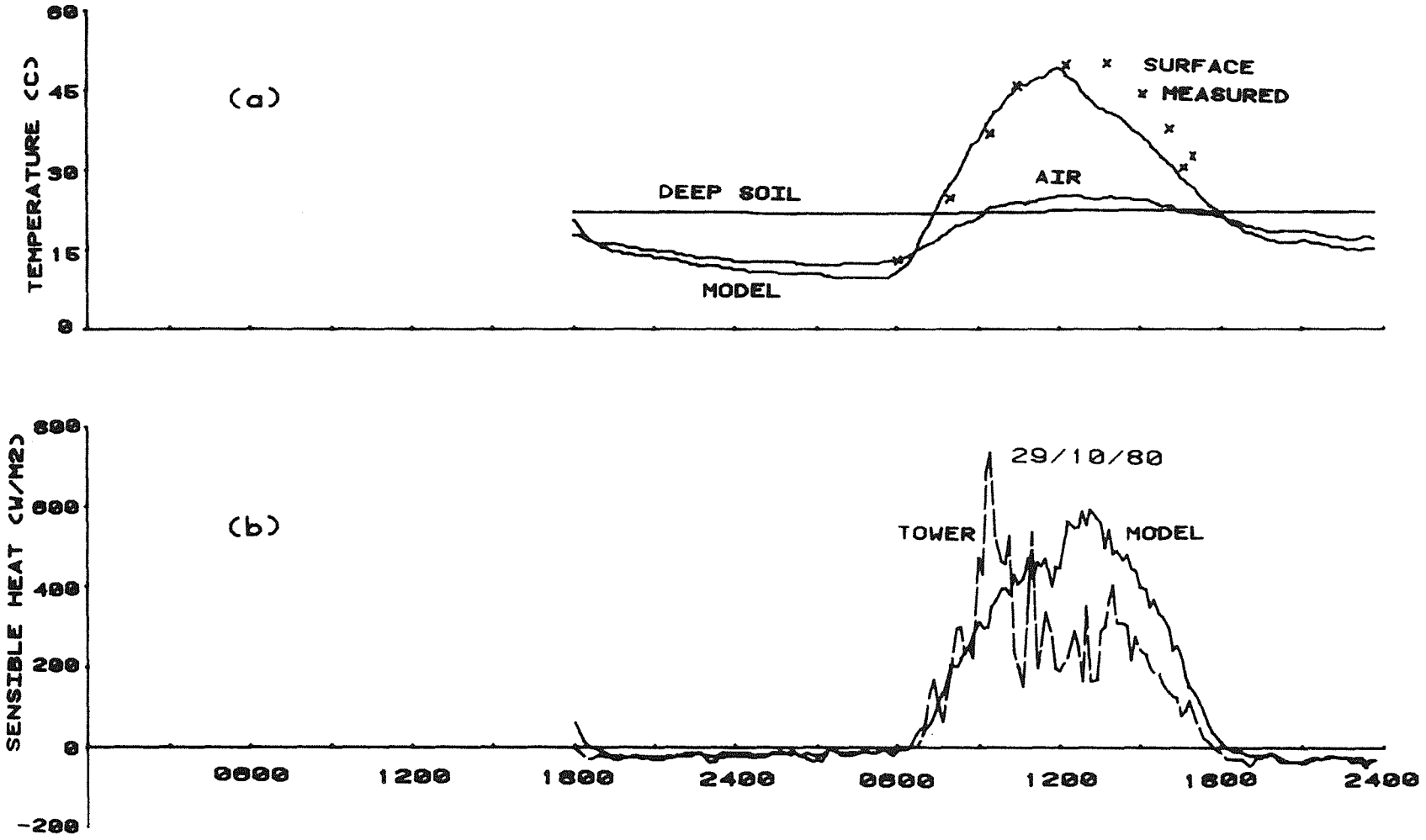

FIG 4.5 RESULTS OF MODEL SOIL

(a) Temperatures of soil and air
(b) Heat flux, compared with tower measurements

the period of interest (midnight to 1200 on 29/10/80) there is generally good agreement between measurements and the calculation methods. Despite the large fluctuations in HVFLUX estimates during daytime hours, the total heat transfer during morning hours matches the SOIL estimate reasonably well.

Figure 4.6 shows the potential temperature profiles obtained from hourly radiosonde releases throughout the study morning. The profile at 0608 shows no effect of mixing near the ground, with a radiation inversion of about 8°C potential between ground level and 350 m height. This profile is used to initialise the model as described in Section 4.5.4.

The simulation was commenced at 2200 on 28/10/80 to allow an examination of the nocturnal boundary layer height estimate. A sample of the acoustic sounder record appears in Figure 4.7, over which has been superimposed the NBL height calculated within the model. The latter decreases steadily towards dawn as the stability increases and u_* becomes smaller. The sounder indicates that some turbulent activity is present at levels well above the predicted NBL height. At 0608 there is a close correspondence between the NBL height indicated by the sounder and the height of the point of inflection in the temperature profile (approximately 350 m), satisfying the criterion proposed by von Gogh and Zib (1978) for determining NBL height. The performance of the NBL equation (4.28) is not good in this instance. In view of the low importance attached to this estimate (Section 4.4) the matter will not be pursued.

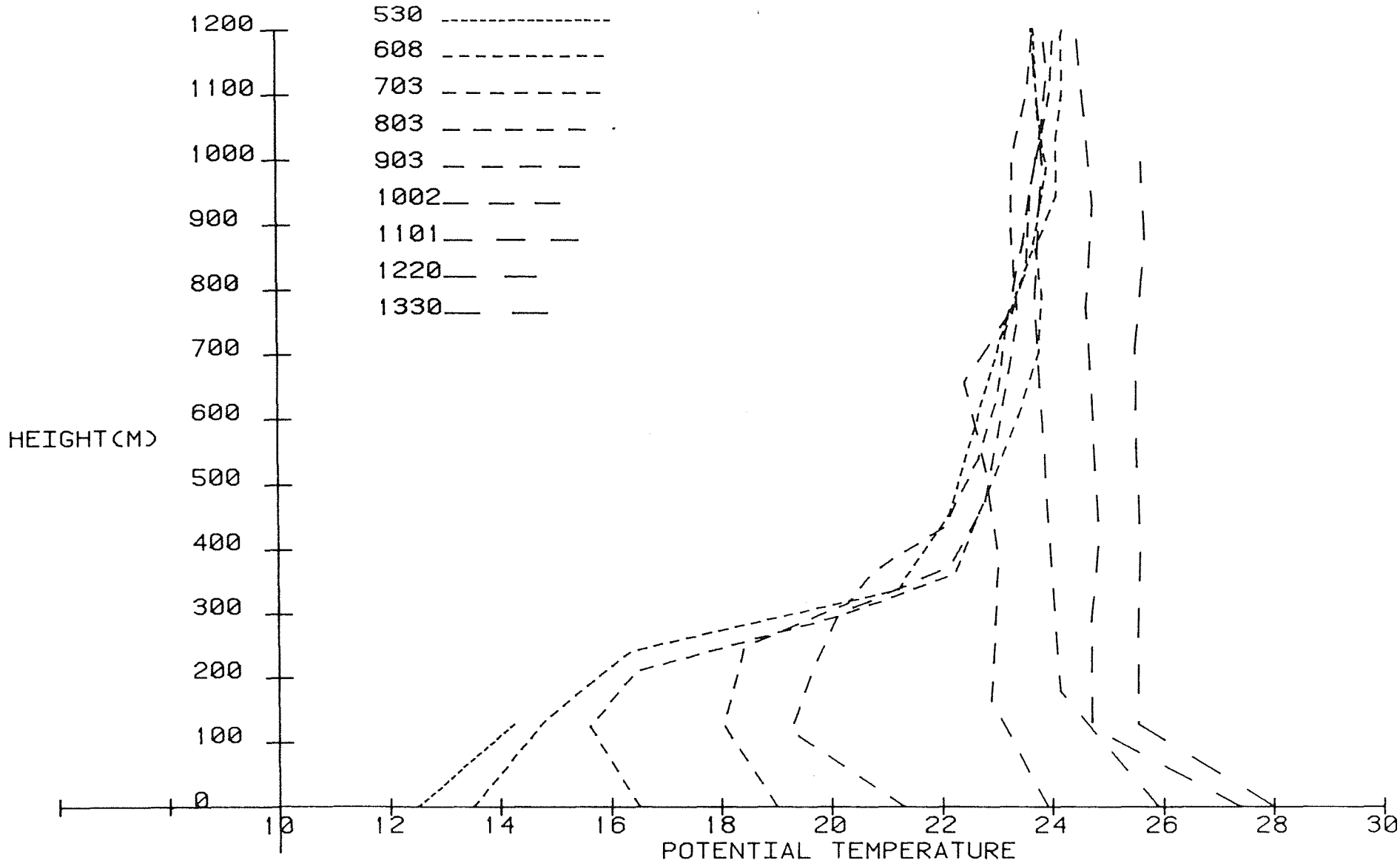

FIG 4.6 POTENTIAL TEMPERATURE PROFILES FROM RADIOSONDES (29/10/80)

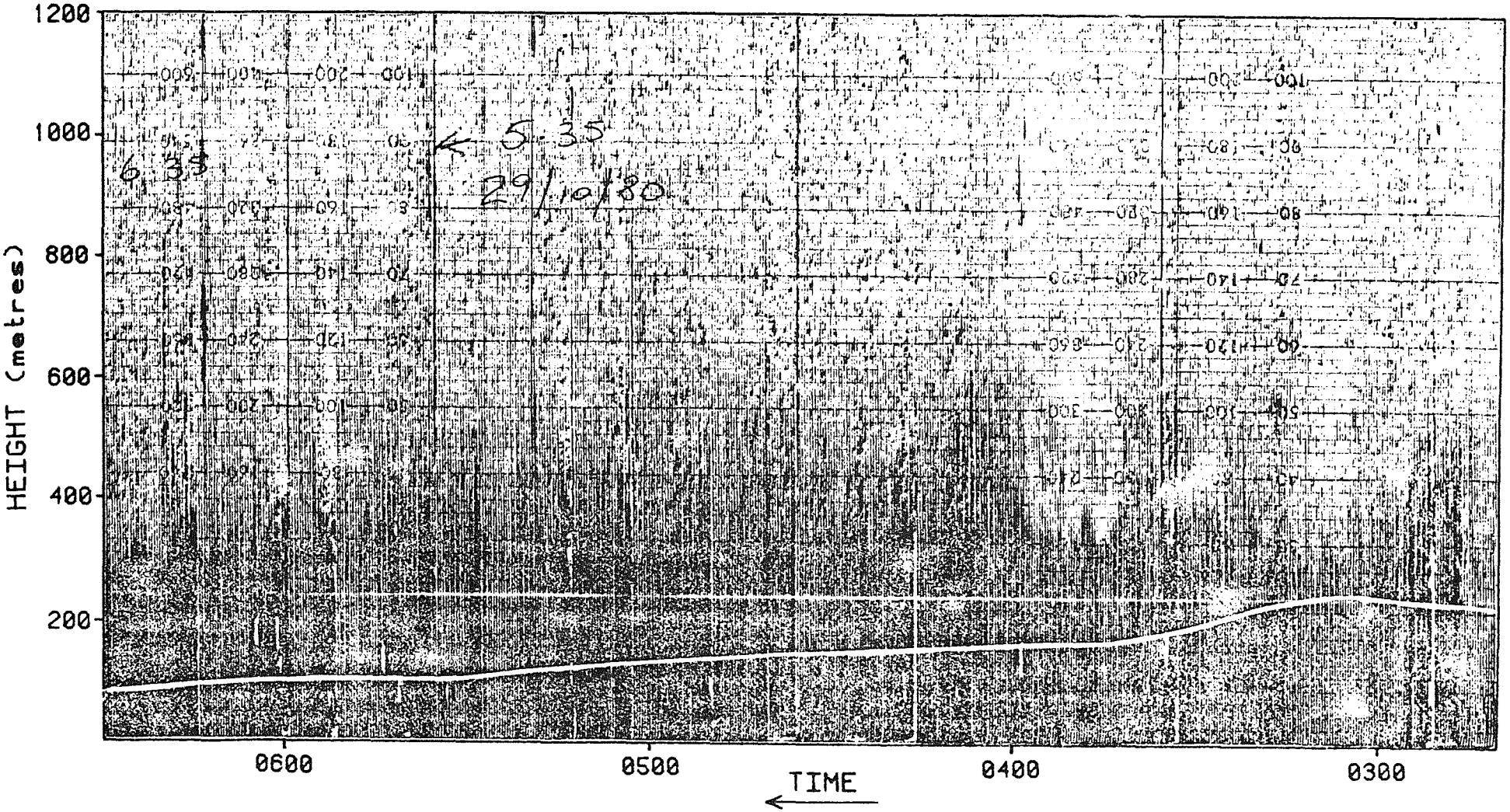

FIG 4.7 ACOUSTIC SOUNDER TRACE WITH MODELLED NBL HEIGHT SUPERIMPOSED

The 0608 potential temperature profile clearly indicates that there is no large scale mixing between ground level and 350 m height. Wind speed and direction profiles plotted in Figure 4.8 show the presence of a nocturnal jet at the top of the ground-based inversion. A mean gradient Richardson No.,

$$Ri = \frac{g}{T_v} \frac{\partial\theta/\partial z}{(\partial U/\partial z)^2} \qquad (4.33)$$

computed for the layer 68 to 288 metres height from the 0608 sonde data has a value of 0.86, well above the 0.25 limit for large scale Kelvin-Helmholtz billows (Emmanuel, 1973). It is apparent however that localised patches in the shear flow become turbulent and that their combined effects produce a strong return on the sounder record. Von Gogh and Zib (1978) note that turbulent fluctuations of the correct order to produce backscatter appear to be almost invariably developed in the presence of inversion conditions.

The experimental results confirm that the NBL height should not be considered as a mixing depth in the same sense as a daytime mixed layer, since the NBL has no distinct inversion "lid" and no large scale mixing which would lead to a uniform vertical distribution of pollutants over its depth. A conventional Gaussian plume dispersion model should therefore conservatively assume slow diffusion over an unlimited mixing depth at night. The NBL height is still required to initialize the NML height when mixing commences.

The model commenced erosion of the inversion at about 0640, as might also be inferred from Figure 4.6. Figures 4.9(a) to (c) compare the potential temperature profiles predicted by the model against those

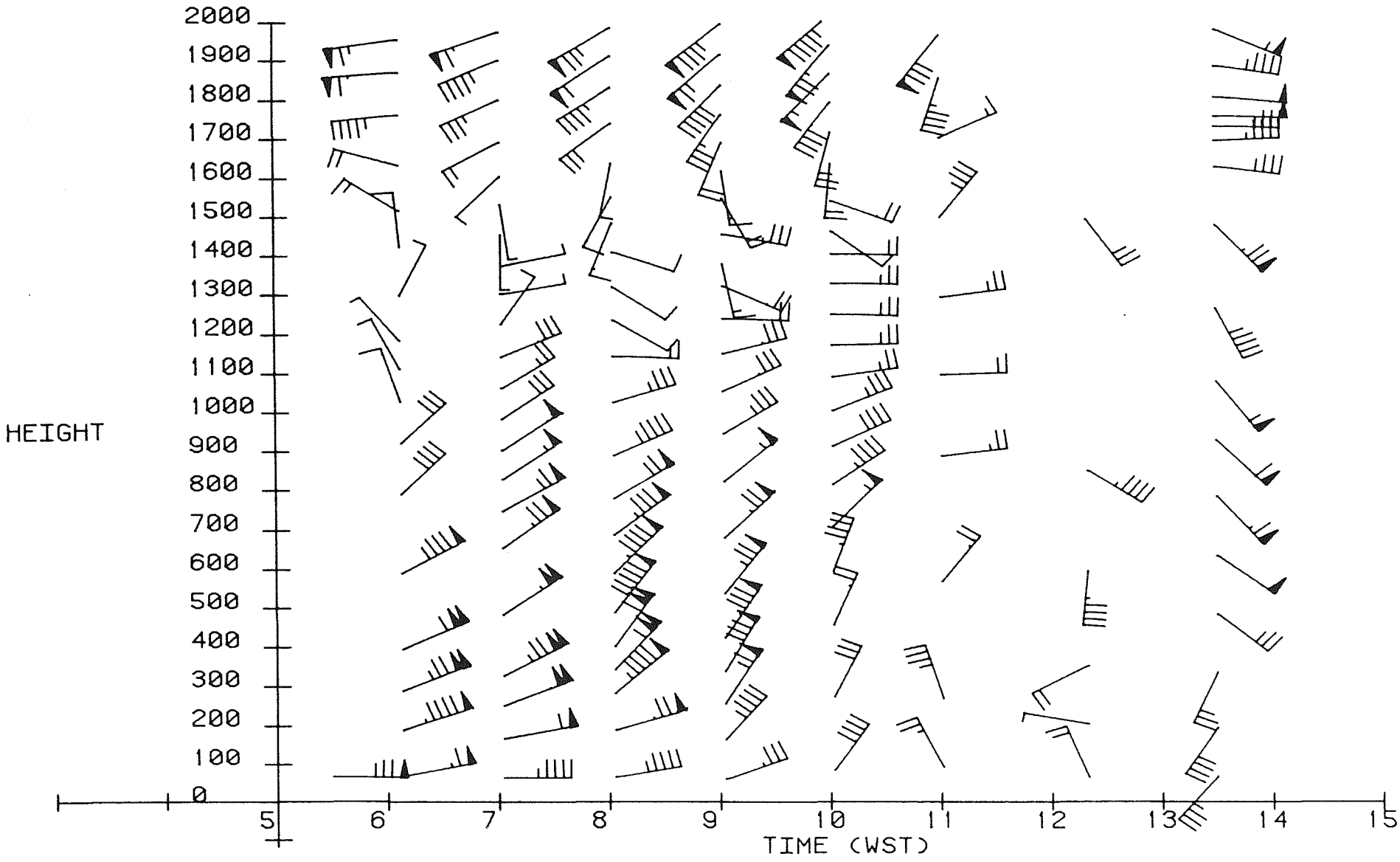

FIG 4.8 WIND SPEED AND DIRECTION PROFILES FROM RADIOSONDES (29/10/80)

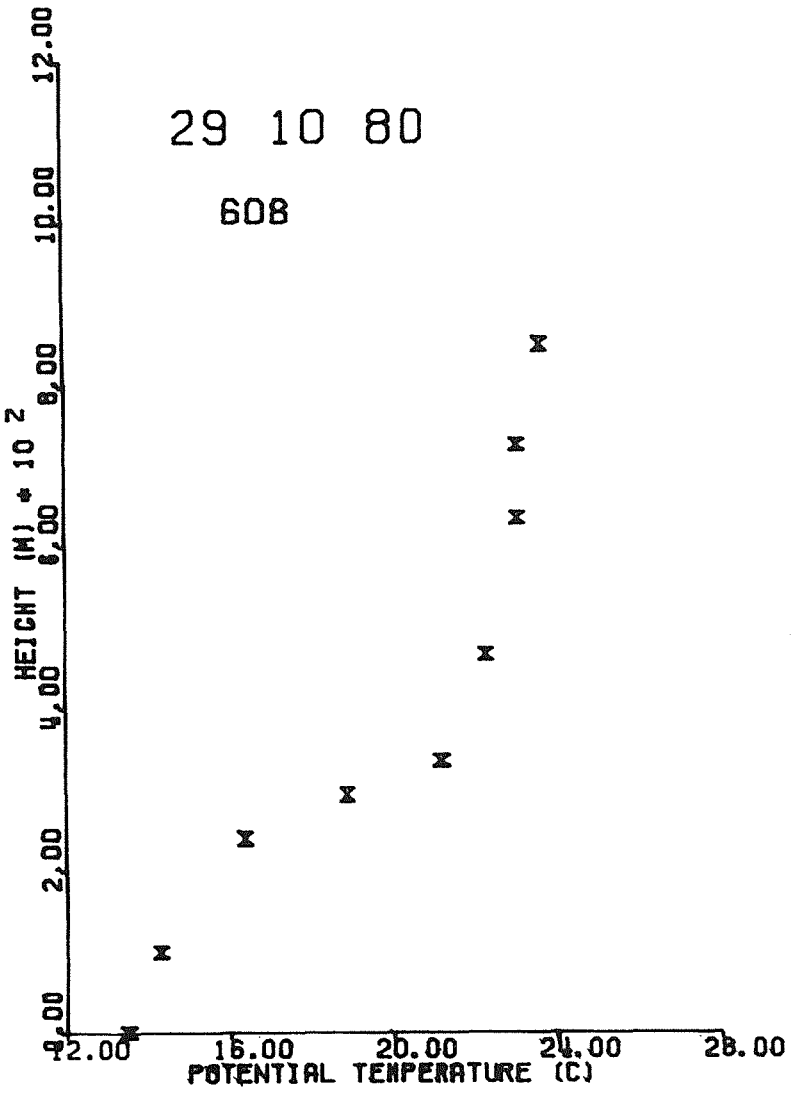

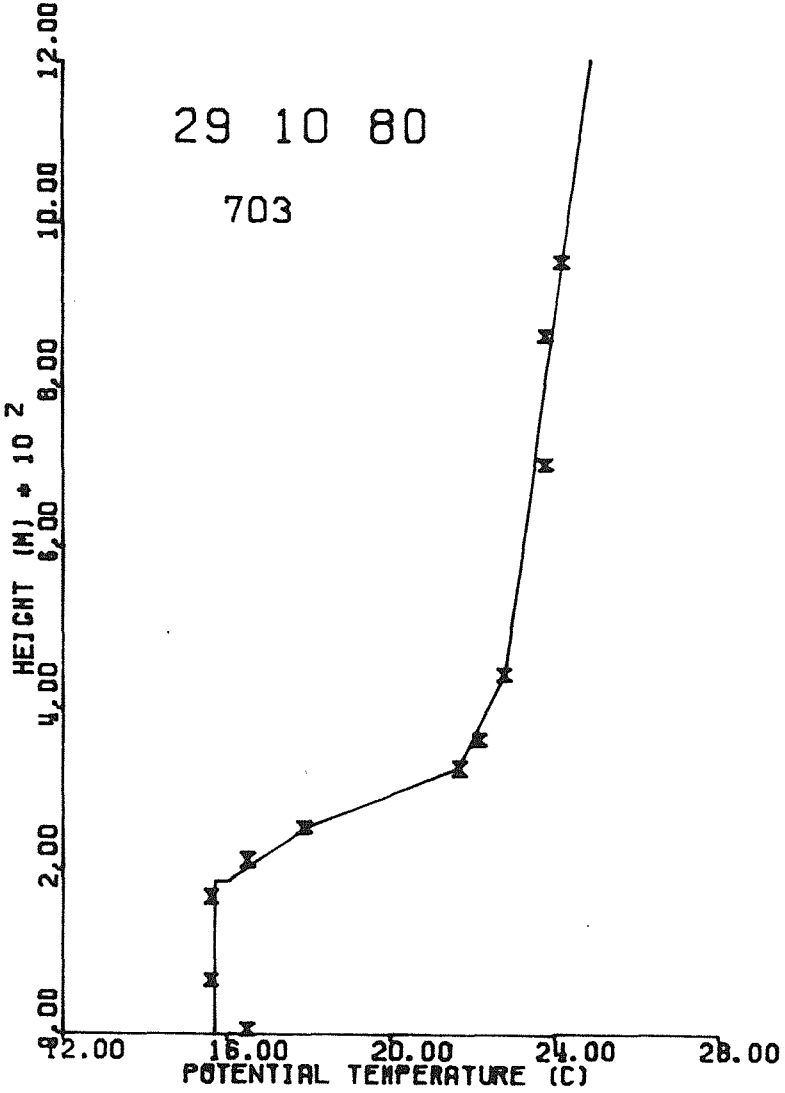

FIG 4.9(a) POTENTIAL TEMPERATURE PROFILES:
Measured (crosses) and Modelled (full line)

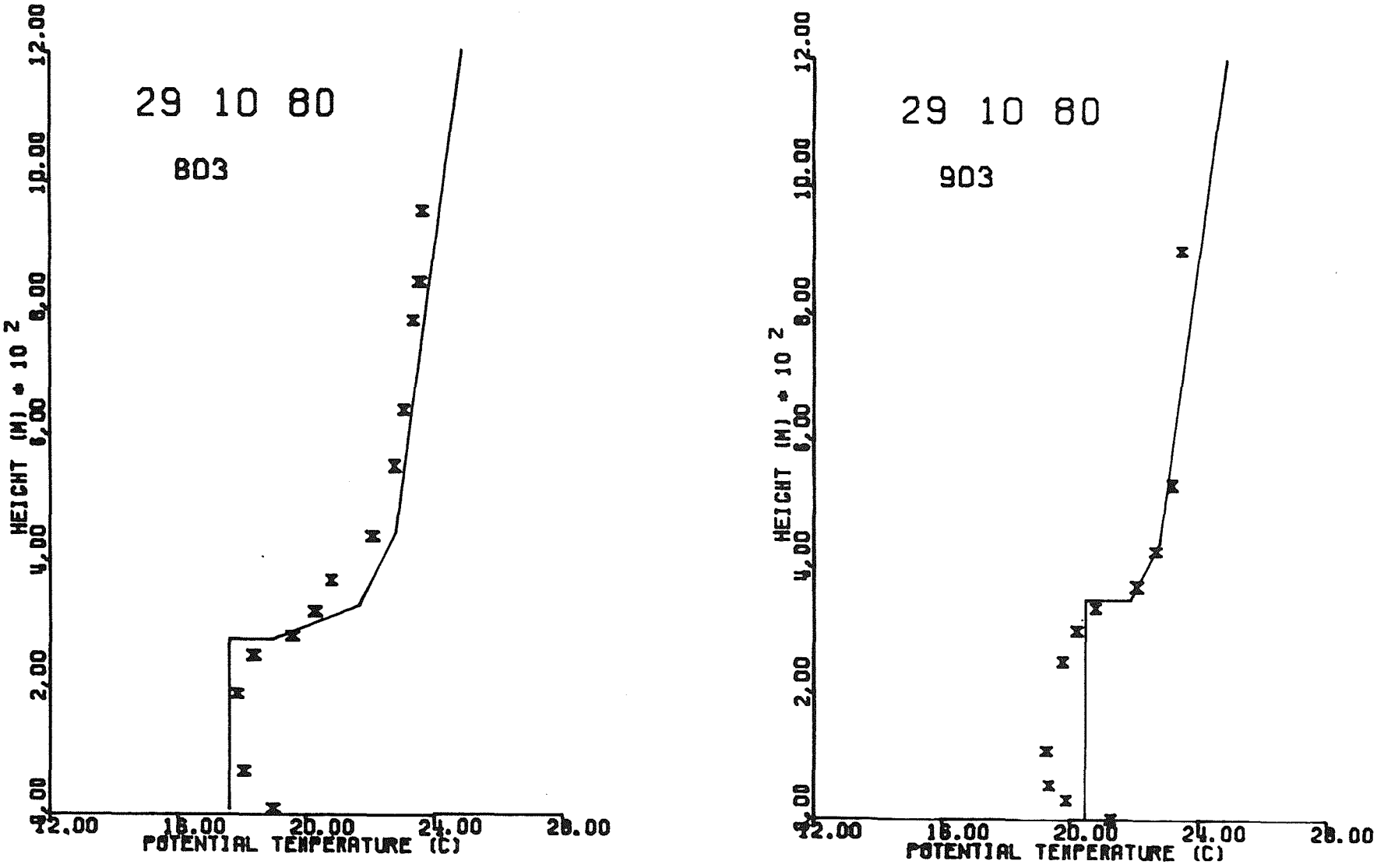
29 10 80
803
HEIGHT (M) * 10 Z
0.00
2.00
4.00
6.00
8.00
10.00
12.00
12.00
16.00
20.00
24.00
28.00
POTENTIAL TEMPERATURE (C)
29 10 80
903
HEIGHT (M) * 10 Z
0.00
2.00
4.00
6.00
8.00
10.00
12.00
12.00
16.00
20.00
24.00
28.00
POTENTIAL TEMPERATURE (C)

FIG 4.9 (b)

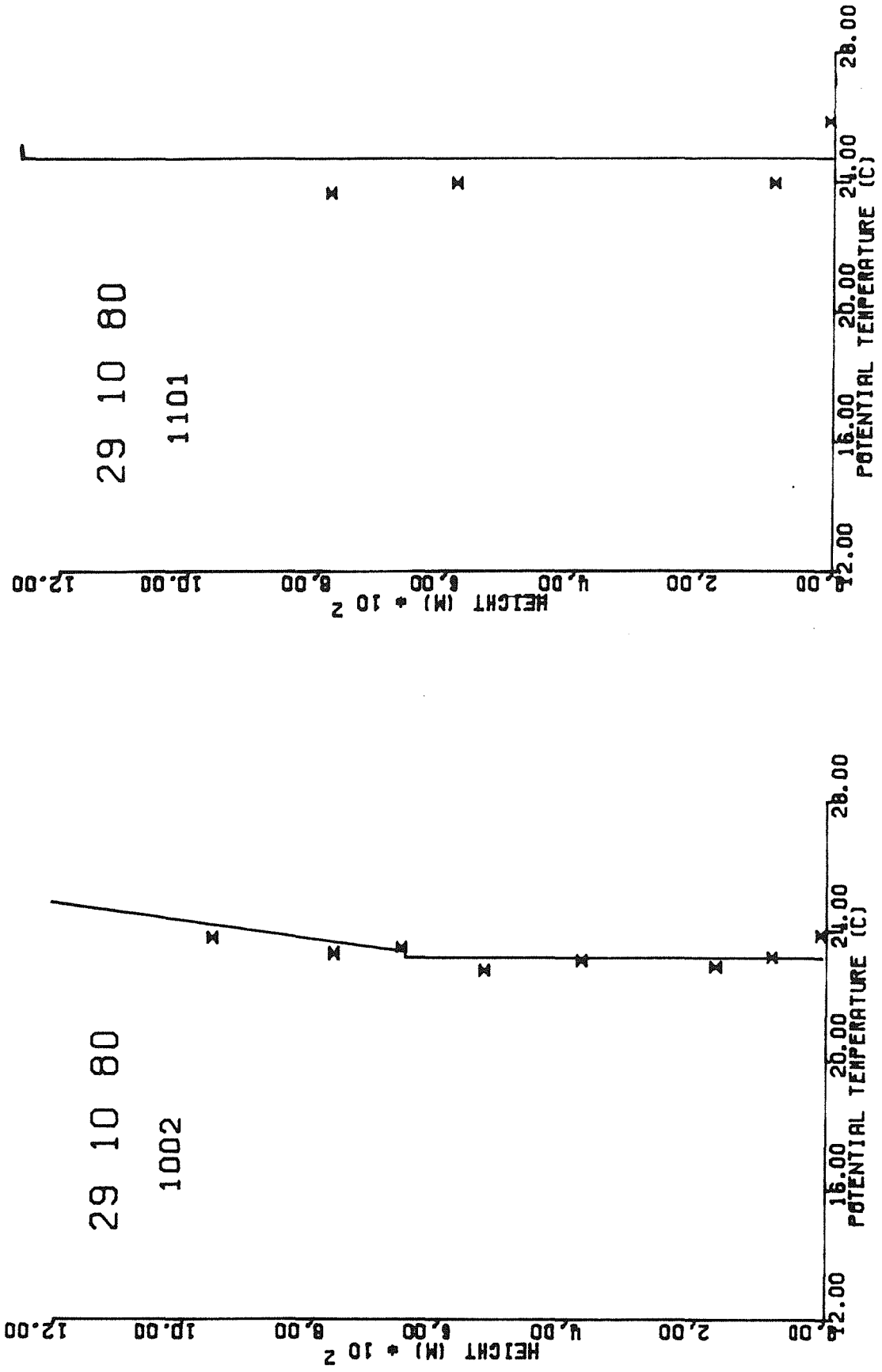
29 10 80
1002
HEIGHT (M) * 10 2
POTENTIAL TEMPERATURE (C)
29 10 80
1101
HEIGHT (M) * 10 2
POTENTIAL TEMPERATURE (C)

FIG 4.9(c)

from the radiosondes. By design, the model profile (solid line) above the WML remains unchanged from the 0608 profile throughout the day. The modelled inversion is plotted as a step, consistent with the model derivation. Up to time 1002, the model simulates the erosion of the inversion in a pleasing fashion, so lending support to the formulations of both models SOIL and WML. The picture at 1101 and onwards is unclear, and also unimportant as the mixing height by this time is large and sea breeze onset is imminent.

The predicted mixing depth throughout the morning is superimposed on the acoustic sounder record in Figure 4.10. Although WML deepening commences at 0640, there is little change in the sounder record until about 0720, consistent with the notion that the sounder is recording the presence of small scale turbulence in the remnant NBL. After this time, the sounder indicates WML deepening at a rate similar to the model, although the trace extends 100 to 150 metres above the model prediction. The sonde profiles in Figure 4.6 indicate that this region above the modelled WML height is in fact the upper portion of the strong capping inversion which is definitely not well mixed. The 'blackness' of the record (which is of relatively low quality in this case) is clearly not a good indicator of the intensity of turbulence and it is therefore not possible to quantify the upper extent of strong turbulent mixing. Other researchers (Russell and Uthe, 1978) report a distinct layer echo associated with the capping inversion above a spikey echo structure associated with the convectively mixed layer. The base of this layer echo is taken as representing the WML height (Kaimal et al., 1982).

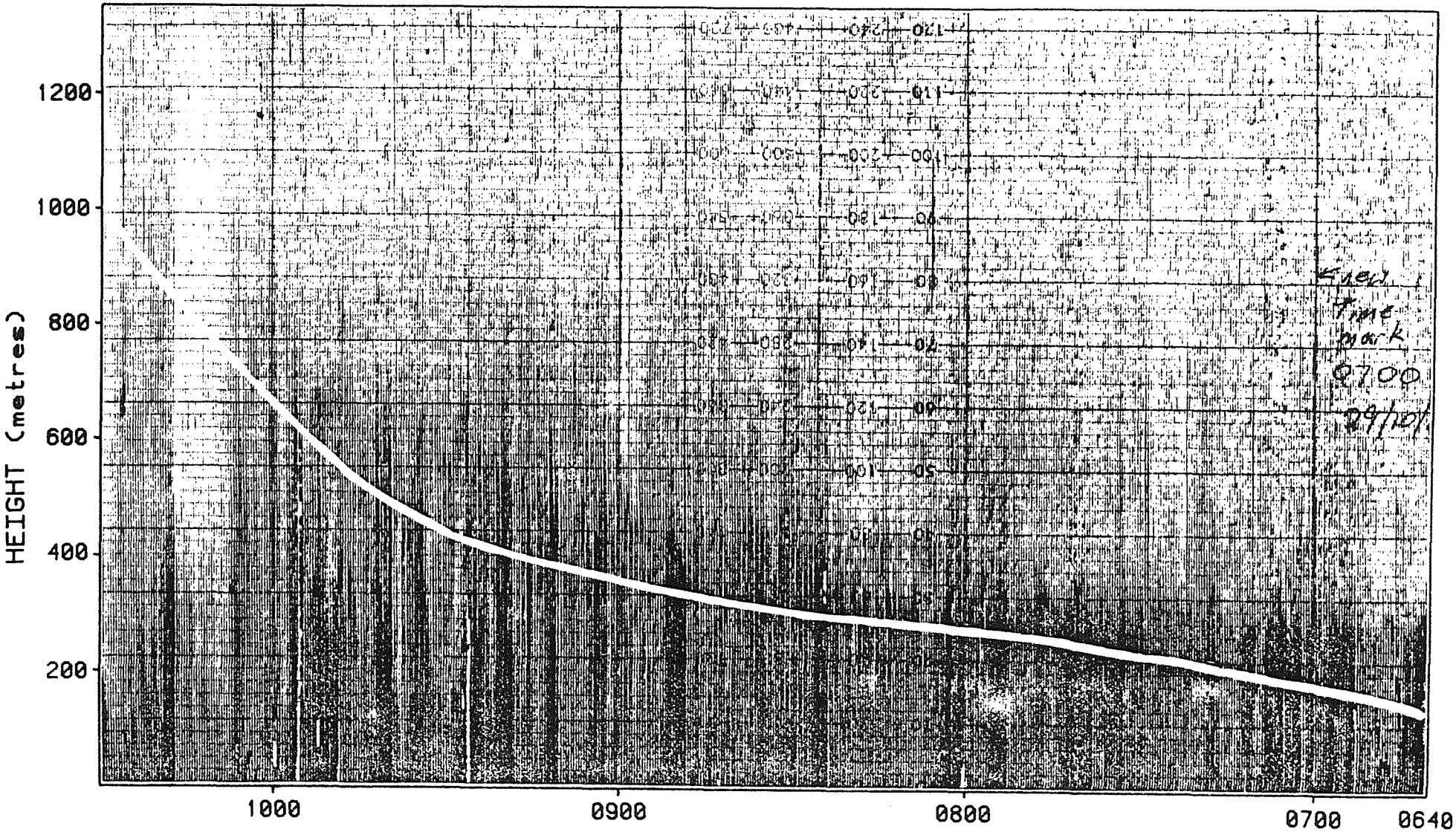

FIG 4.10 ACOUSTIC SOUNDER TRACE WITH MODELLED MIXING DEPTH SUPERIMPOSED

It is of interest to determine whether the turbulence in the strong inversion layer detected by the sounder is simply locally generated small scale turbulence, as observed in the NBL, or whether it is indicative of larger scale Kelvin-Helmholtz billows at the entrainment interface, as described by Hall et al. (1975), Sherman et al. (1978) and others. A Richardson Number criterion for the onset of billowing activity is given in (4.33) above, and this is found by Hall et al. (1975) to be closely matched by values of Ri calculated from field measurements. Spigel et al. (1986) point out that sharp stable density gradients in the presence of mean shear are always unstable and that billowing inevitably occurs, resulting in a stable thickened interface of thickness δ where

$$\delta = 0.3T_v\Delta U^2/(g\Delta\theta) \qquad (4.34)$$

From inspection this is simply a re-organised version of (4.33), implying a slightly different value of Ri = 0.3.

Values of Ri across the entrainment zone may be calculated from the radiosonde profiles of temperature and wind speed, as presented in Table 4.1.

TABLE 4.1 VALUES OF RICHARDSON NUMBER ACROSS THE WELL MIXED LAYER ENTRAINMENT ZONE

TIME	h m	SONDE INTERVAL	$d\theta/dz$ °C/m	dU/dz m/sec/m	Ri
0803	275	246- 315	0.027	0.033	0.83
0903	355	298- 373	0.027	0.017	3.05

The vertical resolution of the sonde values is unfortunately quite coarse, being limited by the double theodolite tracking method employed for wind velocity estimation. However, it is quite apparent from the calculated values of Ri that, if Kelvin-Helmholtz billowing is occurring at the entrainment interface, it is occurring over a vertical scale considerably less than 70 metres (which is about the resolution of the sonde wind speed values). (Note that the layers with Ri < 0.25 described by Hall et al. (1975) were typically 10 m thick.) This conclusion is consistent with the observation that there is no large scale modification of the inversion layer evident in the sonde profiles prior to it being engulfed by the growing mixed layer.

Shear generation of turbulence was obviously not an important mechanism in WML deepening during the field experiment period; this can be demonstrated quantitatively as follows. If we accept a conservatively high value of ΔU = 2 m/sec across the entrainment zone and estimate the entrainment rate dh/dt from the model results (which match the field observations) we may then compare the shear energy contribution $C_S \Delta U^2 dh/dt$ with the surface energy input $C_K q_*^3 = C_K(w_*^3 + C_N^3 u_*^3)$. This is presented in Table 4.2.

The final column gives the percentage error involved in neglecting the shear contribution to the turbulent kinetic energy budget and hence also (approximately) the amount by which the entrainment rate is underestimated. This relatively small conservative error in mixing height prediction is quite acceptable for dispersion modelling. Hence,

TABLE 4.2 COMPARISON OF TERMS IN THE WELL MIXED LAYER GROWTH EQUATION

TIME	ΔU m/sec	dh/dt m/min	$C_s \Delta U^2 dh/dt$ m^3/sec^3	$C_K w_*^3$ m^3/sec^3	$C_K C_N^3 u_*^3$ m^3/sec^3	error %
0803	2	1.25	0.017	0.26	0.04	5
0903	2	1.94	0.026	0.52	0.02	5

the present model appears adequate for daytime convective conditions, but would tend to under-predict the growth of the mixed layer under conditions of limited surface heating and higher wind speeds.

Reference was made in Section 4.3.7 to the high value of K_p accepted by Driedonks (1982). He found that a value of K_p = 5, based on the experimental results of Kantha et al. (1977) was required in order to simulate his field data in conditions where surface shear was an important mixing mechanism. This value of K_p was much larger than that selected by Rayner (1980) (0.42) and gave cause for concern, since the experiment by Kantha et al. (and the forerunner by Kato and Phillips, 1969) was strongly dominated by internal shear-generated turbulence and hence not suited to the task of estimating mixing due to surface shear alone.

Closer examination of Driedonks (1982) methodology has provided a reason for the disparity. The observations of WML height against which his model was compared were all made during morning hours following

sunrise, prior to the time when convection was well developed. Driedonks admitted that the observed temperature profiles during this period looked nothing like the idealised mixed layer model and in fact resembled nocturnal temperature profiles. Since there was no well mixed layer to be observed in his temperature profiles, he determined his observed MML heights from acoustic sounder records.

It has been adequately demonstrated in the literature cited above (e.g. von Gogh and Zib, 1978) and in the Kwinana experiment that an acoustic sounder trace does not necessarily indicate the presence of a well mixed layer, and certainly not at night or just after sunrise. Driedonks has confirmed this fact, although that was not his intention.

It appears therefore that the seemingly good agreement obtained by Driedonks represents the misapplication of both his own data and that of Kantha et al. The analogy between the two data sets is highly tenuous, since the laboratory experiment included a well mixed layer whilst the field data did not.

4.7 APPLICATION OF THE MIXING DEPTH MODEL IN DISPERSION STUDIES

The aim of this modelling exercise, as indicated in the introduction to this Chapter, has been to provide reliable estimates of mixing depth and capping inversion strength for use in dispersion modelling, via a method which is efficient and utilizes routinely available data. The model encompassed in equations (4.26) and (4.2), which is similar in form to other models described in recent literature, achieves the

stated objective. The more generalized model equations (4.17), (4.18), (4.2), (4.5) and (4.6), which include TKE and interface shear terms, may be utilized in situations where greater precision is required and the necessary data are available. Neglect of the shear term leads to a generally small underestimate of MML growth rate. This conservative error is likely to be acceptable to dispersion modellers.

Tennekes and Driedonks (1981) state that use of a simple MML model can provide results (h and θ_m) with adequate accuracy for operational purposes, with relatively little effort. This statement matches the experience in KAMS, during which the model described above was run for a full twelve months' data for very little cost and effort (KAMS, 1982).

The dispersion model which will be described in Chapters 6 and 7 makes use of the $\Delta\theta$ prediction from the MML model to calculate the fraction of plume penetrating the capping inversion. The validity of this procedure warrants discussion.

Figure 4.9 shows modelled values of $\Delta\theta$ which are significantly smaller than the total temperature increase across the smeared temperature inversion above the MML. The latter value would probably be chosen by most modellers although, in practice, it is not obvious where the real MML interface starts and ends. However, it can be argued that any plume with sufficient buoyancy to penetrate $\Delta\theta$, but which cannot fully penetrate the remaining undisturbed inversion structure, will be trapped in the inversion layer and not released until erosion reaches that level some time later, resulting in fumigation at some distance well downwind of the source. Fumigation is an important phenomenon

requiring separate treatment; it is certainly not adequately described by employing the total inversion strength measurement in a dispersion model. If a single mixing height is to be specified, then $\Delta\theta$ as defined by a WML model is believed to be the only available unambiguous estimate of "lid" strength. Fumigation must be modelled separately for predicting dispersion in the far-field, which is beyond the scope of this Study.

Subsequent to KAMS, an intriguing variation of the WML model was employed for an inland location (Collie, Western Australia) where morning radiosonde profiles were not available but where a reliable continuous acoustic sounder record was. Mixing heights at hourly intervals were digitized from the sounder charts. It was desirable to obtain estimates of $\Delta\theta$ for morning hours following sunrise when erosion of stable temperature structure below 1000 m was occurring. This period was defined by the constraints:

$$q_*^3 > q_*^3{}_{min}$$

$$h < 1000 \text{ m}$$

where $q_*^3{}_{min}$ was a specified small value above which daytime mixing might be assumed to be established (e.g. $q_*^3{}_{min} = 0.5 \text{ m}^3/\text{sec}^3$) and q_*^3 was averaged over 10 minutes. The average value of $\Delta\theta$ during an hourly interval (or some other chosen interval), bounded by times i and i+1 is given by :

$$\Delta\theta = C_K T_v Q / [g(h^2_{i+1} - h^2_i)] \qquad (4.35)$$

where $Q = \int_i^{i+1} q_*^3 dt$

These expressions come from integration of (4.26) with the shear and "spin up" terms neglected. Neglect of the "spin up" term will result

in a small overestimate of $\Delta\theta$ which is quite acceptable.

Stated in words, (4.35) uses the observed inversion erosion and the measured input of turbulent energy to infer the average strength of the interface, $\Delta\theta$. The relationship is well behaved if appreciable erosion is occurring ($h_{i+1} > h_i$) and the period average of q_*^3 is greater than $q_*^3{}_{min}$. Outside of the times when the relationship is well behaved, the value of $\Delta\theta$ is of little significance anyway (i.e. within a nocturnal boundary layer or when the mixing height exceeds the height of rise of buoyant plumes). Calculation of $\Delta\theta$ was performed for a full year, giving sensible results. These results are not relevant to the current study and therefore are not presented.

The most commonly used method for estimating daytime mixing heights is to draw a dry adiabat from the surface temperature to the point of intersection with the morning radiosonde profile (e.g. Benkley and Schulman, 1979). Inspection of the field data in Figure 4.9 indicates that reasonably good estimates may be obtained by this method through to mid-morning. The weakness of this method lies in the variety of influences which can corrupt the relationship between the surface measurement and the sonde profile. For example, on days with identical temperature profiles and solar radiation but different wind speeds, the method would predict lower mixing depths for the higher wind speed day, due to the reduction in surface temperature. However, the sensible heat transfer on the higher speed day would be slightly greater (since outgoing long-wave radiation would be reduced), plus there would be a TKE contribution from surface shear, so the mixing depth could be expected to be greater, not smaller. Furthermore, the

selected surface temperature would be strongly dependent on measurement height on calm sunny days, so the method lacks generality.

A second simplified approach for estimating MML depth is to model the encroachment of the MML on the morning temperature profile due to the effects of surface heating alone. This method is appropriate for fully convective conditions only, and is shown by Driedonks (1982) to account for about 80% of the MML deepening in these conditions, with the balance coming from turbulent entrainment. Even though encroachment is a major effect (and for that reason is included in our model via (4.2)), it cannot be assumed to apply in isolation without incurring major errors (e.g. in overcast windy conditions).

4.8 SUMMARY OF FINDINGS

The simplified MML model of (4.26) and (4.2) is recommended for providing reliable conservative input of daytime mixing depth and inversion strength for dispersion calculations. The model has a sound theoretical basis, yet is attractively simple and inexpensive to run. The model and the selected value of its various parameters have been verified in this Study, confirming similar findings of other reseachers. The detailed derivation of (4.26) described herein has served to reconcile the seemingly divergent approaches to modelling atmospheric and oceanographic well mixed layers, and has highlighted a few shortcomings in previous analyses.

Nocturnal boundary layers were also examined as a potential case of limited mixing depth. However, it was shown that, for the purpose of

modelling dispersion over a local distance range (15 km or thereabouts), the mixing height under stable conditions may be conveniently and conservatively assumed to be very large.

CHAPTER 5

COASTAL INTERNAL BOUNDARY LAYERS

Coastal internal boundary layers were identified in Chapter 4 as being an important meteorological phenomena which may limit the mixing depth of pollutants. In addition, plumes from tall chimneys near the coast may interact with coastal internal boundary layers to cause "shoreline fumigation", as briefly discussed in Chapter 1 and illustrated in Figure 1.5.

A dispersion model designed to simulate these effects requires a description of the shape of the coastal internal boundary layer. In particular, as pointed out by Stunder and SethuRaman (1985), the location of predicted fumigation maxima downwind of a tall stack near the coast is highly dependent on the description of coastal internal boundary layers employed by a model.

In the following Sections, simple formulae describing the growth of coastal internal boundary layers will be derived and compared with other formulae which have appeared in the scientific literature. A field study designed to validate the formulae will also be described.

5.1 THEORETICAL DESCRIPTION OF COASTAL INTERNAL BOUNDARY LAYERS

Figure 5.1 shows schematically the various meteorological parameters which can be expected to play a part in the formation of a boundary layer over the land downstream of a shoreline, during daylight hours

when the land temperature T_L is higher than that of the adjacent water, T_W.

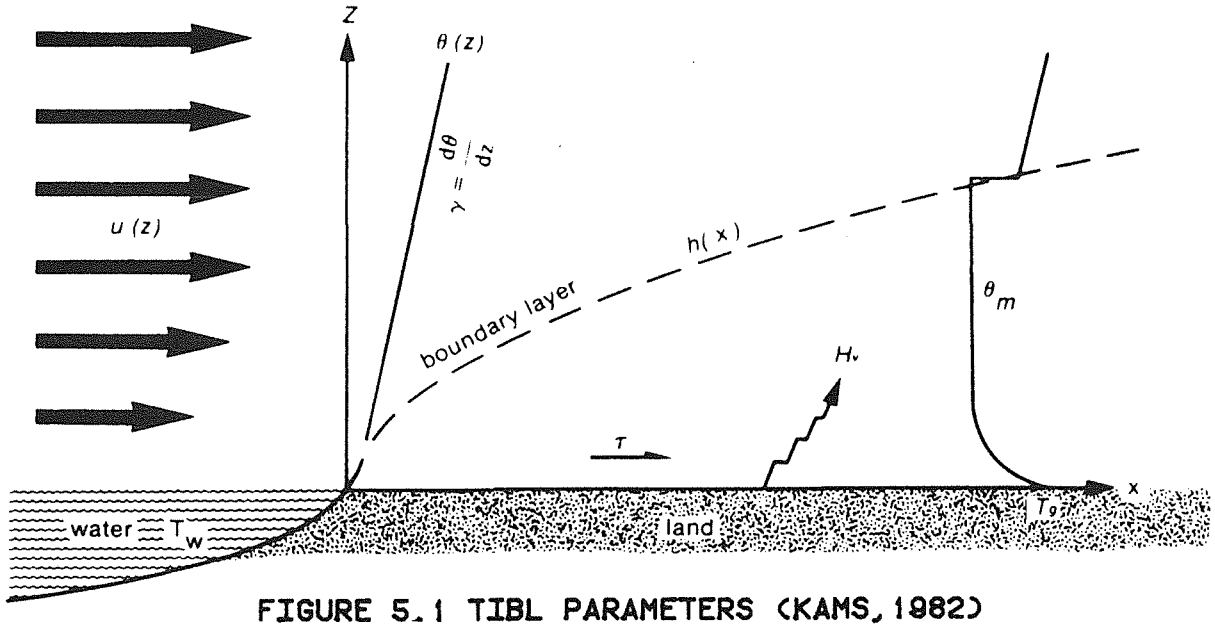

FIGURE 5.1 TIBL PARAMETERS (KAMS, 1982)

The marine air flow, with a stable temperature gradient Γ, will experience surface changes of stress τ and virtual heat flux H_v as it crosses the coast. Both of these turbulent fluxes will lead to turbulent mixing within a surface boundary layer $h(x)$ which grows downstream. The potential temperature θ_m within the layer can be expected to be uniform if mixing is vigorous, with a small step at the top of the boundary associated with turbulent entrainment.

Venkatram (1977) recognised the analogy between the mixing within a coastal boundary layer and that which occurs in the atmospheric well mixed layer under a temperature inversion, as described in the previous Chapter. He proposed the use of a standard WML model (Tennekes 1973) in a Lagrangian framework, i.e. he modelled the mixing within a column of air which is being advected downstream at the mean

flow velocity. The Lagrangian transformation is effected simply by setting $x = U_s t$ where x is distance downwind from the coast.

The concept introduced by Venkatram, together with the theory of well mixed layers described in Chapter 4, may be utilized to derive a theoretical description of coastal internal boundary layers, as follows.

Neglecting the effects of shear across the top of the boundary layer (which is likely to be small) the WML model equations (4.26) and (4.2) may be rewritten as:

$$dh/dt = C_K q_*^3/[C_T q_*^2 + gh\Delta\theta/T_v] \qquad (5.1)$$

$$hd\theta_s/dt = \Delta\theta dh/dt + H_v/(\rho C_p) \qquad (5.2)$$

where $q_*^3 = w_*^3 + C_N^3 u_*^3$ as before.

The "spin-up" term $C_T q_*^2$ will only be important if $\Delta\theta$ is very small, which in turn will only occur if the marine air stability is close to neutral ($r \approx 0$). Neutral flows are not of interest with regard to shoreline fumigation, whilst the flows of major interest (sea breezes) exhibit stable temperature gradients. Therefore the "spin up" term will be neglected.

Following Tennekes (1973), it is now possible to obtain analytical expressions for coastal boundary layer heights for the limiting cases of convective and mechanical turbulence. Convective turbulence is dominant in the planetary boundary layer over land whenever solar insolation is appreciable. Equation (5.1) then reduces to

$$dh/dt = C_K w_*^3 T_v/(gh\Delta\theta) \qquad (5.3)$$

Integrating (5.3) together with the equation for conservation of heat, and applying the initial conditions ($\Delta\theta = h = 0$ at $t = 0$) leads to the expressions

$$h = [(4C_K + 2)H_v t/(\rho C_p r)]^{1/2} \qquad (5.4)$$

$$\Delta\theta = C_K r h/(1 + 2C_K) \qquad (5.5)$$

Applying the Lagrangian transformation and substituting our previously derived value of $C_K = 0.18$ gives

$$h = \left[\frac{2.72\ H_v}{\rho C_p r}\ \frac{x}{U_m}\right]^{1/2} \qquad (5.6)$$

This formula describes the growth of a thermal internal boundary layer (TIBL) inland from the coast. Even though the initial conditions stated above are a good representation of the real situation in sea breeze flows, it is worth noting that the results are quite insensitive to the initial height of the TIBL (Tennekes, 1973).

Mechanical turbulence may determine the growth of a coastal boundary layer under cloudy skies and windy conditions. In this case (5.1) reduces to

$$dh/dt = C_K C_N^3 u_*^3 T_v/(gh\Delta\theta) \qquad (5.7)$$

Integrating (5.7) and the equation for conservation of heat yields the expressions

$$h = (6C_K C_N^3 u_*^3 T_v t/\ gr) \qquad (5.8)$$

$$\Delta\theta = rh/2 \qquad (5.9)$$

Equation (5.7), after substituting for C_K and C_N from Section 4.3.7 transforms to

$$h = \left[\frac{2.5 u_*^3 T_v}{gr}\ \frac{x}{U_m}\right]^{1/3} \qquad (5.10)$$

This formula describes the growth of a mechanical internal boundary

layer (MIBL) inland from the coast. The one-third power law ensures that boundary layer heights predicted by this formula at distances of a few kilometres are less than those from (5.6) except when surface heating is very small (e.g. close to sunset or on very cloudy days). It is probably for this reason that MIBLs have been neglected or overlooked by other researchers. The following review of literature on coastal internal boundary layers refers only to TIBLs.

It does not appear to be possible to derive an analytical expression for the height of the boundary layer in which both mechanical and convective contributions are represented. A conservative estimate of boundary layer depth may be obtained by evaluating (5.6) and (5.10), and choosing the larger value.

TIBL formulae with the same form as (5.6) have appeared elsewhere in the literature (e.g. Weisman, 1976; Steyn and Oke, 1982), with the only difference being the value of the numerical coefficient. The common feature of most interest is the use in the formulae of the sensible or virtual heat flux H_v, with the implied assumption that this flux is essentially constant downwind.

An alternative approach to TIBL formulation, as employed by Venkatram (1977) and Raynor (1975), involves the use of a land-water temperature difference $(T_L - T_W)$ to estimate the heat flux. Venkatram's expression takes the form:

$$h = \frac{u_*}{U}\left[\frac{2(T_L - T_W)x}{r(1 - 2F)}\right]^{1/2} \qquad (5.11)$$

where $F = C_K/(1 + 2C_K)$.

Implicit in this formulation is the assumption that the land temperature, not the heat flux, is horizontally uniform. Although this difference in approach (which is primarily motivated by the availability of temperature data) may seem subtle, it appears to be the starting point for a divergence of methods.

The paper by Kerman et al. (1982) is part of a set of papers describing the comprehensive Nanticoke Shoreline Diffusion Experiment. A stated major finding of this paper is that two internal boundary layers can be detected; one to adjust the bulk buoyancy contrast of the cold onshore flow to the warm land and the other to adjust the flow for the continued solar heating throughout the day. The first boundary layer is seen to reach equilibrium at some distance inland from which point the second is dominant.

The argument advanced by Kerman et al. regarding the first boundary layer is based on an intuitive description of the perceived reduction in air-land temperature difference (and hence also buoyancy difference) as the air is advected inland and warmed. This argument is believed to be a poor representation of the real situation. The picture is made much clearer if one considers a local heat budget at the land surface at any (and all) distances from the coast. Assume for a start that a TIBL is well developed and that incoming solar radiation is roughly constant. Under these conditions, the ground temperature at any particular location will reach a constant equilibrium value. Assuming also that the ground is dry (for simplicity), it is obvious from the local surface heat budget that the spatially uniform incoming solar and long-wave radiation must be

balanced by a spatially uniform total of outgoing sensible heat and long-wave radiation. Since the outgoing long-wave component will vary from place to place by only a few percent due to variations in ground temperature (lower nearer the coast) it follows that the assumption of horizontally uniform heat flux is a good approximation. It is this heat flux which drives the growth of the TIBL - there are no other forcing mechanisms. Consequently, it makes little sense to differentiate between sources of buoyancy or excess temperature as Kerman et al. do. There is just one source - the sun. Their concept of equilibrium height is believed to be a misconstrual of the transient period following the onset of onshore flow, during which time the near-shore land temperature adjusts downward to restore the balance of terms in the local heat budget. Following this period, if steady state were to be reached, one would expect to find the local land-air temperature difference roughly constant for any downwind distance (out to several kilometres), consistent with a spatially uniform sensible heat flux. The land temperatures would therefore exhibit a positive horizontal gradient with distance from the coast, matching that of the air. Experimental evidence of this at Kwinana was documented in Section 3.4.1. This evidence, coupled with observed and modelled rates of soil temperature adjustment, also suggests that the transient period may be quite short (approximately half an hour) so that use of a steady state TIBL equation would not introduce significant errors overall.

Misra and Onlock (1982) state explicitly that the sensible heat flux varies with downwind distance in the TIBL, such that w_* stays roughly constant. They refer to Venkatram (1977) for the basis of this

statement. However, Venkatram gives no such basis. Rather, he assumes constant land and water temperatures for simplicity, recognising this as a source of error but arguing that it should be acceptable in the context of his numerical study.

The short discussion note by Weisman (1976) lends strong support to the assumption of constant heat flux rather than constant land temperatures. He points out that the constant land temperature assumption leads to the unrealistic prediction that atmospheric stability increases inland (as the air warms). This argument is an alternative expression of the local heat budget argument given above.

Venkatram (1986) presents a derivation of TIBL growth formulae which (neglecting coefficient values) reduce exactly to (5.6) if a constant surface heat flux is assumed. He discounts the value of this simplified formula for two reasons:

(i) because surface heat flux data are unlikely to be available in practice, and

(ii) because the formula does not predict an equilibrium height for the TIBL as proposed by Kerman et al. (1982).

The first of these objections is difficult to sustain in relation to serious atmospheric dispersion studies, given that the surface heat flux is a key parameter (as described in Section 1.2) and may be computed from routinely available data. The second objection is discounted here on the basis of the foregoing review of the paper by Kerman et al. (1982). Having adopted the concept of an equilibrium height, Venkatram proposes that its value be determined from a mixed

layer model which requires surface heat flux as an input variable. The proposed model is identical to that which forms the basis of (5.6), expressed in temporal terms (i.e. with advective terms neglected). It would be more meaningful to consider a single model within which advective terms dominate in the near-field and temporal terms dominate in the far-field, as has been done by Steyn and Oke (1982) (described below). Venkatram's proposal to employ an independent modelled estimate of equilibrium height is inappropriate to sea breeze flows in which case the modelled inland mixing depth and temperature structure bear no direct relation to those of the onshore flow.

Stunder and SethuRaman (1985) have evaluated a variety of different TIBL formulations against two suitable field data sets in an effort to ascertain which formulation performs the best overall. The selected data sets were from TIBL experiments over Long Island, New York (Raynor et al., 1979) and Kashimaura (Gammo et al.,1982). The reader is referred to Stunder et al. (1985) for a full discussion of the TIBL formulations, data and statistical methods. Two of the formulae are identical in form to (5.6), varying only in the value of the numerical coefficient. Plate (1971) used a coefficient of 4.0, while Weisman (1976) suggested 2.0, (compared with the value of 2.72 used in (5.6)). The formulae of Raynor (1975) and Venkatram (1977), employing land-water temperature differences were also assessed. The conclusion drawn by Stunder and SethuRaman was that the formula of Weisman (1976) performed best overall, and notably for unstable and isothermal conditions (which encompasses the range of conditions of interest at Kwinana). This finding lends direct support to the form of (5.6) although the value of the coefficient is still in question.

Strong but less direct support for the form of (5.6) is also found in the work of Steyn and Oke (1982). These authors address the problem of determining mixing depths inland from the coast where the TIBL merges into the daytime mixed layer. At these larger distances, both temporal and advective changes to mixed layer temperature are important. They also consider the influence of subsidence at the inversion base although this is found to be relatively unimportant. The method they employ is to obtain expressions for TIBL height and temperature jump which are identical to those derived above (with a coefficient value of 2.8 being almost identical to that in (5.6)). These expressions are then differentiated with respect to downwind distance and substituted back into the material derivatives for mixed layer temperature, temperature jump and inversion heat flux, so that the time derivatives of these variables may be evaluated. Closure is obtained via the known solution to the turbulent kinetic energy equation in convective conditions, namely $H_{s,i} = C_K H_s$, where $H_{s,i}$ and H_s are the sensible heat fluxes at the inversion base and surface respectively.

The procedure of specifying the advection terms a priori must lead to errors in the solution for locations well downwind. In this model, advective effects are superimposed "instantaneously" over the region at each timestep, whereas in reality it takes considerable time (proportional to travel distance) for advective effects to propagate inland, with significant modification occurring on the way.

The model verification results presented by Steyn and Oke both relate to sites close to the coast (5 to 15 km). It is quite apparent from the results, which show significant daytime decreases in mixing depth,

that the advection terms are dominating the solution for these short downwind distances. It would be instructive to view the results from a model run with the temporal terms deleted, to see if there is any significant difference.

As specified in Chapter 1, the modelling exercise in this Study is limited to the local scale, with downwind distances beyond 15 km from the coast not being considered. It is reasonable to assume that the advection of cool marine air over this area would be the dominant influence on mixing depths, and hence the simple TIBL formula of (5.6) should perform almost as well (and certainly quicker) than a 2D model incorporating temporal terms.

Based on the above argument, the excellent comparison of modelled and measured TIBL heights described by Steyn and Oke may be taken as an almost direct verification of (5.6). Furthermore, since the first of the field data sets employed by Steyn and Oke was that from Nanticoke, as used by Kerman et al. (1982), the argument for adopting (5.6) in preference to the model proposed by Kerman et al. (1982) is also substantiated.

In summary, the TIBL formula (5.6) appears to have strong theoretical and experimental support. The value of the numerical coefficient should ideally be fixed with reference to the underlying theory, as was done in the derivation of (5.6). There is a degree of subjectivity in the determination of the TIBL height from experimental data, as noted by Stunder and SethuRaman (1985), which reflects directly on the inferred numerical coefficient. This matter will be discussed in the

light of the results of field experiments described in the next Section.

5.2 FIELD INVESTIGATIONS OF THERMAL INTERNAL BOUNDARY LAYER FORMATION

The TIBL formula (5.6) was utilized in the KAMS dispersion model with reasonable confidence, based on the results of a tracer experiment which will be described in the next Chapter. However, there was no opportunity to directly validate the formula prior to the completion of KAMS. The opportunity to validate the formula came in 1983 as part of an air quality study at Bunbury, Western Australia. Bunbury is a city and regional centre situated on the coast approximately 130 km south of Kwinana. The area is influenced by the same synoptic weather patterns as Kwinana and experiences a similar sea breeze climatology. Roughness length in the Bunbury area was determined (from tower wind speed profiles) as 0.25 m, compared with 0.1 m at Kwinana. Two field experiments, performed on the 3 February and 22 February, 1983, are discussed in this Section. This discussion is preceded by a brief outline of similar field experiments reported in the scientific literature.

5.2.1 REVIEW OF EXPERIMENTAL STUDIES

There have been a number of major field investigations in other countries of the shape of TIBLs and of the shoreline fumigation process. It is worth briefly noting the techniques employed to determine the shape of TIBLs, some of which have been employed in field studies to be discussed later in this Section.

The Brookhaven National Laboratory have been investigating coastal boundary layers for a decade or more. A good discussion of procedures is given by Raynor et al. (1979). Their principal technique involved the use of a sailplane variometer mounted on the wing of a light aircraft to provide a measure of vertical turbulent fluctuations encountered during horizontal traverses inland from the coast. The variometer senses pressure fluctuations associated with the buffeting effect of the turbulence and provides a rapid response analog output for recording purposes. SethuRaman et al. (1979) provide a comprehensive description of the variometer and of its use by the Brookhaven National Laboratory. By flying traverses at successive altitudes, the growth of the boundary layer (identified by the transition from smooth to turbulent air) was mapped and evaluated. Other data collected included radiometric water and land temperatures, vertical atmospheric temperature profiles, pilot balloon soundings and low-level turbulence measurements. Raynor et al. (1979) collected data for a large number of experiments under different meteorological conditions and tested their TIBL formula, which is very similar to (5.11), with moderate success.

Gammo et al. (1982) conducted a series of experiments similar to those reported by Raynor et al. (1979), but using a sonic anemometer and a hot wire anemometer to measure turbulent velocities. The data was used in the same fashion to map the growth of boundary layers. The previously mentioned analysis of TIBL formulae by Stunder and SethuRaman (1985) utilized the data of Gammo et al. (1982) and Raynor et al. (1979).

Details of the Nanticoke Shoreline Diffusion Experiment are given by Portelli (1982). These experiments did not use aircraft to determine the TIBL shape but instead relied on tethered sondes, mini sondes and acoustic sounders. In addition, a comprehensive range of meteorological variables were measured to allow determination of turbulent fluxes via several alternative methods.

5.2.2 EXPERIMENTAL METHODS

The key element of the experiments conducted at Bunbury was the use of an aircraft-mounted sailplane variometer to map the growth of TIBLs inland from the coast, following the method of Raynor et al. (1979) described in the previous Section. The variometer used in this Study was a BORGFLT model MB-1-AV which was modified to produce a voltage as well as an audible signal. The variometer was placed inside the aircraft and was connected to a static pressure head mounted under the wing. The voltage output from the variometer was passed through a high pass filter with a time constant of approximately 18 seconds and then recorded on a single channel chart recorder. The high pass filter was used to eliminate the larger timescale fluctuations due to pilot-induced movements of the plane.

Figure 5.2 shows the static pressure head being fitted under the wing of a Piper Cherokee, and Figure 5.3 shows the instrumentation, including the variometer unit, a strip chart recorder and a data logger. In practice, the chart recorder proved to be sufficient, providing an excellent visual record.

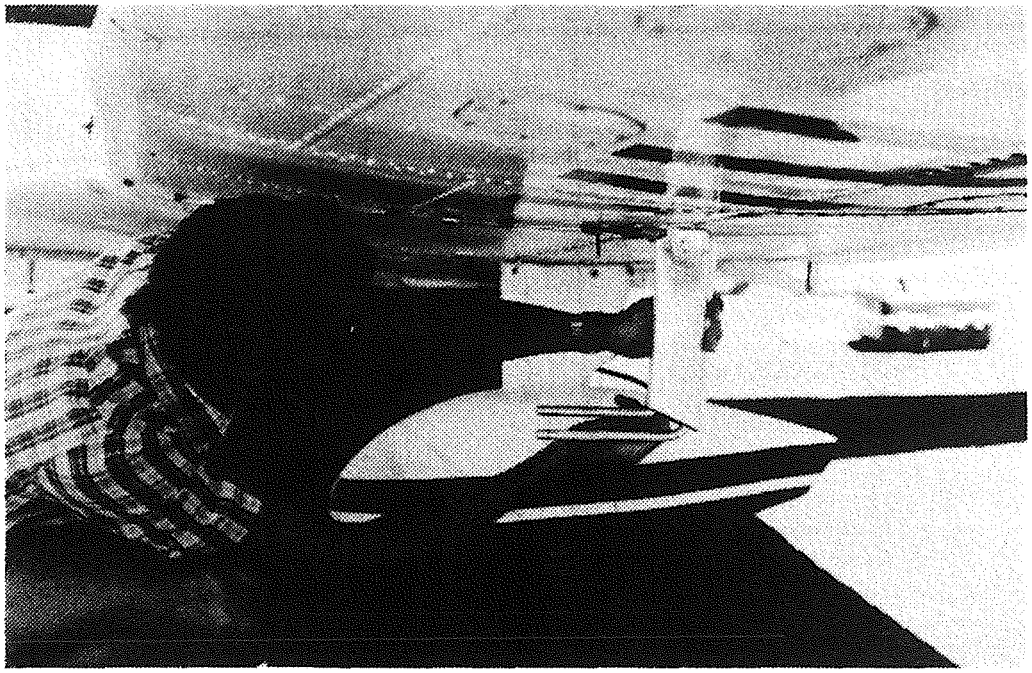

FIGURE 5.2 VARIOMETER STATIC PRESSURE HEAD UNDER AIRCRAFT WING.

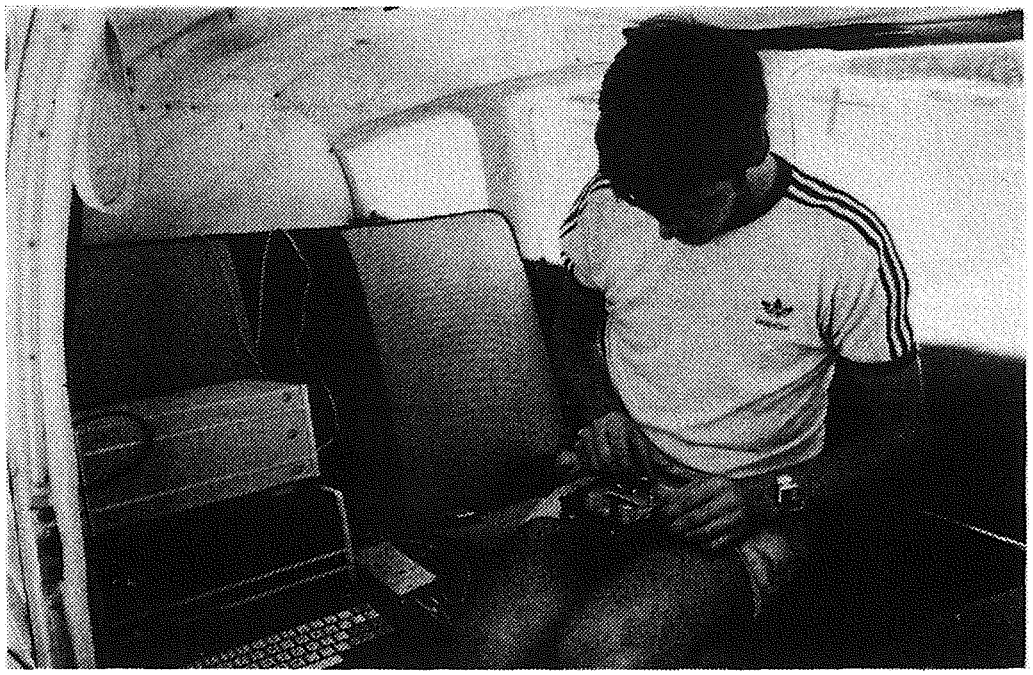

FIGURE 5.3 VARIOMETER AND OTHER INSTRUMENTS INSIDE THE AIRCRAFT.

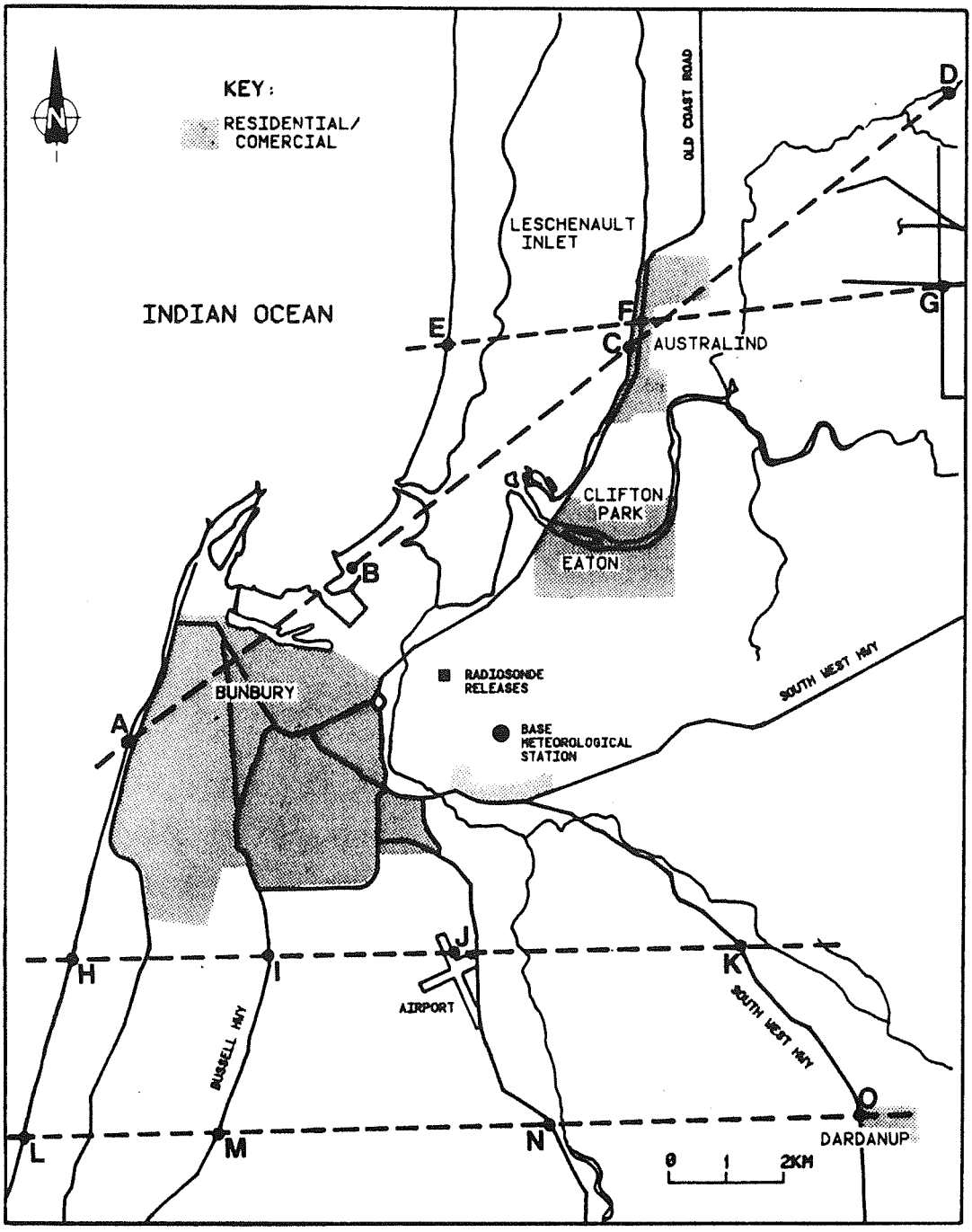

FIGURE 5.4 BUNBURY LOCATION MAP SHOWING AIRCRAFT FLIGHT PATHS

The procedure employed to map the growth of TIBLs was attractively simple. A series of flight paths were first established on a base map of the Bunbury area, as illustrated in Figure 5.4. The capital letters marked along the flight paths denote landmarks (e.g. the coastline, major roads, etc.) which were easily recognisable from the air. A single experiment consisted of several constant speed traverses by the aircraft along the flight path (or part thereof) at selected altitudes within the onshore flow. The variometer output was recorded on the chart recorder for each traverse, as shown on the sample trace in Figure 5.5. Event marks were also recorded on the chart by manually

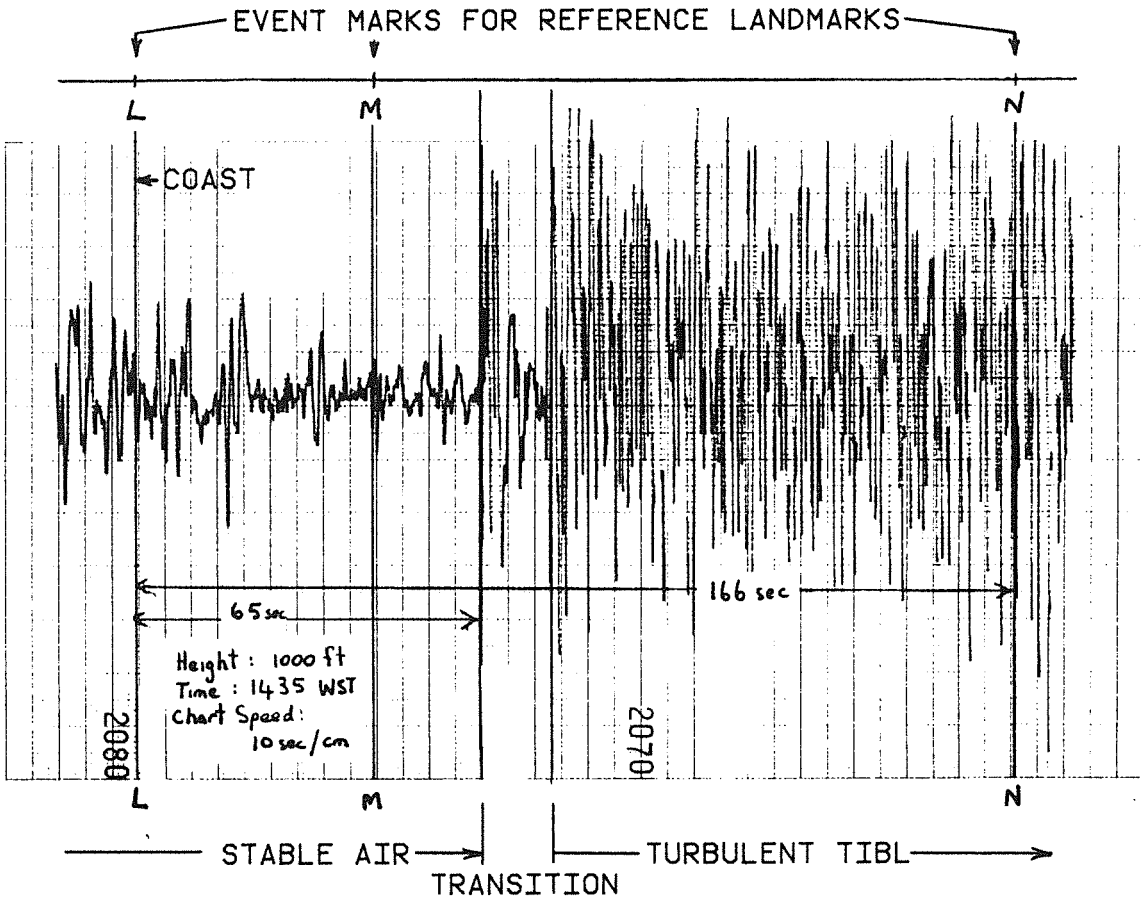

FIGURE 5.5 SAMPLE OUTPUT FROM VARIOMETER

triggering the recorder event marker at the time when the aircraft was directly above the landmarks. Landmark codes are shown adjacent to these event marks.

The sample trace graphically illustrates the change in atmospheric turbulence as the aircraft passes from stable marine air into the TIBL. Given the distance between landmarks, the distance from the coast at which the TIBL turbulence reaches the particular altitude of the traverse is easily determined. Hence the shape of the TIBL may be determined from sequential traces at a range of altitudes, provided the meteorological conditions do not alter significantly during the experiment. Experiments completed within about one hour when the onshore flow is well established are expected to provide reliable information.

The distance data from the two experiments were subsequently transformed from flightpath distance to downwind distance, given the wind direction from the meteorological station (described later) and the shape of the coastline. The flightpaths across Leschenault Inlet required special treatment, as will be discussed in the following Sections.

On the 22 February 1983, some difficulty was experienced in interpreting the TIBL data as it was being recorded. An alternative method involving spiralling the aircraft around a fixed ground point was successfully utilized, although the two data points obtained in this way are not expected to be as accurate in terms of distance from the coast.

The temperature lapse rate Γ in the onshore flow was measured before and after the TIBL mapping experiments by spiralling the aircraft upwards just offshore, commencing close to the water. Data from a wing-mounted temperature sensor (designed and calibrated by Murdoch University staff) were recorded on the chart recorder together with manually actuated event marks at 100 feet intervals of altitude.

Vertical profiles of temperature, wind speed and wind direction over the land were obtained from hourly releases of slow-ascent radiosondes which were tracked by the double theodolite method. The wind profiles were of primary interest, providing estimates of wind speed throughout the TIBL and the bulk of the onshore flow. The temperature profiles provide a useful independent estimate of TIBL height to support aircraft observations. The radiosonde release point is marked on the map in Figure 5.4.

Although attempts were made to run an acoustic sounder during the experiments, this instrument did not function satisfactorily and therefore provided no usable data.

Surface meteorological data was provided by a base meteorological station, located as shown in Figure 5.4. This base station was identical to that installed at Hope Valley during KAMS, as described in Section 2.3, with the additional measurements of incoming long-wave radiation (via a pyrgeometer) and precipitation rate (via a tipping bucket rain gauge). Virtual heat flux and stress were calculated via the heat budget method and verified by the tower profile method, as described in Chapter 3.

5.2.3 EXPERIMENTAL RESULTS

The field experiments performed on the 3/2/83 and 22/2/83 were identical in design, and so the results will be discussed together below.

Figure 5.6 shows the synoptic pressure patterns on the two experimental days, as supplied by the Commonwealth Bureau of Meteorology. On the 3/2/83, a high pressure system was moving eastward across the Great Australian Bight, with a cold front approaching the State from the south west. West to north west winds ahead of the front were well established by early afternoon, with a sea breeze flow superimposed on the onshore flow. The map for 22/2/83 shows a high pressure system ridging eastward across the Bight, producing east to south-west flow across the south west corner of the State. These conditions are conducive to the establishment of a sea breeze along the south west coast, as occurred on this day.

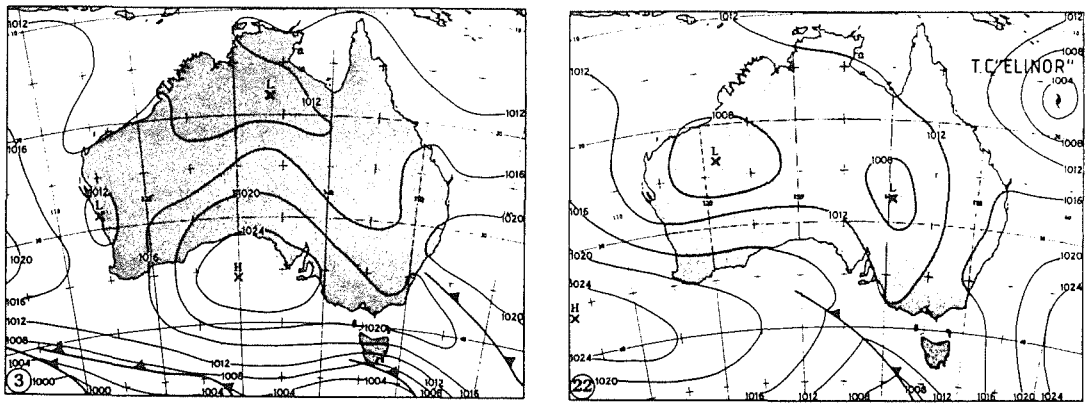

3/2/83 0800 WST 22/2/83 0800 WST

FIGURE 5.6 SYNOPTIC PRESSURE PATTERNS FOR EXPERIMENT DAYS (COMMONWEALTH BUREAU OF METEOROLOGY)

Vertical temperature and wind vector profiles obtained from the radiosonde releases are plotted in Figure 5.7 (a) to (d). Examination of the wind profiles confirms that the two experiment days differred quite distinctly. On the 3/2/85, onshore flow was established over the full vertical range of interest (1 km), ahead of the advancing cold front. The profiles still reveal a wind speed maxima around 400 to 500 metres height however, indicating the superimposed forcing of a sea breeze. The temperature profiles also reveal the development of a cool sea breeze. The wind profiles on the 22/2/83 show a typical summer pattern, with a sea breeze penetrating beneath south easterly flow. The temperature profiles for this day are similarly typical of sea breeze conditions. The sea breeze/synoptic flow interface, centred around 400 metres height, is characterized by a strongly stable temperature gradient, with an overall potential temperature increase of about 2°C across the interface. Very similar sea breeze structures were observed at Kwinana during KAMS, and the sea breeze interfaces were found to present strong barriers to chimney plumes.

Even though there is a marked difference in wind vector profiles on the two days, this difference has no major impact on the development of TIBLs. On both days there was a strong stable layer at the top of the sea breeze flow which would tend to inhibit the growth of a TIBL when it had reached that height.

Temperature profiles obtained by aircraft spirals just offshore at the start and end of experiment periods are plotted in Figure 5.8 (a) and (b). With the exception of the 1410 profile on 22/2/83, these profiles show a close resemblance to those from the radiosondes, without the

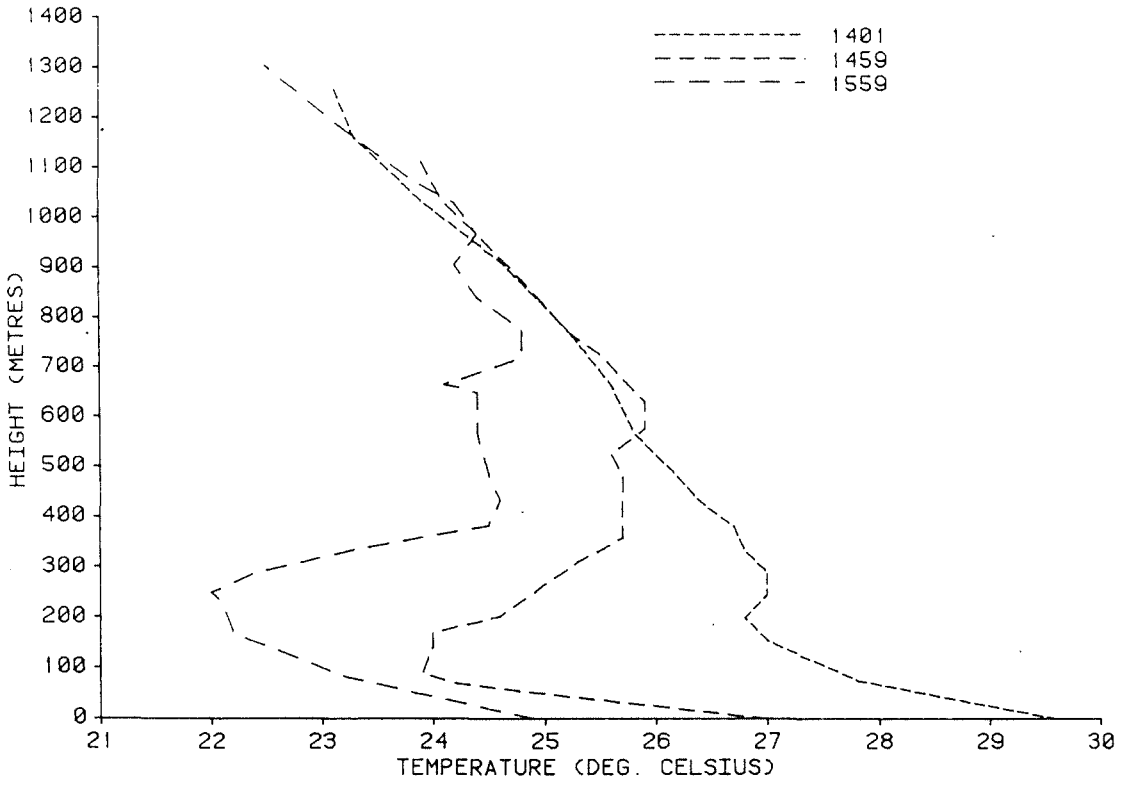

(a) LOW LEVEL TEMPERATURE DATA MEASURED AT BUNBURY ON 03-02-83

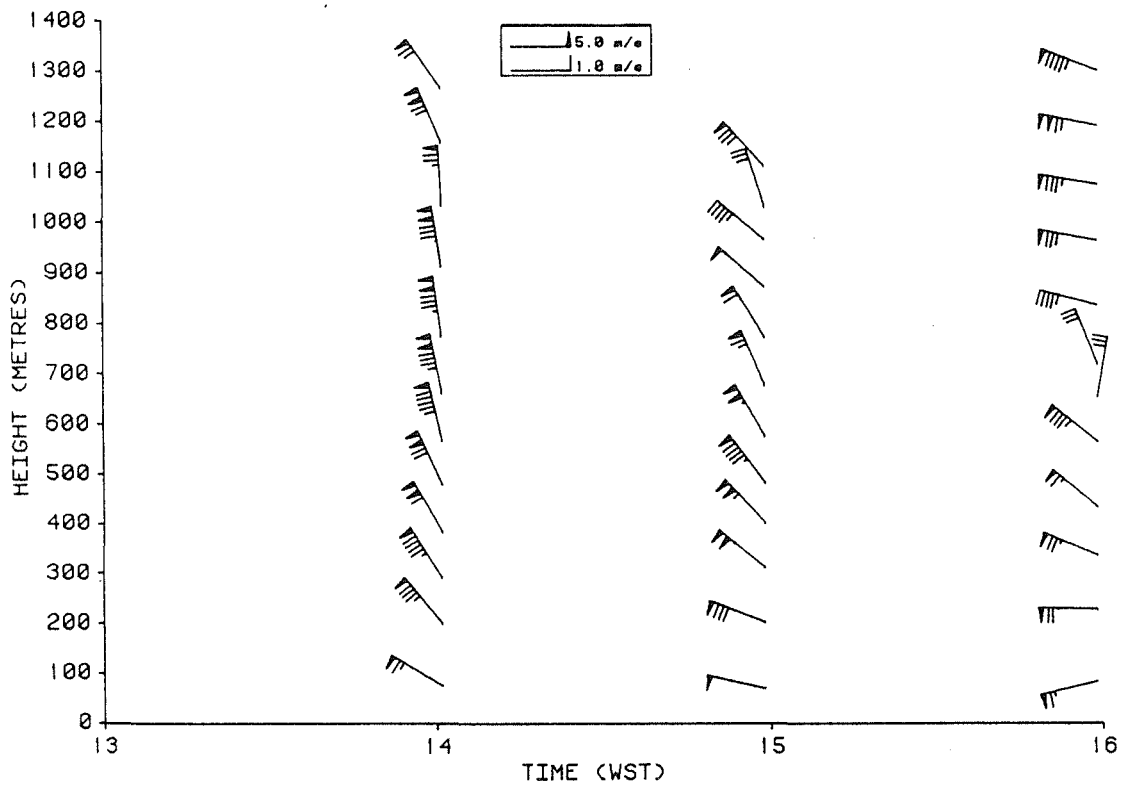

(b) LOW LEVEL WINDS MEASURED AT BUNBURY ON 03-02-83

FIGURE 5.7(a)&(b) TEMPERATURE AND WIND VECTOR PROFILES FROM RADIOSONDES

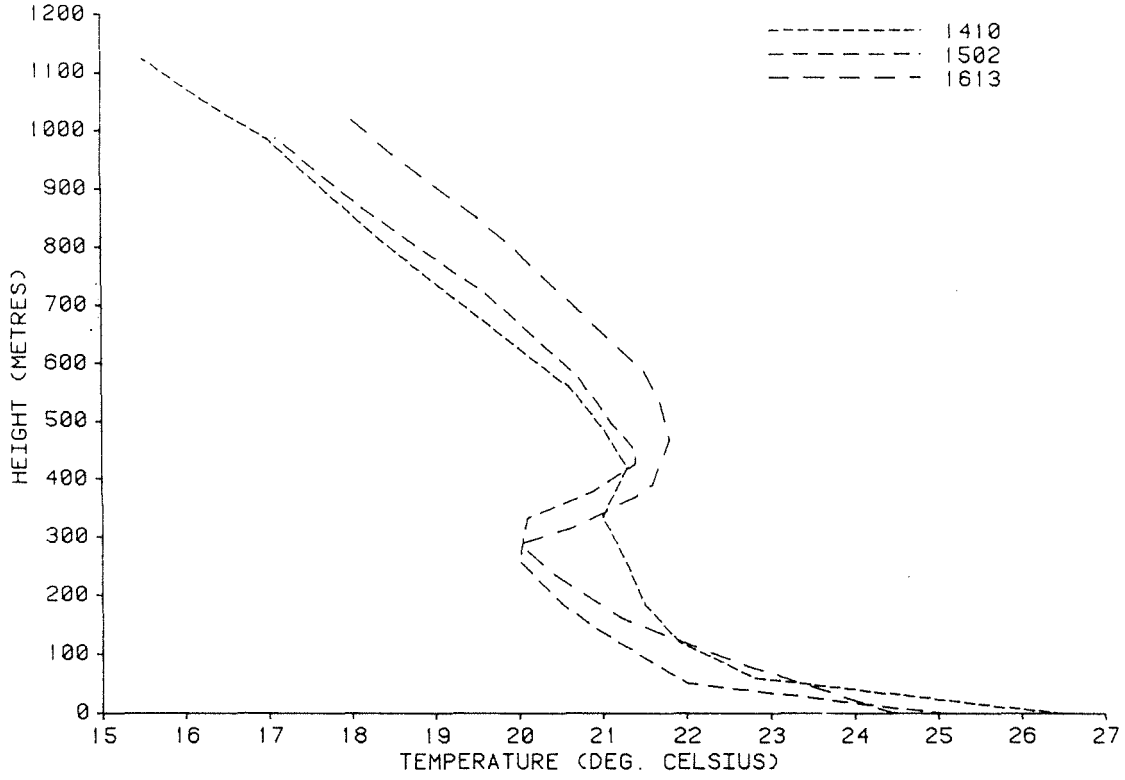

(c) LOW LEVEL TEMPERATURE DATA MEASURED AT BUNBURY ON 22-02-83

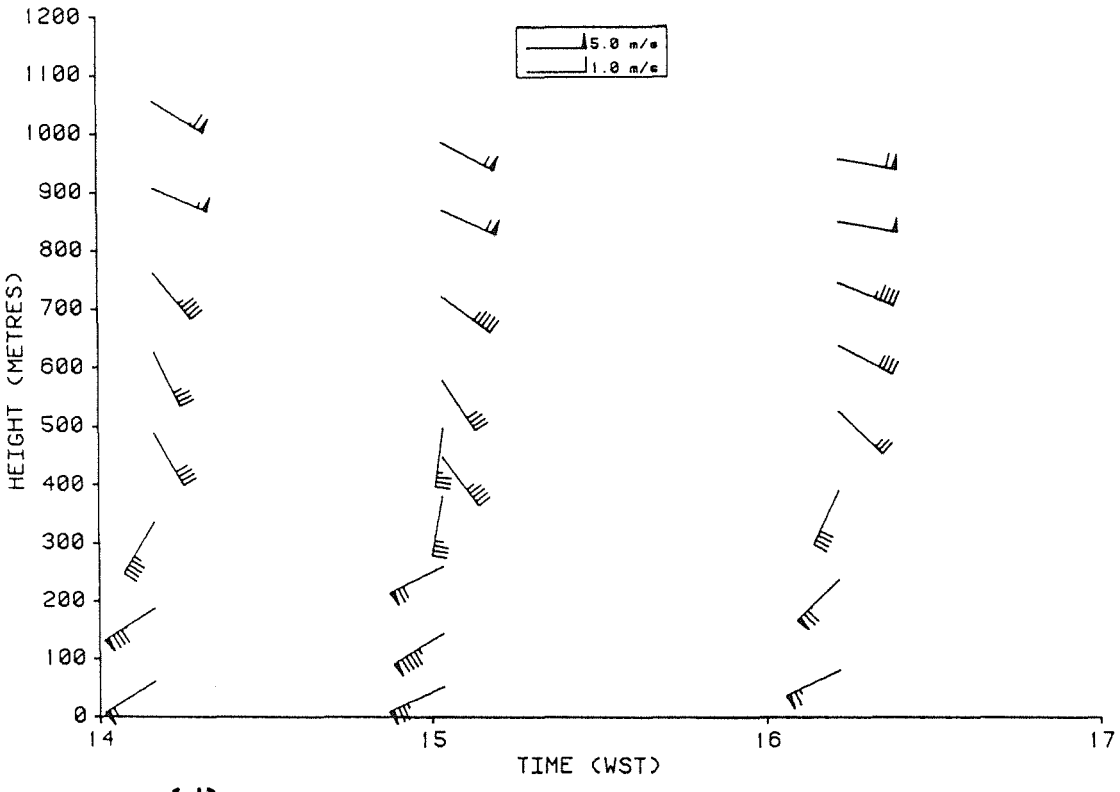

(d) LOW LEVEL WINDS MEASURED AT BUNBURY ON 22-02-83

FIGURE 5.7(c)&(d) TEMPERATURE AND WIND VECTOR PROFILES FROM RADIOSONDES

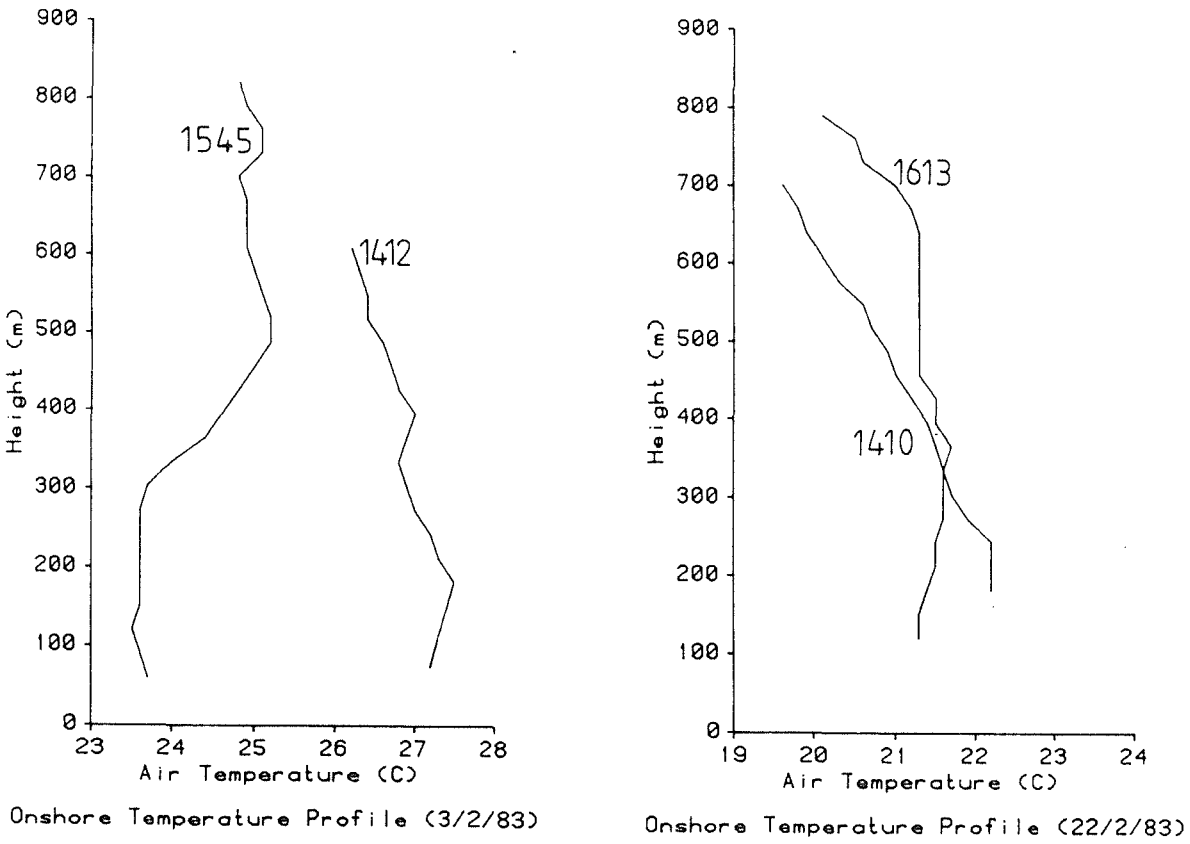

FIGURE 5.8 VERTICAL TEMPERATURE PROFILES MEASURED BY AIRCRAFT SPIRALS OFFSHORE.

effects of surface heating over the land. The 1410 profile on the 22/3/83 shows an unstable warmer region below 300 m, not present in the sonde profile, which must be presumed to be due to erroneous data. Neglecting this anomaly, it may be observed that the profiles up to 300 metres (and sometimes higher) are close to isothermal, i.e. $r \approx 0.0098$ °C/m. This observation is consistent with findings in KAMS, where a figure of $r = 0.0090$ was chosen as representative for well developed sea breezes. The sea breeze data presented by Kerman et al. (1982) also reveal isothermal profiles in the sea breeze flow before it encounters the land, as do the aircraft observations offshore from Perth reported by Walker and Allen (1975). Isothermal profiles in the

sea breeze appear to be a characteristic of this mesoscale flow, providing a useful "rule of thumb" for dispersion modelling.

Table 5.1 gives the important meterological parameters for the two study days, obtained from the meteorological base station. The parameters have been averaged over the experimental period for each day to give the most representative values for use in calculating TIBL heights. The layer mean wind speeds (U_{layer}) were obtained from the radiosonde profiles up to 300 metres height.

TABLE 5.1 METEOROLOGICAL PARAMETERS AVERAGED OVER EXPERIMENTAL PERIODS.

Meteorological Parameter	Experimental Day	
	3/2/83	22/2/83
H_v (W/m^2)	257	471
Direction (deg.)	295	259
U_{27} (m/sec)	4.7	6.2
T_{27} (°C)	26.7	23.1
U_{layer} (m/sec)	7.6	6.2

It is of interest to note that the layer mean wind speed on the 22/2/85 (when the sea breeze / gradient wind counterflow was established) was the same as the tower measurement at 27 metres, which in turn was 1.33 times the 10 metre measurement. Sea breeze observations at Kwinana during KAMS (described in Chapter 6) led to the adoption of a rule of thumb for layer mean winds, namely $U_{layer} \approx 1.2\ U_{10}$. The indication of a larger coefficient for Bunbury is consistent with the greater roughness of the Bunbury site. Such

rules of thumb fail when the counter flow is not present aloft.

The shape of the TIBLs observed on the two field days are plotted in Figure 5.9 (a) and (b) as points with error bars. The vertical error bars represent altitude uncertainty due to altimeter accuracy and pilot error. The horizontal error bars are a composite estimate including inaccuracies in timing of event marks, determining the start of the TIBL on the recorder trace, and in the wind direction estimate used to adjust the distance scale to represent downwind distance.

The point signified by dashed error bars was obtained during a transect across Leschenault Inlet, and will be discussed later as a special case.

5.2.4 DISCUSSION OF RESULTS

The TIBL shapes, calculated from (5.6) with the above data, are plotted as full lines in Figure 5.9 (a) and (b). (A simple check shows that the MIBL effect is negligible).

The two sets of data have distinct characteristics and so will be discussed separately.

The first experiment, 3/2/85, ran very smoothly, with all of the TIBL height observations coming from horizontal aircraft transects. Distinction between stable onshore flow and the TIBL was very easy since the stable air extended over the full height of interest (i.e. there was no turbulent offshore synoptic flow aloft).

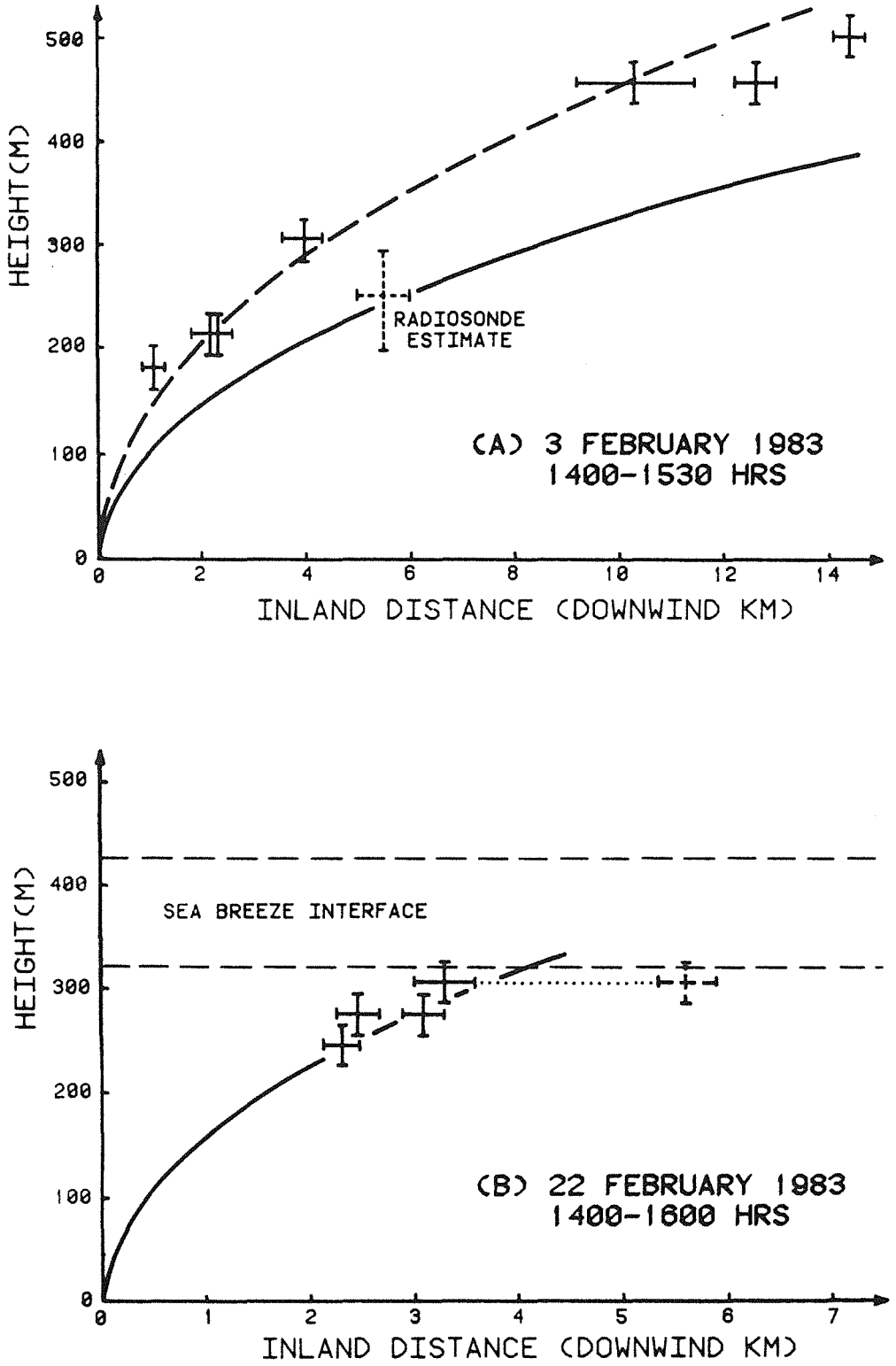

FIGURE 5.9 OBSERVED AND PREDICTED TIBLS

A visual examination of the observed and predicted TIBLs reveals that, whilst the shape of the two are similar, the height of observed turbulent activity extends well above the predicted TIBL envelope. However, the results of Gammo et al. (1982) indicate that the observed disparity is to be expected. They observed that the boundary layer shape defined by the onset of turbulent activity during a horizontal aircraft transect was higher than that defined by a measurable change in air temperature (caused by heating within the TIBL), by a factor of approximately 1.4. The explanation offered by Gammo et al. is difficult to follow, but can be restated as follows. Figure 5.10 shows, for the current model, the idealized temperature profile (full line) and the expected actual profile (dotted) at a distance x downwind of the coast.

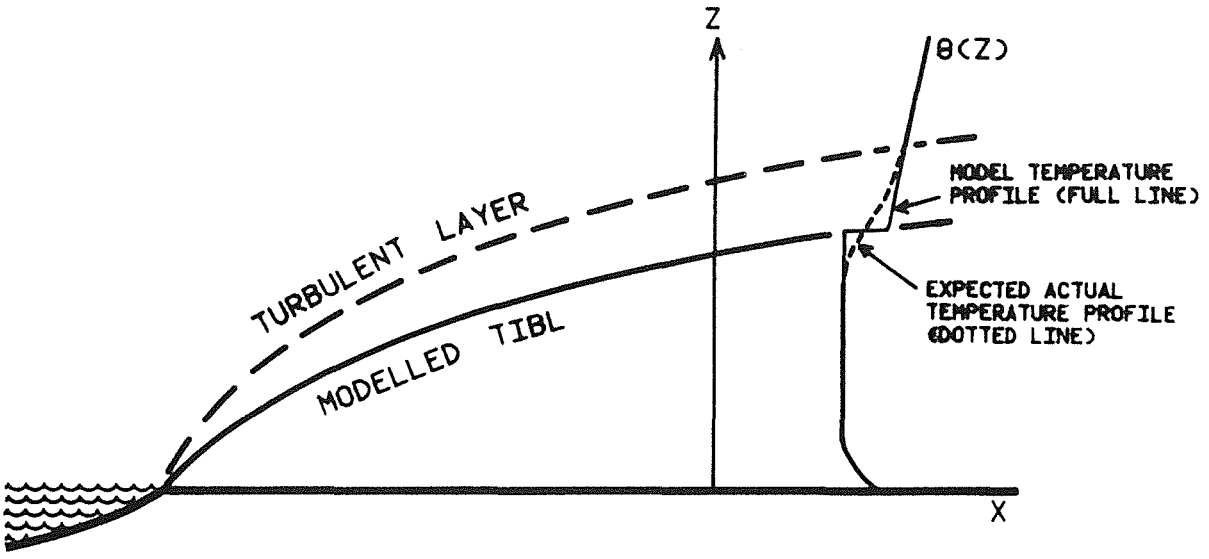

FIGURE 5.10 TIBL TEMPERATURE PROFILE: MODELLED AND ACTUAL

The two differ in that the actual interface at the TIBL top will not be a sharp step but rather a thick smeared layer, similar to that which appears above a one-dimensional well mixed layer as described in Section 4.6. A variometer would detect turbulence as soon as the aircraft encounters the top of this thick interface (i.e. the dashed boundary layer in Figure 5.10), whereas a temperature sensor would not record a discernable change until some further distance downwind. It is not unreasonable to assume that the boundary layer shape defined by discernable temperature changes will approximate to that of the idealized model. Temperature increases above the background value will certainly be detected within the lower half of the interface.

On the basis of the above assumption and Gammo's observations, a dashed line has been drawn on Figure 5.9 (a) to represent 1.4 times the predicted (ideal) TIBL height. This line clearly fits the observations very well. Hence, even though there is some uncertainty associated with the assumption, the basic reason for the difference between observations and predictions is quite clear.

The radiosonde profiles for this day provide a degree of independent support to the analysis above. If we again define the ideal TIBL height to be the centre of the stable interface above the well mixed layer, we obtain a representative TIBL height of 250 ± 50 m from the three sonde profiles. Given that the radiosonde location was 5 to 6 km downwind from the coast, this estimate of TIBL height has been plotted in Figure 5.9 (a) and can be seen to lend strong support to the model prediction, in the same way that radiosonde profiles supported the well mixed layer model predictions rather than acoustic sounder

records in Section 4.6. In other words, the variometer appears to provide a measure of turbulent activity similar to an acoustic sounder, but the turbulent activity at its upper extent is not indicative of strong mixing , as is clearly evidenced by the radiosonde profiles.

Having identified two alternative measures of TIBL height, varying by about 40%, we must decide which form is appropriate for use in dispersion models. In their comparison of different formulae, Stunder and SethuRaman (1985) chose to adopt the "turbulence definition" (i.e. as measured by a variometer), although their diagramatic representation of temperature profiles are not consistent with this definition; they show a fully mixed TIBL with constant potential temperature. (Fortunately, the choice of TIBL definition does not affect their intercomparison of different formulations.) It may be argued that the choice of TIBL definition should be dependent on the use to which it is to be put. In the next Chapter, we will develop an empirical scheme for describing the rapid vertical mixing of smoke plumes after they intersect the TIBL. Since the idealized model description of a TIBL gives the best objective estimate of the height to which strong mixing penetrates, it is believed to provide the best measure of TIBL height for dispersion modelling purposes.

The quality of experimental results and the accuracy of model predictions for the 3/2/83 experiment compare very favourably with those published for other TIBL experiments (i.e. Raynor et al., 1979; Stunder and SethuRaman, 1985), although a thorough comparison is difficult due to the different analytical procedures used and the

limited amount of data presented in accessible form in the literature.

The data obtained on the 22/2/83 has proven to be of limited value for analysis of TIBL growth, for the following reasons. Information from the radiosonde station on the sea breeze depth was not available to the scientists in the light aircraft. Furthermore, there was no other reliable measure of sea breeze depth obtainable from the aircraft. Consequently, these scientists (including the author) experienced great difficulty in differentiating between the turbulence in the TIBL and that in the synoptic easterly flow above the sea breeze. Much time was lost in attempting to define the situation and even then, the need for low level transects (below 200 m) near the coast was not recognised.

Only four reliable data points were able to be extracted from the variometer traces; these are plotted on Figure 5.9 (b). Of these, the two points at 275 m altitude are the most reliable having been determined from a transect below the sea breeze interface. The point at 245 m was obtained from a vertical spiral, but the determination of the onset of turbulence by this method was quite subjective. The uppermost point was transposed horizontally by subtracting out the travel distance across Leschenault Inlet (as indicated by the dotted line). This procedure is believed to be a simple but physically realistic way to account for stagnation of TIBL growth across an inland water body, however further verification is required.

The sea breeze interface determined from the radiosondes is plotted in Figure 5.9 (b). The sonde profiles also show a moderately stable

region below the interface (above 230 m) which is consistent with turbulent entrainment at the top of the mixed layer.

The distribution of data points is not adequate for the task of defining the TIBL shape. All data points fall within the moderately stable region mentioned above, at which level the growth of turbulent activity is suppressed by the strong sea breeze interface. It is not clear at what distance downstream the TIBL reached this level, and therfore it is difficult to comment on the significance of the apparently better correspondence of data points and theoretical prediction compared to the 3/2/86 experiment. However, on the basis of these results it can be argued that the most objective procedure for dispersion modelling is to allow TIBL growth according to (5.6) up to the base of the sea breeze interface. The subsequent erosion of the sea breeze interface has not been addressed in this Study.

5.2.5 SUMMARY OF FINDINGS

In summary, it is apparent that the simple TIBL formula (5.6) describes the essential features of TIBL growth for the purpose of modelling shoreline fumigation. The formula has a sound theoretical base in the well mixed layer theory of Chapter 4 and has received experimental support both directly from the present Study and indirectly from other studies described in the scientific literature. Reliable field data may only be obtained from well designed, comprehensive, expensive field experiments, which no doubt explains the paucity of such data available for theoretical studies (e.g. Stunder and SethuRaman, 1985). Additional field experiments in light

sea breeze conditions are warranted to investigate the rapid growth of the TIBL and its interaction with the sea breeze interface.

CHAPTER 6

ATMOSPHERIC DISPERSION IN A COASTAL REGION

The purpose of this Chapter is to present theoretical relationships and empirical procedures which together form the foundation of a point source dispersion model. Section 6.1 deals with general concepts appropriate to both coastal and inland situations, whilst Section 6.2 concentrates on description of the shoreline fumigation phenomenon introduced in Chapter 1. Experimental verification of a dispersion model employing all the theory and procedures outlined in these Sections is described in Section 6.3.

6.1 GENERAL POINT SOURCE DISPERSION THEORY

A description of general point source dispersion theory must be included here for completeness. However, as identified in Chapter 1, this topic is not a key area of investigation in this Thesis. Accordingly, this Section will simply present selected information as opposed to providing a critical review of alternative methods. The relationships will be, in the main, those adopted for use in the KAMS dispersion model DISPMOD, which will be described in Chapter 7. Alternative relationships or methods will be mentioned only where it is instructive to do so.

It should be noted however, that the capability of employing alternative relationships within DISPMOD to describe any of the meteorological processes which affect plume dispersion is one of the

strengths of the present approach. Within the constraints of the Gaussian plume method, there is scope for employing the comprehensive data output from the well mixed layer model to optimise the description of meteorological processes. In particular, the availability of u_*, w_* (or L) and $\Delta\theta$ data facilitates the application of the bulk of recent advances in atmospheric dispersion theory.

6.1.1 PLUME RISE INTO NEUTRAL OR UNSTABLE AIR

The heading "plume rise" is used to describe plume behaviour generated by its own momentum and buoyancy, out to that distance where atmospheric turbulence becomes dominant and the plume disperses as a passive contaminant.

For the case of neutral atmospheric stability, Briggs (1975) provides an analytical formula for plume trajectory

$$z = \left[\frac{3}{\beta^2}\frac{F_m}{U^2}x + \frac{3}{2\beta^2}\frac{F}{U^3}x^2\right]^{1/3} \qquad (6.1)$$

where the initial momentum flux and buoyancy flux parameters are given by

$$F_m = (\rho_s/\rho)w_s^2 b_s^2 \qquad (6.2)$$

$$F = g(T_s - T)w_s b_s^2/T_s \qquad (6.3)$$

and where:

β is an entrainment coefficient ≈ 0.6

x is downwind distance

ρ_s is efflux density

w_s is efflux velocity

b_s is stack exit radius

T_s is efflux temperature

Equation (6.3) includes the assumption that the plume density and ambient air density at STP are almost equal. The second term in (6.1) dominates as x becomes large, in which case the equation may be rewritten giving:

$$z = 1.6F^{1/3}U^{-1}x^{2/3} \qquad (6.4)$$

For most hot chimney plumes (6.4) holds beyond a downwind distance equal to only a few stack diameters, implying that initial plume momentum is unimportant apart from enabling the plume to clear the stack.

6.1.2 PLUME RISE INTO STABLE AIR

Briggs (1975) reaffirms his 1969 formula for plume rise into a stable constant density gradient, which gives the final height of rise as

$$\Delta H = C_2[F/(Us)]^{1/3} \qquad (6.5)$$

where C_2 is a constant (≈ 2.6) and s is a measure of the atmospheric stability defined as

$$s = gr/T \qquad (6.6)$$

The stack height H_{st} must be added to the estimates from (6.1), (6.4) or (6.5) to give the total plume height H_e.

6.1.3 PLUME PENETRATION OF AN ELEVATED TEMPERATURE INVERSION

The erosion of radiation inversions and the formation of a stable elevated inversion layer ("lid") above a well mixed layer has been fully described in Chapter 4. Use of the modelled lid strength, $\Delta\theta$, in dispersion modelling was discussed in Section 4.7.

Manins (1979) gives the following formulae to predict the fraction FR of plume material which will be trapped under an elevated lid:

$$FR = 0.08/P - (P-0.08), \quad (0<FR<1) \tag{6.7}$$

where $P = F/[Ug\Delta\theta\Delta H^2/T]$ (6.8)

The field observations reported by Manins (1985) support the use of these formulae.

6.1.4 PLUME LEVELLING IN NEUTRAL OR UNSTABLE AIR

The formulae proposed by Briggs (1971) which have gained most widespread acceptance for computing the final rise of plumes in neutral or unstable air are the following:

$$\Delta H = 1.6F^{1/3}U^{-1}(3.5x^*)^{2/3} \tag{6.9}$$

where $x^* = 14F^{5/8}$ for $F < 55\ m^4s^{-3}$

$x^* = 34F^{2/5}$ for $F \geq 55\ m^4s^{-3}$

The plume reaches its final level at the downwind distance $3.5x^*$.

The above formulae will be used in the dispersion model in this Study. However there is a cause for concern in the form of the above relationship which is clearly shared by Briggs (1975) himself, namely that levelling is described in terms of the plume buoyancy F alone, with no reference to the intensity of atmospheric turbulence which is responsible for the transition of the plume to its levelled passive state. Briggs (1975) proposes two alternative formulae for the cases of mechanically and thermally dominated atmospheric turbulence:

Mechanical:

$$\Delta H = 1.3(F/Uu_*^2)(1 + H_{st}/\Delta H)^{2/3} \tag{6.10}$$

Thermal:

$$\Delta H = 4.3(F/U)^{3/5}[H_v g/(\rho C_p T)]^{-2/5} \tag{6.11}$$

For the cases of mechanical and thermal turbulence, u_* and H_v respectively determine the ambient turbulent energy dissipation rate, which may in turn be compared to the decaying plume turbulence dissipation rate to determine the plume height at which atmospheric turbulence dominates and levelling occurs. The results of this analysis are embodied in (6.10) and (6.11). Modified forms of these two equations are given by Hanna, Briggs and Hosker (1982).

Weil and Brower (1984) report improved agreement with observed plume rise by using (6.10) and (6.11). If and when formulae such as (6.10) and (6.11) are better verified and gain wider recognition, they may be easily incorporated in DISPMOD, since u_* and H_v data are directly available.

6.1.5 TRANSPORT OF POLLUTANTS

As described in Chapter 1, the current study is limited to a local scale of less than 15 km. The area of interest is part of a coastal plain with very few significant topographic features. As discussed by Kamst et al. (1980), there are still appreciable variations between the statistics of wind velocity recorded by the network of anemometers deployed during KAMS, primarily due to the change in surface characteristics at the coastline. These variations are believed to be of secondary importance in terms of their effect on the dispersion of plumes from coastal sources (i.e. secondary relative to other meteorological processes which affect dispersion, including shoreline fumigation). In order to proceed with the development of a shoreline fumigation model based on a conventional Gaussian plume approach,

wind-field effects have been neglected.

The variation of wind speed with height in the planetary boundary layer may be described by a power law of the form

$$U(z) = U_1(z/z_1)^p \qquad (6.12)$$

where subscript 1 refers to a reference height (usually 10 metres). Irwin (1979 b) provides estimates for the exponent p as a function of both atmospheric stability and roughness length z_0.

6.1.6 GAUSSIAN PLUME METHOD

For a continuous point source, the general form of the Gaussian plume equation (Turner, 1970) is:

$$\chi(x,y,z) = \frac{Q}{2\pi\sigma_y\sigma_z U}\exp\left[-0.5\left(\frac{y}{\sigma_y}\right)^2\right]\exp\left[-0.5\left(\frac{z-H_e}{\sigma_z}\right)^2\right] \qquad (6.13)$$

where χ is concentration

Q is source emission rate

σ_y is lateral standard deviation

σ_z is vertical standard deviation

x, y, z are downwind, crosswind and vertical coordinates, respectively

The general form of (6.13) is often expanded to include the barrier effects of the ground and an elevated temperature inversion above the mixing height h. "Reflection" of plume material at these two boundaries is achieved by addition to the last exponential term in (6.13), so that expanded term becomes

$$\left\{ \exp\left[-0.5\left(\frac{z-H_e}{\sigma_z}\right)^2\right] + \exp\left[-0.5\left(\frac{z+H_e}{\sigma_z}\right)^2\right] + \exp\left[-0.5\left(\frac{z-(2h-H_e)}{\sigma_z}\right)^2\right] \right.$$

$$\left. + \exp\left[-0.5\left(\frac{z+(2h-H_e)}{\sigma_z}\right)^2\right] \right\} \qquad (6.14)$$

Pasquill (1974) summarizes several field experiments in which averaged crosswind plume profiles were analysed and concludes that, although individual profiles vary considerably, there is no good reason to adopt an analytical form different from Gaussian. The laboratory experiments of Willis and Deardorff (1976) show that the Gaussian distribution adequately describes the ensemble averaged lateral spread of plume material for all downwind distances under convective conditions. This and subsequent experiments by the same authors have shown, however, that vertical spread from an elevated source in strongly convective conditions cannot be adequately described as Gaussian. Further, Pasquill (1974) observes that vertical spread from a ground level source is systematically different from Gaussian, tending toward an exponential form. Apart from the above two exceptions, the precise prescription of plume distribution, be it Gaussian or some similar form, is not as critical as a correct specification of plume spread σ_y and σ_z.

In the Kwinana industrial area, ground level sources were not significant and therefore the Gaussian model capability is only suspect with regard to elevated emissions in unstable conditions. In terms of dispersion overland, the bulk of unstable conditions will be dealt with via special methods for dispersion in TIBLs, to be described in the Section 6.2. For the balance of cases, vertical dispersion calculations will use the most appropriate estimates of σ_z, but no alternatives to the Gaussian plume method will be employed.

6.1.7 ATMOSPHERIC STABILITY DETERMINATION

Good summaries of the historical development of atmospheric stability classification schemes are given by Pasquill (1974), Hanna, Briggs and Hosker (1982) and others. This information will not be repeated here. The approach adopted in KAMS and summarized below was formulated to be consistent (as far as possible) with Hanna et al. (1977).

The input data file for DISPMOD includes the variables h, H_v (which together define w_*), u_*, 10/L, and measured σ_θ. Accordingly, there is no justification for reverting to a stability determination such as that developed by Pasquill and Gifford (Turner, 1970).

Hanna et al. (1977) recommend the use of measured σ_θ where possible for the determination of σ_v. Since σ_θ data are available, this recommendation is easily accommodated. However, alternative approaches were pursued for the following reasons:

i) in line with the Study objectives described in Chapter 1, it is desirable for the model to be applicable in situations where reliable σ_θ data are not available;

ii) the analog Sigma Meter employed in KAMS had a maximum sampling period of three minutes, and therefore tended to underestimate σ_θ in convective conditions. (More recent microprocessor based data logging systems allow σ_θ to be calculated over the full data averaging period, e.g. 10 to 60 minutes).

Two options were open for the application of the available data to classification of stability for dispersion modelling:

(a) use the Monin Obukhov length L and the known roughness length z_0 to determine stability classes, following the method of Golder (1972);

(b) following Irwin (1979a), use the data, together with experimentally determined relationships for planetary boundary layer turbulence, to calculate σ_v and σ_w (and hence $\sigma_\theta = \sigma_v/U$, $\sigma_\phi = \sigma_w/U$), for use in determining σ_y and σ_z as described in the next Section.

Option (b) was chosen, to avoid the coarse resolution of stability classes and to take advantage of the worldwide research effort aimed at relating plume spread (σ_y, σ_z) to atmospheric turbulence (σ_θ, σ_ϕ).

The results of experiments in the planetary boundary layer by Kaimal et al. (1976) and Caughey and Palmer (1979), and the analyses of Panofsky et al. (1977) and Hunt (1982), are summarized in Table 6.1 in a form suitable for dispersion modelling:

TABLE 6.1 EXPRESSIONS FOR σ_v AND σ_w

Expressions for σ_v:

$z/L < 0$: $\sigma_v = u_*(12 - 0.5h/L)^{1/3}$

$z/L \geq 0$: $\sigma_v = 2.3u_*$

Expressions for σ_w:

$z/L < 0$: $\sigma_w = 1.3u_*(1 - A)^{1/3}$

where $A = \begin{cases} 3z/L, & z < 0.08h \\ 0.24h/L, & z \geq 0.08h \end{cases}$

$z/L \geq 0$: $\sigma_w = 1.3u_*$

If the nocturnal boundary layer height is known, the reduction of σ_v with height may be parameterized to match experimental observations in the stable planetary boundary layer (e.g. Caughey et al., 1979)

6.1.8 ESTIMATING PLUME SPREAD PARAMETERS

In view of the selection of Option (b) above for describing atmospheric stability, this Section will concentrate on methods relating σ_y and σ_z directly to σ_θ and σ_ϕ respectively. Discussion of Sigma curves based on stability categories are given by Hanna et al. (1982) and others.

Taylor's (1921) statistical analysis of the spread of particles in a field of homogenous turbulence leads to relationships of the form

$$\sigma_{y,z} = \sigma_{v,w} T \, F_{y,z}(T/\tau_L) \qquad (6.15)$$

where T is travel time and τ_L is the Lagrangian timescale of the turbulence. The only information on the function F which flows directly from Taylor's analysis is that, for short travel times, $F \approx 1$ and for long travel times, F is proportional to $T^{-1/2}$.

Applying the transformations $X = UT$ and $\sigma_{\theta,\phi} \approx \sigma_{v,w}/U$, (6.15) may be rewritten as:

$$\sigma_y = \sigma_\theta X \, F_y(T/\tau_L) \qquad (6.16)$$

$$\sigma_z = \sigma_\phi X \, F_z(T/\tau_L) \qquad (6.17)$$

To utilize these formulae we need estimates of σ_θ and σ_ϕ, and an evaluation of F_y and F_z over all downwind distances (or travel times) of interest.

Pasquill (1976) showed that, provided the sampling times for σ_θ and σ_y

are the same, a single form of F_y will hold (i.e. independent of sampling time). The same should be true in the vertical for elevated plumes. This finding eliminates the need for long sampling times in order to cover the full turbulence spectrum.

The forms taken by F_y and F_z must be determined either from measurements of turbulence spectra, field observations of dispersion, or both. Pasquill (1976) provided a specification of F_y, reproduced in Table 6.2, in which a dependence of F_y on travel distance x was assumed:

TABLE 6.2 VALUES FOR $F_y(X)$ FROM PASQUILL (1976)

x (km)	0.1	0.2	0.4	1	2	4	10	> 10
$F_y(x)$	0.8	0.7	0.65	0.6	0.5	0.4	0.33	$0.33(10/x)^{1/2}$

Irwin (1979a) fitted the following two-part expression to these values:

$$F(x) = [(1 + .0308x^{.4548})]^{-1}, \quad x \leq 10 \text{ km} \qquad (6.18a)$$

$$F(x) = 0.333(10000/x)^{1/2}, \quad x > 10 \text{ km} \qquad (6.18b)$$

where x is in metres. This formulation obeys Taylor's short and long travel time limits.

The form of F_z is less certain. Pasquill (1976), although agreeing that the statistical theory is applicable to vertical dispersion of elevated plumes, did not provide a description of F_z but suggested an interim continued use of the Sigma curves, corrected for surface roughness. The only explicit forms of F_z for elevated sources

mentioned by Hanna et al. (1977) in their review paper were those of Draxler (1976), which take the form:

Unstable: $F_z(t) = 1/[1 + 0.90(t/T_i)^{0.5}]$ (6.19a)

Stable: $F_z(t) = 1/[1 + 0.945(t/T_i)^{0.806}]$ (6.19b)

where T_i is a measure of diffusion time required to reach Taylor's far field limit, evaluated as:

Unstable: T_i = 500 seconds

Stable: T_i = 100 seconds.

Whilst Hanna et al. (1977) did not directly support these formulae, a subsequent comprehensive review of experimental data by Irwin (1983) showed that Draxler's formulae performed creditably and overall the best of the various options evaluated. Irwin's analysis also supported the simple form:

$$F_z = 1 \qquad (6.20)$$

for convective conditions. This expression, coupled with the convective limit of the formula for σ_w in Table 6.1 (i.e. $\sigma_w \approx 0.6w_*$) has received strong support from Weil (1985) and others.

An examination of (6.19a) and (6.19b) reveals that they do not match well at the neutral limit. For the purpose of the current Study, modified versions of these formulae were adopted. These were designed to achieve two goals:

(i) agreement with the important features of Taylor's statistical theory embodied in (6.19 a and b), and a close correspondence to these formulae in the ranges where they are believed to be most applicable (moderate instability, moderate to strong stability);

(ii) a reasonable correspondence with the Pasquill-Gifford-Turner sigma curves (Turner, 1970) and Briggs sigma relations (Gifford, 1975) (corrected for surface roughness), which are still widely

recognised in regulatory modelling applications (Hanna, 1982).

The expressions which were adopted are as follows:

Unstable/neutral: $F_z(x) = 1/[1 + 0.018(x)^{0.5}]$ (6.21a)

Stable: $F_z(x) = 1/[1 + 0.098(x/30)^E]$ (6.21b)

where the exponent E varies linearly between 0.5 and 0.81 as the Monin-Obukhov scale 10/L varies from 0 to 3. The first of these expressions comes from Draxler's expression for a median wind speed of 5 m/s, while the second is an empirical expression designed to match (6.19 a) in the neutral limit and (6.19 b) in the stable limit, again for a median wind speed of 5 m/s. Equation (6.20) was reserved for the convective conditions encountered in thermal internal boundary layers, as discussed in the next Section.

It is expected that improvements to the formulae for F_y and F_z will be forthcoming from future international research efforts, and it will be a trivial task to incorporate these in the model. A more detailed analysis of alternative formulae is beyond the scope of this Study.

Hanna (1982) suggests a simple scheme for including the effects of buoyancy-induced spread in the estimates of σ_y and σ_z, which entails setting both of these parameters equal to $0.3\Delta H$ at the distance where final rise is achieved and then calculating a virtual source location (e.g. from (6.18a)) to give a matching value of σ_y at the final rise distance. A single virtual source cannot match both the σ_y and σ_z buoyancy-spread values.

6.1.9 SUMMARY

The foregoing discussion has presented, without exhaustive review, selected formulations for the various components required within a conventional Gaussian plume dispersion model. Attention can now be focussed on one of the main developmental areas in this Study, namely the description of dispersion in onshore flows.

6.2 DISPERSION IN ONSHORE FLOWS WITH COASTAL INTERNAL BOUNDARY LAYERS

Onshore winds have dispersion characteristics which are quite different to that of winds which have travelled over an expanse of land, as discussed by Lyons (1975). There are also significant differences to be seen within the general classification of onshore winds. The most obvious differentiation is based on whether the wind has been generated by synoptic or mesoscale pressure patterns (i.e. sea breezes). Sea breezes characteristics (e.g. time of onset, depth, strength) also vary significantly. An important area of future work is the classification of sea breeze characteristics in terms of synoptic and other external parameters.

The onshore flow feature of particular interest in the present Study is the formation of coastal internal boundary layers and the impact of these on dispersion of chimney plumes from coastal industries. A brief introduction to the problem was given in Section 1.2.1 and portrayed in Figure 1.5.

An intuitive examination of Figure 1.5 reveals that the shoreline

fumigation process is well beyond the scope of standard procedures such as the uniform Gaussian plume description for continuous point sources. The rate of both vertical and horizontal diffusion changes quite suddenly as plume material enters a TIBL. A corresponding but less dramatic change in dispersion rate would be seen when a plume enters an internal boundary layer dominated by mechanical turbulence (MIBL). McRae et al. (1981) correctly point out that atmospheric stability (which varies markedly from the marine air to the air within a TIBL or MIBL) cannot be meaningfully classified in the conventional way.

For clarity, the term "shoreline fumigation" will be restricted to the effect of TIBLS, with the effect of MIBLS being considered separately as a case of enhanced dispersion.

The basic reason for the level of worldwide interest in the shoreline fumigation process is the potential of this process to produce high, localised, short term concentrations of pollutants at distances well beyond those which would be predicted by conventional theory. Unlike the transient fumigation events associated with the erosion of radiation inversions, the shoreline fumigation process may persist for a period of a few hours on any particular day, as noted by Kerman et al. (1982). During this period the location of peak concentrations may move around over a wide area downwind, as various meteorological and source parameters change. If the meteorology of a coastal region is such that a regular pattern of onshore winds occurs over a season or longer, then a particular locality downwind of the industrial sources may experience high level fumigation events as frequently as daily

over that time of the year. Such is the case at Kwinana, where sea breezes occur on more than 50% of days over the months of October to March (Hounam ,1945) and less frequently in the remaining autumn and spring months. This may be compared to the figures provided by Portelli et al. (1982) for the Nanticoke Study; 25% of days between April and September and 30% of days between May and July have the potential for shoreline fumigation.

The inherent variability of the shoreline fumigation process, caused by variations in mean (10-30 minute average) meteorological and source parameters, calls for special procedures to investigate it. Portelli et al. (1982) show (by implication) that this variability, and the localised nature of concentration maxima, renders investigation via fixed monitoring stations inadequate. Stunder and SethuRaman (1985) and Weisman (1976) point to the need for a model in which the TIBL and source plumes are accurately described in relation to each other, and since these are independent fluid-flow phenomena, each must be independently and accurately described. Specifically, the model must be able to describe the important features of the fumigation process which are:

(i) intersection of the plume and the TIBL and subsequent entrainment of pollutants into the TIBL;

(ii) rapid vertical mixing of pollutants within the TIBL

(iii) enhanced lateral spread of pollutants within the TIBL.

A corresponding description of enhanced dispersion within a MIBL is also required in the model.

6.2.1 REVIEW OF SHORELINE FUMIGATION MODELS

Lyons (1975) has provided a comprehensive review of plume dispersion in a coastal region where TIBLs occur. The schematic on which his fumigation model is based is reproduced below in Figure 6.1. As can

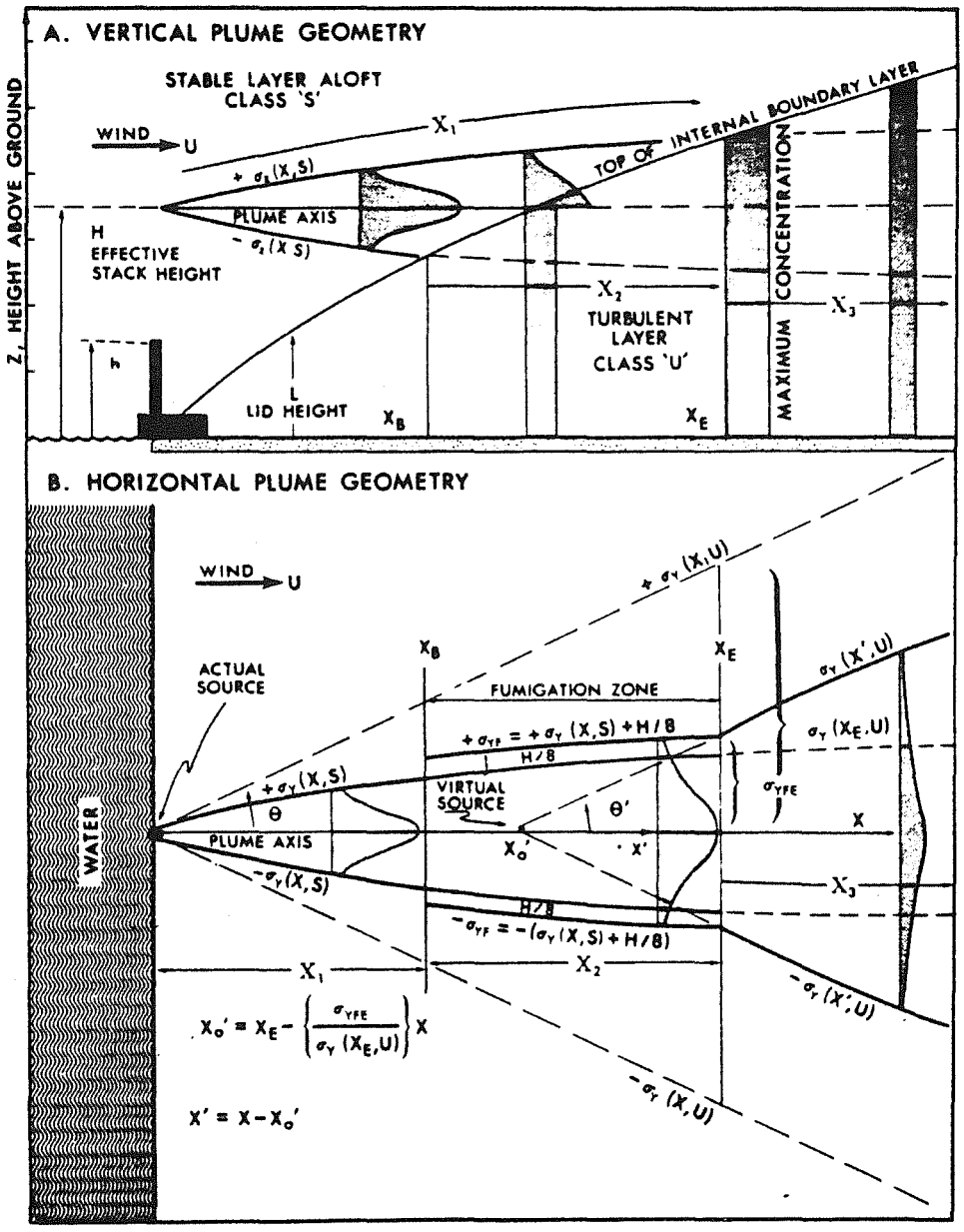

FIGURE 6.1 SCHEMATIC OF SHORELINE FUMIGATION MODEL (LYONS & COLE, 1973, LYONS, 1975)

be seen from this schematic, Lyons considers the plume dispersion in three zones.

In the first zone, prior to the downwind distance X_B, the plume disperses slowly in the stable marine air, with $\sigma_y(s,x)$ and $\sigma_z(s,x)$ determined for Pasquill's stability class E or F (where the parameter s implies stable atmospheric conditions). At X_B, the lower edge of the plume encounters the growing TIBL. (The lower and upper edges of the plume are defined as minus and plus 2.15 σ_z from the plume centreline level H_e respectively).

In the second zone, the plume is progressively entrained into the growing TIBL and mixed uniformly over the TIBL depth L(X) (h in the current notation). At the same time, lateral spread is enhanced due to the strong convective mixing and so a modified value of σ_y is used:

$$\sigma_{yf}(s,x) = \sigma_y(s,x) + H_e/8 \qquad (6.22)$$

This form of relation was proposed by Turner (1970) to describe the lateral spread of an elevated plume as it is being fumigated to ground during morning inversion break-up. With this value of σ_y, ground level concentrations are calculated in the normal manner for a vertically mixed Gaussian plume, except that the source strength is modified by a factor QF, being that fraction of plume entrained into the TIBL at a distance x, given by:

$$QF = \int_{-\infty}^{p} (2\pi)^{-1/2} \exp(-p^2/2)\,dp \qquad (6.23)$$

where $p = [L(x) - H_e]/\sigma_z(s,x)$

Zone three commences after X_E, the distance at which all of the plume

has been entrained into the TIBL. Ground level concentrations are now calculated from the standard Gaussian formula for uniform vertical mixing, except that the mixing height h continues to grow downstream. As the dispersion in this zone is now completely determined by the strong convective turbulence, a more rapid spreading rate must be used, giving greater values of lateral spread $\sigma_y(u,x)$ (where the parameter u implies unstable atmospheric conditions). Lyons employs a simple geometric procedure (which is clearly displayed in Figure 6.1) to define a virtual source x_0' which lies between X_B and X_E. With this new origin, lateral spread $\sigma_y(u,x')$ is given by Pasquill's curves for stability A or B (i.e. unstable conditions).

Misra (1980) adopts a more formal approach to obtain an expression for the concentration field within the TIBL, which depends on the prescribed plume distribution above and within the layer. Whilst this model avoids the somewhat arbitrary simplification to the lateral dispersion calculation in Lyons' model, its routine application in dispersion models is limited due to the computer time which would be necessary to perform the numerical integration at each timestep.

For the purpose of modelling dispersion in a coastal area over extended periods of data (e.g. 12 months or more) it is necessary to employ a description of shoreline fumigation which is relatively simple and which executes rapidly. The scheme of Lyons (1975) is commendable in that it achieves these requirements whilst describing the essential features of TIBL fumigation, namely the initial slow plume spread in stable marine air, rapid vertical mixing of that part of the plume entrained in the growing TIBL, and enhanced lateral

spread of the plume in the TIBL. Experience with the use of this model has revealed two significant weaknesses however:

(i) Lateral spread in the downwind half of zone two and all of zone three is under-predicted. Clearly, the lower plume segments entrained near X_B will have spread much wider in the TIBL than those entrained further downstream; hence the $\sigma_{y,f}$ associated with the latter (as used by Lyons) will under-predict the former. In particular, the virtual source as defined is too far downstream, being applicable only to the upper plume segments entrained near X_E, not the total plume.

(ii) Although vertical mixing within the TIBL is relatively strong, the assumption that the elevated plume is mixed instantaneously following entrainment is obviously an over-simplification. The maximum vertical velocities expected (Venkatram 1980b), would be about $0.6w_*$ (e.g. about 1.5m/sec in strongly convective conditions). Hence with a 5 m/sec mean wind, a plume at 200 metres elevation would require at least 0.6 km travel before any ground level concentrations would be registered. Although the concept of instantaneous mixing has been widely employed (van Dop et al.; 1979, Misra, 1980), other reseachers have also noted the above-mentioned shortcoming (McRae et al., 1981; Misra and Onlock, 1982).

In view of the above, a revised scheme for computing TIBL fumigation was developed, drawing heavily on the concepts laid down by Lyons, but incorporating an updated description of dispersion and fumigation consistent with the theory of previous Sections.

6.2.2 A MODIFIED SHORELINE FUMIGATION SCHEME

The modified representation of shoreline fumigation within TIBLs, which was employed in DISPMOD (KAMS, 1982), is shown schematically in Figure 6.2. The most obvious new feature represented in Figure 6.2 is the finite rate of vertical mixing in the TIBL. Pollutants entering the TIBL at X_B, X_I and X_E are not mixed to ground until the plume has travelled an additional distance to X_{BF}, X_{IF} and X_{EF} respectively.

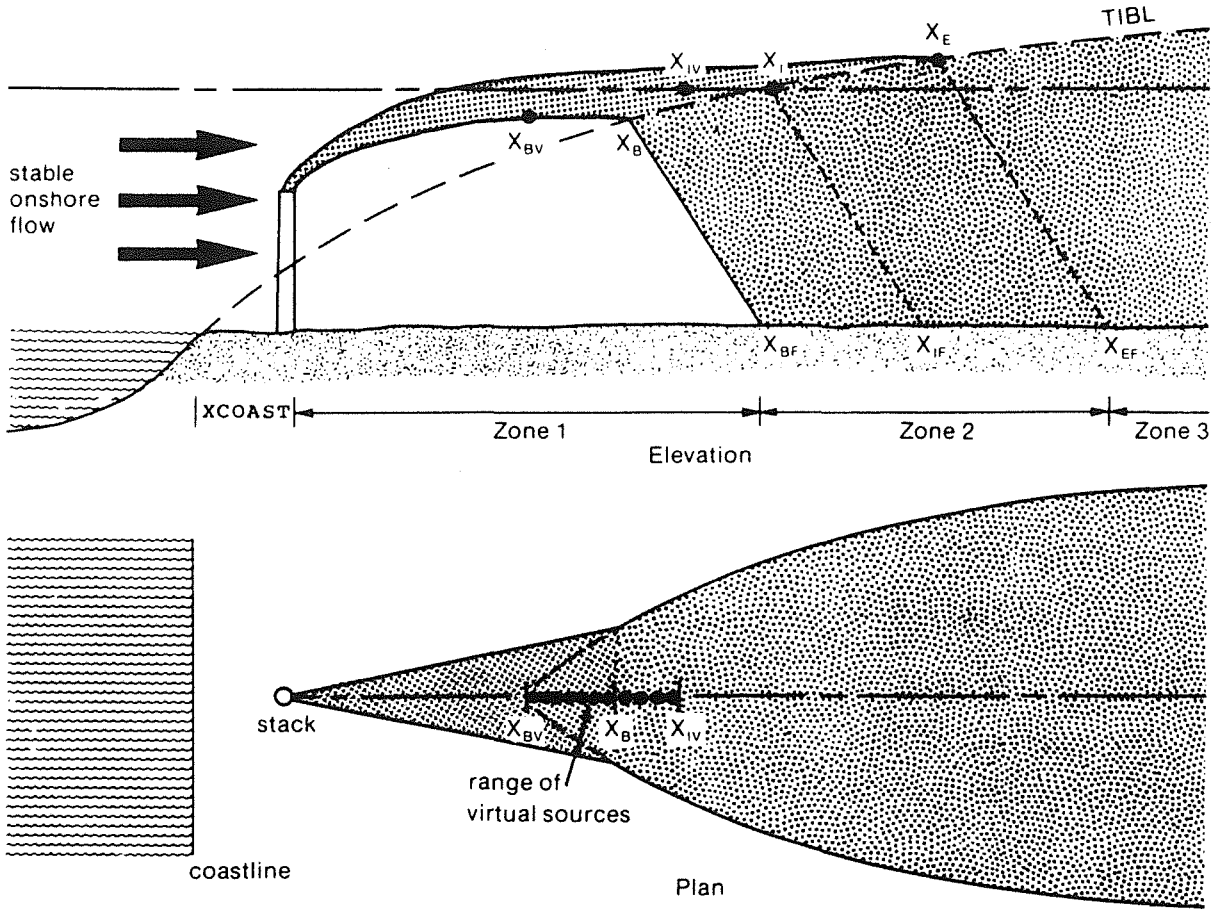

FIGURE 6.2 PLUME GEOMETRY USED TO MODEL FUMIGATION UNDER A TIBL (KAMS, 1982)

These additional distances are evaluated as follows. The maximum vertical velocity scale, $\sigma_w \approx 0.6 w_*$ defines a maximum angle of decent, $\sigma_\phi \approx 0.6 w_*/U$. Hence, from geometry, we can write:

$$X_{BF} = X_B + h_B/\sigma_\phi \qquad (6.24)$$

and similarly for X_{IF} and X_{EF}. This formulation ignores any change in dispersion rate with time or distance of travel; i.e. $F_z(t/\tau_L)$ in (6.17) is constant at unity, as given by (6.20) for convective conditions.

Other researchers have also addressed the question of finite mixing rates within TIBLs. Stunder et al. (1985) have evaluated the theoretical study of convective mixing by Misra (1982) and the tank study of convective mixing timescales by Deardorff and Willis (1982). They find the application of results from both studies leads to significant under-estimates of the mixing rate observed in the Nanticoke Study (Portelli, 1982), and that the instantaneous mixing assumption fits the data reasonably well. This conclusion is surprising (in view of the fact that it is physically unrealistic) and suggests that there may be inadequacies in either the analysis or the data employed. The current scheme expressed in (6.24) is believed to be a good first-order correction to the instantaneous mixing assumption and, in view of all of the other uncertainties in the calculation procedure, it is doubtful whether more precise schemes are warranted.

Where plumes have been released above the TIBL as shown in Figure 6.2, their levelling height $H_* (= \Delta H + H_{*i})$ is computed from (6.5). This height is limited to just less than the specified sea breeze depth,

given the strength of the sea breeze inversion as discussed in Section 5.2.3.

The distance at which the levelled plume centreline intersects the growing TIBL may be obtained from (5.6) with $h = H_e$. If, however, the plume has not reached its final level at this distance, the true intersection point must be found by equating (6.4) and (5.6) and solving for the distance by iteration. (Neglecting the effects of stability in computing the plume trajectory via (6.4) is a minor source of error.) The plume may be assumed to level out in the TIBL at the height of intersection, in view of the strong convective mixing in the TIBL.

Following Lyons (1975), X_B and X_E are the TIBL intersection points of the upper and lower plume edges, defined as $+2.15\ \sigma_z$ and $-2.15\ \sigma_z$ from the plume centreline. Vertical plume spread σ_z is a function of X whilst the TIBL height is a function of distance from the coast, X + XCOAST, as shown in Figure 6.2. Consequently, the intersection points must be obtained by iteration. (This procedure is a necessary generalization of Lyons' model, which only considers stacks immediately on the shoreline). Lyons (1975) suggests the use of a stable PGT category to obtain σ_z estimates. An alternative approach which avoids the use of stability categories is to use specified values of σ_θ and σ_ϕ in equations (6.16) and (6.17). These values of σ_θ and σ_ϕ may be calculated from the equations for stable flow in Table 6.1, which in turn require estimates of u_*/U. By definition, $u_*/U = C_D^{1/2}$, where C_D in this case is the drag coefficient over water, having a typical value at ten metres of 1.3×10^{-3}. Therefore,

typical ten metre values of $\sigma_{\theta s}$ and $\sigma_{\phi s}$ (where subscript s refers to stable conditions) are 4.7° and 2.7° respectively. These values give plume spread similar to that for Pasquill Category F.

In practice, a Newton-Raphson iteration for X_B and X_E converges to within 1% relative accuracy in about 4 steps. On the assumption that TIBL growth is impeded significantly when it reaches the sea breeze depth, X_E is limited to the distance at which that occurs.

Within Zone Two, the ground level concentration at any downwind distance is due to the plume fraction which has fumigated to earth prior to and at that point. For example, the source strength Q appropriate to distance X_{IF} will be determined by the fraction of plume entrained out to the distance X_I, given by (6.23) where $x = X_I$. The obvious effect of using (6.24) is to introduce a time lag into the fumigation process. Another effect which follows directly from the first is the enhanced lateral spread in Zone Two and beyond; this is achieved by allowing the plume to spread according to σ_θ in the TIBL over the fumigating distance (e.g. X_B to X_{BF}). At X_B, the plume has a lateral spread

$$\sigma_y(s, X_B) = \sigma_{\theta s} X_B F_y(X_B) \qquad (6.25)$$

with $F_y(X_B)$ from (6.18). Hence we can solve for a virtual source distance ΔX_B from

$$\sigma_y(s, X_B) = \sigma_\theta \Delta X_B F_y(\Delta X_B) \qquad (6.26)$$

where σ_θ is the unstable TIBL value. The solution is performed iteratively, given an initial estimate $\Delta X_B = \sigma_y(s, X_B)/\sigma_\theta$. Lateral dispersion at X_{BF} is then computed from the virtual source at X_{BV}, where $X_{BV} = X_B - \Delta X_B$. This procedure has the same sort of effect as

(6.22) used by Lyons but is physically more realistic for TIBL fumigation.

As noted above, Lyons' scheme under-estimates lateral plume spread at ground level in the downwind portion of Zone Two and all of Zone Three because he uses only one virtual source (for Zone Three only). A similar under-estimate would result if the above procedure was used to determine virtual sources for all points in Zone Two (up to X_{EF}) as plotted in Figure 6.3, curve (a), for values of meteorological parameters and stack location typical of Kwinana. To investigate this effect, a numerical exercise was carried out in which the plume in Zone Two was divided into fifty downwind segments, and the plume spread at any ground level location was calculated from the average of the mass- weighted variances of all those segments entrained to that point. The result is plotted in Figure 6.3, curve (b). This procedure is thought to give an accurate picture of TIBL fumigation but is clearly too unwieldly to incorporate into a dispersion model. Hence an empirical simplification was postulated, as follows. It is reasonable to presume that the effective virtual source for a plume well downstream in Zone Three will be somewhere close to X_{IV}, as it is from this point that the most concentrated pollutants spread into the TIBL. There seems therefore no justification for considering virtual sources beyond X_{IV}. Prior to X_{IV}, a simple interpolation scheme may be used to define virtual sources between X_{BV} and X_{IV}:

$$X_V = X_{BV} + (X_{IV} - X_{BV})(X - X_{BF})/(X_{IF} - X_{BF}) \qquad (6.27)$$

There is no physical justification for this scheme and its acceptability must rest on its performance. As can be seen from Figure 6.3 ,curve(c), the scheme predicts ground level lateral spread which

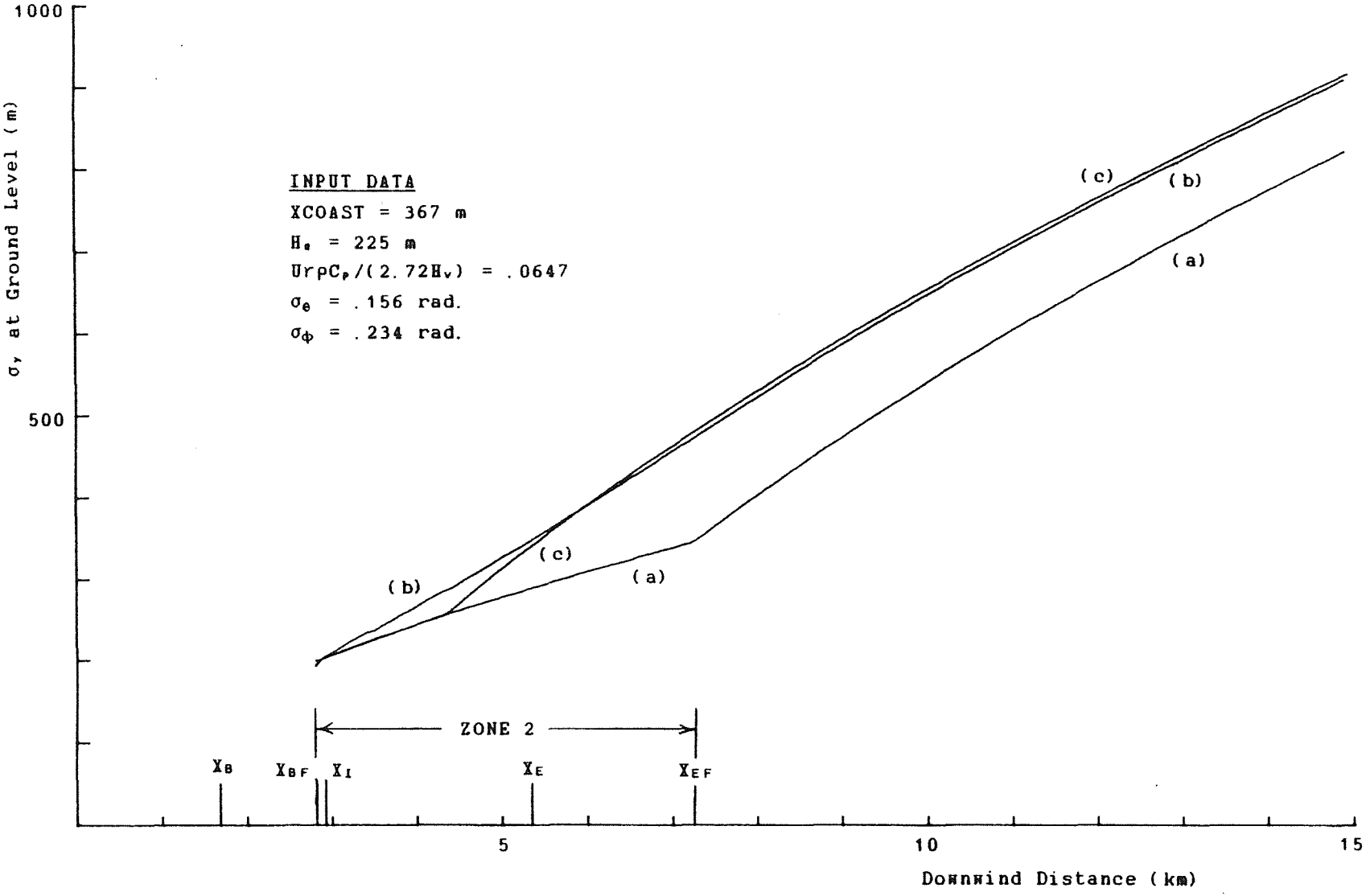

FIGURE 6.3 ESTIMATES OF σ_y AT GROUND LEVEL WITHIN A TIBL

closely approximates the numerical results. It has therefore been incorporated in the dispersion model.

Buoyancy-induced spread, discussed in Section 6.1.8, has been neglected in the calculation scheme described above. The scheme is already complicated by iteration procedures and the determination of virtual sources , and it was thought that an additional procedure to determine a virtual source which accounts for buoyancy-induced spread should be avoided if possible. Alternative interpolation formulae (e.g. Pasquill, 1976) over-estimate plume spread near the final rise distance relative to the method of Hanna (1982) and have therefore been rejected for the present application. The scheme described above for calculating plume spread in stable onshore flow is by no means exact and it therefore seemed sensible to seek experimental evidence before further complicating the scheme. As will be described in Section 6.3.2, neglect of the specifics of buoyancy-induced spread appears to be an acceptable simplification.

Whilst the vertical mixing of pollutants in Zone 2 occurs at a finite rate, as described above, uniform vertical distribution of pollutants up to the mixing height (TIBL height) is still assumed for any given downwind distance. These two assumptions may appear to be incompatible in the light of classical dispersion theory, but the uniform distribution assumption is nevertheless the most appropriate simple approach for modelling highly convective turbulence as found in TIBLs (Venkatram, 1980b).

In order to calculate the fraction QF of a plume which is mixed to

ground level at some downwind distance in Zone 2, it is first necessary to iteratively solve the reverse form of (6.24) to determine the associated plume travel distance to the point of intersection with the TIBL (e.g. to determine X_B from X_{BF}). Equation (6.23) may then be solved by numerical means.

6.2.3 ENHANCED DISPERSION WITHIN A MECHANICAL INTERNAL BOUNDARY LAYER

Neutral or stable conditions prevail over land in onshore flows at night or on very cloudy days, especially following rain. In this case the turbulent heat flux from the ground, H_v, will be close to zero or negative (i.e. downward) and a TIBL will not form. However, the mechanical internal boundary layer (MIBL), which forms over the land due to the change in surface friction, may have an important modifying influence on dispersion of chimney plumes. The growth of a MIBL is given by (5.10).

It would be possible in principle to develop a plume dispersion scheme similar to that for TIBLs, in which the plume from an elevated stack impacts the MIBL at some downwind distance and is dispersed downward at a rate enhanced by the MIBL turbulence. The task would be more complicated than that for TIBLs however, as rapid vertical mixing cannot be assumed. Nevertheless the effect of MIBLs may still be significant, as it is intuitively clear that a plume which levels out high above the MIBL will disperse much more slowly than one which levels within the MIBL. The following simple procedure has therefore been adopted (see Figure 6.4 for a schematic illustration). The distance of impact of the plume centreline with a growing MIBL is

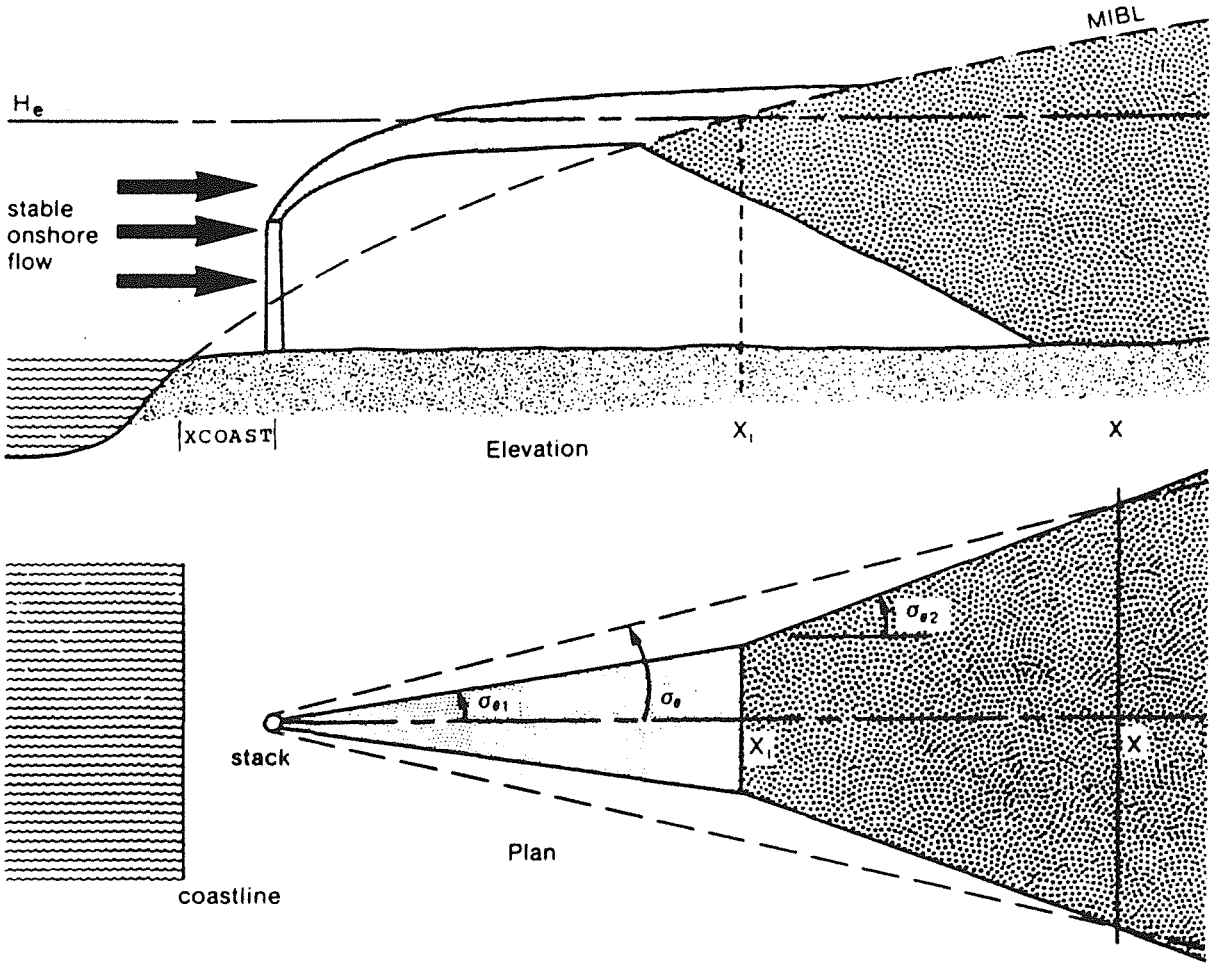

FIGURE 6.4 PLUME GEOMETRY USED TO MODEL PLUME ENTRAINMENT INTO A MIBL (KAMS, 1982)

given by:

$$X_I = H_e^3[grU/(2.5u_*^3T_v)] - XCOAST \qquad (6.28)$$

We would like to know the effective enhanced spread of a plume which has entered a MIBL somewhere between the stack and a distance X downwind of the stack. Figure 6.4 shows that the lateral plume spread is determined inside and outside the MIBL by the respective values of σ_θ (and similarly σ_ϕ for vertical spread). The superimposed dotted line shows identical plume spread at distance X, while progressively over-predicting spread for distances closer to the stack and

progressively under-predicting spread for distances beyond X. The effective value of σ_θ which would produce the dotted line is given by

$$\sigma_\theta = Tan^{-1}[(X_1 Tan\sigma_{\theta 1} + (X - X_1)Tan\sigma_{\theta 2})/x] \qquad (6.29)$$

and a corresponding expression gives σ_ϕ. This expression may be solved as part of the dispersion calculations at every model gridpoint or, as an efficiency measure, it may be solved once at the start of a timestep for a representative distance of interest (taken as 10 km in the current Study). The loss of accuracy involved in the latter option is relatively small. As with procedures developed for TIBLs, this expression is quite empirical, but it will reproduce the essential effect of a MIBL, correctly differentiating between high and low plumes, enabling approximate but meaningful dispersion estimates to be obtained.

6.3 FIELD INVESTIGATION OF SHORELINE FUMIGATION WITHIN A SEA BREEZE

As a part of KAMS, a field experiment was conducted on the 31/1/80 to investigate dispersion of a plume from a coastal power station in sea breeze conditions. The experiment followed an earlier experiment on 2/3/78 in which the shoreline fumigation phenomena had been identified but without adequate data to allow a quantitative investigation. The 31/1/80 experiment was designed to provide a comprehensive data set to allow an evaluation of dispersion models.

6.3.1 EXPERIMENTAL METHODS

The primary experimental method employed on the 31/1/80 was the release of sulphur hexafluoride (SF_6) from the 137 m stack at the

Kwinana Power Station and the sampling of SF_6 concentrations at a variety of downwind locations. Freon$_{11}$ gas was also released, but was a less reliable tracer due to higher background levels.

The use of SF_6 as a tracer in plume dispersion studies is common and well documented (e.g. McRae, Shair and Seinfeld, 1981). In the 31/1/80 study, SF_6 was released into the base of the stack between 1400 and 1430 hours at a constant rate of 0.03 kg/sec. Sampling at each of 24 downwind locations (which will be identified in the discussion of results) was performed manually by gradually filling a Mylar bag with a hand operated pump. Five bags were filled at each location over a total elapsed time of 30 minutes. The start time of the first bag was delayed beyond 1400 hours by a period estimated to be (approximately) the travel time of the plume from the stack to the sampling location. Hence there is believed to be a reasonable time correspondence between the sampling interval for each location and the tracer release interval.

Sample bags were taken immediately after the experiment for analysis on a gas chromatograph at the University of Western Australia. Results of this analysis were tabulated as concentrations of SF_6 ($\mu g/m^3$) for each sample location and bag.

Black smoke was released from the stack over short periods at pre-arranged intervals throughout the experiment, to facilitate photography of the plumes. Photographs were taken with a 35 mm SLR camera, with a 35 mm wide-angle lens, mounted on a levelled platform at the Hope Valley Base station with a recorded orientation. The

photographs were subsequently analysed via the method described by Halitsky (1961) to determine plume trajectories.

Slow-ascent radiosondes were released at approximately 45 minute intervals throughout the afternoon from a site approximately 6 km directly inland from the power station and about 16 km downwind of the coast. The radiosondes were tracked via double theodolites, giving wind vector profiles in addition to accurate temperature profiles. A second radiosonde release station was located at the coast a few kms south of the power station in order to measure the undisturbed temperature and velocity profiles in the sea breeze. The recording equipment at this station unfortunately failed and no data were collected.

The acoustic sounder located at the Hope Valley Base Station operated throughout the experiment, providing a clear indication of convective mixing. In addition, the Hope Valley Base Station provided continuous measurements of mean (10 minute average) meteorological data, allowing the subsequent computation of H_v and u_* via the methods described in Chapter 3.

6.3.2 DISCUSSION OF EXPERIMENTAL RESULTS

The main synoptic feature influencing the meteorology on the 31/1/80 was a high pressure system situated south west of the State and ridging eastward, directing south easterly flow across the south west of the State. The sea breeze front had crossed the coast before noon and the sea breeze was well established by 1400 hours, with wind

speeds of 8-9 m/sec at 10 metres, from a direction of 220° (SW).

The temperature and velocity profiles from the inland radiosonde are reproduced in Figure 6.5. These profiles reveal a strong sea breeze/synoptic flow interface, approximately 150 m thick, with its base rising from 300 to 400 m altitude between 1335 and 1535 hours. The layer below the interface is well mixed in all profiles, and it is therefore apparent that the TIBL growth has been arrested by the sea breeze interface at this distance downwind (approximately 16 km). The sea breeze interface is very stable in all but the 1335 profile, with a potential temperature increase of about 3°C from bottom to top.

A further point of interest which arises from the sonde profiles (and which was briefly mentioned in Chapter 5) is the magnitude of velocities within the sea breeze layer. Rather than increasing monotonically with height, the wind speed is roughly constant throughout the layer, which has led to the adoption of a rule of thumb for mean layer wind speed:

$$U_{LAYER} \approx 1.2\ U_{10} \qquad (6.30)$$

This rule holds only when there is a counter flow of synoptic wind and sea breeze.

Mixing height inferred from the acoustic sounder is plotted in Figure 6.6. During the tracer release period the sounder indicated turbulent mixing up to above 400 m, indicating that the TIBL above the sounder had reached the sea breeze interface. Due to the angle of the coastline upwind of the sounder location, the overland distance is difficult to specify (being somewhere between 5 and 14 km).

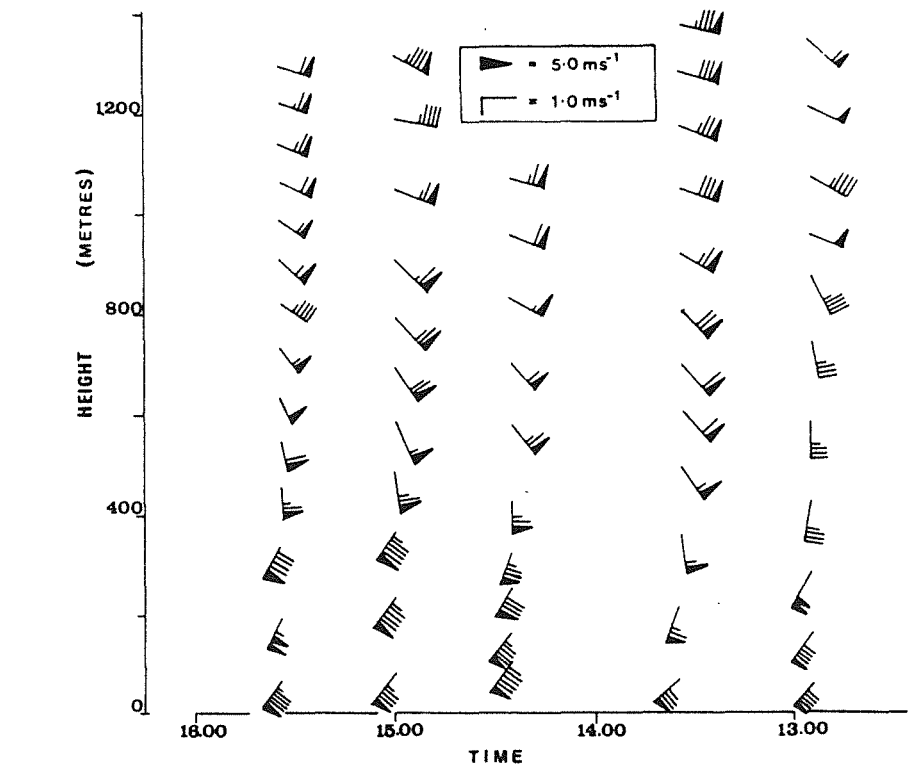

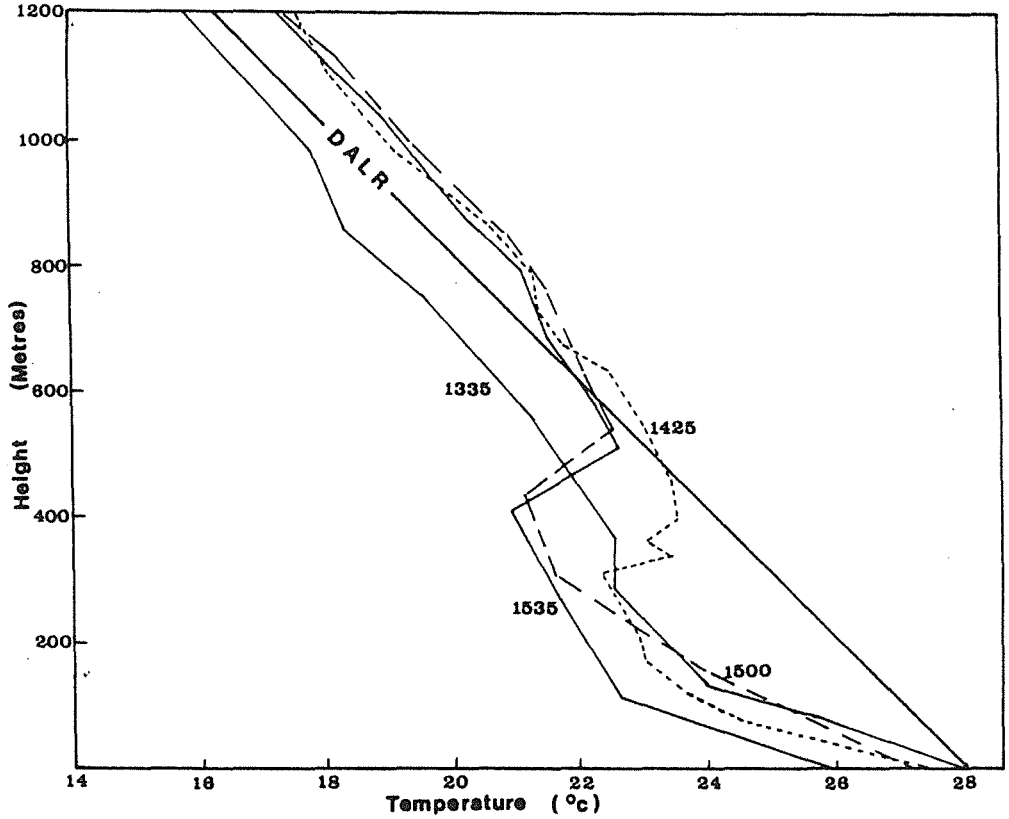

FIGURE 6.5 RADIOSONDE WIND AND TEMPERATURE PROFILES FOR 31 JANUARY 1980.

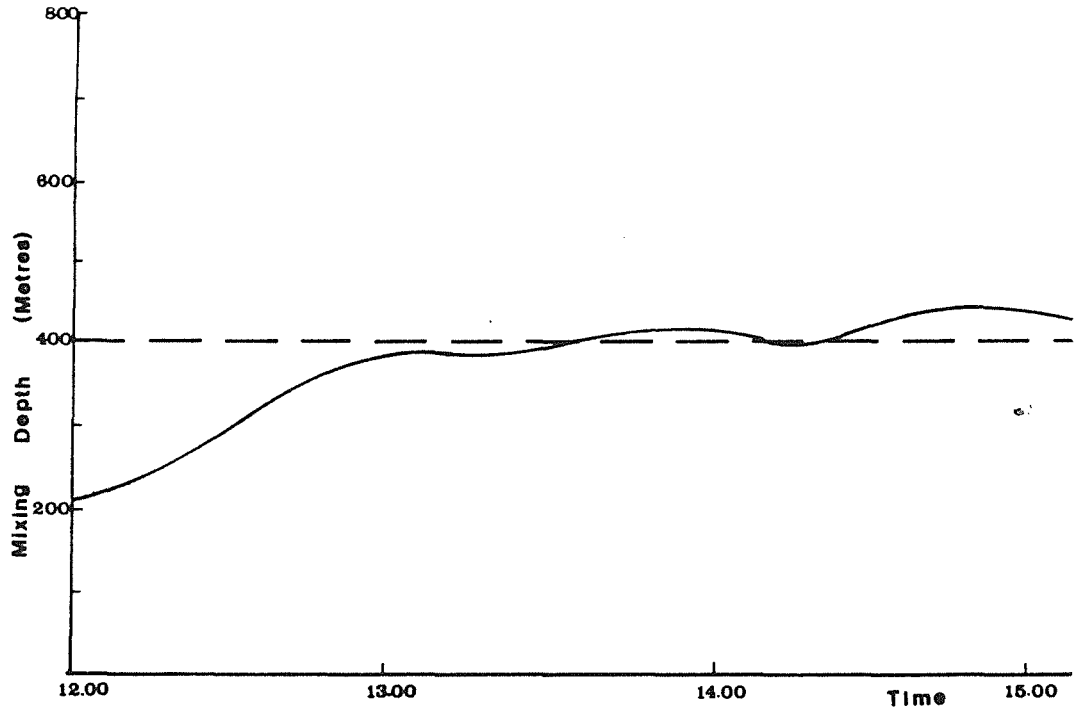

FIGURE 6.6 ACOUSTIC SOUNDER RECORD FOR 31 JANUARY 1980

Three photographs of plume trajectory spanning the tracer release period were analysed to obtain an estimate of mean plume rise. The plume trajectories during this period, which are plotted in Figure 6.7 (a) to (c), were quite smooth with an absence of looping behaviour, indicating that the marine air was gravitationally stable. The average plume rise at 1 km downwind of the stack was estimated to be 80 ± 20 metres, as indicated by the composite plume envelope plotted in Figure 6.7 (d).

During the period of tracer release, the power station plume average flow rate was 126 m^3/sec at a temperature of 142°C, giving a buoyancy parameter value of F = 110 m^4/sec^3 from (6.3). Substituting this value and a mean wind velocity of 9.6 m/sec into Briggs neutral plume rise formula (6.4) gives a predicted rise above stack height of 79 m.

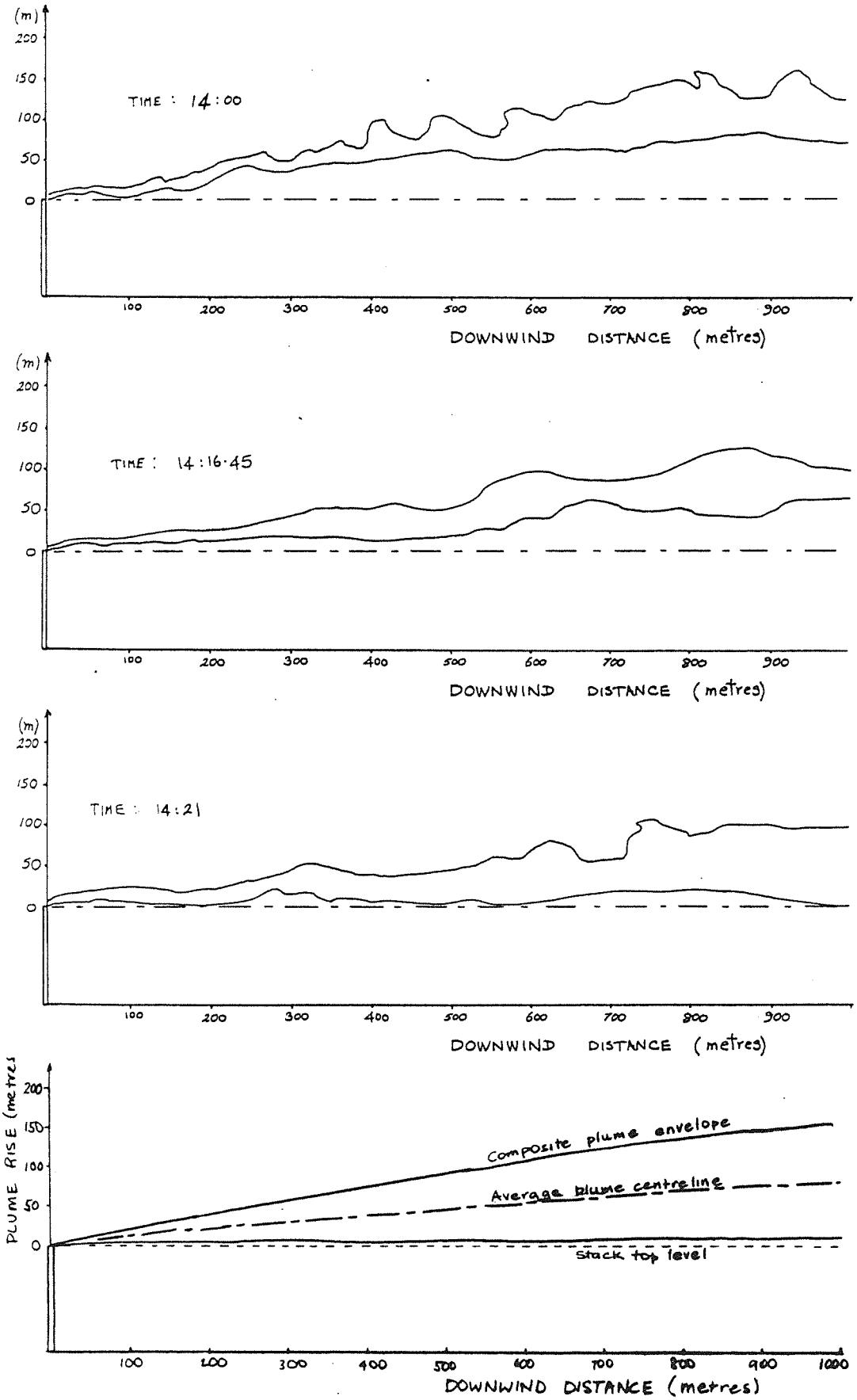

FIGURE 6.7 PLUME TRAJECTORIES FROM PHOTOGRAPHS AND A COMPOSITE PLUME ENVELOPE

Alternatively, if stable air with an isothermal lapse rate (.0098°C/m) is assumed, then Briggs formula (6.5) estimates a final rise height of 85 m. The plume observations are consistent with either of these cases (and any intermediate stability) providing a high degree of confidence in the plume rise portion of the shoreline fumigation simulation.

If the final rise height of the plume is taken as 80 m, then the calculated buoyancy-induced spread is $\sigma_y = \sigma_z = 24$ m at the distance of final rise (Hanna, 1982). The distance to the point of final rise is about 1 km (estimated by comparing predicted rise heights with Figure 6.7 and equation (6.9)). The values of σ_y and σ_z at this distance, calculated using $\sigma_{\theta s}$ and $\sigma_{\phi s}$ with 10/L = 3, are 48 m and 18 m respectively. The conservatively stable value of 10/L matches Lyons' (1975) use of stability category F in the onshore flow. A more realistic value of 10/L ≈ 1, inferred by matching the sea breeze lapse rate with stability category E (Sedefian and Bennett, 1980) and the stability category with 10/L for a very small roughness length (Golder, 1972) gives $\sigma_z \approx 26$ m. The calculated value of σ_y more than accommodates the buoyancy spread, so that application of Hanna's (1982) scheme is not warranted in this case. Similarly, the alternative calculated values of σ_z straddle the buoyancy spread estimate, indicating that the uncertainty in the former is probably more significant (in terms of model accuracy) than the contribution of the latter. Whilst it is difficult to quantify σ_y and σ_z from Figure 6.7, the instantaneous plume widths are consistent with the theory behind Hanna's (1982) scheme (i.e. plume width ≈ height of rise). In summary, there seems to be little point in further complicating the estimation of σ_y and σ_z to explicitly account for buoyancy spread.

This simplifying assumption would need to be reviewed for pollutant sources with plume buoyancy greater than that of the sources at Kwinana.

Computation of turbulent fluxes and stability parameters for this experiment day was discussed in detail in Section 3.4.1 and presented in graphical form in Figure 3.3 (c) and (d). Important measured and calculated parameters for the experimental period are presented here in Table 6.3. Note that the three records are 10 minute averages commencing at the nominated time.

TABLE 6.3 IMPORTANT MEASURED AND CALCULATED METEOROLOGICAL PARAMETERS FOR THE TRACER EXPERIMENT PERIOD ON 31/01/80.

TIME PERIOD	H_v W/m^2	u_* m/sec	10/L	T_{10} °C	U_{10} m/sec	Direct. degrees
1400-1410	593	.779	-.141	24.8	8.0	223
1410-1420	621	.856	-.111	24.4	8.9	220
1420-1430	562	.777	-.135	24.4	8.0	221

No direct measure of r in the sea breeze was available due to the failure of the coastal radiosonde. A value of r = 0.009 (close to isothermal) has been chosen as a likely value because:

(i) it was predicted by a mesoscale sea breeze model run for this

experiment period (Rye, 1980);

(ii) subsequent experiments at Bunbury and experiments described by other researchers (Kerman et al., 1982; Walker and Allen, 1975) indicate that this figure is typical of cooling sea breezes (i.e. where the water temperature is cooler than that of the offshore synoptic flow). This observation was discussed in Section 5.2.3.

The data given above allow estimates ot TIBL heights to be made via (5.6). For the representative values H_v = 590 W/m^2 and U = 9.6 m/sec, TIBL height is given by h = 3.94 $x^{1/2}$. Taking the base of the sea breeze interface to be at 400 m, we can see that the TIBL will grow to this level 10.3 km downwind of the coast. Hence the acoustic sounder record described above is not inconsistent with predicted TIBL heights. The lower limit of downwind distance for the sounder location, 5 km, has an associated TIBL height of 280 m, but it is likely that the sounder would record turbulent activity at higher levels as did the variometer described in Section 5.2.4.

For the purposes of simulating the shoreline fumigation pattern observed in the tracer experiment, the tracer concentration results were averaged over the half hour sampling period and plotted as figures on the location map shown in Figure 6.8. The reason for this averaging procedure was to minimise as far as possible the errors associated with estimating the travel time of the tracer material.

Computer simulation of the observed dispersion pattern was performed by the model DISPMOD, which incorporates all of the shoreline

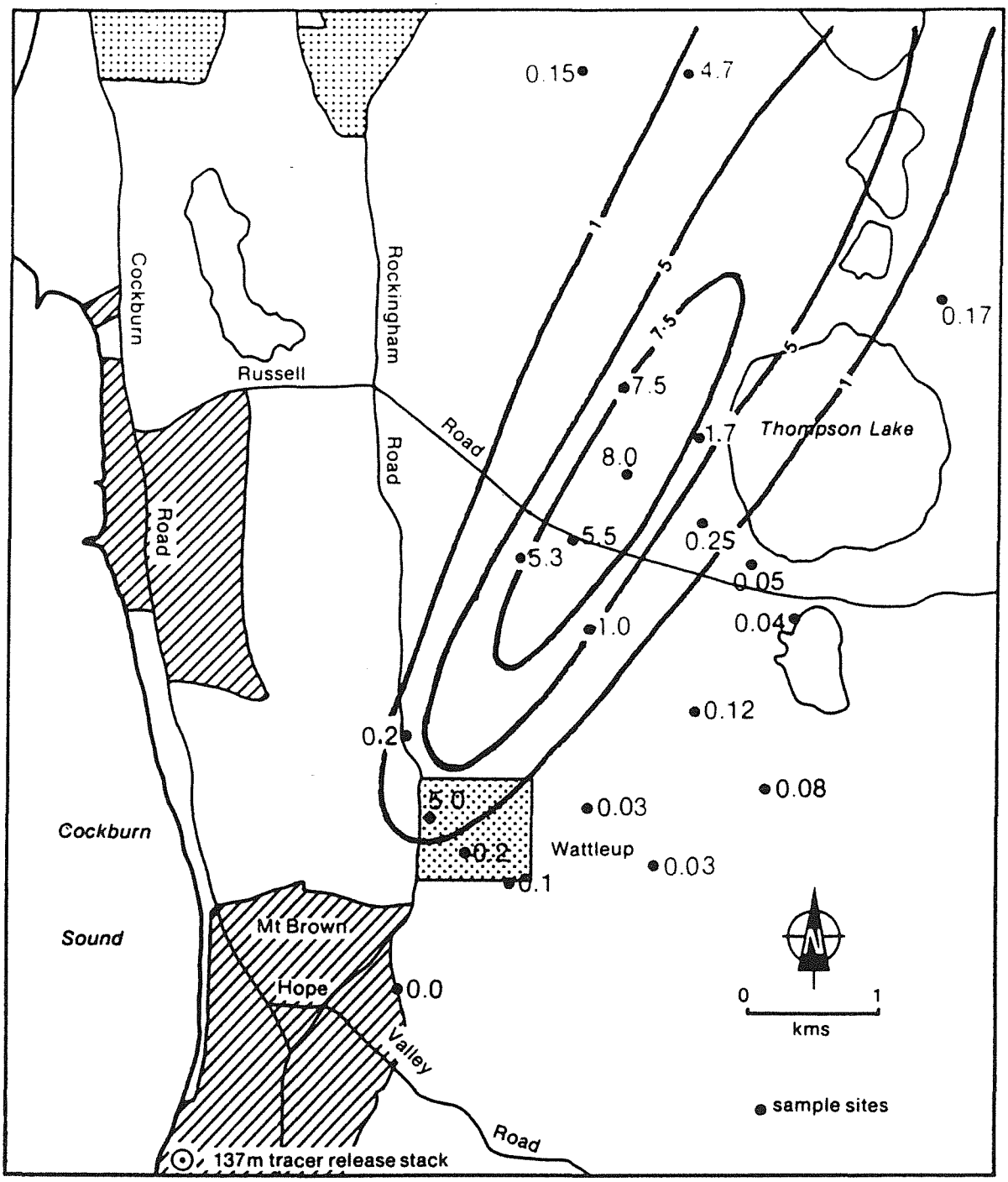

Figure 6.8. The 31 January 1980 tracer study showing estimated 30-minute average SF_6 contours and the measured values (●). All concentrations are in $\mu g/m^3$.

fumigation description outlined in Section 6.2 and the general plume dispersion relations of Section 6.1. A description of the structure of DISPMOD will be given in Chapter 7. It is sufficient to note here that the application of DISPMOD to the 31/1/80 experiment is an unambiguous test of the theory presented in this Chapter and Chapter 5.

DISPMOD results are plotted on Figure 6.8 as concentration isopleths, for comparison with the observed concentrations. The isopleths represent the average of three 10 minute model timesteps, employing the data of Table 6.3, and hence are directly comparable to the half hour average observations.

Although inadequacies can be seen in the spread of observation data, the general agreement between observations and predictions would have to be classed as very good. The location and magnitude of maximum concentrations appears to have been predicted fairly accurately, and certainly far better than the "factor of 2" generally considered acceptable (Hanna et al., 1977). Although the distribution of observed concentrations is far from smooth, the lateral spread of the predicted plume also appears to be representative.

6.3.3 SUMMARY OF FINDINGS

The shoreline fumigation model developed in this Chapter has been seen to exhibit a high degree of skill in simulating observed dispersion patterns from a coastal power station in sea breeze conditions. The success of this model points to the successful development of its various inputs and components, including the meteorological

measurements, calculated turbulent fluxes and stability parameters, calculation of TIBL height and simulation of the fumigation of an elevated plume into the growing TIBL.

The simple mechanistic approach employed to describe the fumigation process has two advantages:

(i) it facilitates the incorporation of physical concepts without the need for costly complex solution techniques;

(ii) it is readily incorporated into a model for long-term simulations.

CHAPTER 7

AN EFFICIENT GAUSSIAN DISPERSION MODEL FOR USE IN COASTAL OR INLAND AREAS

The objectives of this Study, and the implications of these objectives in determining the direction of model development, were outlined in Chapter 1. In brief, a dispersion model meeting the following criteria was required:

(i) efficient (i.e. relatively low computing costs for operation over long periods);

(ii) flexible and robust (i.e. applicable to widely varying conditions and scenarios without major changes to computer code);

(iii) capable of application to both coastal and inland sites, with all important meteorological processes described to an acceptable level of accuracy;

(iv) able to run on routinely available data as far as possible.

The modelling exercise was completed in three parts, for reasons described in Section 1.2.2, but the final product may be viewed as a package which fulfils the Study objectives and meets the above criteria. The heat budget and mixing depth models were designed with particular emphasis on criterion (iv). The final component (the subject of this Chapter) is a Gaussian plume dispersion model which utilizes the combined output of the heat budget and mixing depth models as input data, and incorporates the effects of coastal internal boundary layers described in Chapters 5 and 6. Development of this

model was achieved by incorporating segments for coastal effects and dispersion parameterization within the framework of an existing efficient Gaussian dispersion model.

The following description of the final Gaussian dispersion model will be limited to a broad overview of the model structure and discussion of model features which were designed with the Study objectives and the above criteria in mind. A summary of the model's performance against SO_2 measurements obtained during KAMS will also be presented.

7.1 STRUCTURE AND OPERATION OF THE MODEL DISPMOD

7.1.2 OVERVIEW OF MODEL STRUCTURE

A block diagram of DISPMOD is included in Appendix D to provide an overview of the model's structure.

The model structure follows simple conventional lines. The program control file sets the context of the model run, including the run period, a physical description of all sources including their location and distance from the coastline and the dimensions, resolution and reference location of the model grid. A full day's meteorological and emissions data is then accessed and dispersion calculations peformed for all sources (or groups of sources), for each model timestep (10 minutes in KAMS). The model accumulates average concentrations and statistics of exceedences of nominated air quality standards for each grid point, and stores this information on disk once per day. A post-processing program accesses the disk file to produce contour

plots and tables of average concentrations and the exceedence statistics.

In view of the previously stated objective that the model be applicable to both coastal and inland areas, considerable care was taken to build the special coastal dispersion features into the model in a modular fashion, and in a way which would allow these features to be disabled easily if the model was to be applied to an inland situation. The modular approach is shown in Appendix D. Nearly all of the mainline portion of the model dealing with onshore flow is contained in two discrete sections, one near the start of the timestep loop and the other within the central source loop. In the former section, the first step is a check to see whether the wind is onshore or not, and all subsequent processing of coastal effects occurs only if a positive determination is made at this point. Conversion of the model to run efficiently for inland situations is simply achieved by disabling the determination of onshore flow.

7.1.2 DESCRIPTION OF IMPORTANT FEATURES

The theoretical basis for DISPMOD was set out in Chapter 6 and will not be discussed further here. However, there are several features of the model, depicted in Appendix D, which warrant further explanation.

The model grid is defined in the program control file by the Australian Map Grid coordinates of the south west corner, the numbers of E-W and N-S grid points, and the distance interval between grid points. The standard grid employed in KAMS covered an area of 15 km

(E-W) x 22 km (N-S), with 1 km spacing. All pollutant sources are assigned coordinates within the grid; they are not constrained to be located on grid points. The E-W distance from the coastline is also specified so that downwind distances from the coast may be calculated.

The model obtains a variable mixing depth value from one of two sources:

(i) from the input meteorological data for offshore flow, as computed by the daytime mixing depth model (Chapter 4);

(ii) from the TIBL height whenever the flow is onshore and the surface stability is unstable.

For all stable surface conditions (onshore and offshore winds) the mixing height is set to 999 metres, i.e. there is no limit to vertical mixing within the scale of the model.

The depth of sea breezes and the temperature lapse rates within them are not available in the data set, and so must be specified. As indicated in Section 6.2, an important area of future work is the classification of sea breeze types and other onshore flows to provide broad indications of flow characteristics, including depth and temperature lapse rate. For the present study, it has been necessary to adopt an interim classification scheme based on limited information (see Section 5.2.3) and a fair degree of intuition. Table 7.1 presents this scheme.

TABLE 7.1 ONSHORE FLOW CLASSIFICATION

TIME OF ONSET (WST)	LAPSE RATE (°C/100m)	DEPTH (metres)
after 1000	0.9	500
0700 - 1000	0.4	750
before 0700	0.2	1000

The range of lapse rates is similar to that adopted by Rye (1984). An improved classification scheme may be easily incorporated into the model at a future date.

The procedures for calculating dispersion of plumes which are entrained into TIBLs or MIBLs have been fully discussed in Chapter 6. The procedures employed by the model to analyse plumes which are released within a TIBL or MIBL are described below.

Plumes which obviously reach their final height within a MIBL are assumed to simply disperse downwind according to the strength of turbulence within the MIBL. Plumes which have a final level higher than the height of the MIBL above the stack are treated as described in Section 6.2.3.

Similarly, plumes which are released within a TIBL may be sufficiently elevated and buoyant to penetrate into the stable flow and subsequently fumigate back into the TIBL. A simple approach is adopted, which allows plumes to escape the TIBL only if they have

sufficient buoyancy to do so completely, as determined by the formulae for plume penetration into elevated stable layers given by Briggs (1975). Plumes which are only capable of partial escape are held completely within the TIBL, with the mixing height set equal to the TIBL height and the plume height constrained to be equal to the TIBL height until the final plume level is reached.

The most time consuming part of Gaussian models is the calculation of concentrations at multiple grid points via the Gaussian formula (6.13, 6.14). Efficiency measures employed in DISPMOD are:

(i) transition to a simple "vertically mixed" Gaussian formula when $\sigma_z \geq h$, avoiding the need for continued calculation of reflection terms, as defined in (6.14). (Note that the alternative limit of $\sigma_z = 0.8h$ (Hanna et al., 1977) is not appropriate when reflection terms are significant.);

(ii) use of a look-up table of calculated exponential values (501 elements) rather than calculation of exponentials at every grid point;

(iii) rapid pre-determination of the range of grid points at which concentrations may be registered from each source at each timestep, so that calculation of zero or negligible concentrations is minimised.

The final version of DISPMOD is believed to be very efficient relative to other Gaussian models in current use. In a comparison test, DISPMOD executed in approximately one quarter of the time required by the USEPA model ISC.

7.2 RESULTS OF MODEL OPERATION IN KAMS

The major final modelling exercise in KAMS concentrated on the period 1st July 1979 to 30th June 1980, during which high grade data were available.

The KAMS Final Report (KAMS, 1982) provides extensive analysis of model results in terms of various health standards and other criteria for air quality. It is not the intention of this Thesis to analyse or draw any conclusions about the air quality at Kwinana, and hence the modelling results will not be presented in detail. The only results which will be presented below are those which illustrate the skill of the model DISPMOD.

The continuous SO_2 monitoring results from the Wattleup Base Station 1 were the only reliable source of validation data available during the Study period. These data are known to be of high quality with minimal gaps. The data from the Hope Valley Base Station 3 is also of high quality but unfortunately did not overlap sufficiently with the emissions data. The data from the 24 hour sequential SO_2 samplers (described in Section 2.3) proved to be unreliable for the purpose of model checking. The measurement method employed by these samplers is inherently variable, and the accuracy is severely impacted by the instability of the chemical complex over a period of a few days at normal ambient temperatures.

A comparison of the results of DISPMOD and the monitoring results from Base Station 1 are presented in Table 7.2. The various averaging times

Table 7.2. Comparison of measured and modelled sulphur dioxide statistics for the Wattleup base station site for the period July 1979 to June 1980. Reference levels were chosen to approximate Victorian EPA 1-hour objectives and WHO 24-hour guidelines.

	MODEL 1*	
	Measured	Modelled
Annual average concentration ($\mu g/m^3$)	44	43
Frequency of 24-hour average concentrations exceeding:		
100 $\mu g/m^3$	49	51
150 $\mu g/m^3$	19	18
Frequency of 1-hour average concentrations exceeding:		
500 $\mu g/m^3$	183	169
1000 $\mu g/m^3$	14	4
1400 $\mu g/m^3$	4	1
Frequency of daily maximum 1-hour average concentrations exceeding:		
500 $\mu g/m^3$	82	87

* Calculated for 24 fixed 1-hour periods per day at 0°C

and reference concentration levels were chosen to compare with relevant health standards. The comparison between annual modelled and measured estimates is obviously excellent. The same may be said for 24 hour estimates, which are described in terms of exceedence statistics in Table 7.2 and in terms of relative accuracy in Figure 7.1. The latter Figure shows that only 20% of 24 hour average concentration predictions fell outside the "factor of 2" criterion commonly accepted, and that 50% of predictions were within 20% of the measured value. Furthermore, the relative errors are evenly distributed about the line of perfect agreement, indicating that there is no significant bias in the results. Consequently it may be inferred that there is a good level of accuracy, without significant bias, in the following model components and inputs:

(i) the raw meteorological data;

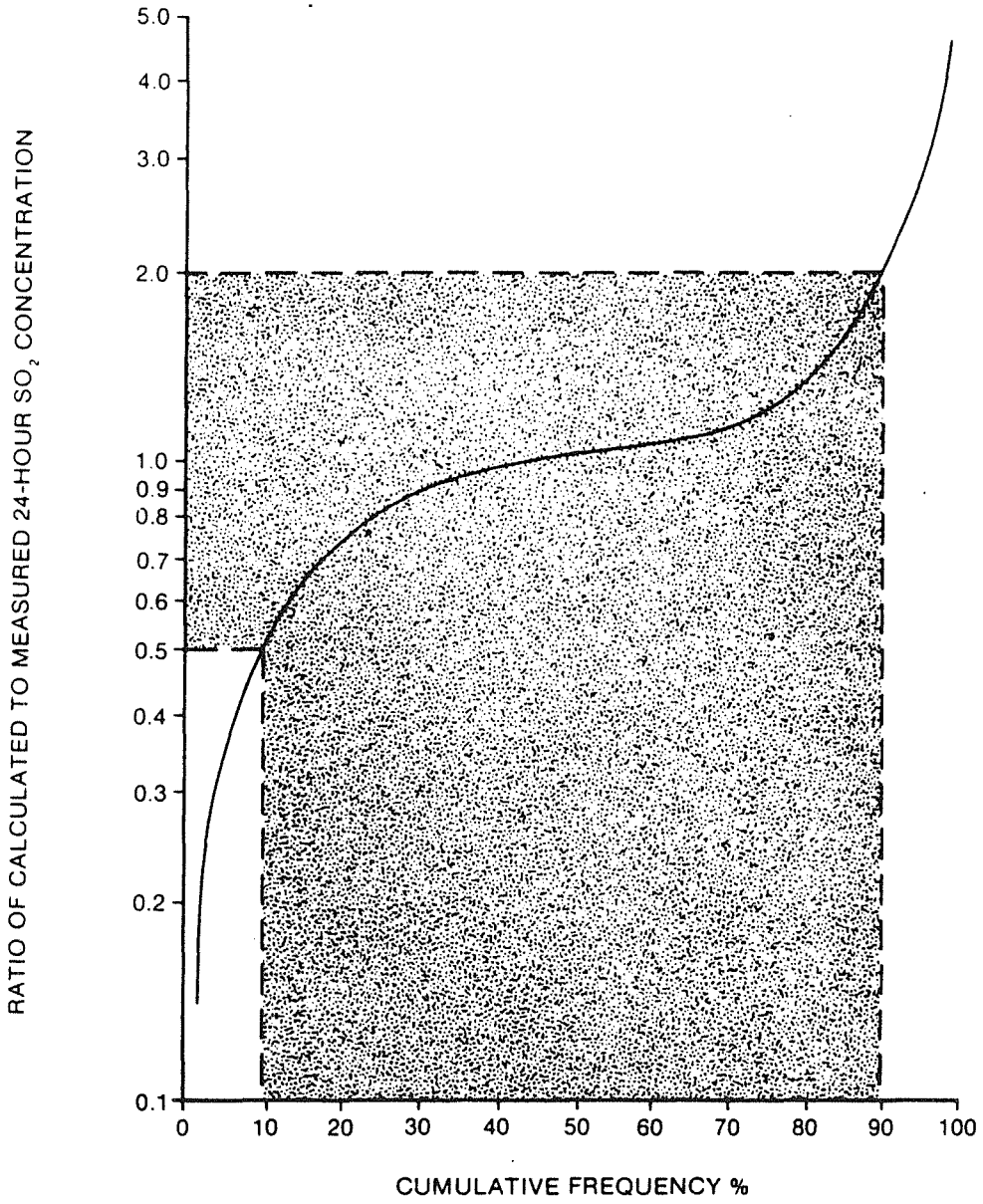

Figure 7.1. The comparison of measured 24-hour average sulphur dioxide concentrations measured at Wattleup and those calculated using **DISPMOD** for the year July 1979 to June 1980. The shaded area indicates the proportion of the calculated values which are within a factor of 2 of the measured concentrations.(KAMS,1982)

(ii) the computed turbulent fluxes and mixing heights (including TIBLs and MIBLs);

(iii) the emissions data;

(iv) plume rise and levelling calculations;

(v) the vertical dispersion calculations, including fumigation within TIBLs and enhanced dispersion within MIBLs.

Very little may be inferred about lateral dispersion calculation accuracy, since any inaccuracies would be largely smoothed out over 24 hour averages. Similarly, temporal inaccuracies due to the model's neglect of plume travel time would be smoothed out.

Comparison of hourly estimates and measurements over the Study period are given in Table 7.2 in the form of exceedences of reference levels. This method of viewing the results is consistent with the context of most short term health standards (in which the allowable number of exceedences is specified) and it also averages out the temporal errors which would be involved in a direct comparison of hourly concentration values. The two entries for the 500 $\mu g/m^3$ level show favourable comparison of prediction and measurement but the predicted exceedences for the 1000 and 1400 $\mu g/m^3$ levels are significantly lower than those extracted from measurements. It should be noted that the actual number of exceedences (less than 14) is a very small fraction of the hours in a year and that the comparison of exceedences of high concentrations is highly sensitive to relatively small absolute differences between predictions and measurements. Nevertheless, a tendency for the model to under-predict high hourly concentrations is indicated. The combination of accurate prediction of long term averages and under-prediction of 1 hour averages suggests one of the following possibilities:

(a) The assumption of uniform mixing within a TIBL of a fumigating plume does not adequately describe the high concentrations which may occur at ground level due to the down-mixing of segments of the plume in convective downdrafts, as described by Lamb (1978).

A discrepancy between the statistics of measured and predicted high short term averages is therefore to be expected.

(b) The use of a 10 minute timestep within the model may lead to an over-estimate of effective dispersion for travel times beyond 10 minutes, given that changes in wind direction between timesteps lead to a shift in plume location which is linear with distance. For distances between about 3 and 10 km, a model timestep of 30 minutes is thought more appropriate, with the lateral spread at these distances tending towards $x^{1/2}$ behaviour (as in equation 6.18). Resultant centreline concentrations would be higher at any given distance than the average of three 10 minute predictions, and this would be reflected in the increased incidence of high hourly averages at any location in the area of impact.

A ten minute timestep was originally chosen for consistency with published sigma curves (e.g. Turner, 1970) and it is still thought to be the optimum timescale for evaluating the primary pollution impact of most industrial sources. The issue raised above is an implicit limitation of the Gaussian plume modelling approach and will not be addressed further here.

7.3 ALTERNATIVE APPLICATIONS OF THE MODEL

The efficiency and relative simplicity of DISPMOD make it a very useful tool which may be applied with relatively high confidence and relatively little expense.

Apart from the foregoing task of predicting existing pollution concentrations from an established industrial complex, uses to which the model can (and in most cases has) been put are:

(i) environmental impact analysis of proposed new industries, including site selection studies;

(ii) stack height optimisation;

(iii) preparing Pollution Potential Maps for various regions to assist in land use planning, including the establishment of adequate "buffer zones" between industry and residential development;

(iv) source reconciliation studies (i.e. determining the source of pollutants detected in a particular area);

(v) modelling the impact of accidental toxic emissions as an input to risk analyses (limited to emissions which may be classified as coming from point sources and quasi continuous).

CHAPTER 8

SUMMARY AND CONCLUSIONS

The objectives of this Study, and the implications of these in terms of the direction of work and methodology employed, are listed below.

A. Provide predictive tools (computer models) for use in assessing air quality constraints on land use planning in the Kwinana area. The implications of this objective were:

   (i) Models needed to be efficient (not expensive to run), flexible and robust;

   (ii) Models needed to demonstrate acceptable accuracy (which primarily depends on the model description of important meteorological processes which influence dispersion);

   (iii) Attention was limited to the impact of primary pollutants on a local scale.

B. Develop atmospheric dispersion models which could be adapted to apply elsewhere in the State, both on the coast and inland. The implication of this objective was that models needed (as far as possible) to operate on routinely available meteorological data, as opposed to specialised and/or difficult-to-obtain data.

The methodology employed in the Study was to identify important meteorological processes and to focus on the development and validation of conceptually simple but acceptably accurate models for each of these. The final product was comprised of three models, one

each for surface layer turbulent transfers, daytime mixing in the planetary boundary layer and dispersion of plumes from point sources. Shoreline fumigation within coastal internal boundary layers was incorporated into the final model. Each of these models has demonstrated a pleasing degree of skill in simulating the results of the field experiments.

The heat budget model described in Chapter 2 formalises the approach which is implicit in the Pasquill-Gifford (PG) method of categorising atmospheric stability. The model accounts directly for the important effects of surface roughness and surface moisture content, plus other variable surface parameters. Neither the model in its present form nor the PG scheme account for the heat storage and evapotranspiration effects of dense vegetation. However the model is believed to be applicable to sparsely vegetated areas, which fairly describes the bulk of Western Australia and the coastal plain near Perth specifically. Favourable comparison of the model results and those calculated from meteorological tower profiles supports this contention. The model successfully meets the objectives listed above; in particular it fulfils the requirement for a reasonably accurate model which can run on routinely available, single height meteorological data.

The model of daytime well mixed layer growth described in Chapter 4 similarly achieves the Study objectives successfully. The only input data required by the model apart from the output of the heat budget model are morning (near sunrise) radiosonde temperature profiles (which is a requirement common to any rigorous mixing depth model).

Such data are available from the Commonwealth Bureau of Meteorology for various regions in the State, and the shape of these profiles may be taken as being representative over a fairly wide area (subject to experimental verification). The model is soundly based on theoretical principles and experimental evidence, and has demonstrated a level of accuracy which is quite adequate for dispersion modelling purposes. The model output, including h, w_*^3 and $\Delta\theta$ is ideally suited for accommodating state-of-the-art calculations of plume behaviour (including levelling and penetration of inversions) and dispersion within a convective boundary layer. The effects of wind shear thickening the inversion "lid" and enhancing mixed layer growth has been neglected as a secondary effect, but may be included if the necessary data (horizontal temperature gradients) are available. Similarly, subsidence is a secondary effect which may be included, given the necessary data.

The simple analytical formula for a thermal internal boundary layer (TIBL) described in Chapter 5 was derived directly from the mixing depth model described above, as was the associated formula for a mechanical internal boundary layer (MIBL). The TIBL formula is attractively simple and appears to agree well with experimental observations both in the current Study and other studies described in the scientific literature, although the analysis is complicated by the presence of mechanical turbulence up to 40% higher than the boundary layer defining thermal adjustment. It was argued in Chapter 5 that the simple TIBL formula was appropriate for use within the simulation of shoreline fumigation described in Chapter 6. Application of the TIBL formula is limited to the local scale within which travel time is

short compared to the diurnal timescale of convective boundary layer deepening. Rapid growth of the TIBL is clearly limited by the strongly stable interface at the top of a sea breeze; this may be simply described in a shoreline fumigation model if the sea breeze depth is known. The requirements to measure or estimate the sea breeze depth and the temperature lapse rate within onshore flows are two unavoidable departures from the objective of using routinely available data. The main area of future work identified in this Study is to seek to develop parameterizations for these two variables in terms of available synoptic data. There are strong indications from the present Study that this can be achieved in relation to lapse rate at least.

The shoreline fumigation model described in Chapter 6 is reliant on accurate descriptions of TIBL growth and of plume rise from near-shore tall stacks. The algorithm employed for computing plume entrainment and subsequent fumigation within a growing TIBL is based on the model of Lyons (1975) but incorporates significant improvements in the description of vertical mixing rate and lateral dispersion within the TIBL. The model is conceptually simple, executes very rapidly and has demonstrated a high degree of skill in simulating the results of a tracer gas dispersion experiment. Statisitics of high concentration predictions from an annual run of the dispersion model DISPMOD point to possible under-prediction of peak levels caused by convective down-mixing of plumes within a TIBL. It may be possible to develop empirical procedures to emulate this effect, but such has not been attempted in the current Study. An empirical procedure was developed to describe enhanced dispersion of plumes within a MIBL, correctly differentiating between high and low sources. As with the shoreline

fumigation model, the procedure combines conceptual simplicity with acceptable accuracy in the context of Study objectives.

The point source Gaussian plume dispersion model, DISPMOD, was developed with a view to employing recent findings from planetary boundary layer turbulence and dispersion studies. The results provided by the surface layer and mixed layer models are employed directly within DISPMOD to compute turbulence statistics and plume spread parameters from analytical formulae, avoiding the conventional stability categories and sigma curves. Refinements to these formulae may be easily incorporated as and when they are reported in the scientific literature. The simulation of coastal fumigation has been incorporated into DISPMOD as a modular feature which can be simply disabled for inland application. Close attention was paid to enhancing the computational efficiency of the model; as a consequence the model may be run over an extended period for a modest cost, making it a viable tool for case studies and evaluation of alternative development proposals. The model has demonstrated excellent accuracy in predicting annual and 24 hour concentrations at the location of a continuous monitoring station. The model tends to under-predict high short term (1 hour) averages as described above. In its present form the model takes no account of topographic effects (which are insignificant, in relation to dispersion from tall chimneys, throughout most of Western Australia) and it is directly applicable only on a local scale (e.g. 10 - 20 km from the source), in that it does not account for wind direction veer with height or fumigation into growing convective mixed layers.

Areas of work which have been identified in this Study as requiring further attention are:

(i) parameterization of the sea breeze depth and onshore flow (including sea breeze) temperature lapse rate in terms of synoptic data;

(ii) determination of soil heat and moisture characteristics for Western Australian soils, for use in the heat budget model;

(iii) additional field experiments to study TIBL growth and confirm (or otherwise) the observations and hypothesis regarding the differing vertical extent of mechanical turbulence and thermal adjustment;

(iv) investigation of possible empirical descriptions of convective downwash of plumes within a TIBL;

(v) refinement of plume spread formulae as and when new information becomes available.

REFERENCES

Benkley, C. W. and Schulman, L. L. 1979. Estimating hourly mixing depths from historical meteorological data. J. Appl. Meteorol., 18, 772-780.

Berkowicz, R. and Prahm, L. P. 1982a. Sensible heat flux estimated from routine meteorological data by the resistance method. J. Appl. Meteorol., 21, 1845-1864.

Berkowicz, R. and Prahm, L. P. 1982b. Evaluation of the profile method for estimation of surface fluxes of momentum and heat. Atmos. Environ., 16, 2809-2819.

Binkowski, F. S. 1983. A simple model for the diurnal variation of the mixing depth and transport flow. Bound.- Layer Meteorol., 27, 217-236.

Blackadar, A. K. 1976. Modelling the nocturnal boundary layer. Proc. Third Symposium on Atmospheric Turbulence, Diffusion and Air Quality, American Meteorological Society, Boston, Mass. 46-49.

Briggs, G. A. 1971. Some recent analyses of plume rise observation. Proc. of the Second International Clean Air Congress, edited by H. M. England and H. T. Berry, Academic Press, New York, 1029.

Briggs, G. A. 1975. Plume rise predictions. Lectures on Air Pollution and Environment Impact Analyses. Ed. D. A. Haugen. American Meteorological Society, Boston, Mass., 59-105.

Carlson, T.N., Dodd, J.K., Benjamin, S.G. and Cooper, J.N. 1981. Satellite estimation of the surface energy balance, moisture availability and thermal inertia. J. Appl. Meteorol., 20, 67-87.

Carson, D.J. and Richards, P.J.R. 1978. Modelling surface turbulent fluxes in stable conditions. Bound. - Layer Meteorol., 14, 67-81.

Caughey, S.J. and Palmer, S.G. 1979. Some aspects of turbulence structure through the depth of the convective boundary layer. Quart. J. Roy. Meteorol. Soc., 105, 811-827.

Caughey, S.J., Nyngaard, J.C. and Kaimal, J.C. 1979. Turbulence in the evolving stable boundary layer. J. Atmos. Sci., 36, 1041-1052.

Clark, G.H., Charash, E. and Bendun, E.O.K. 1977. Pattern recognition studies in acoustic sounding. J. Appl. Meteorol., 16, 1365-1368.

Clarke, R.H., Dyer, A.J., Brook, R.R., Reid, D.G. and Troup, A.J. 1971. The Hangara experiment: boundary layer data. CSIRO Div. Meteorol. Phys., Melbourne, Australia. Tech. Paper No. 19, 358 pp.

Davies, J.A., Schertzer, W. and Nunez, M. 1975. Estimating global solar radiation. Bound. - Layer Meteorol., 9, 33-52.

Deardorff, J.W. 1968. Dependence of air-sea transfer coefficients on bulk stability. J. Geophys. Res., 73, 2549-2557.

Deardorff, J.W. 1970. Convective velocity and temperature scales for the unstable planetary boundary layer.
J. Atmos. Sci., 27, 1211-1213.

Deardorff, J.W. 1978. Efficient prediction of ground surface temperature and moisture, with inclusion of a layer of vegetation.
J. Geophys. Res., 83, 1889-1903.

Deardorff, J.W. 1979. Prediction of convective mixed-layer entrainment for realistic capping inversion structure.
J. Atmos. Sci., 36, 424-436.

Deardorff, J.W. 1983. A multi-limit mixed-layer entrainment formulation. J. Phys. Oceanogr., 13, 988-1002.

Deardorff, J.W. and Willis, G.E. 1983. Response to ground-level concentration due to fumigation into an entraining mixed layer.
Atmos. Environ., 17, 1030-1032.

DeHeer-Amissah, A., Hogstrom, U. and Smedman-Hogstrom, A. 1981. Calculation of sensible and latent heat fluxes, and surface resistance from profile data. Bound. - Layer Meteorol., 20, 35-49.

Denman, K.L. 1973. A time dependent model of the upper ocean.
J. Phys. Oceanogr., 3, 173-184.

Draxler, R.R. 1976. Determination of atmospheric diffusion parameters.
Atmos. Environ., 10, 99-105.

Driedonks, A.G.M. 1982. Models and observations of the growth of the atmospheric boundary layer. Bound. - Layer Meteorol., 23, 283-306.

Driedonks, A.G.M. and Tennekes, H. 1984. Entrainment effects in the well-mixed atmospheric boundary layer. Bound. - Layer Meteorol., 30, 75-105.

Dyer, A.J. 1974. A review of flux-profile relationships. Bound. - Layer Meteorol., 7, 363-372.

Emmanuel, C.B. 1973. Richardson number profiles through shear instability wave regions observed in the lower planetary boundary layer. Bound. - Layer Meteorol., 5, 19-27,

Gamo, M., Yamamoto, S. and Yokoyama, O. 1982. Airborne measurements of the free convective internal boundary layer during the sea breeze. J. Meteorol. Soc. Japan, 60, 1284-1298.

Garratt, J.R. 1978a. Flux profile relations above tall vegetation. Quart. J. Roy. Meteorol. Soc., 104, 199-211.

Garratt, J.R. 1978b. Transfer characterisitics for a heterogeneous surface of large aerodynamic roughness. Quart. J. Roy. Meteorol. Soc., 104, 491-502.

Gifford, F.A. 1975. Atmospheric dispersion models for environmental pollution applications. Lectures on Air Pollution and Environmental Impact Analyses. Ed. D.A. Haugen. American Meteorological Society, Boston, Mass. 35-58.

Golder, D. 1972. Relations among stability parameters in the surface layer. Bound. - Layer Meteorol., 3, 47-58.

Halitsky, J. 1961. Single camera measurements of smoke plumes. Int. J. Air and Water Pollut., 4, 185-189.

Hall, F.F., Edinger, J.G. and Neff, W.D. 1975. Convective plumes in planetary boundary layer, investigated with an acoustic echo sounder. J. Appl. Meteorol., 14, 513-523.

Hanna, S.R. 1982. Review of atmospheric diffusion models for regulatory applications. Technical Note No. 177., World Meteorological Organization, Geneva, Switzerland. 37 pp.

Hanna, S.R., Briggs, G.A., Deardorff, J.W., Egan, B.A., Gifford, F.A. and Pasquill, F. 1977. AMS workshop on stability classification schemes and sigma curves - summary of recommendations. Bull. Amer. Meteor. Soc., 58, 1305-1309.

Hanna, S.R., Briggs, G.A. and Hosker, R.P. 1982. Handbook on Atmospheric Diffusion. U.S. Department of Energy. 102 pp.

Hicks, B.B. 1975. A procedure for the formulation of bulk transfer coefficients over water. Bound. - Layer Meteorol., 8, 515-524.

Hicks, B.B. 1976. Wind profile relationships from the Wangara experiment. Quart. J. Roy. Meteorol. Soc., 102, 535-551.

Hoffert, M.I. and Storch, J. 1979. A scheme for computing surface fluxes from mean flow observations.
Bound. - Layer Meteorol., 17, 429-442.

Hounam, C.E. 1945. The sea breeze at Perth.
Weather Develop. Res. Bull., 3, 20-55.

Hunt, J.C.R. 1982. Diffusion in the stable boundary layer.
Atmospheric Turbulence and Air Pollution Modelling.
Eds. F.T.M. Nieuwstadt and H. van Dop. D. Reidel Publishing Company.
Dordrecht : Holland. 358 pp.

Imberger, J. 1985. The diurnal mixed layer.
Limnol. Oceanogr., 30, 737-770.

Irwin, J.S. 1979a. Estimating plume dispersion - a recommended generalized scheme. Preprints Fourth Symposium on Turbulence, Diffusion and Air Pollution. Am. Meteorol. Soc., 45 Beacon Street, Boston, Mass. 02108, 62-69.

Irwin, J.S. 1979b. A theoretical variation of the wind profile power - law exponent as a function of surface roughness and stability.
Atmos. Environ., 13, 191-194.

Irwin, J.S. 1983. Estimating plume dispersion - a comparison of several sigma schemes. J. Climate Appl. Meteor., 22, 92-114.

Kahle, A.B. 1977. A simple thermal model of the earth's surface for geological mapping by remote sensing.
J. Geophys. Res., 82, 1673-1680.

Kaimal, J.C., Wyngaard, J.C., Haugen, D.A., Cote, O.R., Izumi, Y., Caughey, S.J. and Readings, C.J. 1976. Turbulence structure in the convective boundary layer. J. Atmos. Sci., 33, 2152-2169.

Kaimal, J.C., Abshire, N.L., Chadwick, R.B., Decker, M.T., Hooke, W.H., Kropfli, R.A., Neff, W.D. and Pasqualucci, F. 1982. Estimating the depth of the daytime convective boundary layer.
J. Appl. Meteorol., 21, 1123-1129.

KAMS 1982. Kwinana Air Modelling Study. Department of Conservation and Environment, Western Australia, Report 10. 96 pp.

Kamst, F.H., Lyons, T.J. and Carras, J.N. 1980. Windfield analysis of the Kwinana Industrial Region.
Arch. Met. Geoph. Biokl., Ser. B., 28, 15-30.

Kantha, L.H., Phillips, O.M. and Azad, R.S. 1977. On turbulent entrainment at a stable density interface.
J. Fluid Mech., 79, 753-768.

Kato, H. and Phillips, O.M. 1969. On the penetration of a turbulent layer into stratified fluid. J. Fluid Mech., 37, 643-655.

Kerman, B.R., Mickle, R.E., Portelli, R.V. and Trivett, N.B. 1982. The Nanticoke shoreline diffusion experiment, June 1978-II-internal boundary layer structure. Atmos. Environ., 16, 423-437.

Kraus, E.B. and Turner, J.S. 1967. A one-dimensional model of the seasonal thermocline. Tellus, 19, 98-106.

Kristensen, L. 1982. Report from the panel discussion. Atmospheric Turbulence and Air Pollution Modelling. Eds. F.T.M. Nieuwstadt and H. van Dop. D. Reidel Publishing Company. Dordrecht : Holland. 358 pp.

Lamb, R.G. 1978. A numerical simulation of dispersion from an elevated point source in the convective planetary boundary layer. Atmos. Environ., 12, 1297-1304.

Lyons, T.J. and Edwards, P.R. 1982. Estimating global solar irradiance for Western Australia, Part I. Arch. Met. Geoph. Biokl., Ser. B., 30, 357-369.

Lyons, W.A. 1975. Turbulent diffusion and pollutant transport in shoreline environments. Lectures on Air Pollution and Environmental Impact Analysis, pp. 136-208. American Meteorological Society, Boston, Mass.

Lyons, W.A. and Cole, H.S. 1973. Fumigation and plume trapping on the shores of Lake Michigan during stable onshore flow. J. Appl. Meteorol., 12, 494-510.

McCumber, M.C. 1980. A numerical simulation of the influence of heat and moisture fluxes upon mesoscale circulations. Ph.D. dissertation, Univ. of Virginia, 255 pp.

McCumber, M.C. and Pielke, R.A. 1981. Simulation of the effects of surface fluxes of heat and moisture in a mesoscale numerical model. 1 Soil layer. J. Geophys. Res., 86, 9929-9938.

McKay, D.J. 1978. A sad look at commercial humidity sensors for meteorological applications. Fourth Symposium on Meteorological Observations and Instrumentation, American Meteorological Society. Boston, Mass., U.S.A. 563 pp.

McRae, G.J., Shair, F.H. and Seinfield, J.H. 1981. Continuous downmixing of plumes in a coastal environment. J. Appl. Meteorol., 20, 1312-1324.

Mahrt, L. 1981. Modelling the depth of the stable boundary-layer. Bound. - Layer Meteorol., 21, 3-19.

Mahrt, L. and Lenschow, D.H. 1976. Growth dynamics of the convectively mixed layer. J. Atmos. Sci., 33, 41-51.

Manins, P.C. 1979. Partial penetration of an elevated inversion layer by chimney plumes. Atmos. Environ., 13, 733-741.

Manins, P.C. 1982. The daytime planetary boundary layer: A new interpretation of Wangara data.
Quart. J. Roy. Meteorol. Soc., 108, 689-705.

Manins, P.C. 1985. Chimney plume penetration of the sea breeze inversion. Atmos. Environ., 18, 2239-2344.

Misra, P.K. 1980. Dispersion from tall stacks into a shoreline environment. Atmos. Environ., 14, 396-400.

Misra, P.K. 1982. Dispersion of non-buoyant particles inside a convective boundary layer. Atmos. Environ., 16, 239-243.

Misra, P.K. and Onlock, S. 1982. Modelling continuous fumigation of the Nanticoke generating station plume. Atmos. Environ., 16, 479-489.

Monin, A.S. and Obukhov, A.M. 1954. Basic laws of turbulent mixing in the atmosphere near the ground.
Jr., Akad. Nauk SSSR Geofiz. Inst., No. 24 (151), 163-187.

Monteith, J.L. 1973. Principles of Environmental Physics,
E. Arnold Ltd., London. 241 pp.

Niiler, P.P. and Kraus, E.B. 1977. One-dimensional models of the upper ocean. p 143-172. Modelling and Prediction of the Upper Layers of the Ocean. (Ed. E.B. Kraus). Permagon Press, N.Y.

Ookouchi, Y., Segal, M., Kessler, R.C. and Pielke, R.A. 1984. Evaluation of soil moisture effects on the generation and modification of mesoscale circulations. Monthly Weather Review, 112, 2281-2292.

Paltridge, G.W. 1970. Day-time long-wave radiation from the sky. Quart. J. Roy. Meteorol. Soc., 96, 645-653.

Paltridge, G.W. 1974. Solar radiation statistics for Australia. CSRIO Div. Atmos. Phys., Melbourne, Australia. Tech. Paper No. 23. 22 pp.

Paltridge, G.W. and Platt, C.M.R. 1976. Radiative processes in meteorology and climatology. Elsevier Scientific Publishing Company, Amsterdam - Oxford - New York. 318 pp.

Paltridge, G.W. and Proctor, D. 1976. Monthly mean solar radiation statistics for Australia. Solar Energy, 18, 235-243.

Panofsky, P.A., Tennekes, H., Lenschow, D.H. and Wyngaard, J.C. 1977. The characteristics of turbulent velocity components in the surface layer under convective conditions. Bound. - Layer Meteorol., 11, 355-361.

Pasquill, F. 1974. Atmospheric diffusion. 2nd Edition. John Wiley and Sons, London. 429 pp.

Pasquill, F. 1976. Atmospheric dispersion parameters in Gaussian plume modelling. Part II. Possible requirements for change in the Turner Workbook Values. EPA-600/4-76-030b. 44 pp.

Paulson, C.A. 1970. The mathematical representation of wind speed and temperature profiles in the unstable atmospheric surface layer. J. Appl. Meteorol., 9, 857-861.

Peterson, E.W. 1969. Modification of mean flow and turbulent energy by a change in surface roughness under conditions of neutral stability. Quart. J. Roy. Meteorol. Soc., 95, 561-575.

Penman, H.L. 1948. Natural evaporation from open water, bare soil and grass. Proc. Roy. Soc., A193, 120-146.

Plate, E.J. 1971. Aerodynamic Characteristics of Atmospheric Boundary Layers, United States Atomic Energy Commission 190 pp.

Pollard, R.T., Rhines, P.B. and Thompson, R.O.R.Y. 1973. The deepening of the wind-mixed layer. Geophys. Fluid Dyn., 3, 381-404.

Portelli, R.B. 1982. The Nanticoke shoreline diffusion experiment, June, 1978 - 1. Experimental design and program overview. Atmos. Environ., 16, 413-421.

Raupach, M.R. and Thom, A.S. 1981. Turbulence in and above plant canopies. Ann. Rev. Fluid Mech., 13, 97-129.

Rayner, K.N. 1980. Diurnal Energetics of a Reservoir Surface Layer. M.Eng.Sc. Thesis, University of Western Australia. 227 pp.

Raynor, G.S., Michael, P., Brown, R.M. and SethuRaman, S. 1975. Studies of atmospheric diffusion from a nearshore oceanic site. J. Appl. Meteorol., 14, 1080-1094.

Raynor, G.S., SethuRaman, S. and Brown, R.M. 1979. Formation and characteristics of coastal internal boundary layers during onshore flows. Bound. - Layer Meteorol., 16, 487-514.

Russell, P.B. and Uthe, E.E. 1978. Regional patterns of mixing depth and stability : Sodar network measurements for input to air quality models. Bull. Amer. Meteor. Soc., 10, 1275-1287.

Rye, P.J. 1980. A model for pollutant dispersal by the sea breeze; 1. Structure and validation of sea breeze model. Western Australian Institute of Technology, Department of Physics Internal Report PD 239/1980/AM 34. (Tech. Report KAMS-08, Department of Conservation and Environment, Western Australia.) 25 pp.

Rye, P.J. 1984. Gaussian air pollution models for air quality management in Western Australia. Structure and Validation. Report SPG/1984/AP 86, School of Physics and Geosciences, Western Australian Institute of Technology. 33 pp.

Sedefian, L. and Bennett, E. 1980. A comparison of turbulence classification schemes. Atmos. Environ., 14, 741-750.

SethuRaman, S., Brown, R.M., Raynor, G.S. and Tuthill, W.A. 1979. Calibration and use of a sailplane variometer to measure vertical velocity fluctuations. Bound. - Layer Meteorol., 16, 99-105.

Sherman, F.S., Imberger, J. and Corcos, G.M. 1978. Turbulence and mixing in stably stratified waters. Ann. Rev. Fluid Mech., 10, 267-288.

Smith, F.B. and Blackall, R.M. 1979. The application of field-experiment data to the parameterization of dispersion of plumes from ground-level and elevated sources. Mathematical Modelling of Turbulent Diffusion in the Environment. Ed. C.J. Harris, Academic Press, London. 500 pp.

Spigel, R.H., Imberger, J. and Rayner, K.N. 1986. Modelling the diurnal mixed layer. Limnol. Oceanogr., 31, 533-556.

Steyn, D.G. and Oke, T.R. 1982. The depth of the daytime mixed layer at two coastal sites: a model and its validation. Bound. - Layer Meteorol., 24, 161-180.

Stull, R.B. 1976. The energetics of entrainment across a density interface. J. Atmos. Sci., 33, 1260-1267.

Stunder, M.J. and SethuRaman, S. 1985. A comparative evaluation of the coastal boundary - layer height equations. Bound. - Layer Meteorol., 32, 177-204.

Stunder, M.J., SethuRaman, S., Misra, P.K. and Sahota, H. 1985. Downwind non-uniform mixing in shoreline fumigation processes. MEAS Technical Report.

Swinbank, W.C. 1963. Longwave radiation from clear skies. Quart. J. Roy. Meteorol. Soc., 89, 339-348.

Taylor, G.I. 1921. Diffusion by continuous movements. Proc. London Math. Soc., 20, 196-202.

Tennekes, H. and Lumley, J.L. 1972. A First Course in Turbulence. The MIT Press, Cambridge. 300 pp.

Tennekes, H. 1973. A model for the dynamics of the inversion above a convective boundary layer. J. Atmos. Sci., 30, 558-567.

Tennekes, H. and Driedonks, A.G.M. 1981. Basic entrainment equations for the atmospheric boundary layer. Bound. - Layer Meteorol., 20, 515-531.

Turner, D.B. 1970. Workbook of atmospheric dispersion estimates. Office of Air Programs, Environmental Protection Agency, Research Triangle Park, North Carolina. 64 pp.

TVA. 1972. Heat and mass transfer between a water surface and the atmosphere. Div. Water Resources Research Laboratory Report No. 14, Tennessee Valley Authority. 168 pp.

Van Dop, H., Steenkist, R. and Nieuwstadt, F.T.M. 1979. Revised estimates for continuous shoreline fumigation.
J. Appl. Meteorol., 18, 133-137.

Van Ulden, A.P. and Holtslag, A.A.M. 1985. Estimation of atmospheric boundary layer parameters for diffusion applications.
J. Climate Appl. Meteor., 24, 1196-1207.

Venkatram, A. 1977. A model of internal boundary layer development.
Bound. - Layer Meteorol., 11, 419-437.

Venkatram, A. 1980a. Estimating the Monin Obukhov length in the stable boundary layer for dispersion calculations.
Bound. - Layer Meteorol., 19, 481-485.

Venkatram, A. 1980b. The relationship between the convective boundary layer and dispersion from tall stacks. Atmos. Environ., 14, 763-767.

Venkatram, A. 1986. An examination of methods to estimate the height of the coastal internal boundary layer.
Bound. - Layer Meteorol., 36, 149-156.

Von Gogh, R.G. and Zib, P. 1978. Comparison of simultaneous tethered balloon and monostatic acoustic sounder records of the statically stable lower atmosphere. J. Appl. Meteorol., 17, 34-39.

Walker, D.R. and Allen, S.C. 1975. Perth sea breeze project 1966: data.
Bureau of Meteorology, Australia. 33 pp.

Webb, E.K. 1975. Evaporation from catchments. Prediction in Catchment Hydrology, Australian Academy of Science. 203-236.

Webb, E.K. 1984. Evaluation of evapotranspiration and canopy resistance: An alternative combination approach. Evapotranspiration From Plant Communities. Ed. M.L. Sharma. Elsevier Science Publishers B.V.

Weil, J.C. and Brower, R.P. 1984. An updated Gaussian plume model for tall stacks. J. Air Pollut. Control Assoc., 34, 818-827.

Weil, J.C. 1985. Updating applied diffusion models. J. Climate Appl. Meteorol., 24, 1111-1130.

Weisman, B. 1976. On the criteria for the occurrence of fumigation inland from a large lake - a reply. Atmos. Environ., 12, 172-173.

West, P.W. and Gaeke, G.C. 1956. Fixation of sulphur dioxide as sulfiteomercurate III and subsequent colorimetric determination. Anal. Chem., 23, 1816.

Willis, G.E. and Deardorff, J.W. 1974. A laboratory model of the unstable planetary boundary layer. J. Atmos. Sci., 31, 1297-1307.

Willis, G.E. and Deardorff, J.W. 1976. A laboratory model of diffusion into the convective planetary boundary layer. Quart. J. Roy. Meteorol. Soc., 102, 427-445.

Hu, J. 1973. Wind-induced turbulent entrainment across a stable density interface. J. Fluid Mech., 61, 275-287.

Zeman, O. and Tennekes, H. 1977. Parameterization of the turbulent energy budget at the top of the daytime atmospheric boundary layer. J. Atmos. Sci., 34, 111-123.

APPENDIX A

SOLAR RADIATION

Solar radiation is a parameter which is readily measured. For the purposes of dispersion modelling, however, there are a few additional items of information required which are derived from theoretical considerations. A simplified treatment of solar radiation theory is given below, providing the required information.

This section draws heavily on a report from the Tennesse Valley Authority (1972).

Extra-terrestrial Solar Radiation

The radiation Q_{so} impinging on a horizontal plane at the top of the atmosphere is

$$Q_{so} = \frac{I_o}{r} \sin\alpha \qquad (A.1)$$

with I_o solar constant = 1353W/m^2,

r radius vector

α solar altitude (radians).

The solar altitude is defined as

$$\sin\alpha = \sin\phi \sin\delta + \cos\phi \cos\delta \cosh , \qquad (A.2)$$

with ϕ latitude (radians),

δ declination of sun (radians)

h local hour angle of sun (radians)

The variables r and δ may be considered constant over a day and are given by:

$$r = 1 + 0.017 \cos\left[\frac{2\pi}{365}(186 - D)\right] \qquad (A.3)$$

$$\delta = 23.45\left(\frac{\pi}{180}\right) \cos\left[\frac{2\pi}{365}(172 - D)\right] \qquad (A.4)$$

The local hour angle h comes from its equivalent in hours, LHA. LHA is measured westward around the axis of the celestial sphere from the upper meridian of the observation point to the meridian of the sun. In other words, for the hours around local noon:

12 <LHA < 24	before local noon
LHA = 0	at local noon
0 <LHA < 12	after local noon.

LHA is computed from a two-part formula

(a) for the sun east of the local meridian

$$LHA = ST + 12 - DTSL + ET, \qquad (A.5)$$

(b) for the sun west of the local meridian

$$LHA = ST - 12 - DTSL + ET \qquad (A.6)$$

with ST standard time of time zone,

DTSL difference between local and standard time,

ET the equation of time.

ET, accounting for the apparent irregular angular motion of the sun, is given by:

$$ET = -60(0.123570\sin d - 0.004289\cos d + 0.153809\sin 2d + 0.060783\cos 2d), \qquad (A.7)$$

where $d = \frac{2\pi}{365.242}(D-1)$

and D is the day number of the year.

Sunrise and Sunset.

Sunrise and sunset are defined as those times when the centre of the sun is at the altitude of the horizon. Hence, if there are no horizon obstructions,

$$\alpha_{SR} = 0$$

$$\alpha_{SS} = \pi$$

From the definition of local hour angle, it follows that

$$\pi < h_{SR} < 2\pi$$

$$0 < h_{SS} < \pi$$

Figure A.1 shows these hour angles in the Celestial Sphere, viewed from above the north pole. From (A.2)

$$\cos h_{ss} = \frac{\sin \alpha_{ss} - \sin\phi \ \sin\delta}{\cos\phi \ \cos\delta} \qquad (A.8)$$

ST_{ss} may be evaluated from (A.6). h_{SR} also satisfies (A.8), and may be simply evaluated as

$$h_{SR} = 2\pi - h_{SS}$$

ST_{SR} is then evaluated from (A.5).

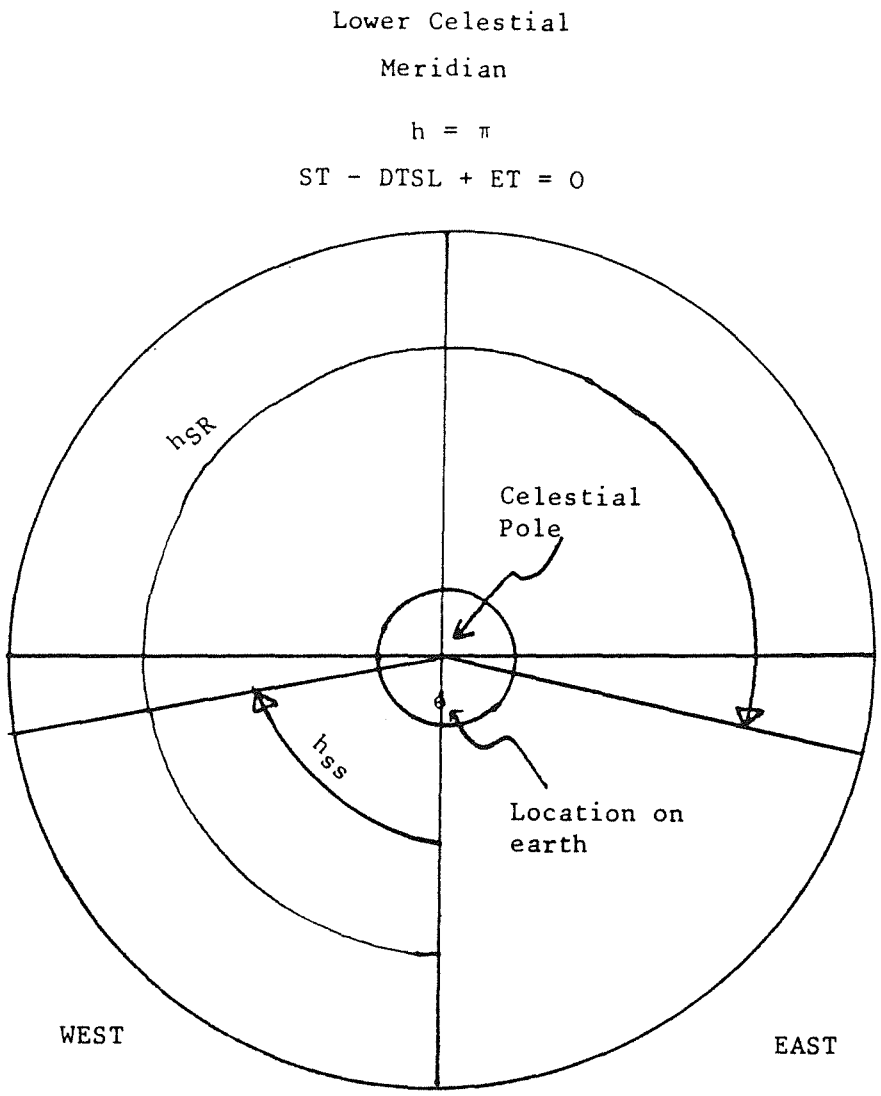

FIGURE A.1 Celestial sphere, showing hour angles for sunrise and sunset during winter.

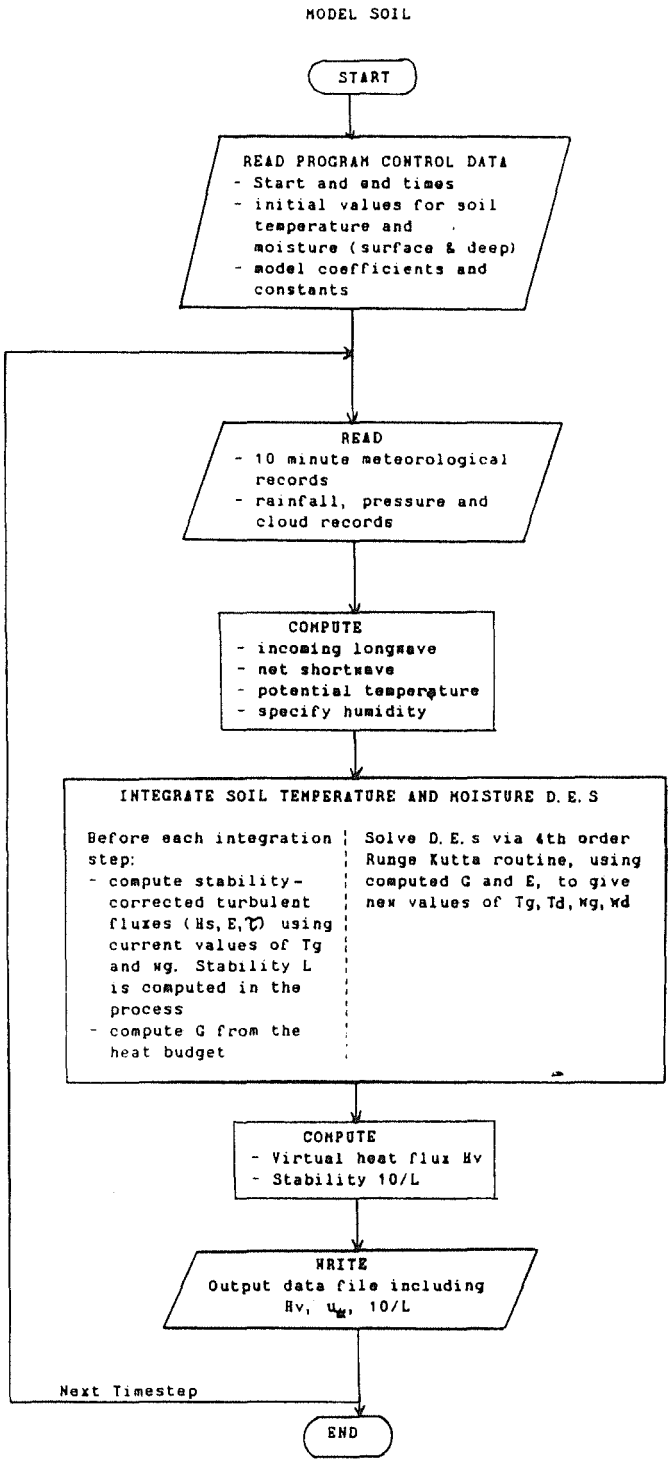

APPENDIX B FLOWCHART FOR THE SURFACE LAYER HEAT BUDGET MODEL

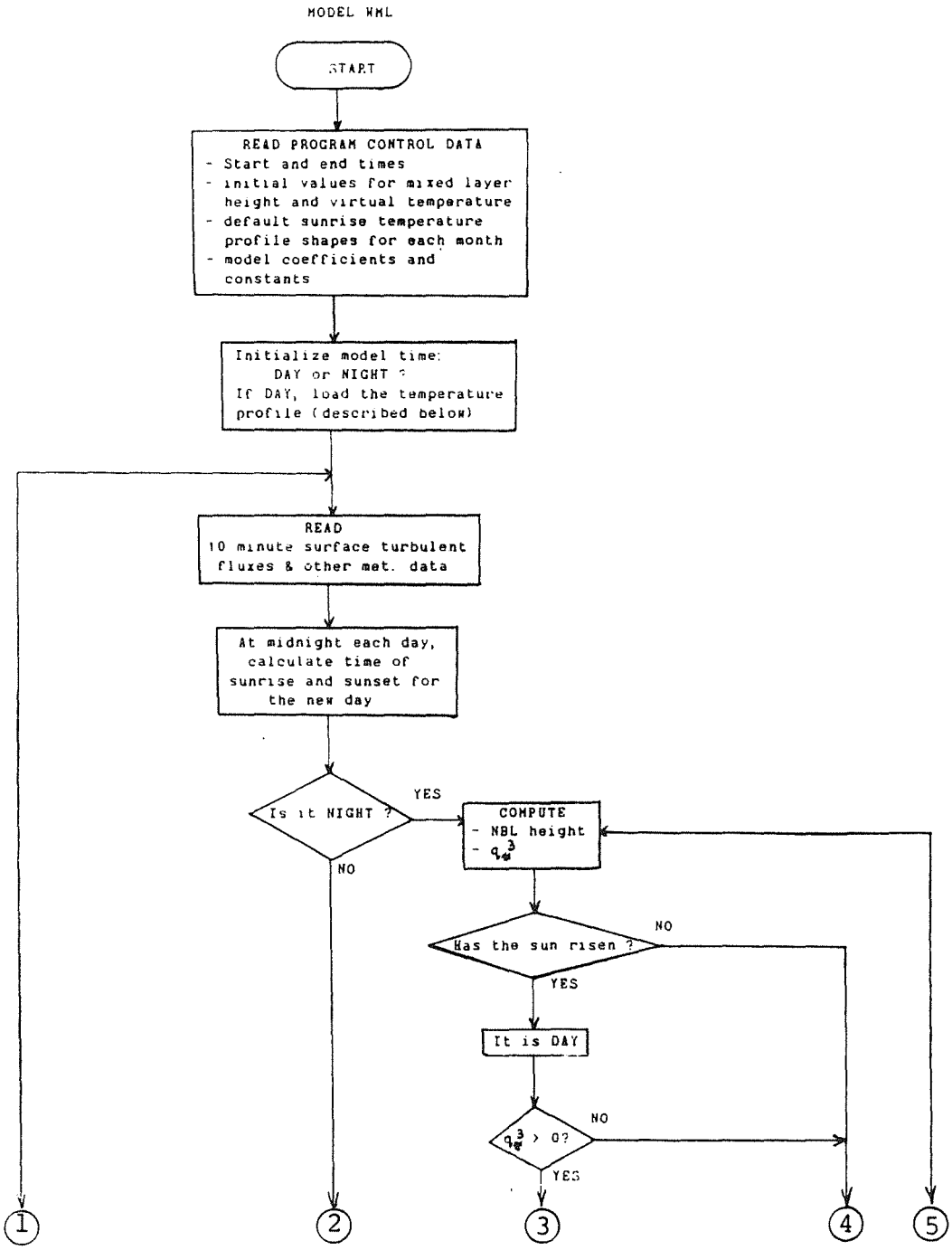

APPENDIX C FLOWCHART FOR THE ATMOSPHERIC MIXING DEPTH MODEL

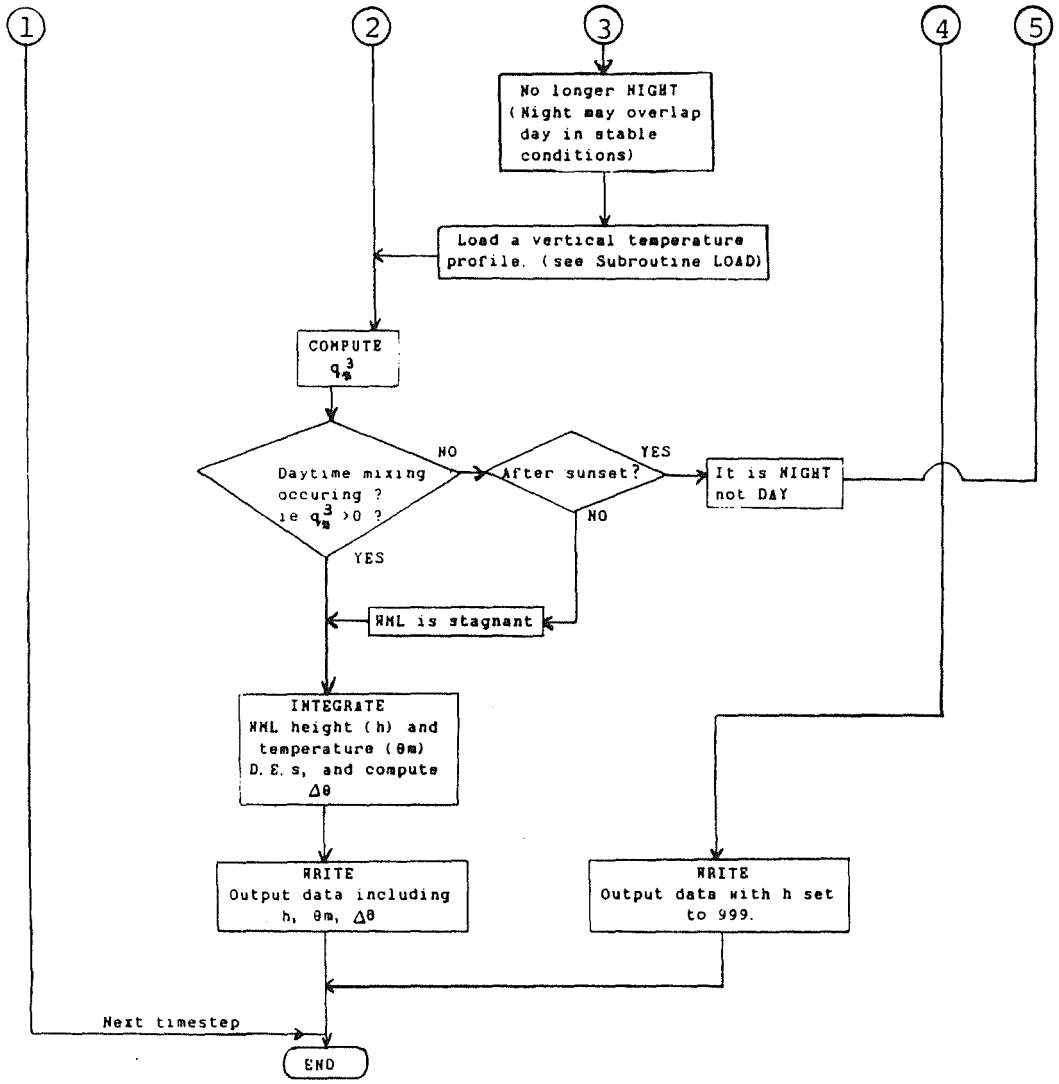
1
2
3
4
5
No longer NIGHT (Night may overlap day in stable conditions)
Load a vertical temperature profile. (see Subroutine LOAD)
COMPUTE q_s^3
Daytime mixing occuring ? ie $q_s^3 > 0$?
NO
YES
After sunset?
YES
NO
It is NIGHT not DAY
YES
NML is stagnant
INTEGRATE NML height (h) and temperature (θ_m) D. E. s, and compute $\Delta\theta$
WRITE Output data including h, θ_m, $\Delta\theta$
WRITE Output data with h set to 999.
Next timestep
END

SUBROUTINE LOAD

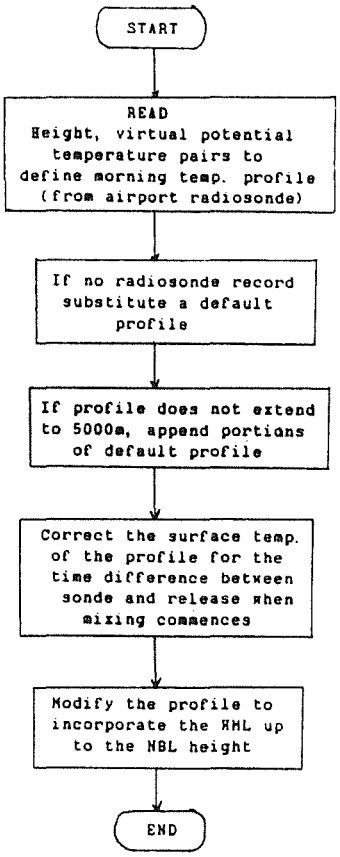

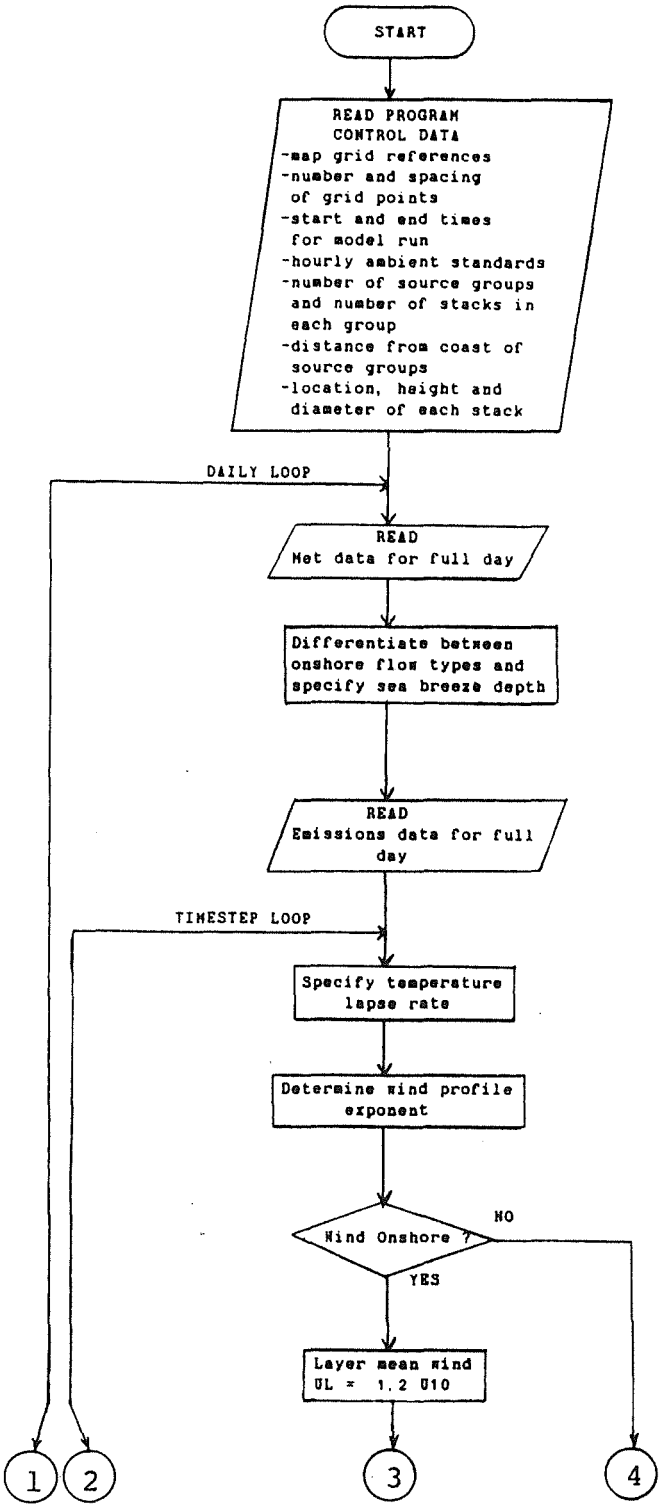

APPENDIX D FLOWCHART FOR THE GAUSSIAN PLUME DISPERSION MODEL

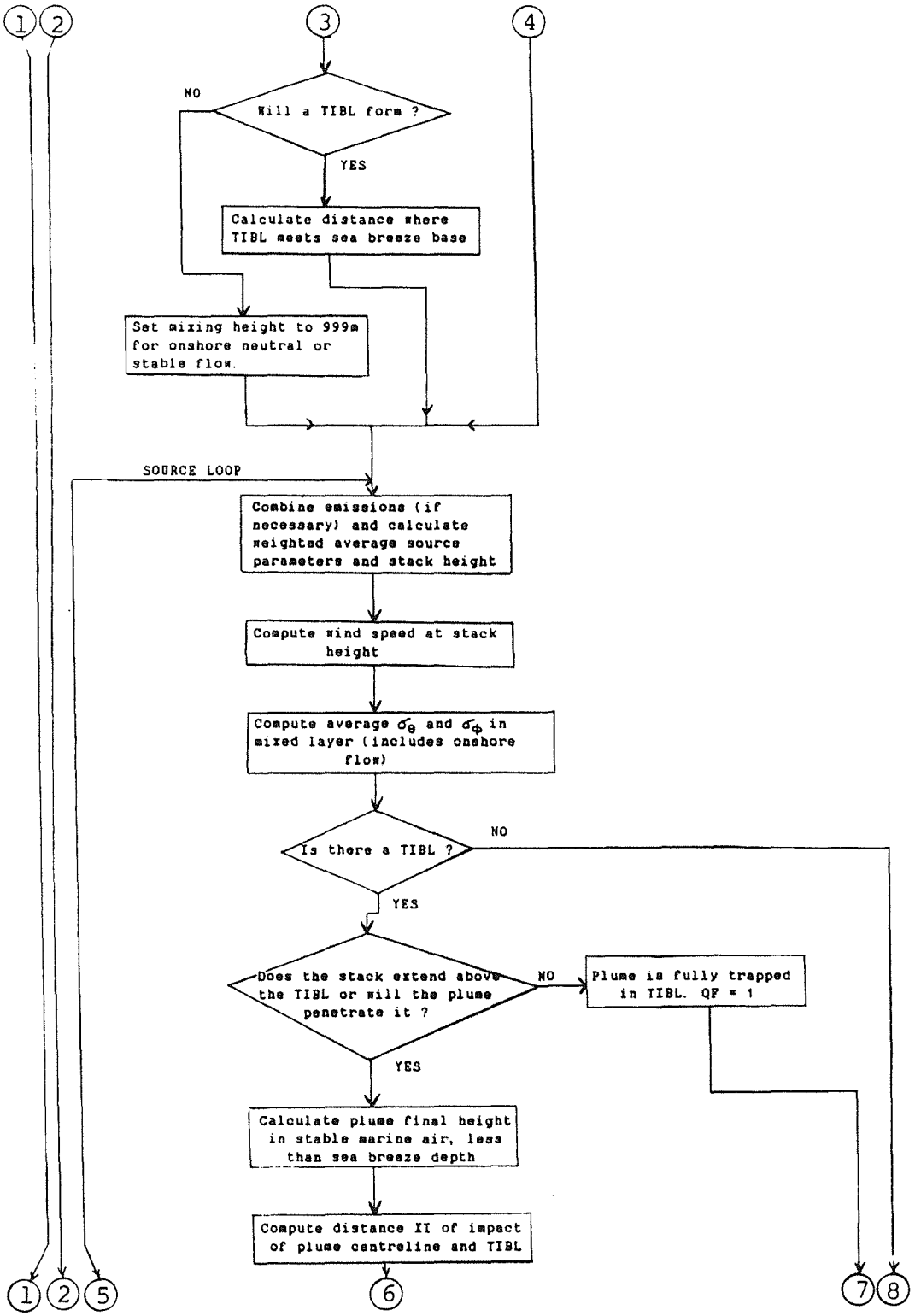
1
2
3
4
NO
Will a TIBL form ?
YES
Calculate distance where TIBL meets sea breeze base
Set mixing height to 999m for onshore neutral or stable flow.
SOURCE LOOP
Combine emissions (if necessary) and calculate weighted average source parameters and stack height
Compute wind speed at stack height
Compute average σ_θ and σ_ϕ in mixed layer (includes onshore flow)
Is there a TIBL ?
NO
YES
Does the stack extend above the TIBL or will the plume penetrate it ?
NO
Plume is fully trapped in TIBL. QF = 1
YES
Calculate plume final height in stable marine air, less than sea breeze depth
Compute distance XI of impact of plume centreline and TIBL
1
2
5
6
7
8

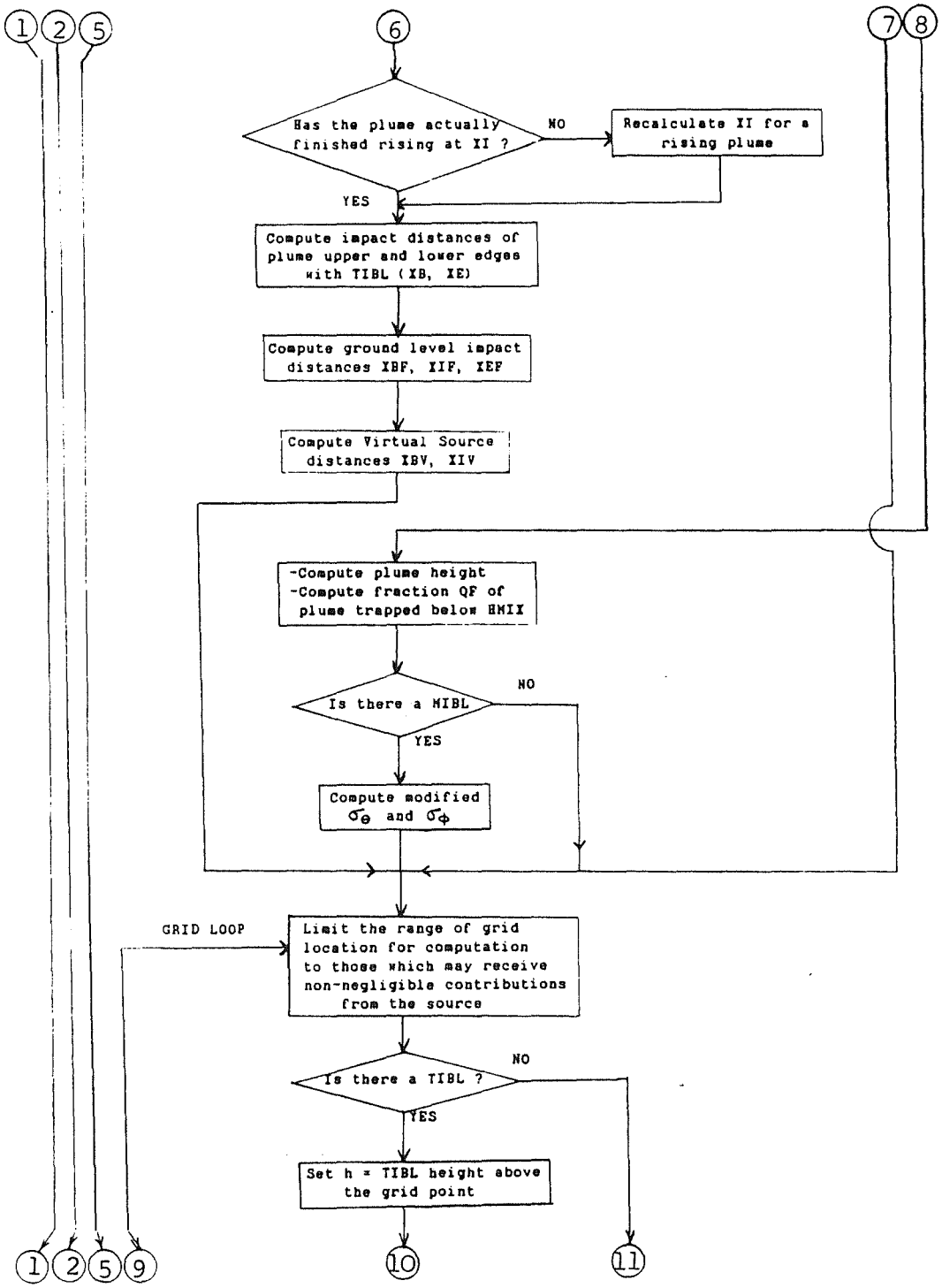
1
2
5
6
7
8
Has the plume actually finished rising at XI ?
NO
Recalculate XI for a rising plume
YES
Compute impact distances of plume upper and lower edges with TIBL (XB, XE)
Compute ground level impact distances XBF, XIF, XEF
Compute Virtual Source distances XBV, XIV
-Compute plume height
-Compute fraction QF of plume trapped below HMIX
Is there a MIBL
NO
YES
Compute modified σ_θ and σ_ϕ
GRID LOOP
Limit the range of grid location for computation to those which may receive non-negligible contributions from the source
Is there a TIBL ?
NO
YES
Set h = TIBL height above the grid point
1
2
5
9
10
11

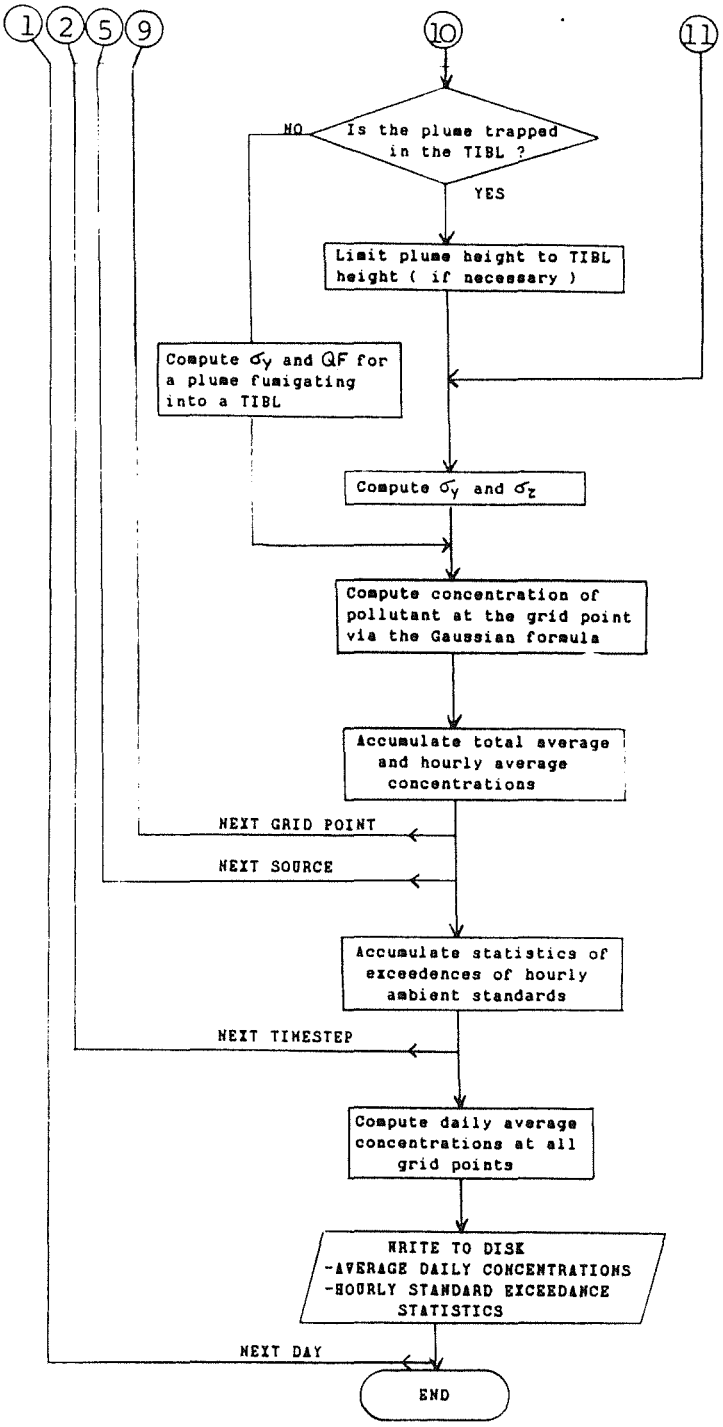
1
2
5
9
10
11
Is the plume trapped in the TIBL ?
NO
YES
Limit plume height to TIBL height (if necessary)
Compute σy and QF for a plume fumigating into a TIBL
Compute σy and σz
Compute concentration of pollutant at the grid point via the Gaussian formula
Accumulate total average and hourly average concentrations
NEXT GRID POINT
NEXT SOURCE
Accumulate statistics of exceedences of hourly ambient standards
NEXT TIMESTEP
Compute daily average concentrations at all grid points
WRITE TO DISK
-AVERAGE DAILY CONCENTRATIONS
-HOURLY STANDARD EXCEEDANCE STATISTICS
NEXT DAY
END